CONTROLLING FACTORS OF RIVER WATER STABLE ISOTOPE COMPOSITIONS AND MIDDLE TO LATE CENOZOIC DEPOSITION AND SUFACE UPLIFT HISTORY OF THE SOUTHERN ROCKY MOUNTAINS, U.S.A.

by

LU ZHU

Presented to the Faculty of the Graduate School of

The University of Texas at Arlington in Partial Fulfillment

of the Requirements

for the Degree of

DOCTOR OF PHILOSOPHY

THE UNIVERSITY OF TEXAS AT ARLINGTON

August 2019

Acknowledgements

I would first like to express my deep gratitude to Dr. Majie Fan for her guidance and support throughout the course of my study and the preparation of my dissertation. I appreciate the great amount of time and patience that Dr. Fan has spent with me in the field and laboratory, and on helping me improve critical thinking and scientific writing skills. I would also like to thank the members of my dissertation committee, Drs. Asish R. Basu, Arne M. E. Winguth, James P. Grover, Qinhong Hu, and Elizabeth M. Griffith for their time, comments, and guidance throughout the preparation and review of this dissertation.

Special thanks are extended to Dr. Brian Hough for his contribution, helpful discussion and instructions on ArcGIS in the first project; and to Drs. Andres Aslan, Jon J. Smith, and Thomas E. Yancey, for their generosity and kindness of providing samples and information in the second and third projects. Special thanks also go to Emma Gains, Jackie Garcia and Dr. Min Gao for their help in the field, and to Hepeng Tian and Dr. Lin Li for their help in the lab separating heavy minerals. Thank Dr. Hyeong-Moo Shin for help with multivariate regression analysis, and Dr. Chao Ma for help with R programing. Great thanks to my family and friends for their support and encouragement.

This research was supported by NSF grant EAR-1119005 and 1454802, and one Geological Society of America graduate student research grant.

August 15, 2019

Abstract

CONTROLLING FACTORS OF RIVER WATER STABLE ISOTOPE COMPOSITIONS AND MIDDLE TO LATE CENOZOIC DEPOSITION AND SUFACE UPLIFT HISTORY OF THE SOUTHERN ROCKY MOUNTAINS, U.S.A.

Lu Zhu, PhD

The University of Texas at Arlington, 2019

Supervising Professor: Majie Fan

The Cenozoic topographic evolution of the Rocky Mountains (Rockies) and Great Plains in the western U.S.A. reflect a combination of mantle geodynamic, crustal deformation and surface erosional processes. This region was near sea-level during the Late Cretaceous and is characterized by high topography and high relief at present. Different hypotheses involving crustal shortening and thickening, mantle dynamic process, and enhanced erosion induced by climate change have been proposed to interpret the Cenozoic surface uplift. The timing and magnitude of surface uplift hold the key to test these different hypotheses. This dissertation identifies the controlling factors of modern river water isotopic lapse rate and latitudinal gradient in the southern Rockies in Wyoming and Colorado, and the

Great Plains from south Texas to Nebraska; and examines the depositional processes and reconstructs the paleoelevations of the southern Rockies in Colorado and the adjacent Great Plains in Kansas.

Table of Contents

List of Figures

List of Tables

Chapter 1 Introduction

The southern Rocky Mountains (Rockies) in Colorado and New Mexico is a region of high elevation and high relief within the western interior of the USA. The region is bounded by the Colorado Plateau to the west, Rio Grande rift to the south, the Great Plains to the east, and extends to the central Rockies in northern Colorado and Wyoming. Well-preserved Late Cretaceous marine sedimentary rocks suggest that the region was at sea level during the Late Cretaceous. Currently, the southern Rockies is ~2500 m above the adjacent Great Plains with local relief greater than 1600 m. Despite the fact that the uplift history of the Rockies has been studied for decades, the timing and tectonic processes that produced the modern topography remain ambiguous. Quantitative paleoelevation reconstruction hold the key to better understand the topographic history and assess the geodynamic drivers of uplift.

Stable isotope paleoaltimetry is a major approach of reconstructing paleoelevation. Despite the fact that it has been applied to reconstruct the Cenozoic elevation history of many mountains belts, including the central Rockies, it has not been applied to the southern Rockies in the past. In addition, many studies have shown that stable isotope paleoaltimetry is sensitive to climate change and vapor moisture change in continental interiors. Therefore, it is important to understand the controlling factors of modern surface water isotope values and assess the influence of climate change on latitudinal and altitudinal gradients before applying such understanding to reconstruct the paleoelevation of the Rockies. Three projects presented in Chapters 2-4 are designed to understand the controlling factors of modern surface water isotope values and reconstruct the mid-late Cenozoic paleoelevation of the southern Rockies.

Chapter 2 is entitled *Spatiotemporal distribution of river water stable isotope compositions and variability of lapse rate in the central Rocky Mountains: Controlling factors and implications for paleoelevation reconstruction*. This paper was published in *Earth and Planetary Science Letters* in 2018. The paper presents an extensive river water isotopic dataset collected in one spring and two summers of two different years from Wyoming and western Nebraska. It examines the spatial and temporal variations of river water isotope compositions, and their relationships with climatic and geographic parameters, as well as moisture sources through back trajectory analysis. We elucidate the influence of elevation and climatic parameters on the spatiotemporal variation of river water isotopic values in the central Rockies. The river water isotopic compositions show no correlation to elevation because river water from the high mountains dominants the river in the lower intermountain basins. The isotope values of river water generally increase from the central Rockies to the adjacent Great Plains, which is mainly controlled by the elevation-induced temperature difference between the two areas with a combination of evaporation. We suggest that paleoclimate and atmospheric circulation pattern must be carefully evaluated when applying stable isotope-based paleoaltimetry in continental interiors.

Chapter 3 is entitled *Detrital zircon provenance record of middle Cenozoic landscape evolution in the southern Rockies, USA*. This paper was published in *Sedimentary Geology* in 2018. The paper presents 1284 new detrital zircon U-Pb ages of Eocene-Miocene sedimentary rocks in south-central Colorado to constrain the depositional ages and sediment provenances. The detrital zircon ages are integrated with interpretation of sedimentary environments and the detrital zircon signatures of potential sources to interpret landscape and paleodrainage evolution. Our results indicate that the Laramide Orogeny did not contribute to the high elevation of the Sangre de Cristo Range, and the Wet Mountain was the dominant topographic feature in the early Eocene with paleo-Arkansas River draining from north to south. During the Eocene-early Oligocene, aggradation of the Wet Mountain Valley and the Huerfano Basin formed a low-relief surface; subsequently the river changed its course to the west. By the Miocene time, the Sangre de Cristo Range raised, most likely related to the opening of the Rio Grande Rift. Opening the Rift formed the north-south orientated upper Arkansas River valley and connected the upper valley with the east-west orientated lower Arkansas River valley.

Chapter 4 is entitled *Late Eocene low elevation and subsequent differential uplift of the southern Rocky Mountains*. The manuscript compiles and analyzes the controlling factors of modern river water isotopic compositions from the near sea-level region in south Texas to the southern Rockies, and then apply the understanding to the late Eocene-Miocene surface water δD values reconstructed from the δD values of hydrated volcanic glass samples from the high southern Rockies, its adjacent high Great Plains and near sea-level region in south Texas to constrain the surface uplift history. The modern river water δD values show a latitudinal gradient from south Texas to Kansas and a lapse rate along the transect of the southern Rockies and its adjacent Great Plains, and the rates are both mainly controlled by air temperature. Our quantitative paleoelevation reconstructions show that the southern Rockies has a low mean elevation during the latest Eocene, and experienced differential uplift throughout the Oligocene and Miocene. The Arkansas River valley near the San Juan volcanic field gained nearly its modern elevation, and the South Park farther away from the field gain its partial elevation by the early Oligocene, suggesting that mid-Cenozoic crustal inflation associated with ignimbrite flare-up magmatism has caused localized uplift. The Wet Mountains gained most of its elevation by the late Miocene, likely associated with crustal thinning and thermal heating related to the opening of the Rio Grande Rift. Paleoelevation estimates of the Great Plains and the central Rockies further show along-strike variation of surface uplift process and mechanisms.

My future work will calibrate clumped isotope paleoaltimetric proxy of carbonate cement and apply the proxy to constrain and refine the surface uplift history of the southern Rockies.

Chapter 2 Spatiotemporal distribution of river water stable isotope compositions and variability of lapse rate in the central Rocky Mountains: Controlling factors and implications for paleoelevation reconstruction

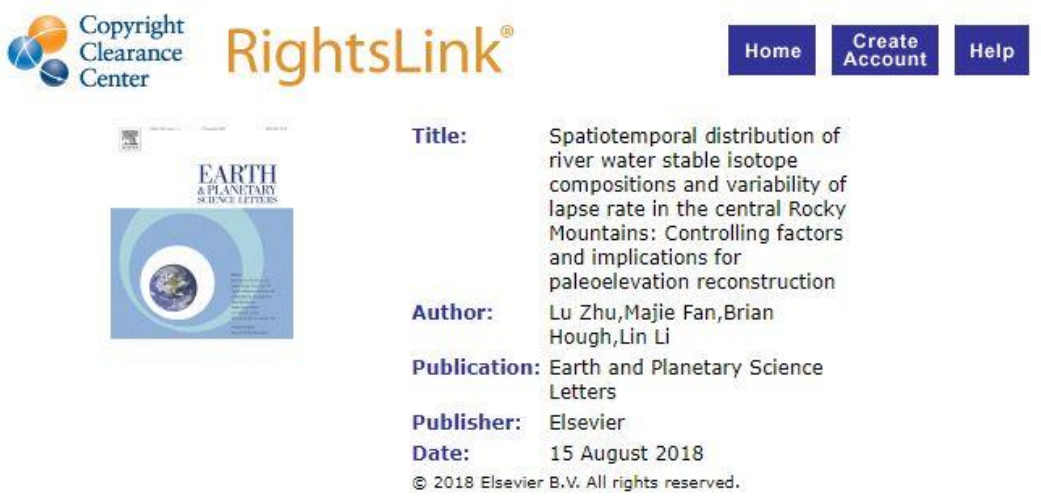

Abstract

Stable isotope-based paleoaltimetry is the most widely used approach for paleoelevation reconstruction. Interpretations of stable isotope data in continental interiors, however, are undermined by surface water isotope compositions that are influenced by multiple factors. Here we present a stable isotope dataset of modern river water samples collected over two summers and one spring from the central Rocky Mountains (Rockies) and the adjacent Great Plains. By examining the spatial and temporal variations of river water $\delta^{18}O$, δD and d-excess values, and their relationships with climatic and geographic parameters, as well as through back trajectory analysis of moisture sources, we elucidate the influences of elevation and

climatic parameters on the spatiotemporal variation of river water isotopic values. In the Bighorn River drainage, a typical intermontane drainage in the central Rockies, the isotopic difference between highland and lowland rivers is small, which we attribute to highland precipitation that dominates lowland river discharge. In the North Platte River drainage across the central Rockies and Great Plains, the river water $\delta^{18}O$ values show poor correlation with elevation west of 105°W (central Rockies), but increase as elevation decrease east of 105°W (in the western Great Plains). This eastward increase across the western Great Plains leads to an average oxygen isotope lapse rate of -2.3‰/km, which we interpret as being caused primarily by condensation temperature-controlled isotopic fractionation at various elevations, and secondarily by evaporation in the upper reaches of streams that contribute to the North Platte River plus direct contribution of moisture from the Gulf of Mexico in the Great Plains. In this continental interior setting, multiple moisture sources, including recycled continental moisture, contribute to surface water, and evaporation influences river water isotope values to various degrees depending on the relative humidity within an individual river catchment. These results suggest that paleoclimate and atmospheric circulation pattern must be carefully evaluated when applying stable isotope-based paleoaltimetry in continental interiors. Our findings have implications for paleoelevation reconstruction in the study area, including that 1) within the central Rockies, the isotopic difference of river water and unevaporated basinal precipitation can be used to infer paleorelief of the Laramide ranges with respect to the basin floors; 2) along a regional transect crossing the central Rockies and Great Plains, the modern isotope lapse rate of the North Platte River drainage can be used to constrain the paleorelief between the two regions in semi-arid climate.

Keywords: river water, stable isotopes, Rocky Mountains, paleoelevation, evaporation, Great Plains

2.1 Introduction

Rayleigh distillation of a predominant moisture source in an open system along the windward side of mountains is a fundamental assumption of stable isotope-based paleoaltimetry (e.g., Rowley et al., 2001; Rowley and Garzione, 2007). By applying an empirical isotopic lapse rate of modern surface water or a theoretical lapse rate based on Rayleigh distillation modeling, histories of surface uplift and collapse of mountains and plateaus have been reconstructed from the stable isotope compositions of many suitable geologic materials. Examples of such geologic materials include, but are not limited to, lacustrine and paleosol carbonate, groundwater carbonate cements, hydrous silicate minerals, fossil mollusks, and plant remains (e.g., Garzione et al., 2000; Mulch and Chamberlain, 2007; Fan and Dettman, 2009; Hoke et al., 2009; Hren et al., 2010). In continental interiors, a major challenge for stable isotope-based paleoaltimetry is the characterization of a surface water isotope lapse rate, which can vary from -11.4 ‰/km (Poage and Chamberlain, 2001) to nearly 0 ‰/km (Bershaw et al., 2012). This large variation was interpreted to be influenced by multiple controlling factors. Previous studies, mostly conducted in the Tibetan Plateau and Andean Plateau, have suggested that the controlling factors include vapor recycling through surface water evaporation, sub-cloud evaporation, convective storms, and snow sublimation (e.g., Bershaw et al., 2012, 2016; Lechler and Niemi, 2012; Rohrmann et al., 2014; Li and Garzione, 2017), and moisture mixing governed by atmospheric circulation patterns and climate changes (e.g., Froehlich et al., 2008; Liu et al., 2011; Poulsen and Jeffery, 2011; Licht et al., 2017).

The Cenozoic history of surface uplift and collapse of the Rocky Mountains (Rockies), the worlds' longest intracontinental mountain belt, has drawn a great amount of interest in paleoelevation reconstruction (e.g., Wolfe et al., 1998; Cather et al., 2012; Chamberlain et al., 2012; Feng et al., 2013). Many of these studies use stable isotope proxies and have yielded fruitful insights regarding the growth history and geodynamic drivers of the Rockies (e.g., Fricke, 2003; Sjostrom et al., 2006; Fan and Dettman, 2009; Fan et al., 2011, 2014a, 2014b; Fan and Carrapa, 2014; Licht et al., 2017). In these studies, paleoelevation estimates were determined either through the application a theoretical lapse rate based on Rayleigh distillation modeling (Rowley and Garzione, 2007), or by comparing reconstructed surface water isotope compositions from high to low regions with modern surface water in the same regions (Fan et al., 2014b, 2014a) or with GCM simulation-predicted paleoprecipitation isotope compositions for the same regions (Feng et al., 2013).

However, like in the interiors of other continents, vapor sources are complex and recycled moisture contributes to precipitation. Furthermore, the relative contributions of moisture sources may change during the geologic past when atmospheric circulation patterns were likely different from today (e.g., Liu et al., 2010). Additionally, the mountain ranges in the Rockies, particularly in the central Rockies, are of various orientations, which may cause orographic precipitation on some mountain flanks, but not others. Therefore, the contribution of each vapor source in the Rockies may be spatially and temporally heterogeneous, and subject to the influence of climate changes.

Understanding the controlling factors of isotopic compositions of modern surface water in the Rockies is fundamental to paleoelevation reconstructions that use stable isotope proxies and assessment of their uncertainties. Despite the fact that several studies have been conducted to characterize surface water isotope compositions in the region (Copeland and Kendall, 2000; Kendall and Coplen, 2001; Dutton et al., 2005; Vachon et al., 2010a, 2010b), none of the studies have high enough resolution to understand the heterogeneity of surface water isotope compositions and their controlling factors. In this study, we present an extensive river water isotopic dataset collected in one spring and two summers of two different years from Wyoming and western Nebraska (Fig.2-1A) to understand the spatiotemporal distribution of river water isotopes and variations in isotope lapse rate in the central Rockies and the adjacent Great Plains. By analyzing climatic patterns and vapor trajectories in the major rainy seasons before and during each sampling period, we constrain the controlling factors on river water isotope distribution and lapse rate. This new understanding sheds light on the paleoelevation reconstruction of the Rockies.

.

2.2 Background

2.2.1 Geography and climate

The study area is located in the central Rockies in Wyoming and the adjacent Great Plains in western Nebraska (Fig. 2-1). Western and central Wyoming (west of 105°W) is mountainous with a mean elevation of ~2.0 km. Eastern Wyoming and western Nebraska (east of 105°W) are relatively flat, with the mean elevation decreasing eastward gradually from 1.4km to 0.8km. The central Rockies of Wyoming are bounded to the west by the Sevier thrust belt. Major mountain ranges in Wyoming and its adjacent regions include the W-E striking Granite, Owl Creek, and Uinta mountains, NW-SE striking Wind River Range and Beartooth Mountains, and N-S striking Bighorn and Laramie mountains (Fig. 2-1A). The Bighorn River drainage ranges from 1.1 to 4.1 km in elevation, and is the largest river drainage in northwestern Wyoming (Fig. 2-1A). The Wind River flows northward from the Wind River Range through the Wind River Basin and Owl Creek Mountains, and becomes the Bighorn River in the Bighorn Basin. With major tributaries sourced in the Bighorn Mountain, the Powder River drainage is the largest river drainage in northeastern Wyoming (Fig. 2-1A). The North Platte River drainage is the largest river drainage in southern Wyoming (Fig. 2-1A). The river rises in northern Colorado and merges with the Sweetwater River sourced from the Wind River Range in central Wyoming, then flows eastward to the low plains in western Nebraska. The catchment elevation of the North Platte River ranges from 0.8 to 4.1 km, following the relief contrast between the central Rockies and Great Plains. The upper Green River drainage consists of the southward-flowing rivers in southwestern Wyoming.

The climate in Wyoming and western Nebraska is semiarid. The major rainy season in the mountainous area is spring and early summer (March–June), which contributes 50–70% of the annual precipitation amount (Arguez et al., 2010). The major rainy season on the plain area is spring and summer (April-August), which contributes ~75% of the annual precipitation amount (Arguez et al., 2010). Precipitation amount is generally higher on the plains than in the mountainous area. Within the mountainous area, precipitation amount is higher on the mountain flanks than on the basin floors.

2.2.2 Moisture sources and transport

Four major moisture sources contribute to precipitation in the study area, including northern cold moisture from the Hudson Bay and regions east of Canadian Rocky Mountains (N), moisture from the north Pacific and the tropical Pacific (P), moisture from the Gulf of Mexico (GM), and continental recycled moisture (C) (Fig. 2-1B) (Ting and Wang, 2006; Liu et al., 2010). Atmospheric water vapor from N, C, and north Pacific sources contribute to precipitation in the study area throughout the year, while the tropical Pacific and GM sources contribute more to precipitation during summer time than other seasons via the North American Monsoon (Adams et al., 1997). The GM moisture follows two transport paths, which either transports water vapor directly to western Nebraska along the front of the Rockies, or mixes with the tropical Pacific moisture near Arizona before transport northward to Wyoming (e.g., Adams et al., 1997)

.

2.3 Methods

2.3.1 River water samples and isotope analysis

A total of 242 river water samples were collected during three field seasons: one in late July in 2010 during the rainy season of western Nebraska and after the main rainy season of Wyoming, and the other two in late April and early August in 2016, which are in the rainy season of Nebraska, but during and after the rainy season of Wyoming (Fig. 2-2B). Most of the samples were collected in the Bighorn River drainage and the North Platte River drainage (Fig. 2-1A). By sampling along these two drainages, our samples follow the changes in relief between the Laramide mountain ranges and basin floor, and between the central Rockies and the Great Plains, respectively. Additional samples were collected from mountain flanks in the upper Green River and Powder River drainages. Most of the samples were collected from the same localities over the three sampling seasons. Because river samples in each locality integrate surface water over the entire upper stream drainage, the elevation of the water sample is best represented by the mean drainage elevation above the sampling site. These elevations were extracted from a 90 m digital elevation model using ArcGIS.

All river water samples were stored in plastic vials with screw tops that were sealed with Teflon tape to avoid any vapor exchange during transport and storage. The $\delta^{18}O$ and δD values of the samples collected in 2010 were analyzed using a liquid water isotope analyzer (model LWI-24d) with a GC-PAL auto-sampler at the University of Rochester, and the samples collected in 2016 were analyzed using Picarro L1102-i isotopic liquid water analyzer with a GC-PAL auto-sampler at the Iowa State University. Each analysis conducted at the University of Rochester consists of 14 water injections whereas those conducted at the Iowa State University consists of a minimum of 6 injections. To account for memory effects, the first three injections were omitted from calculations of mean isotopic values. Reference standards (VSMOW and VSLAP in University of Rochester, VSMOW, USGS 48 and USGS 47 in the Iowa State University) were used for regression-based isotopic corrections, and all the data were reported relatve to the VSMOW standard. At least one reference standard or an in-house standard that was calibrated to VSMOW and VSLAP was used for every 3-5 samples for standardization. The uncertainty, including analytical uncertainty determined from multiple injections and average correction factor, is less than 0.15‰ for $\delta^{18}O$ and 1.0‰ for δD for all samples.

We constructed contour maps of $\delta^{18}O$, δD, and d-excess values using Kriging interpolation in ArcGIS. Using this interpolation method, the value of each query point was determined based on the scattered set of input samples and their weights to the query point by considering the statistical relationships among the input. This interpolation method is most appropriate when a spatially correlated distance or directional bias exists in the data. It is important to note that the Kriging interpolation also makes predictions in the areas with few input data points and the estimates in those areas are of higher uncertainty.

An ANOVA test was used to test the differences of river water stable isotope compositions in different years and seasons. Any two groups of data would be considered similar to each other when the P value is greater than 0.05.

2.3.2 Climate factors and statistical analysis

The climatic parameters, including mean seasonal temperature, mean cumulative daily precipitation, and mean seasonal relative humidity (RH), of each sampling site during sampling seasons were extracted from the North American Regional Reanalysis dataset (NARR data). The NARR data is an average of daily data of March-May for the spring sampling season, and June-August for the summer sampling season. Contour maps of mean RH, mean temperature, and mean cumulative precipitation were also generated from grid data using Natural Neighbor interpolation tool with default settings in ArcGIS (Fig. 2-2). Climate parameters used for multivariate linear regression analysis for each sampling site in different seasons were extracted from these maps using ArcGIS.

Meteoric water isotope values are mainly influenced by elevation, RH, precipitation amount, and temperature (Dansgaard, 1964). A multivariate linear regression model was used to test the influence of these climate parameters on water stable isotope compositions. The mean seasonal temperature, mean cumulative daily precipitation, and mean seasonal RH are assumed to be independent variables in our regression models. The corresponding P-value of each independent variable in the regression helps identify the major factors influencing the river water $\delta^{18}O$ values. Any geographic or climatic parameters with P values greater than 0.05 would be excluded from subsequent regression analysis for having no statistically significant influence on water isotope values.

2.3.3 Moisture trajectories and vapor mixing

Moisture trajectories in each river drainage during the spring and summer seasons were modeled using the Hybrid Single-Particle Lagrangian Integrated Trajectory model (HYSPLIT, Draxler and Rolph, 2014) in order to track the sources of rain before and during the sampling seasons. We conducted moisture trajectory analyses for the cities of Lander, Thermopolis, and Ten Sleep in the Bighorn River drainage, for Rawlins, Wheatland, and Ogallala in the North Platte

River drainage, for Buffalo on the eastern side of the Bighorn Mountain, and for Pinedale on the western side of the Wind River Range (Fig. 2-1).

For each representative locality, back trajectories were computed every 12 hours from March–May for the spring of 2016, and from June–August for the summers of 2011 and 2016. We use 120-hour back trajectories for each analysis episode. Moisture sources were determined based on the locations of end points of the back trajectories. While it is not guaranteed that the ultimate source can be determined by the analysis, the relative contribution of each source to the precipitation can be well approximated based on the end points of the back trajectories. The initial air parcel was set at 1 km above ground, because most atmospheric moisture is in the lower troposphere 0–2 km above ground level and there is no significant difference in results for initiation at 0.5, 1.0, or 1.5 km level (Li and Garzione, 2017). Among the computed results of back trajectories, we only consider the trajectories that produced rain at the study area during the sampling periods. At each representative locality, the contribution of each rain-producing trajectory to each precipitation episode was determined based on its rain amount. The contribution of each source to each season was determined by the sum of its contribution to all precipitation episodes in the season.

2.4 Results

2.4.1 Spatial and temporal patterns of river water isotope compositions

The $\delta^{18}O$, δD, and d-excess values of the river water samples vary from -19.2 to -11.7‰, -144.6 to -88.8‰, and -11.7 to 11.3‰, respectively (Fig. 2-3). These data are consistent with published river water isotope data of the same sampling months, but different years, in a previous study (Kendall and Coplen, 2001). The distribution patterns of $\delta^{18}O$ and δD values are similar in the study area (Fig. 2-3), thus we only describe and discuss the $\delta^{18}O$ and the d-excess values. In the Bighorn River drainage, the $\delta^{18}O$ values on the flanks of the Bighorn Mountains and the Wind River Range are on average 1-3‰ lower than those on the basin floors (Fig. 2-3). The d-excess values are on average up to 2.4‰ higher on the mountains than on the basin floors (Fig. 2-3). In the North Platte River drainage, the $\delta^{18}O$ values west of 105° W are 4-6‰ lower than those east of 105° W (Fig. 2-3), and the d-excess values are high in the upper stream reaches near the Wind River Range, and low in central and eastern Wyoming and western Nebraska. The d-excess values in the North Platte River drainage are generally lower than those in the Bighorn River drainage, but with larger variations. The lowest d-excess value is on the basin floor in central Wyoming (Fig. 2-3). The general spatial patterns of the river water stable isotope values in the three sampling seasons are similar (Fig. 2-3).

Linear regression of all the river water isotope values generates a local river water line: $\delta D = 6.4 * \delta^{18}O - 21.2$ ($R^2 = 0.94$, n = 242) (Fig. 2-4), and the water samples from elevations above 3.0 km generate a high-elevation river water line: $\delta D = 7.0 * \delta^{18}O - 9.9$ ($R^2 = 0.98$, n = 32). The river water lines have lower slope and d-excess values than the previously reported local meteoric water line of the north-central Great Plains ($\delta D = 7.7 * \delta^{18}O + 4.9$; Harvey and Welker, 2000), which includes the eastern part of our study area, and the local line to the northwest of our study area ($\delta D = 7.9 * \delta^{18}O + 8.1$; Benjamin et al., 2004).

We compare local river water lines and d-excess values at high- and low-elevation regions (Fig. 2-3; Table 2-1). Based on the variation of drainage mean elevation, we arbitrarily use 3.0 km of drainage mean elevation as the elevation cutoff of high- and low-elevation regions for the Bighorn River drainage, and 2.2 km of drainage mean elevation for the North Platte River drainage. In the Bighorn River drainage, the local water lines have lower slopes, but lower d-excess values in the low-elevation region than those in the high-elevation region (Fig. 2-3 and Table 2-1). Although the pattern exists in spring and summer, the slopes are higher in spring (-0.4‰/km) than in summer (-0.7‰/km). In the North Platte River drainage, the trend is different from that in the Bighorn River drainage. The local water lines have higher slopes, but smaller d-excess values in the low-elevation region than those in the high-elevation region (Fig. 2-3 and Table 2-1), and the pattern exists in both spring and summer. The slope of the river water line is lower in summers than in spring in the Bighorn River drainage, but the seasonal difference is not consistent in the North Plate River drainage (Table 2-1). The slope of water lines in mountains flanks of different orientation shows small variability (Table 2-1).

2.4.2 Spatial and temporal patterns of river water isotope lapse rates

The $\delta^{18}O$ lapse rate in the Bighorn River drainage varies from -1.4‰/km (R^2 = 0.39) in the summer of 2011 to -0.7 and -0.4‰/km in the summer and spring of 2016 (Fig.2-5A). The $\delta^{18}O$ lapse rate in the North Platte River drainage was relatively stable through the study period. The rate is -2.5‰/km (R^2 = 0.58) in the summer of 2011 and -2.1‰/km (R^2 = 0.23 and 0.17) in the spring and summer of 2016 (Fig. 2-5B). In all the drainages, isotope values of river water with drainage mean elevation higher than 2 km are not correlated (P value > 0.05, and lapse rate ~0‰/km) with drainage mean elevation (Fig. 2-5).

2.4.3 Geographic and climate parameters and their relationships with water isotope compositions

RH in the study area varies between 30% and 75%, and the majority of the study area has a RH lower than 50% (Fig. 2-2). Mountains generally have higher RH than the basin floors in the central Rockies and the adjacent western Great Plains (Fig.2). The surface air temperature is lower in the central Rockies than in the western Great Plains (Fig. 2-2).

In the Bighorn River drainage, the $\delta^{18}O$ values are inversely correlated with RH in the summer, and correlated with mean seasonal temperature in spring (Table 2-2). In the North Platte River drainage, the $\delta^{18}O$ values are correlated with RH and with mean seasonal temperature in the spring and sometimes in the summer (Table 2-2).

2.4.4 Vapor trajectory

The contribution of each moisture source varies temporally and spatially (Fig. 2-6). In the central Rockies, moistures from N, P, and C sources contribute to precipitation in the spring, and the contribution from N decreases significantly in the summer (Fig. 2-6). In the western Great Plains (Ogallala in Fig. 2-6), the N, P, C, and GM moisture sources all contribute precipitation in the summers, and the region receives less contribution from the GM moisture source, but more from the N moisture source in the spring.

2.5 Discussion

2.5.1 Relationship between precipitation and river water isotopic compositions

A previous study (Dutton et al., 2005) has shown that river waters have lower isotopic values than local precipitation in the western U.S.A. because these rivers integrate precipitation over the entire upper stream catchments. We compare published monthly river water $\delta^{18}O$ values (Kendall and Coplen, 2001) to monthly precipitation $\delta^{18}O$ values from nearby stations (Harvey and Welker, 2000; Vachon et al., 2010a) in Wyoming and western Nebraska to further define the relationship between local precipitation and river water (Fig. 2-7). River water $\delta^{18}O$ values are relatively stable (~4‰ variation) throughout the year whereas precipitation $\delta^{18}O$ values may vary by 19‰. Published rissssver water $\delta^{18}O$ values (Fig. 2-7) and our new data (Fig. 2-3) both show minor increases from spring to summer, reflecting higher precipitation $\delta^{18}O$ values in summer than in spring (Benjamin et al., 2004; Vachon et al., 2010a), or reduced snowmelt discharge in summer than in spring. The small seasonal fluctuation in river water $\delta^{18}O$ values suggests that the influence of local seasonal precipitation on river water isotope compositions is small, and that river waters in the study area are mostly derived from by high-elevation surface water. The river water $\delta^{18}O$ values are 0–4‰ lower than those of mean annual precipitation in the central Rockies, and the river water $\delta^{18}O$ values are ~2‰ higher or lower than those of the mean annual precipitation on the Great Plains (Fig. 2-7 A and B).

Published data (Kendall and Coplen, 2001) and our data all show that most of the rivers have d-excess values smaller than the d-excess (10‰) of the global meteoric water line (Fig. 2-7C and D). Previous observations have shown that moisture recycling from evaporation of water bodies such as lakes, and sub-cloud evaporation can influence the isotopic compositions of vapor and precipitation, and such influences are associated with kinetic fractionation (e.g., Bershaw et al., 2012, 2016; Li and Garzione, 2017). Precipitation derived from recycled moisture and reevaporated moisture typically has a d-excess greater than 10‰ (Gat and Airey, 2006). Although moisture recycling and sub-cloud evaporation typically occur in arid climates, the low d-excess of the river water in this study suggests that such processes do not influence the river water isotope composition.

In the central Rockies, the river water d-excess generally increases as drainage mean elevation increases (Fig. 2-7C), but as drainage area decreases (Fig. 2-7D). On the Great Plains, the d-excess values of small rivers have less variation than those of small rivers in the central Rockies, and the d-excess of the North Platte River is in the middle of the d-excess range for rivers in the central Rockies (Fig. 2-7C and D). Kinetic evaporation processes in moisture source regions and in sub-cloud layers increase precipitation d-excess, while post-precipitation surface evaporation decreases surface water d-excess (Gat and Airey, 2006). The low d-excess of river waters in the study area suggests that post-precipitation evaporation occurs in most rivers. In the central Rockies, the lower d-excess values in low-elevation regions compared to those in high-elevation regions suggest stronger evaporation on the Laramide basin floors than in the mountain ranges (Fig. 2-7C), consistent with the observation made from RH data (Fig. 2-2). The intermediate d-excess of small rivers on the Great Plains (Fig. 2-7D) suggests that evaporation is less strong on the Great Plains than in some regions in the central Rockies. The low d-excess of the North Platte River in Nebraska not only reflects the contribution of river water with low d-excess from the central Rockies, but also evaporation within its drainage.

The slopes of the local river water lines also support the interpreted evaporation pattern of river water in our study area (Fig. 2-4; Table 2-1). Our local river water lines have lower slopes than the local meteoric water line derived from precipitation, which could not be explained by sub-cloud evaporation. Sub-cloud evaporation, if it occurred, should influence both precipitation and river water isotope compositions and cause similar slopes. The lower slopes could not have been caused by mixing of snowmelt that had undergone sublimation (Lechler and Niemi, 2012). The addition of snowmelt should influence the river water line in high-elevation regions more and cause lower slopes than those in low-elevation regions, because waters in high-elevation regions have proportionally more snowmelt input. Instead, in the Bighorn River drainage, the water line of rivers with high mean elevations (> 3.0 km) has higher slopes than those with low elevations (< 3.0 km) (Table 2-1). Therefore, we attribute the low slopes in low elevation areas to surface evaporation. Given that evaporation should have a minimal influence on running water in river channels, we suggest that evaporation must occur to both local precipitation and groundwater in the vadose zone of local river catchments, particularly on the basin floors of the central Rockies. This interpretation is supported by previous studies which found that evaporation influences groundwater isotope compositions, particularly when soil has high porosity and low vegetation cover (e.g., Gat and Dansgaard, 1972; Allison et al., 1983). The influence of groundwater evaporation on river water suggests that in semiarid climates, river water isotope compositions may not be good approximations of local mean annual precipitation isotope compositions.

2.5.2 Isotope distribution and lapse rate in the Bighorn River drainage

In the Bighorn River drainage, RH governs the spatiotemporal variations of river water isotopic compositions based on our multivariate analysis (Table 2-2). On the basin floors where RH is generally lower than in the mountains, the river water line has a lower slope (Table 2-1) and lower d-excess value (Figs. 2-3 and 2-7) than those in the mountains, suggesting that stronger evaporation of river water occurs on the basin floors than in the mountains. The higher water line slopes in summer than in spring (Table 2-2) suggests stronger evaporation in the entire catchment during summer than during spring, consistent with the observation of RH (Fig. 2-2).

In the Bighorn River drainage and other drainages in the central Rockies, the river water lapse rate is very small or close to 0‰/km (Fig. 2-5), which we attribute to highland surface water being the major source of recharge of lowland rivers. It is tempting to think that the different mountain orientations in the central Rockies may block certain vapor masses, but cause rainout of others, thereby causing river water isotope lapse rates on one side of a mountain to be different from those on the other. However, such a hypothesis cannot be validated because the dominant contribution of highland surface water to rivers leads to a lack of isotopic lapse rates on all the Laramide range flanks (Fig. 2-5) and to a lack of major difference in local water line slopes (Table 2-1). While lowland rivers in this drainage are influenced by evaporation, evaporation is not the cause of the lack of lapse rate. Strong evaporation should increase river water lapse rate by increasing river water $\delta^{18}O$ values on the basin floors, which is contrary to our observation of lack of lapse rate.

2.5.3 Isotope distribution and lapse rate in the North Platte River drainage

In the North Platte River drainage, the controlling factors on the spatiotemporal variations of river water isotopic compositions are complex. The multivariate analysis shows that temperature and RH sometimes play key roles (Table 2-2). The eastward increase in river water $\delta^{18}O$ values is consistent with the general trend of eastward decrease in elevation and increase in temperature, suggesting that vapor condensation temperature, changing with elevation, is the primary factor. In addition to these factors, variation of moisture sources in different segments of the river should also affect this isotopic pattern. For instance, our back-trajectory analysis shows that in Ogallala, the GM moisture source contributed more precipitation to the Great Plains (Fig.2-6).

The influence of elevation on the distribution and lapse rate of the river water isotope compositions in the North Platte River drainage is not simply governed by progressive rainout and Rayleigh distillation. Although Rayleigh distillation of water vapor from the east along the central Rockies-Great Plains transect offers a possible explanation, our HYSPLT back trajectory model shows that almost none of the moisture that reached the central Rockies had traveled from the Great Plains (Fig.2-1B), and both the central Rockies and Great Plains have multiple moisture sources (Fig. 2-6). Therefore, the assumption of Rayleigh distillation during progressive rain out of a single vapor source is clearly not met in our study area.

The river water lapse rate east of 105°W is controlled by moisture mixing and by vapor condensation temperature-induced isotope fractionation. The lapse rate of the North Platte River drainage is steeper in 2011 than in 2016 (Fig. 2-5B). Moisture from the Gulf of Mexico has higher δ^{18}O values than moisture from other sources (Liu et al., 2010), resulting in relatively high precipitation δ^{18}O values on the Great Plains (Harvey and Welker, 2000). Although the degree of vapor mixing is variable in the three sampling seasons (Fig. 2-6), the river water lapse rate persisted, suggesting condensation temperature-induced isotope fractionation is the primary cause of the lapse rate. It is also possible that convective storms, which influence the Great Plains as far north as the northern Great Plains (Pu and Dickinson, 2014), contribute to the lapse rate by increasing precipitation δ^{18}O values on the Great Plains.

The average lapse rate of the North Platte River drainage (~-2.3‰/km) is lower than the average global precipitation lapse rate (-2.9‰/km; Poage and

Chamberlain, 2001), which we suggest has two major causes. First, as in the Bighorn River drainage, highland water contributes to lowland water in the North Platte River drainage and reduces the lowland river $\delta^{18}O$ value (Figs. 2-3 and 2-5). Second, central Wyoming is subject to more evaporation than the Great Plains (Figs. 2-2 and 2-3). Evaporation increases river water $\delta^{18}O$ values and lowers the slope of the river water line in this highland region during the summers (Table 2-1).

2.5.4 Controlling factors of isotope distribution

Our results show that in the mountainous central Rockies, highland water dominates lowland water discharge, and that the downstream contribution of highland water yields a negligible isotope lapse rate. In the regional transect from the central Rockies to the Great Plains, the influence of highland discharge persists, but becomes progressively smaller and the influence of local precipitation becomes progressively larger to the east of 105°W. The moisture sources in the central Rockies and its adjacent Great Plains are complex mixtures of multiple vapor masses, and the assumption of Rayleigh distillation of a homogeneous vapor mass is not met. However, the temperature difference, in association with the elevation difference from west to east, appears to control the precipitation $\delta^{18}O$ value, and thus influences the regional pattern of river water $\delta^{18}O$ values. Therefore, highland discharge and condensation temperature are primary controlling factors of the regional river water isotope distribution.

Our results also show that evaporation, associated with low RH and low precipitation, on the basin floors in the Bighorn River drainage and in central Wyoming, influences local river water $\delta^{18}O$ values. Direct addition of moisture derived from the Gulf of Mexico to the Great Plains increases local precipitation $\delta^{18}O$ values, and increases the isotope lapse rate of the North Platte River, particularly during summers. Although recycled continental moisture contributes up to 48% of precipitation in the study area (Fig. 2-6), it does not contribute to this regional isotope pattern because its contribution in the central Rockies is not significantly different from that in the Great Plains (Fig. 2-7). Our finding regarding the amount of recycled moisture in precipitation is consistent with observations from other continental interiors. For example, recycled moisture contributes up to ~70% of precipitation in the Western Cordillera in South America (Van Der Ent et al., 2010), and ~63% on the Tibetan Plateau (Curio et al., 2015). However, unlike the Tibetan Plateau and the Western Cordillera, where recycled moisture contributes more to downwind precipitation and increases precipitation $\delta^{18}O$ values, the influence of recycled moisture on the spatiotemporal isotope patterns is overprinted by mixing of multiple moisture sources in the central Rockies and the adjacent Great Plains. Therefore, evaporation, vapor mixing, and moisture recycling are secondary controlling factors of river water isotope distribution.

2.5.5 Implications for paleoaltimetry study

In the central Rockies, the timing and magnitude of surface uplift of the Laramide mountains are critical to the understanding of geodynamic drivers of the Laramide orogeny. The regional elevation of the central Rockies with respect to the adjacent Great Plains is critical to the understanding post-Laramide modification of the regional topography. Our interpretation of the modern river water isotope values in the Bighorn River and the North Platte River drainages sheds light on reconstructions of paleoelevation of Laramide mountain ranges with respect to the basin floors, and paleoelevation of the central Rockies relative to the adjacent Great Plains. Although the sampling period is too short compared to the geologic past, our observations of modern water isotope variability imply that the temporal variations in distribution and lapse rate of river water isotope compositions in the continental interior are sensitive to climate changes in the geologic past. Our results highlight that paleoclimate must be assessed before the application of stable isotope-based paleoaltimetry in continental interior settings.

Our study shows that in the Laramide intermontane basins, lowland rivers clearly record the isotopic signature of highland precipitation. Therefore, the existence of relief between the Laramide basin floor and mountain ranges can be inferred from the isotopic difference between lowland river water or shallow-ground water and unevaporated basinal precipitation (Fig. 2-8A). The isotope compositions of river and shallow-ground water can be reconstructed from aquatic fossil mollusks, and shallow-groundwater carbonate cement because these carbonates are formed in equilibrium with river and shallow-ground water (e.g., Fan et al., 2011). The isotope compositions of basinal precipitation can be reconstructed from paleosol carbonate because pedogenic carbonates form under equilibrium with soil water (with possible seasonal bias), and soil water is from basinal precipitation (e.g., Fan et al., 2011 and references therein). In modern semiarid climates, despite the influence of evaporation and highland discharge to lowland rivers, by using the isotopic difference of basinal precipitation and river water and the global precipitation lapse rate of -2.9‰/km, relief of the Bighorn Basin drainage was calculated and the reconstructed relief matches modern relief well (Fig. 2-8B). In wet climates during some periods in the geologic past, the basinal precipitation and lowland river water should have experienced minimal evaporation and their $\delta^{18}O$ values can be directly used for paleorelief reconstruction. Paleoclimate in the early Paleogene was generally wet in the Laramide basins based on paleoclimate modeling (Snell et al., 2012) and paleosol geochemistry (e.g., Kraus and Riggins, 2007). The precipitation isotope lapse rate has also been modeled for the early Paleogene using an isotope-enabled global circulation model (Feng et al., 2013). Therefore, paleoelevation of the Laramide mountains with respect to the basin floors can be inferred from highland and basinal precipitation isotope values reconstructed from the associated carbonate. Using published isotope data for the lowland river and basinal precipitation associated carbonate in the Bighorn Basin, we estimate the early Eocene paleorelief of the Bighorn Basin to be ~2km using a modern isotope lapse rate of -2.9‰/km (Fig. 2-8B), and to be at least 2km using the early Paleogene isotope lapse rate based on global circulation modeling (Feng et al., 2013). The paleorelief estimate is likely a minimum because the addition of basinal precipitation into river water on basin floors reduces the isotopic difference between the two types of water.

The Oligocene and Miocene relief between the central Rockies and the adjacent Great Plains was constrained previously by the difference of surface water isotope values, and the surface water isotope values were reconstructed from the stable isotope compositions of authigenic minerals and volcanic glass along a regional transect (Sjostrom et al., 2006; Fan et al., 2014a, 2014b). In the North Platte River drainage, an isotope lapse rate is present to the east of 105°W, which is primarily caused by a condensation-temperature decrease associated with the decrease in surface elevation. Before applying this mean modern regional lapse rate (-2.3‰/km) to paleo-river water $\delta^{18}O$ values to constrain the elevation contrast between the Great Plains and the Rockies, atmospheric circulation patterns and paleoclimate must be assessed based on proxy data and model simulations. During the Oligocene and Miocene, the paleoclimate in the region was wetter and warmer than today (Fan et al., 2014a, 2014b). A stronger North American monsoon may have existed under these warmer climate conditions which would have brought more GM moisture to the Great Plains and therefore increase the isotope lapse rate.

Alternatively, warm paleoclimate conditions may reduce isotope lapse rate by reducing the temperature gradient across the troposphere and by increasing highland precipitation $\delta^{18}O$ values (Poulsen and Jeffery, 2011), thereby overwhelming the effect of mixing more GM moisture. Despite the influence of evaporation and highland discharge to lowland rivers, modern relief of the central Rockies can be reconstructed using the isotopic difference across the drainage of the North Platte River using the modern mean regional lapse rate (Fig. 2-8D). By applying the mean lapse rate and reconstructed Oligocene-Miocene shallow groundwater $\delta^{18}O$ values (Fig. 2-8C) (Fan et al., 2014b), we estimated the paleorelief of the central Rockies with respect to the Great Plains to be 1-2.5 km (Fig. 2-8D), which is comparable to or larger than modern relief.

2.6 Conclusions

We investigate the controlling factors of river water isotope compositions in the central Rockies and the adjacent Great Plains by integrating analyses of spatiotemporal patterns of river water isotope values, back trajectory analysis of precipitation, and statistical analysis of the relationships between river water isotope values and climate and geographic factors. Our vapor trajectory analysis shows that vapor masses from tropical and high-latitude Pacific, Gulf of Mexico, northern region in the Canadian Rockies and Hudson Bay, and continental recycled moisture all contribute to precipitation in the study area, and the Great Plains receives more moisture from the Gulf of Mexico than the central Rockies.

Therefore, Rayleigh distillation of a single vapor source is not a valid assumption for surface water isotope fractionation in the region.

Our isotope results show that in the Bighorn River drainage, a typical intermontane drainage in the central Rockies, the isotope difference between highland and lowland rivers is small, which we attribute to low $\delta^{18}O$ highland precipitation that governs the isotopic composition of lowland river discharge. In the North Platte River drainage across the central Rockies and Great Plains, river water $\delta^{18}O$ values show eastward increase east of 105°W, with an average isotope lapse rate of -2.3‰/km. This eastward increase in $\delta^{18}O$ values follows the decrease in elevation and is mainly caused by condensation temperature-induced isotope fractionation in precipitation, and secondarily by more moisture from the Gulf of Mexico on the Great Plains than in the central Rockies and strong evaporation in the headwaters of the North Platte River. Our statistical analysis and low d-excess suggest that rivers in the study area are generally influenced by evaporation, and strong evaporation occurs on the basin floors of the Bighorn River drainage, where relative humidity is very low, and river catchments are large. We suggest that evaporation occurs in groundwater and local precipitation in the vadose zone of river catchments. Because of the influence of highland discharge and evaporation, small catchment area rivers in both the central Rockies and the adjacent Great Plains are not good representatives of local mean annual precipitation.

Our understanding of the controlling factors on river water isotope compositions has implications for paleorelief reconstruction. We suggest paleoclimate and atmospheric circulation pattern must be evaluated in order to constrain the influence of evaporation and vapor mixing on water isotope proxies. Existence of paleorelief between the Laramide mountain ranges and basin floors can be inferred from the differences of reconstructed river water and basinal precipitation isotope values in the Laramide intermontane basins. By using the modern lapse rate a paleorelief of the central Rockies relative to the Great Plains can be derived for the Oligocene and Neogene.

Acknowledgements

This research was supported by National Science Foundation grants (EAR-1119005 and -1457802) and a Geological Society of America graduate student grant. We would like to thank Dr. Min Gao, Jackie Lynn Garcia and Emma Gains for their help collecting river water samples in the field; Dr. Hyeong-Moo Shin for help with multivariate regression analysis; and Dr. Chao Ma for help with R programing. We would also like to thank Dr. Carmala Garzione and two anonymous reviewers for constructive comments that helped to improve this work.

References

Adams, D.K., Comrie, A.C., Adams, D.K., Comrie, A.C., 1997. The North American Monsoon. Bulletin of the American Meteorological Society 78, 2197–2213. doi:10.1175/1520-0477(1997)078<2197:TNAM>2.0.CO;2

Allison, G.B., Barnes, C.J., Hughes, M.W., Leaney, F.W.J., 1983. Effect of climate and vegetation on oxygen-18 and deuterium profiles in soils, in: Isotopes Hydrology: Proceedings of the International Symposium on Isotope Hydrology for Water Resources Development. Int. At. Energy Agency, Vienna, Austria, pp. 105–123.

Arguez, A., Durre, I., Applequist, S., Squires, M., Vose, R., Yin, X., Bilotta, R., 2010. NOAA's U.S. Climate Normals (1981-2010). NOAA National Centers for Environmental Information. doi:10.7289/V5PN93JP

Benjamin, L., Knobel, L.L., Hall, L.F., Cecil, L.D., Green, J.R., 2004. Development of a Local Meteoric Water Line for Southeastern Idaho, Western Wyoming, and South-Central Montana, U.S. Geological Survey Scientific Inversitygations Report 2004-5126.

Bershaw, J., Penny, S.M., Garzione, C.N., 2012. Stable isotopes of modern water across the Himalaya and eastern Tibetan Plateau: Implications for estimates of paleoelevation and paleoclimate. Journal of Geophysical Research: Atmospheres 117, 1–18. doi:10.1029/2011JD016132

Bershaw, J., Saylor, J.E., Garzione, C.N., Leier, A., Sundell, K.E., 2016. Stable isotope variations (d18O and dD) in modern waters across the Andean Plateau. Geochimica et Cosmochimica Acta 194, 310–324. doi:10.1016/j.gca.2016.08.011

Cather, S.M., Chapin, C.E., Kelley, S.A., 2012. Diachronous episodes of Cenozoic erosion in southwestern North America and their relationship to surface uplift, paleoclimate, paleodrainage, and paleoaltimetry. Geosphere 8, 1177–1206. doi:10.1130/GES00801.1

Chamberlain, C.P., Mix, H.T., Mulch, A., Hren, M.T., Kent-Corson, M.L., Davis, S.J., Horton, T.W., Graham, S.A., 2012. The Cenozoic climatic and topographic evolution of the western north American Cordillera. American Journal of Science 312, 213–262. doi:10.2475/02.2012.05

Copeland, P., Kendall, C., 2000. Stable hydrogen and oxygen isotope ratios for selected sites of the U.S. Geological Survey's NASQAN and Benchmark surface-water networks. US Geological Survey Open-File Report 00-160.

Curio, J., Maussion, F., Scherer, D., 2015. A 12-year high-resolution climatology of atmospheric water transport over the Tibetan Plateau. Earth System Dynamics 6, 109–124. doi:10.5194/esd-6-109-2015

Dansgaard, W., 1964. Stable isotopes in precipitation. Tellus 16, 436–468. doi:10.3402/tellusa.v16i4.8993

Draxler, R.R., Rolph, G.D., 2014. HYSPLIT (HYbrid Single-Particle Lagrangian Integrated Trajectory) Model access via NOAA ARL READY Website (http://www.arl.noaa.gov/HYSPLIT.php). NOAA Air Resources Laboratory, College Park, MD. NOAA Air Resources Laboratory.

Dutton, A., Wilkinson, B.H., Welker, J.M., Bowen, G.J., Lohmann, K.C., 2005. Spatial distribution and seasonal variation in 18O/16O of modern precipitation and river water across the conterminous USA. Hydrological Processes 19, 4121–4146. doi:10.1002/hyp.5876

Fan, M., Carrapa, B., 2014. Late Cretaceous-early Eocene Laramide uplift, exhumation, and basin subsidence in Wyoming: Crustal responses to flat slab subduction. Tectonics 33, 509–529. doi:10.1002/2012TC003221

Fan, M., DeCelles, P.G., Gehrels, G.E., Dettman, D.L., Quade, J., Peyton, S.L., 2011. Sedimentology, detrital zircon geochronology, and stable isotope geochemistry of the lower Eocene strata in the Wind River Basin, central Wyoming. Geological Society of America Bulletin 123, 979–996. doi:10.1130/B30235.1

Fan, M., Dettman, D.L., 2009. Late Paleocene high Laramide ranges in northeast Wyoming: Oxygen isotope study of ancient river water. Earth and Planetary Science Letters 286, 110–121. doi:10.1016/j.epsl.2009.06.024

Fan, M., Heller, P., Allen, S.D., Hough, B.G., 2014a. Middle Cenozoic uplift and concomitant drying in the central Rocky Mountains and adjacent Great Plains. Geology 42, 547–550. doi:10.1130/G35444.1

Fan, M., Hough, B.G., Passey, B.H., 2014b. Middle to late Cenozoic cooling and high topography in the central Rocky Mountains: Constraints from clumped isotope geochemistry. Earth and Planetary Science Letters 408, 35–47. doi:10.1016/j.epsl.2014.09.050

Feng, R., Poulsen, C.J., Werner, M., Chamberlain, C.P., Mix, H.T., Mulch, A.,

2013. Early cenozoic evolution of topography, climate, and stable isotopes in precipitation in the north American cordillera. American Journal of Science 313, 613–648. doi:10.2475/07.2013.01

Fricke, H.C., 2003. Investigation of early Eocene water-vapor transport and paleoelevation using oxygen isotope data from geographically widespread mammal remains. GSA Bulletin 115, 1088–1096.

Froehlich, K., Kralik, M., Papesch, W., Rank, D., Scheifinger, H., Stichler, W., 2008. Deuterium excess in precipitation of Alpine regions - moisture recycling. Isotopes in environmental and health studies 44, 61–70. doi:10.1080/10256010801887208

Garzione, C.N., Quade, J., DeCelles, P.G., English, N.B., 2000. Predicting paleoelevation of Tibet and the Himalaya from d18 O vs. altitude gradients in meteoric water across the Nepal Himalaya. Earth and Planetary Science Letters 183, 215–229.

Gat, J.R., Airey, P.L., 2006. Stable water isotopes in the atmosphere/biosphere/lithosphere interface: Scaling-up from the local to continental scale, under humid and dry conditions. Global and Planetary Change 51, 25–33. doi:10.1016/j.gloplacha.2005.12.004

Gat, J.R., Dansgaard, W., 1972. Stable isotope survey of the fresh water occurrences in Israel and the Northern Jordan Rift Valley. Journal of Hydrology 16, 177–211. doi:10.1016/0022-1694(72)90052-2

Harvey, F.E., Welker, J.M., 2000. Stable isotopic composition of precipitation in the semi-arid north-central portion of the US Great Plains. Journal of Hydrology 238, 90–109. doi:10.1016/S0022-1694(00)00316-4

Hoke, G.D., Garzione, C.N., Araneo, D.C., Latorre, C., Strecker, M.R., Williams, K.J., 2009. The stable isotope altimeter: Do Quaternary pedogenic carbonates predict modern elevations? Geology 37, 1015–1018. doi:10.1130/G30308A.1

Hough, B.G., Fan, M., Passey, B.H., 2014. Calibration of the clumped isotope geothermometer in soil carbonate in Wyoming and Nebraska, USA: Implications for paleoelevation and paleoclimate reconstruction. Earth and Planetary Science Letters 391, 110–120. doi:10.1016/j.epsl.2014.01.008

Hren, M.T., Pagani, M., Erwin, D.M., Brandon, M., 2010. Biomarker reconstruction of the early Eocene paleotopography and paleoclimate of the northern Sierra Nevada. Geology 38, 7–10. doi:10.1130/G30215.1

Kendall, C., Coplen, T.B., 2001. Distribution of oxygen-18 and deuterium in river waters across the United States. Hydrological Processes 15, 1363–1393. doi:10.1002/hyp.217

Kraus, M.J., Riggins, S., 2007. Transient drying during the Paleocene-Eocene Thermal Maximum (PETM): Analysis of paleosols in the bighorn basin, Wyoming. Palaeogeography, Palaeoclimatology, Palaeoecology 245, 444–461. doi:10.1016/j.palaeo.2006.09.011

Lechler, A.R., Niemi, N. a., 2012. The influence of snow sublimation on the isotopic composition of spring and surface waters in the southwestern United States: Implications for stable isotope-based paleoaltimetry and hydrologic studies. Bulletin of the Geological Society of America 124, 318–334. doi:10.1130/B30467.1

Li, L., Garzione, C.N., 2017. Spatial distribution and controlling factors of stable isotopes in meteoric waters on the Tibetan Plateau: Implications for paleoelevation reconstruction. Earth and Planetary Science Letters 460, 302–314. doi:10.1016/j.epsl.2016.11.046

Licht, A., Quade, J., Kowler, A., De Los Santos, M., Hudson, A., Schauer, A., Huntington, K., Copeland, P., Lawton, T., 2017. Impact of the north American monsoon on isotope paleoaltimeters: Implications for the paleoaltimetry of the American southwest. American Journal of Science 317, 1–33. doi:10.2475/01.2017.01

Liu, Z., Bowen, G.J., Welker, J.M., 2010. Atmospheric circulation is reflected in precipitation isotope gradients over the conterminous United States. Journal of Geophysical Research Atmospheres 115, 1–14. doi:10.1029/2010JD014175

Liu, Z., Kennedy, C.D., Bowen, G.J., 2011. Pacific/North American teleconnection controls on precipitation isotope ratios across the contiguous United States. Earth and Planetary Science Letters 310, 319–326. doi:10.1016/j.epsl.2011.08.037

Mulch, A., Chamberlain, C.P., 2007. Stable Isotope Paleoaltimetry in Orogenic Belts The Silicate Record in Surface and Crustal Geological Archives. Reviews in Mineralogy and Geochemistry 66, 89–118. doi:10.2138/rmg.2007.66.4

NARR, n.d. NARR data provided by the NOAA/OAR/ESRL PSD, Boulder, Colorado, USA, from their Web site at http://www.esrl.noaa.gov/psd/ [WWW Document].

Poage, M.A., Chamberlain, C.P., 2001. Empirical relationships between elevation and the stable isotope composition of precipitation and surface waters: considerations for studies of paleoelevation change. American Journal of Science 301, 1–15.

Poulsen, C.J., Jeffery, M.L., 2011. Climate change imprinting on stable isotopic compositions of high-elevation meteoric water cloaks past surface elevations of major orogens. Geology 39, 595–598. doi:10.1130/G32052.1

Pu, B., Dickinson, R.E., 2014. Diurnal spatial variability of Great Plains summer precipitation related to the dynamics of the low-level jet. Journal of the Atmospheric Sciences 71, 1807–1817. doi:10.1175/JAS-D-13-0243.1

Rohrmann, A., Strecker, M.R., Bookhagen, B., Mulch, A., Sachse, D., Pingel, H., Alonso, R.N., Schildgen, T.F., Montero, C., 2014. Can stable isotopes ride out the storms? The role of convection for water isotopes in models, records, and paleoaltimetry studies in the central Andes. Earth and Planetary Science

Letters 407, 187–195. doi:10.1016/j.epsl.2014.09.021

Rowley, D.B., Garzione, C.N., 2007. Stable Isotope-Based Paleoaltimetry. Annual Review of Earth and Planetary Sciences 35, 463–508. doi:10.1146/annurev.earth.35.031306.140155

Rowley, D.B., Pierrehumbert, R.T., Currie, B.S., 2001. A new approach to stable isotope-based paleoaltimetry: Implications for paleoaltimetry and paleohypsometry of the High Himalaya since the late Miocene. Earth and Planetary Science Letters 188, 253–268. doi:10.1016/S0012-821X(01)00324-7

Sjostrom, D.J., Hren, M.T., Horton, T.W., Waldbauer, J.R., Chamberlain, C.P., 2006. Stable isotopic evidence for a pre–late Miocene elevation gradient in the Great Plains–Rocky Mountain region, USA. Geological Society of America Special Papers 398, 309–319. doi:10.1130/2006.2398(19).

Ting, M.F., Wang, H.L., 2006. The role of the north American topography on the maintenance of the great plains summer low-level jet. Journal of the Atmospheric Sciences 63, 1056–1068. doi:10.1175/JAS3664.1

Vachon, R.W., Welker, J.M., White, J.W.C., Vaughn, B.H., 2010a. Monthly precipitation isoscapes (d18O) of the United States: Connections with surface temperatures, moisture source conditions, and air mass trajectories. Journal of Geophysical Research Atmospheres 115, 1–17. doi:10.1029/2010JD014105

Vachon, R.W., Welker, J.M., White, J.W.C., Vaughn, B.H., 2010b. Moisture source temperatures and precipitation δ18O- temperature relationships across the United States. Water Resources Research 46, 1–14. doi:10.1029/2009WR008558

Van Der Ent, R.J., Savenije, H.H.G., Schaefli, B., Steele-Dunne, S.C., 2010. Origin and fate of atmospheric moisture over continents. Water Resources Research 46, 1–12. doi:10.1029/2010WR009127

Wolfe, J.A., Forest, C.E., Molnar, P., 1998. Paleobotanical evidence of Eocene and Oligocene paleoaltitudes in midlatitude western North America. Bulletin of the Geological Society of America 110, 664–678. doi:10.1130/0016-7606(1998)110<0664:PEOEAO>2.3.CO;2.

Figures and tables

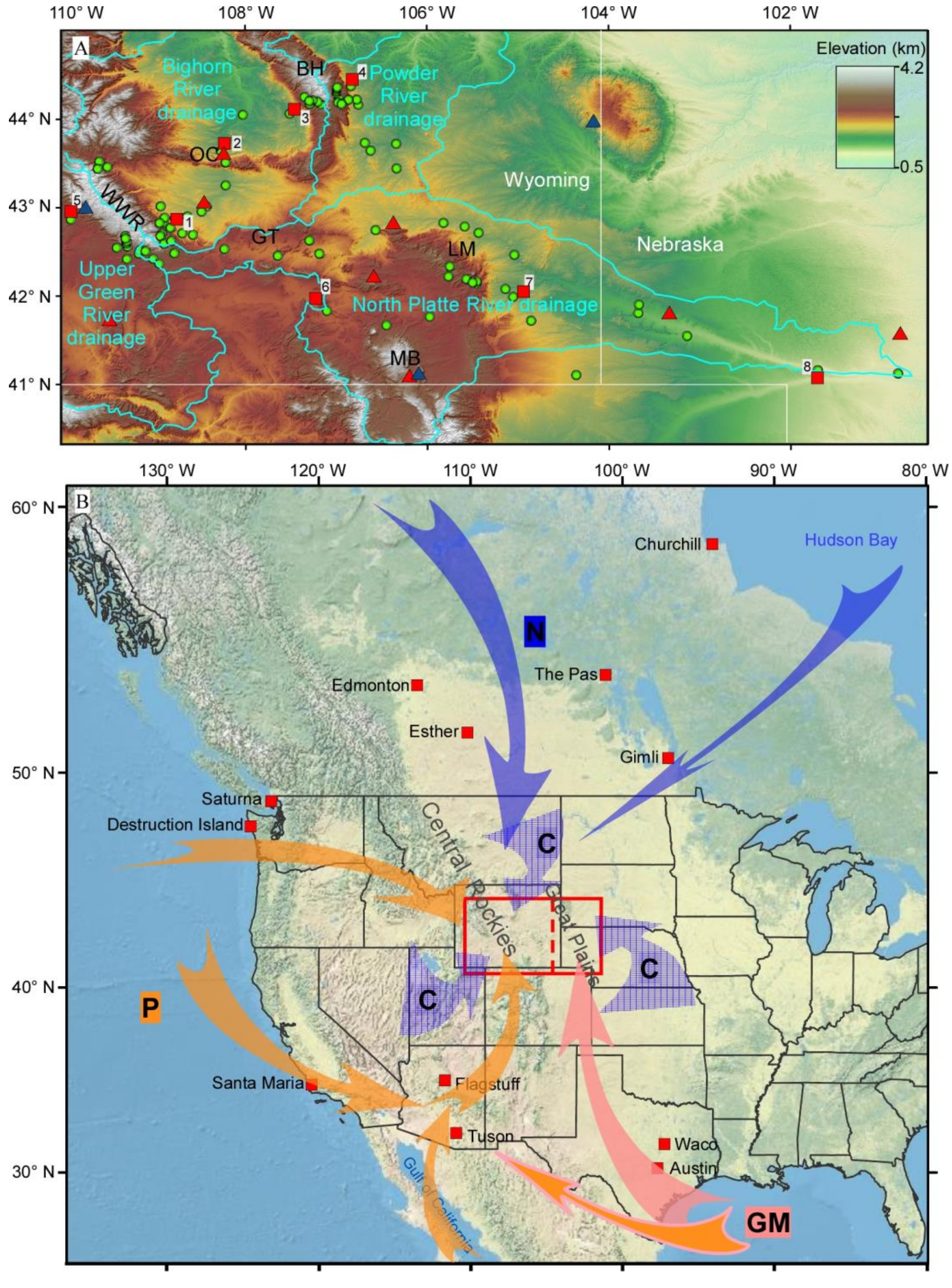

Figure 2-1 (A) Digital elevation map of the study area in the central Rockies and its adjacent Great Plains. Green dots are sampling sites in this study. Red triangles are river water sample sites in Kendall and Copeland (2001), and blue triangles are precipitation sample sites in Harvey and Welker (2000) and Vachon et al. (2010a). These published data are used for Figure 8. Red squares are representative localities of vapor trajectory analysis using the HYSPLIT model. 1= Lander. 2= Thermopolis. 3=Ten Sleep. 4=Buffalo. 5=Pinedale. 6=Rawlins. 7=Wheatland. 8=Ogallala. Blue lines outline the Bighorn River, North Platte River, Powder River, and upper Green River drainages. BH=Bighorn Mountain. OC=Owl Creek Mountain. WWR=Wind River Range. GT=Granite Mountains. LM=Laramie Mountain. MB=Medicine Bowl Mountain. (B) Map of moisture sources and their general transport paths. Red box represents the study area in A. Red squares represent the stations whose precipitation isotope data were used for the Monte Carlo simulation of moisture mixing in this study. N (purple arrows)=northern moisture derived from east of the Canadian Rocky Mountains and the Hudson Bay. GM (pink arrow)= moisture derived to the Gulf of Mexico transports along the front of the Rockies. P+GM (orange arrows)=moistures from the North Pacific, tropical Pacific, and the Gulf of Mexico. Note that the three moistures meet near Arizona and transport to the central Rockies as a group of moisture and the North Pacific moisture also transports eastward directly to the study area. C (shaded purple arrows) = recycled continental moisture.

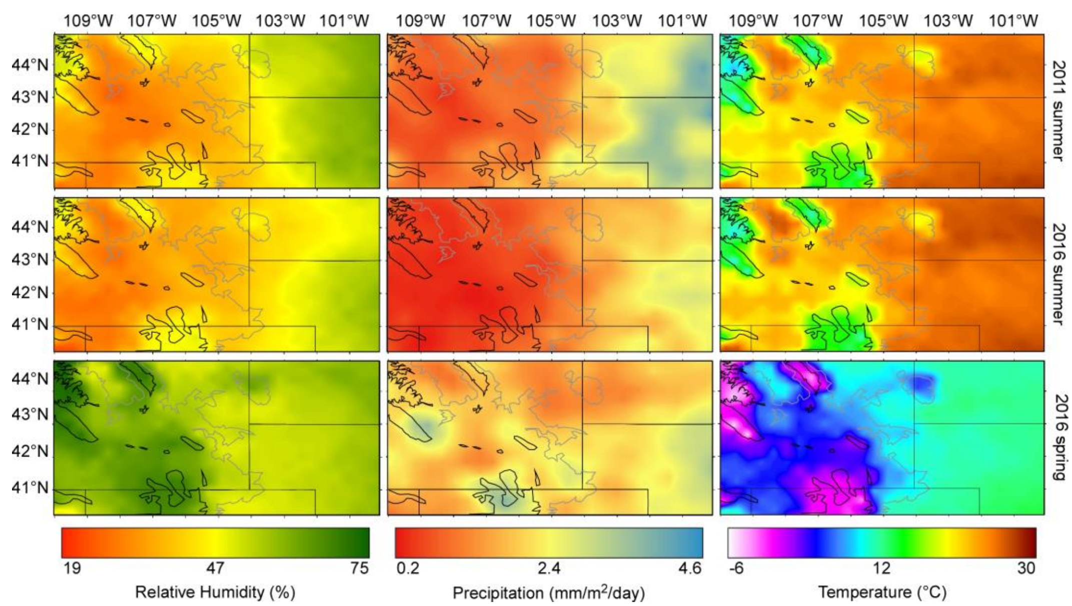

Figure 2-2 Maps of relative humidity, precipitation, and temperature in the study area during the sampling seasons. Raw data is from North American Regional

Reanalysis dataset (NARR dataset). Irregular black lines are contour lines of 2.5 km, and grey lines are contour lines of 1.5 km.

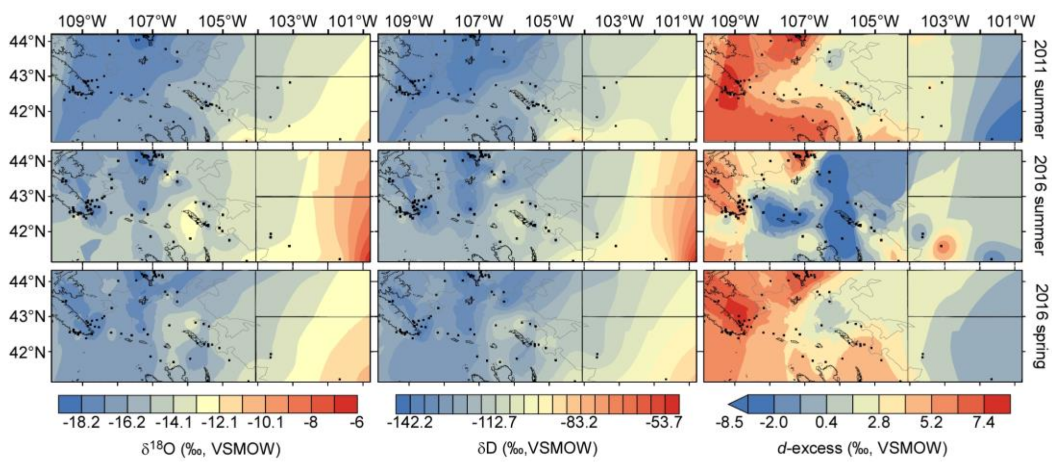

Figure 2-3 Maps of river water $\delta^{18}O$, δD, and *d*-excess distributions in different years in the study area. Black rectangles are sample locations. Irregular black lines are contour lines of 2.5 km, and grey lines are contour lines of 1.5 km.

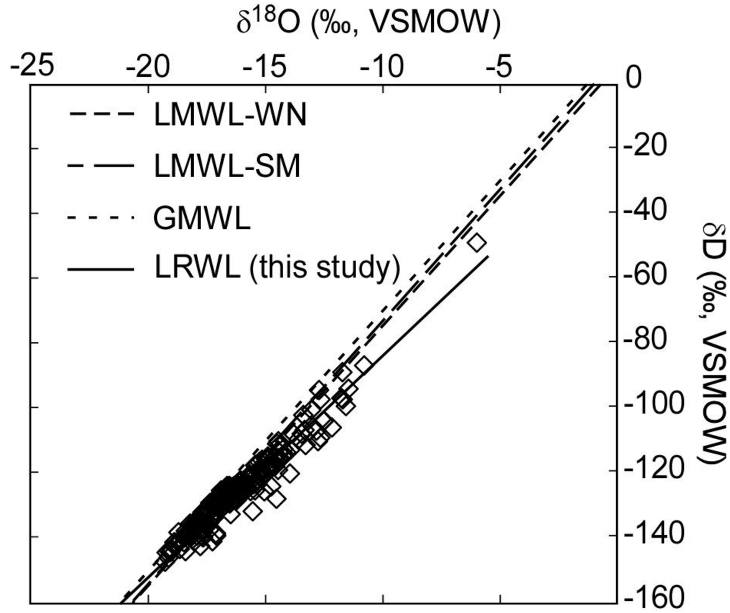

Figure 2-4 Local river water line from this study is compared with other published local meteoric water lines in adjacent regions. LRWL is the local river water line derived from the linear regression of 242 $\delta^{18}O$ and δD data (black diamonds) in this study. LMWL-WN is the local meteoric water line in western Nebraska (Harvey and Welker, 2000). LMWL-SM is the local meteoric water line in southern Montana, western Wyoming, and eastern Idaho (Benjamin et al., 2004). GMWL is the global meteoric water line.

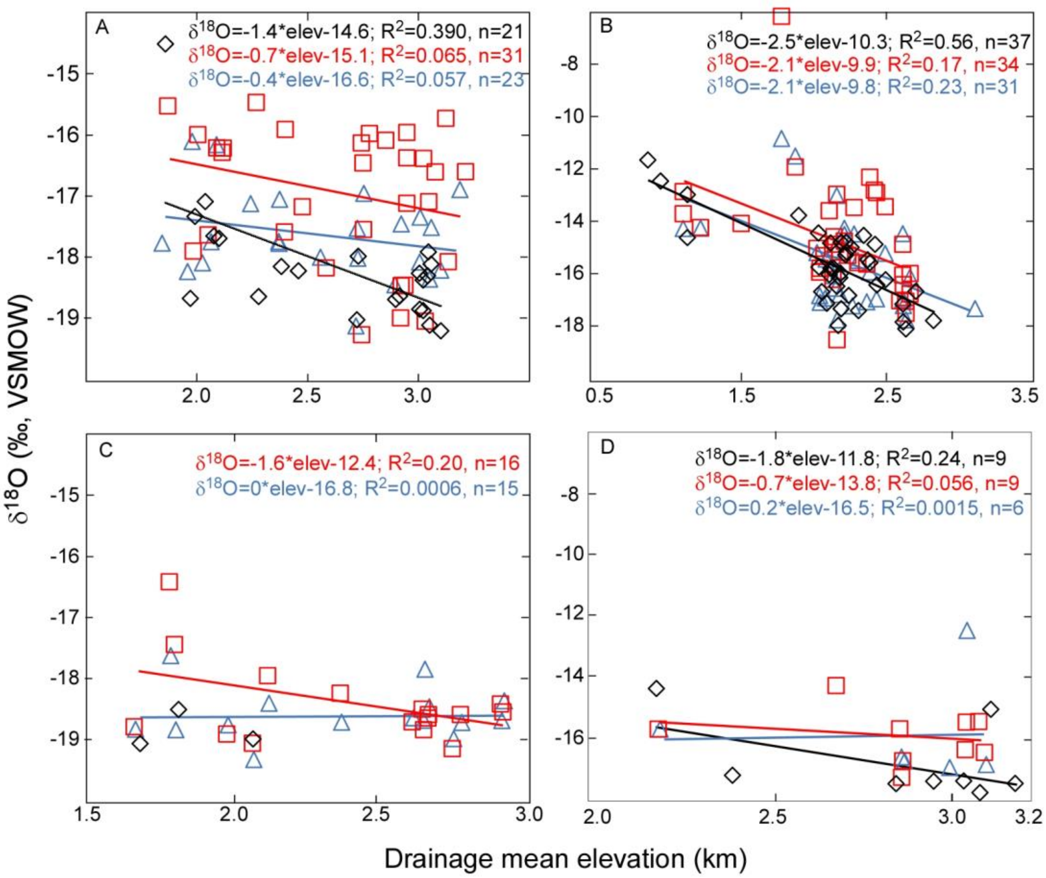

Figure 2-5 . The $\delta^{18}O$ values of river water in the (A) Bighorn River drainage, (B) North Platte River drainage, (C) Powder River drainage, and (D) upper Green River drainage plot against drainage mean elevation. The slopes of the linear regression lines are isotope lapse rates. Black diamond = summer of 2011. Red square = summer of 2016. Blue triangle = spring of 2016.

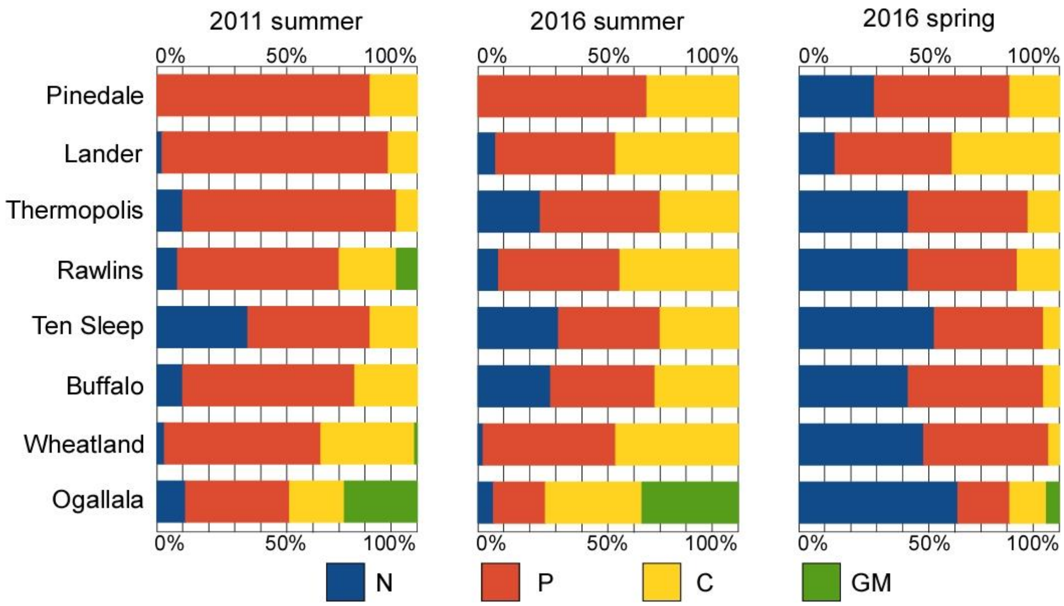

Figure 2-6 Moisture fraction of each source for representative localities. See Figure 2-1A for the geographic locations of each locality. Moisture fraction was determined by the sum of its contribution to each precipitation episode based on our vapor trajectories analysis. See Methods section for details.

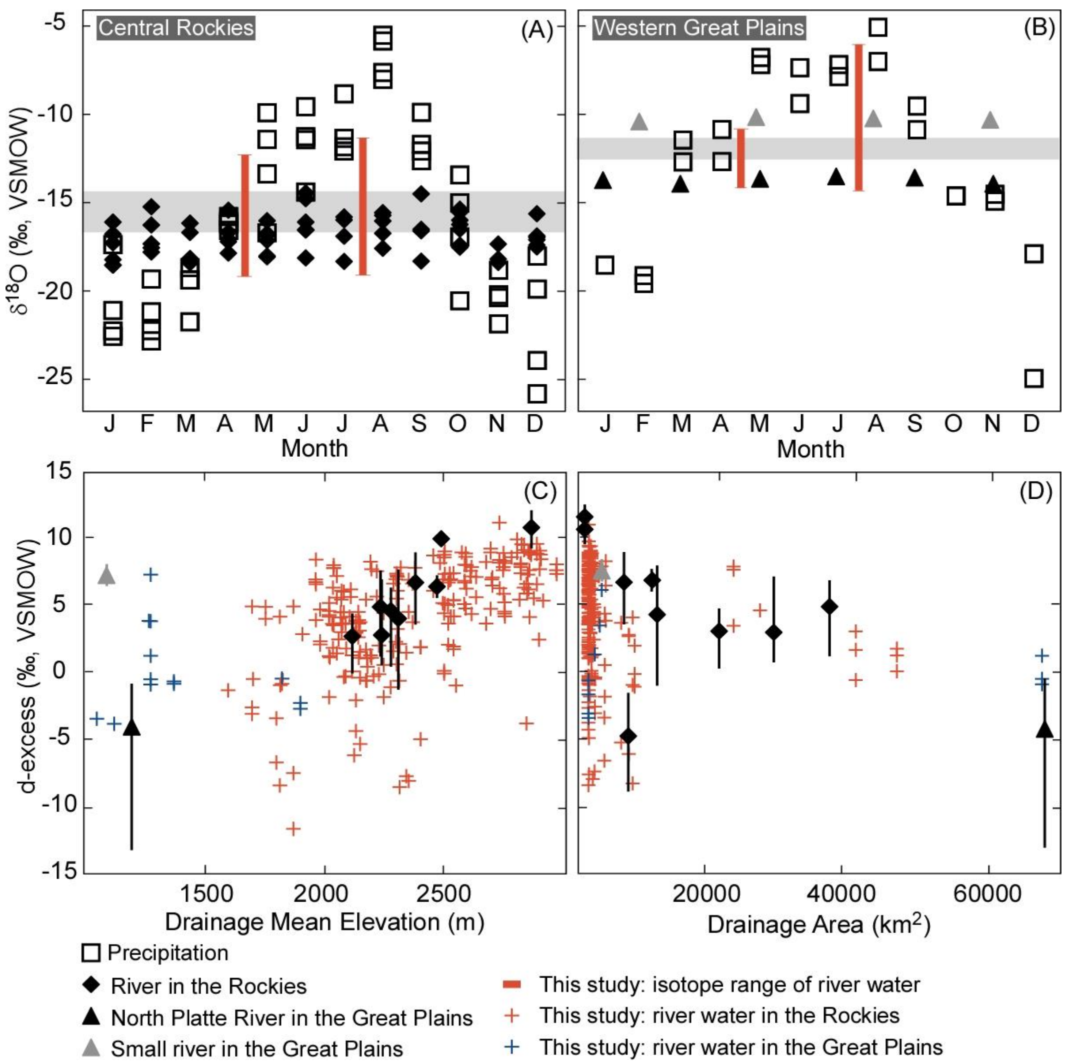

Figure 2-7 (A) and (B) Distribution of monthly average of precipitation and river water isotope compositions. All data are from Kendall and Copeland (2001), Harvey and Welker (2000), and Vachon et al. (2010a) Shaded grey areas represent the ranges of mean annual precipitation calculated from the monthly data. (C) Relationship between river water d-excess and drainage mean elevation. (D) Relationship between river water d-excess and drainage area. Published data are from Kendall and Copeland, 2001. Solid vertical lines in (C) and (D) represent the range of monthly d-excess.

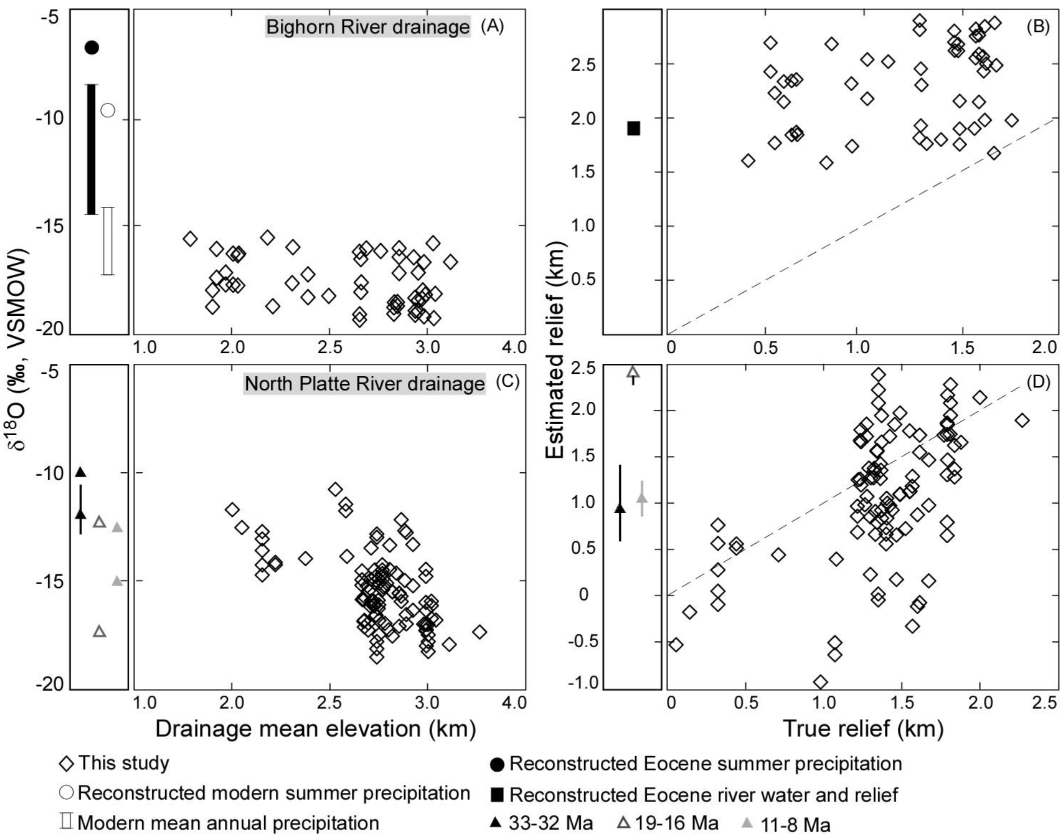

Figure 2-8 (A) Relationship between modern and reconstructed early Eocene precipitation and river water $\delta^{18}O$ values in the Bighorn River drainage. (B) Reconstructed early Eocene paleorelief and relationship between reconstructed modern relief and true relief in the Bighorn River drainage. (C) Relationship between modern and reconstructed Oligocene-Miocene precipitation and river water $\delta^{18}O$ values in the North Platte River drainage. (D) Reconstructed Oligocene-Miocene paleorelief and relationship between estimated modern relief and true relief in the North Platte River drainage. Modern precipitation data are calculated from modern soil carbonate (Fan et al., 2011; Hough et al., 2014) using local carbonate clumped isotope temperature (Hough et al., 2014). Modern river water data are from this study. Early Eocene precipitation data are reconstructed from paleosol carbonate in the Wind River Basin (Fan et al., 2011) and Bighorn Basin (Snell et al., 2012) using early Eocene carbonate clumped isotope temperature (Snell et al., 2012). The reconstructed precipitation $\delta^{18}O$ value is biased to summer precipitation $\delta^{18}O$ values, and 6‰ was subtracted to correct for the observed difference between summer and mean annual precipitation $\delta^{18}O$ values (Hough et al., 2014). Oligocene and Miocene data are constructed from carbonate cement $\delta^{18}O$ in Fan et al. (2014b) using clumped isotope temperature in the same study.

Paleorelief and modern relief are estimated using an average precipitation isotope lapse rate of -2.9 ‰/km for the U.S.A. (Dutton et al., 2005) in the Bighorn River drainage, and an average of local isotope rate of -2.3 ‰/km in the North Platter River in this study. Dashed lines in B and D show the 1:1 trends of the estimated and true relief.

Table 2-1 Local river water lines and average d-excess (±σ) in areas with different elevations

Bighorn River drainage – local seasonal river water line				
Seasons	Entire basin	Subarea based on mean drainage elevation		d-excess
summer	$\delta D = 6.0 * \delta^{18}O - -29.6$; $R^2 = 0.91$ (n=51)	>3000 m	$\delta D = 6.5 * \delta^{18}O - 19.4$; $R^2 = 0.97$ (n=16)	7.4 ± 2.0
		<3000 m	$\delta D = 6.0 * \delta^{18}O - 30.0$; $R^2 = 0.89$ (n=35)	4.8 ± 3.3
spring	$\delta D = 6.9 * \delta^{18}O - 12.7$; $R^2 = 0.89$ (n=23)	>3000 m	$\delta D = 8.5 * \delta^{18}O - 16.9$; $R^2 = 0.97$ (n=6)	8.1 ± 0.9
		<3000 m	$\delta D = 6.7 * \delta^{18}O - 16.7$; $R^2 = 0.90$ (n=17)	6.7 ± 2.0
North Platte River drainage – local seasonal river water line				
Seasons	Entire basin	Subarea based on mean drainage elevation		d-excess
summer	$\delta D = 6.7 * \delta^{18}O - 18.3$; $R^2 = 0.94$ (n=70)	>2200 m	$\delta D = 5.1 * \delta^{18}O - 42.3$; $R^2 = 0.94$ (n=36)	2.1 ± 4.8
		<2200 m	$\delta D = 7.3 * \delta^{18}O - 8.6$; $R^2 = 0.96$ (n=34)	1.5 ± 3.5
spring	$\delta D = 6.3 * \delta^{18}O - 24.6$; $R^2 = 0.90$ (n=31)	>2200 m	$\delta D = 6.1 * \delta^{18}O - 25.8$; $R^2 = 0.91$ (n=15)	4.1 ± 3.4
		<2200 m	$\delta D = 6.8 * \delta^{18}O - 15.6$; $R^2 = 0.98$ (n=16)	2.8 ± 3.1

Bighorn Mountains		**Wind River Range**	
Flanks	Local river water line	Flanks	Local river water line
East flank	$\delta D = 5.8 * \delta^{18}O - 32.6$; $R^2 = 0.83$ (n=34)	East flank (Powder River drainage)	$\delta D = 6.4 * \delta^{18}O - 22.3$; $R^2 = 0.89$ (n=39)
West flank (Upper Green River drainage)	$\delta D = 6.2 * \delta^{18}O - 29.6$; $R^2 = 0.92$ (n=22)	West flank	$\delta D = 5.5 * \delta^{18}O - 34.6$; $R^2 = 0.97$ (n=18)

Table 2-2 Multivariate linear regression results of controlling factors on water isotope composition

Drainage basins	Season	Regression Models	Coefficient (P-value)		Interception (‰)	R^2
			Relative Humidity (‰/%)	Temperature (‰/°C)		
Bighorn River drainage	2011 summer	RH (n = 21)	-0.07 ($1.6*10^{-6}$)		-15.65	0.71
	2016 summer	RH (n = 31)	-0.17 (0.0002)		-12.51	0.38
	2016 spring	TEMP (n = 23)		0.15 (0.002)	-18.14	0.41
North Platte drainage	2011 summer	RH + TEMP (n=37)	0.13 ($6.6*10^{-6}$)	0.23 ($1.8*10^{-6}$)	-25.34	0.71
	2016 summer	RH (n=33)	0.22 (0.0002)		-22.85	0.37
	2016 spring	TEMP (n=31)		0.37 ($8.5*10^{-6}$)	-17.33	0.50

Table 2-3 River water isotopic composition data from this study

2011 summer					
Latitude	Longitude	Drainage Mean Elevation (m)	$\delta^{18}O$	δD	d-excess
42.018	-105.016	2121	-14.9	-115.4	3.7
41.755	-104.814	2038	-14.5	-111.0	4.6
41.158	-104.317	1716	-11.7	-88.8	5.0
41.840	-103.635	1135	-14.7	-117.9	-0.5
42.679	-103.430	1127	-14.4	-111.3	3.9
42.789	-105.542	2042	-15.8	-125.2	1.2
42.828	-105.785	2142	-15.9	-122.6	4.2
42.750	-106.521	2190	-16.0	-125.2	3.2
42.637	-107.248	2174	-18.0	-141.2	3.1
43.426	-106.290	1654	-17.8	-142.7	-0.5
43.697	-106.295	1790	-16.5	-132.7	-0.9

43.780	-106.626	2053	-17.6	-137.2	3.7
44.132	-107.122	2917	-18.7	-141.3	7.9
44.158	-107.158	2898	-18.7	-138.4	11.3
44.174	-107.213	3023	-18.9	-141.5	9.6
44.182	-107.217	3102	-19.2	-144.6	9.2
44.211	-107.302	2723	-19.0	-144.3	8.1
44.169	-107.250	3052	-19.1	-144.1	9.0
44.139	-107.246	3007	-18.9	-142.7	8.2
44.051	-107.385	2279	-18.7	-143.6	5.7
44.030	-107.464	1971	-18.7	-141.0	8.5
44.016	-107.972	1992	-17.4	-134.1	4.8
43.622	-108.222	2101	-17.7	-135.5	6.2
42.953	-108.433	1858	-14.5	-128.0	-11.7
42.901	-108.588	2077	-17.7	-135.7	5.7
42.869	-108.837	3046	-17.9	-137.2	6.3
42.737	-108.837	3059	-18.1	-136.0	9.0
42.502	-107.865	2096	-17.2	-132.9	4.6
42.489	-107.140	2165	-16.5	-129.4	2.8
42.472	-107.600	2194	-17.4	-137.6	1.6
42.542	-108.180	2314	-17.5	-135.2	4.5
42.695	-108.559	2038	-17.1	-138.7	-1.8
42.495	-108.732	2640	-18.2	-138.5	6.8
42.379	-108.899	2622	-17.9	-134.1	9.1
42.330	-109.515	2400	-17.4	-131.4	7.9
42.867	-109.895	2188	-14.6	-115.4	1.1
42.556	-109.363	2855	-17.7	-132.1	9.3
42.651	-109.259	3119	-15.3	-116.6	5.4
42.705	-109.270	3187	-17.7	-133.7	7.7
42.666	-109.266	2960	-17.6	-132.2	8.7
42.627	-109.255	3089	-18.0	-134.8	8.9
42.605	-109.283	3044	-17.6	-131.6	9.1
42.533	-109.205	2988	-18.2	-135.7	10.0
42.492	-109.123	2500	-16.3	-128.4	1.9
42.479	-109.025	2831	-17.8	-134.4	8.3
42.880	-108.728	2729	-18.0	-135.3	8.7
42.875	-108.964	3006	-18.3	-138.1	8.1
42.861	-108.919	3023	-18.4	-137.9	9.2

42.851	-108.948	3043	-18.3	-139.2	7.4
42.813	-108.893	2459	-18.2	-139.2	6.7
41.860	-107.052	2061	-16.7	-125.8	8.1
41.751	-107.948	2471	-16.7	-125.6	7.9
41.747	-106.771	2186	-16.2	-125.0	4.6
41.705	-106.402	2619	-17.2	-128.8	8.9
41.799	-105.926	2441	-16.5	-127.2	4.6
42.090	-105.580	2229	-14.9	-117.8	1.1
42.108	-105.617	2263	-15.1	-120.7	-0.3
42.262	-105.474	2709	-16.7	-124.8	9.0
42.170	-105.464	2247	-16.9	-126.7	8.3
42.213	-105.357	2393	-15.6	-125.7	-0.6
42.207	-105.360	2227	-15.3	-123.3	-0.6
42.207	-105.360	2378	-15.5	-123.6	0.6
42.160	-105.410	2112	-16.1	-122.6	6.1
42.197	-105.307	2232	-15.2	-121.3	0.5
42.198	-105.304	1902	-13.8	-107.7	2.9
42.165	-105.176	2194	-14.9	-119.1	-0.4
42.104	-105.093	2349	-14.6	-117.8	-1.1
42.351	-105.706	2427	-14.9	-117.9	1.5
42.720	-105.389	2124	-15.9	-125.0	1.8
41.211	-101.649	951	-12.5	-104.0	-3.8
41.588	-103.100	1135	-13.0	-100.4	3.9
41.195	-100.812	863	-11.7	-97.1	-3.4
2016 spring					
41.175	-100.782	1799	-10.8	-86.7	-0.4
41.211	-101.663	1892	-11.5	-93.9	-2.3
41.838	-103.635	1135	-14.2	-112.5	1.3
41.931	-103.628	1253	-14.2	-114.4	-0.6
41.155	-104.265	1648	-13.4	-102.1	5.0
41.755	-104.812	2038	-15.1	-115.9	5.2
42.104	-105.095	2290	-14.4	-113.4	2.1
42.200	-105.301	2224	-14.5	-110.1	5.5
42.160	-105.410	2147	-16.0	-122.4	5.7
42.210	-105.412	2100	-15.4	-117.6	5.5
42.212	-105.524	2376	-17.0	-129.1	7.0
42.240	-105.721	2395	-15.9	-124.9	2.2

42.721	-105.389	2154	-15.0	-118.8	1.3
42.789	-105.542	2057	-16.8	-127.8	6.4
42.830	-105.775	2173	-13.0	-105.8	-2.0
42.750	-106.521	2224	-14.2	-114.2	-0.6
43.428	-106.291	1649	-17.3	-141.2	-3.1
43.698	-106.296	1789	-17.3	-134.1	4.2
43.623	-106.576	1771	-14.5	-119.1	-3.4
43.708	-106.639	2059	-18.4	-139.5	7.9
44.127	-106.712	2112	-16.3	-125.7	4.5
44.183	-106.728	2363	-17.0	-129.2	6.7
44.181	-106.820	1970	-17.1	-130.0	6.8
44.167	-106.920	2752	-17.6	-133.8	7.2
44.196	-106.927	2613	-16.8	-127.7	7.0
44.256	-106.952	2652	-15.0	-115.6	4.2
44.278	-106.950	2919	-16.9	-126.5	9.0
44.301	-106.947	2780	-17.0	-128.9	7.2
44.319	-106.942	2927	-16.2	-125.2	4.2
44.332	-106.793	2648	-16.9	-127.9	7.5
44.135	-106.895	2667	-16.4	-125.8	5.4
44.158	-107.158	2898	-18.5	-139.4	8.3
44.182	-107.218	3102	-18.2	-138.0	7.8
44.169	-107.250	3052	-18.4	-139.3	7.7
44.212	-107.302	2723	-19.1	-146.2	6.9
44.137	-107.249	3007	-18.1	-137.3	7.5
44.030	-107.465	1971	-18.2	-139.3	6.6
44.017	-107.979	1992	-16.1	-126.8	2.1
43.622	-108.222	2101	-16.2	-126.3	3.1
43.242	-108.168	2253	-17.1	-129.3	7.8
43.009	-108.377	2382	-17.1	-130.4	6.2
42.953	-108.433	1858	-17.8	-137.3	5.0
42.901	-108.588	2077	-17.8	-134.8	7.3
42.880	-108.727	2729	-17.5	-131.4	9.0
43.011	-108.882	2758	-17.0	-127.8	7.9
43.444	-109.467	2732	-18.0	-136.2	8.1
43.426	-109.560	3188	-16.9	-127.9	7.4
42.871	-108.886	3010	-17.4	-129.2	9.6
42.830	-108.851	2565	-18.0	-135.3	8.8

42.776	-108.775	2925	-17.5	-131.3	8.4
42.734	-108.845	3059	-17.5	-131.4	8.9
42.716	-108.645	2380	-17.8	-135.0	7.3
42.379	-108.898	2622	-17.2	-129.9	7.4
42.492	-109.122	2500	-15.2	-119.4	1.9
42.528	-109.107	2667	-16.1	-126.6	2.0
42.562	-109.062	3106	-17.3	-129.3	8.9
42.533	-109.205	2988	-17.0	-126.9	9.0
42.570	-109.248	2863	-16.8	-127.0	7.2
42.605	-109.258	3036	-12.5	-103.8	-3.8
42.627	-109.254	3089	-16.9	-125.4	9.7
42.557	-109.363	2855	-16.6	-124.1	9.0
42.866	-109.869	2188	-15.7	-122.1	3.7
42.381	-108.898	2279	-17.2	-129.8	7.6
42.496	-108.732	2640	-17.7	-139.6	2.1
42.715	-108.644	2379	-17.8	-134.6	7.4
42.698	-108.528	2038	-18.1	-140.5	4.3
42.542	-108.182	2314	-15.4	-122.9	0.6
42.510	-107.892	2096	-16.9	-130.8	4.2
42.467	-107.595	2194	-16.7	-130.1	3.8
42.491	-107.139	2165	-16.5	-129.1	2.9
42.637	-107.249	2174	-17.7	-137.7	3.9
41.704	-106.402	2619	-14.4	-115.4	-0.1
41.799	-105.926	2441	-16.9	-128.2	7.0
41.704	-106.402	2619	-16.9	-126.8	8.7
41.741	-106.773	2186	-15.8	-124.0	2.7
41.862	-107.056	2061	-17.0	-128.5	7.9
2016 summer					
41.175	-100.782	1799	-6.0	-48.7	-0.8
41.211	-101.663	1892	-11.8	-96.8	-2.7
41.588	-103.100	1135	-12.7	-94.3	7.4
41.838	-103.635	1135	-13.6	-109.4	-0.9
41.931	-103.628	1253	-14.1	-113.6	-0.8
41.755	-104.812	2038	-14.9	-114.9	4.2
42.104	-105.095	2290	-13.3	-106.7	-0.1
42.160	-105.410	2147	-16.1	-122.4	6.3
42.212	-105.524	2376	-15.5	-121.7	2.3

42.240	-105.721	2395	-12.2	-105.9	-8.6
42.721	-105.389	2154	-14.4	-115.5	0.1
42.478	-104.997	1527	-13.9	-112.8	-1.3
42.789	-105.542	2057	-15.8	-124.6	1.9
42.830	-105.775	2173	-12.8	-106.9	-4.4
42.750	-106.521	2224	-14.6	-115.2	1.7
43.428	-106.291	1649	-17.1	-139.4	-2.6
43.698	-106.296	1789	-14.0	-120.1	-8.5
43.623	-106.576	1771	-11.6	-99.3	-6.7
43.708	-106.639	2059	-17.7	-138.2	3.6
44.127	-106.712	2112	-15.1	-121.5	-0.3
44.183	-106.728	2363	-15.8	-124.9	1.6
44.181	-106.820	1970	-17.4	-132.1	7.0
44.167	-106.920	2752	-17.9	-135.8	7.7
44.196	-106.927	2613	-16.9	-130.1	5.2
44.256	-106.952	2652	-17.2	-130.7	7.0
44.278	-106.950	2919	-16.2	-123.9	5.9
44.301	-106.947	2780	-16.6	-127.4	5.7
44.319	-106.942	2927	-16.5	-124.1	8.3
44.332	-106.793	2648	-16.4	-124.5	7.0
44.151	-106.932	2669	-16.6	-128.8	4.2
44.135	-106.895	2667	-16.8	-128.7	5.5
44.132	-107.121	2917	-18.5	-140.1	7.7
44.158	-107.158	2898	-19.0	-143.6	8.5
44.175	-107.213	3023	-17.1	-130.5	6.4
44.212	-107.302	2723	-19.3	-147.5	6.8
44.137	-107.249	3007	-19.1	-144.6	7.9
44.030	-107.465	1971	-17.9	-139.4	4.0
44.017	-107.979	1992	-16.0	-125.7	2.4
43.622	-108.222	2101	-16.3	-126.8	3.7
43.242	-108.168	2253	-15.5	-122.8	1.1
43.009	-108.377	2382	-15.9	-124.1	3.3
42.953	-108.433	1858	-15.5	-131.9	-7.5
42.901	-108.588	2077	-16.2	-128.4	1.5
42.880	-108.727	2729	-16.5	-127.0	4.8
43.011	-108.882	2758	-16.0	-123.5	4.4
43.444	-109.467	2732	-17.6	-134.2	6.3

42.830	-108.851	2565	-18.2	-139.3	6.2
42.776	-108.775	2925	-16.4	-126.5	4.6
42.492	-109.122	2500	-13.3	-111.3	-5.0
42.528	-109.107	2667	-15.9	-125.2	1.8
42.570	-109.248	2863	-16.7	-127.1	6.6
42.605	-109.258	3036	-16.3	-124.0	6.7
42.627	-109.254	3089	-16.4	-124.7	6.6
42.557	-109.363	2855	-15.7	-120.5	4.8
42.866	-109.869	2188	-15.7	-121.4	3.9
42.496	-108.732	2640	-17.4	-135.5	3.7
42.715	-108.644	2379	-17.6	-135.2	5.6
42.698	-108.528	2038	-17.7	-140.0	1.3
42.542	-108.182	2314	-15.4	-125.4	-1.8
42.467	-107.595	2194	-15.0	-125.7	-5.3
42.491	-107.139	2165	-14.7	-124.2	-6.2
42.637	-107.249	2174	-18.4	-144.3	3.0
41.704	-106.402	2619	-14.7	-117.8	0.1
41.799	-105.926	2441	-12.8	-110.1	-8.1
41.704	-106.402	2619	-15.9	-122.9	4.5
41.862	-107.056	2061	-15.7	-121.8	3.6
41.158	-104.317	1716	-12.7	-97.2	4.1
42.017	-105.010	2121	-13.5	-107.9	-0.2
42.185	-105.411	2086	-15.2	-118.9	2.5
42.175	-105.455	2247	-15.2	-120.0	1.3
42.351	-105.706	2427	-12.7	-109.1	-7.8
44.169	-107.250	3052	-16.6	-128.8	4.2
43.493	-108.168	2106	-16.2	-126.1	3.7
43.502	-109.556	2722	-16.1	-124.0	5.2
43.423	-109.573	3188	-16.6	-124.8	8.1
42.885	-108.840	2831	-16.1	-125.1	3.7
42.828	-108.894	2459	-17.2	-133.7	3.8
42.776	-108.775	2925	-17.1	-131.8	5.3
42.776	-108.775	2925	-16.0	-123.3	4.5
42.710	-108.868	3099	-15.7	-123.5	2.5
42.684	-108.885	3110	-18.1	-136.2	8.5
42.600	-108.845	3000	-16.4	-125.7	5.5
42.630	-108.765	2900	-18.5	-141.5	6.3

42.434	-108.964	2638	-16.9	-130.3	5.1
42.380	-108.898	2622	-16.3	-125.1	5.2
42.528	-109.105	2667	-16.7	-125.7	7.5
42.520	-109.048	2599	-16.9	-127.0	8.2
42.432	-109.252	2679	-14.2	-114.9	-0.9
42.686	-109.271	3073	-15.4	-117.8	5.6
42.657	-109.267	3039	-15.4	-117.5	6.0
42.556	-109.363	2860	-17.2	-130.9	7.0
2012 summer*					
44.406	-106.744	2162	-16.9	-130.1	5.1
44.319	-106.942	2944	-17.1	-129.4	7.5
44.277	-106.948	2387	-17.2	-131.2	6.5
44.259	-107.215	2785	-17.1	-131.0	6.0
44.245	-106.435	1759	-8.8	-87.4	-16.7
44.204	-107.240	2665	-17.2	-131.6	6.1
44.174	-107.213	3021	-17.5	-134.2	5.8
44.174	-106.890	2657	-17.5	-133.1	7.0
44.158	-107.158	2768	-18.8	-143.0	7.1
44.138	-107.246	2308	-16.9	-131.3	4.1
44.131	-107.121	2740	-18.3	-140.4	6.0
44.106	-107.089	2858	-18.1	-136.4	8.3
44.082	-107.310	2826	-18.7	-142.8	6.6
44.061	-107.384	1467	-19.0	-145.4	6.3
44.052	-107.399	1418	-17.8	-138.7	4.0
43.781	-106.626	1473	-17.5	-136.1	3.8
42.880	-108.728	1629	-16.7	-129.5	4.2
42.777	-109.213	3351	-17.2	-129.0	8.4
42.766	-109.212	3389	-16.1	-119.2	9.5
42.763	-109.212	3375	-16.8	-126.0	8.1
42.757	-109.207	3364	-16.8	-126.7	8.0
42.756	-109.206	3184	-16.3	-122.7	7.6
42.742	-109.200	2989	-16.8	-127.5	7.0
42.738	-109.208	2999	-17.0	-126.6	9.6
42.737	-109.198	3083	-15.3	-120.3	1.9
42.736	-108.836	2093	-16.3	-124.4	5.7
42.725	-108.984	2762	-18.5	-140.9	7.0
42.725	-108.949	3175	-16.6	-127.2	6.0

42.724	-108.995	2765	-18.3	-140.1	6.1
42.72	-108.949	2759	-19.0	-141.7	9.9
42.717	-108.972	2722	-15.3	-123.5	-0.8
42.715	-108.996	2797	-16.2	-126.3	3.5
42.689	-109.269	3186	-16.6	-125.6	7.1
42.688	-109.038	3290	-16.8	-125.8	8.4
42.641	-108.347	1714	-16.3	-123.5	6.8
42.641	-108.337	1716	-17.7	-141.8	0.0
42.627	-109.255	2760	-17.1	-126.8	9.6
42.560	-108.714	2520	-18.0	-140.0	3.8
42.492	-107.138	1797	-14.5	-122.2	-6.1
42.468	-107.595	1892	-14.0	-120.9	-8.6
42.379	-108.982	2265	-16.8	-128.9	5.5
41.929	-105.412	2411	-9.4	-87.2	-12.3
41.845	-105.221	1640	-14.5	-114.1	2.0

*The data of 2012 summer was not included in the discussion due to its limited spatial coverage, though it shows similar patterns to the data of 2011 and 2016.

Chapter 3 Detrital Zircon Provenance Record of Middle Cenozoic Landscape Evolution in the Southern Rockies, USA

Abstract

The high-elevation, high-relief landscape of the southern Rocky Mountains (Rockies), USA, reflects interactions between tectonics, paleoclimate, and surface processes. The southern Rockies experienced several episodes of uplift, extension, and major climate changes during the Cenozoic, but the landscape and river drainage evolution remain poorly constrained. Here we apply detrital zircon U-Pb geochronology to Eocene-Miocene strata in south-central Colorado to constrain the depositional ages and sediment provenance. A total of 1284 concordant U–Pb ages were determined and are grouped into 75–11 Ma, 1500–1300 Ma, and 1800–1500 Ma populations. Intense late Eocene-Oligocene regional volcanism provided abundant air fall zircons into the latest Eocene-Oligocene sedimentary systems where maximum depositional ages can be used to closely proximate depositional ages and improve the chronostratigraphy. The new data are integrated with interpretation of sedimentary environments, and the detrital zircon signatures of potential source terranes and age-equivalent strata in other nearby basins to interpret landscape and paleodrainage evolution. Specifically, the new provenance data show that (1) after the main phase of the Laramide deformation, the Wet Mountains, but not the Sangre de Cristo Range, was the dominant local topographic feature, and a southward-flowing river connected the Wet Mountain Valley with

the Huerfano and Raton Basins to the south; (2) during the Eocene-early Oligocene, aggradation of the Wet Mountain Valley and the Huerfano Basin formed a low-relief surface, and subsequent river erosion changed the drainage pattern eastward and likely formed the modern lower Arkansas River valley; and (3) during the Miocene, dissection of the low-relief surface by the opening of the Rio Grande Rift formed the upper Arkansas River valley, and the upper valley was connected with the lower valley to establish the modern drainage pattern of the Arkansas River in the southern Rockies.

Keywords: Detrital zircon; Provenance; Southern Rocky Mountains; Landscape evolution; Paleodrainage patterns

3.1 Introduction

The southern Rocky Mountains (Rockies) in Colorado and New Mexico (Fig. 3-1A) is a region of high-elevation and high-relief within the western USA. The region is bounded by the Colorado Plateau to the west and the Great Plains to the east. The southern Rockies extends to the central Rockies in northern Colorado and Wyoming, and is dissected by the Rio Grande Rift in the south. Well-preserved Late Cretaceous marine sedimentary rocks suggest that the region was at sea level at that time (Dick and Nish, 1966). At present, the southern Rockies is ~3 km above the adjacent Great Plains and has an average relief greater than 1.6 km. Deep river canyons with a local relief of ~3 km are present around the northern Rio Grande Rift. The tectonic history of the southern Rockies has been studied for decades (e.g., Epis et al., 1980; Wolfe et al., 1998; Roy et al., 2004; McMillan et al., 2006; Eaton, 2009; Copeland et al., 2011; Chapin et al., 2014). The history includes the latest Cretaceous-early Paleogene Laramide orogeny, late Paleogene regional epeirogenic uplift (Eaton, 1987, 2008), Neogene extension of the Rio Grande Rift (Landman and Flowers, 2013; Ricketts et al., 2016), and late Neogene mantle-driven dynamic uplift (Karlstrom et al., 2012). It is well known that the Laramide orogeny produced discrete uplifts and basins in the southern Rockies. However, the landscape evolution in response to the late Paleogene-Neogene tectonic history remains poorly constrained. In the southern Rockies, one intriguing observation of the modern landscape is that the Arkansas River valley follows the northern Rio Grande Rift initially, but abandons the path and turns eastward to cut through basement rocks of the northern Wet Mountains (Fig. 3-1). Because modern studies have suggested that river drainages and sediment routing are sensitive to tectonics (e.g., Bonnet, 2009; Castelltort et al., 2012), the drainage pattern of the Arkansas River is likely a result of long-term channel migration in response to regional tectonic. Here we collect 1284 new detrital zircon U–Pb ages to constrain sediment provenance and reconstruct paleodrainage patterns in order to understand the landscape evolution of the southern Rockies during the early Eocene-middle Miocene. The data are also used to test the hypothesis that the drainage pattern of the Arkansas River was a result of landscape change in response to tectonic deformation. The maximum depositional ages improve chronostratigraphy of the late Eocene–middle Miocene strata in south-central Colorado.

3.2 Tectonic setting and stratigraphy

The southern Rockies experienced the latest Cretaceous-Paleogene Laramide orogeny and several episodes of epeirogenic, long-wavelength uplift during the late Paleogene-Neogene (e.g., Epis et al., 1976, 1980; Gregory and Chase, 1994; Gregory and McIntosh, 1996; Wolfe et al., 1998; Eaton, 2009; Copeland et al., 2011; Cather et al., 2012; Donahue, 2016). The Laramide orogeny caused by low-angle subduction of the Farallon plate had produced discrete high mountain ranges and low intermontane basins (Cather et al., 2012), and the orogeny may have continued until the late Oligocene in the southern Rockies (Copeland et al., 2011; Tomlinson et al., 2013). During the middle to late Eocene, following a period of tectonic quiescence (Roberts et al., 2012) or basin subsidence (Cather et al., 2012), a low-relief erosional surface was developed on beveled Precambrian basement rocks and basin-fill of the Laramide intermontane basins (Epis et al., 1976, 1980). The erosion was suggested to have been resulted from thermal uplift induced by middle Cenozoic magmatism (Eaton, 2009; Roberts et al., 2012; Donahue, 2016) or lithosphere isostatic rebound induced by foundering the Farallon plate(Cather et al., 2012). The magmatism in the southern Rockies, as part of the middle Cenozoic ignimbrite flare-up in the broad western USA, was mostly intensive during the latest Eocene-early Oligocene (Chapin et al., 2004; McIntosh and Chapin, 2004). During the Neogene, extension associated with the opening of the Rio Grande Rift modified some of the Laramide intermontane basins into grabens (Kellogg, 1999), and the Rio Grande Rift propagated northward (Leonard, 2002; Cosca et al., 2014) or was synchronous along its strike (Landman and Flowers, 2013; Ricketts et al., 2016). Another episode of erosion occurred during the late Miocene in the southern Rockies, which is generally attributed to a mantle anomaly (Eaton, 2008; Coblentz et al., 2011; Karlstrom et al., 2012; Hansen et al., 2013; Lazear et al., 2013; Rosenberg et al., 2014). An alternative interpretation is that the erosion was caused by seasonal snowmelt related to late Neogene global cooling (Pelletier, 2009).

Our study sites in the southern Rockies include the Wet Mountain Valley, Huerfano Basin, upper Arkansas Valley, and South Park Basin (Fig. 3-1B). The Wet Mountain Valley is bounded by the Sangre de Cristo Range to the west, the Arkansas River to the north, and the Wet Mountains to the east. The Valley is separated from the Huerfano Basin to its south by the Promontory Divide. The Huerfano Basin is bounded also by the Wet Mountains and Sangre de Cristo Range, and is connected to the Raton Basin to the south (Dick and Nish, 1966; Scott and Taylor, 1975). At present, the Wet Mountain Valley is a graben bounded by normal faults on the east and west sides. The major basin-bounding thrust is at the foot of the Sangre de Cristo Range, and has been previously attributed to the latest Cretaceous-early Paleogene Laramide deformation (Scott and Taylor, 1975).

In the central and eastern parts of the Wet Mountain Valley and the Huerfano Basin, middle and late Cenozoic sedimentary rocks, including the middle Eocene Huerfano Formation and Farisita Conglomerate, the upper Eocene-lower Oligocene Devils Hole Formation, and the Miocene-Pliocene Santa Fe Formation, are exposed (Scott and Taylor, 1975). On the east side of Highway 69, the Farisita Conglomerate intertongues with and partially overlies the Huerfano Formation. The Huerfano Formation contains red and maroon silty mudstone and lenticular sandstone (Johnson, 1959; Scott and Taylor, 1975). The Farisita Conglomerate contains yellowish-grey cobble to boulder conglomerate and coarse-grained sandstone. The Huerfano Formation and the Farisita Conglomerate were interpreted to be alluvial deposits with fluvial channel sub-environments, and sourced primarily from Meso- and Paleoproterozoic rocks of the Wet Mountains (Johnson, 1959; Scott and Taylor, 1975; Rasmussen and Foreman, 2017). The Huerfano Formation and the Farisita Conglomerate have no volcanic ash, and the depositional ages were estimated to be early to middle Eocene based on mammal fossils (Robinson, 1966; Scott and Taylor, 1975; Robinson et al., 2004). The Devils Hole Formation contains light grey tuffaceous, cross-stratified sandstone and pumice conglomerate (Johnson, 1959). This formation was deposited in debris flow environments and was intertongued with lahars (Scott and Taylor, 1975). A pumice-bearing sandstone was dated to be 32.1±0.9 Ma, and an ash flow was dated to be 27.5±2.8 Ma based on zircon U-Pb geochronology near Rosita, Colorado

(Scott and Taylor, 1975 and references therein). The Devils Hole Formation is currently exposed on the Greenhorn Mountains at ~3.5 km above sea level (Fig. 3-1B). The Santa Fe Formation is salmon-pink colored, and contains crudely stratified, interbedded conglomerate and coarse- to medium-grained, muddy sandstone. This formation was interpreted to be deposited in debris flow environments (Dick and Nish, 1966; Scott and Taylor, 1975; Epis et al., 1980). No identifiable ash beds or vertebrate fossils were found in the Santa Fe Formation, and the age was roughly estimated to be Miocene-Pliocene based on biostratigraphy correlation to the Santa Fe Group in New Mexico (Scott and Taylor, 1975).

The Arkansas River rises near Leadville, flows southward in its upper valley surrounding Salida, Colorado before it changes flow direction abruptly to east toward its lower valley surrounding Canon City (Fig. 3-1B). The Arkansas River valley near Salida is bounded by the Sawatch Range to the west, the Mosquito Range to the east, and is separated from the San Luis Basin to the south by the Poncha Pass (Fig. 3-1B). The upper valley is bounded by normal faults associated with extension of the Rio Grande Rift (e.g., Landman and Flowers, 2013; Ricketts et al., 2016; Abbey and Niemi, 2018). The Dry Union Formation is exposed in the Arkansas Valley. The formation consists of interbedded, crudely stratified conglomerate and poorly sorted, medium- to coarse-grained muddy sandstone deposited in an alluvial fan environment (Tweto, 1961). The depositional age of the formation was estimated to be Miocene-Pliocene based on vertebrate fossils (Van

Alstine and Lewis, 1960). Two ash beds are present in the upper part of the formation, and were estimated to be 11-8 Ma based on geochemical correlation with Yellowstone hotspot ashes (Hubbard et al., 2001).

Separated by the Front Range and lower Arkansas River valley, the South Park Basin is located to the north of the Wet Mountain Valley (Fig. 3-1B). The Basin is a syncline and the deposition was interrupted by volcanic rocks of the Thirty-nine Mile volcanic filed during the Oligocene (Maughan, 1988). Outcrops of Cenozoic rocks are sparse in the South Park Basin. The Oligocene Balfour and Antero Formations, Miocene Wagontongue Formation, and Pliocene Trump Formation were previously described in the Basin (Stark et al., 1949). The Antero Formation was determined to be Oligocene based on mammal fossils, including *Mesohippus* sp., a species of brontothere or titanothere (Stark et al., 1949) that is characteristic to the Chadronian Stage of the North American Land Mammal Age (Prothero and Emry, 2004). The underlying Balfour Formation was estimated to be older than the Antero Formation only based on stratigraphic relationships (Stark et al., 1949). The Balfour Formation changes upward from conglomerate with interbedded tuff and muddy sandstone deposited in an alluvial fan environments into interbedded mudstone, and fine-grained muddy sandstone with tuff deposited in a lacustrine environment (Stark et al., 1949). The Wagontongue Formation is the most well exposed Cenozoic strata, and its distribution is limited to the west part of the Basin (Stark et al., 1949). The Wagontongue Formation consists of poorly consolidated conglomerate, sandstone, mudstone, and reworked ash and pumice, and was interpreted to be deposited in a fluvial environment (Stark et al., 1949). Identification of the species of silicified wood and roots placed the formation in the late Miocene or early Pliocene (Stark et al., 1949).

3.3 Methods

A total of nine medium- to coarse-grained sandstone and conglomerate samples were collected from outcrops and processed for detrital zircon provenance study. Details of locations and sedimentological descriptions of the samples are listed in Table 3-1. Our sedimentological observations to the studied strata are generally consistent with previous descriptions and interpretations of depositional environments. Zircon grains were separated from disaggregated samples by panning, passing through Frantz magnetic separator and heavy liquid. Zircon grains were mounted together with Sri Lanka zircon standard and analyzed using a laser ablation multi-collector inductively coupled plasma mass spectrometry (LA-MC-ICPMS) at the Arizona LaserChron Center following Gehrels (2012). The isotope ratios of $^{207}Pb/^{206}Pb$ are used for grains that are greater than 900 Ma, and ratios of $^{206}Pb/^{238}U$ are used for grains that are less than 900 Ma. These ages were filtered by 20% discordance and 5% reverse discordance. All the samples have 100-200 best ages with more than 90% confidence of showing all age populations (Vermeesch, 2004).

The maximum depositional ages were calculated using Isoplot. For samples that their youngest group of zircons contains more than 20 grains, we used TuffZirc to calculate the maximum depositional ages. TuffZirc is an algorithm that is generally insensitive to Pb loss and inheritance (Ludwig and Mundil, 2002), therefore is preferred in use on the samples that contains relatively great numbers of young zircons. For samples whose youngest groups contain less than 10 grains and TuffZirc is not applicable, the maximum depositional ages were calculated as the weighted mean ages of the youngest group of zircons. The youngest group has at least three grains with overlapping ages.

3.4 Results

3.4.1 Maximum depositional ages

Six of the samples contain clusters of youngest zircons with maximum depositional ages younger than or equivalent to the previously estimated depositional ages (Table 3-1). The oldest sample from the Farisita Conglomerate yields a maximum depositional age of 66.3±0.3 Ma (n=3, Mean Square Weighted Deviation (MSWD)=1.6). This age is considerably older than the expected early Eocene depositional age based on mammal fossils in the Farisita Conglomerate and its intertonguing Huerfano Formation (Robinson, 1966; Scott and Taylor, 1975). The maximum depositional ages of samples from the Devils Hole Formation in the Greenhorn Mountains, and the Balfour Formation in South Park are 33.5+0.2/-0.3 Ma (n=45, 95% confidence) and 34.1+0.3/-0.2 Ma (n=19, 93.6% confidence), respectively (Fig. 3-3). The maximum depositional ages of the two samples from the Dry Union Formation are 35.8 ±0.2 Ma (n=52, 95% confidence) and 33.8+0.2/-0.4 Ma (n=19, 93.6% confidence), respectively (Fig. 3-3).

The abundant latest Eocene-earliest Oligocene zircons were most likely from the intense syndepositional eruption of the nearby Silver Cliff-Rosita, Thirty-nine, and San Juan volcanic fields (McIntosh and Chapin, 2004) (Fig. 3-1B), therefore, the maximum depositional ages of these samples closely represent the depositional ages. The ages of the Devils Hole Formation and the Balfour Formation place the two formations in the latest Eocene-earliest Oligocene, consistent with the expected depositional ages based on stratigraphic correlation and the principle of superposition (Table 2-1). However, the ages of the Dry Union Formation are older than the expected late Miocene-early Pliocene depositional age based on vertebrate remains and tephrochronology (Van Alstine and Lewis, 1960; Hubbard et al., 2001; Kellogg et al., 2017). The maximum depositional ages of the two samples from the Santa Fe Formation in the Wet Mountain Valley and the Wagontongue Formation in South Park are 11.5±0.3 Ma (n=4, MSWD=0.9) and 16.7±0.3 Ma (n=3, MSWD=0.4), respectively, and these ages place the two formations in the Miocene (Fig. 3-3).

3.4.2 Detrital zircon age distributions

A total of 1284 new detrital zircon U-Pb ages range from Archean (2700 Ma) to Miocene (11 Ma). These ages are divided into five populations based on known basement provinces and magmatic events in the North America (Fig. 3-1A), including latest Cretaceous–Miocene population (A: 75–11 Ma), late Mesozoic–middle Mesoproterozoic population (B: 1300–75 Ma), middle–late Mesoproterozoic population (C: 1500–1300 Ma), Mesoproterozoic–Paleoproterozoic population (D: 1800–1500 Ma), and Archean–Paleoproterozoic population (E: 2709–1800 Ma) (Fig. 3-4).

Population A is further divided into A1 (23–11 Ma), A2 (50–23 Ma), and A3 (75–50 Ma) subpopulations, and population B is further divided into B1 (500–75 Ma), B2 (550–500 Ma), and B3 (1300–550 Ma) subpopulations based on potential sources following Link et al. (2005) (Fig. 3-4). Populations A, C, D are major populations, and populations B and E are minor populations, constituting ~10% and <4%, respectively, of the total grains. B2 subpopulation dominates population B (Fig. 3-4).

The abundances of zircon populations are variable among the nine samples (Fig. 3-5). The abundance of population A (75–11 Ma) varies from 0% to 94% (Fig. 3-5). Subpopulation A3 (75–50 Ma) only exists in three samples and the abundance is negligible (Fig. 3-5). The abundance of subpopulation B2 (550–500 Ma) is relatively high in the three samples of the Farisita Conglomerate and decreases stratigraphically upward (Figs. 3-4, 3-5). Populations C and D are present in all the samples, but dominate (>50%) the samples from the Wagontongue Formation and Farisita Conglomerate.

3.4.3 Potential zircon sources

The nearest potential sources of subpopulation A1 are volcanisms related to the extension of the Basin and Range and the Rio Grande Rift (Chapin et al., 2004; Ricketts et al., 2016) and in the Snake River Plain (Perkins and Nash, 2002). The sources of subpopulation A2 are the intense and frequent middle Cenozoic volcanism related to ignimbrite flare-up that extends from Mexico to northwestern Nevada, including mainly the local San Juan, Silver Cliff-Rosita, and Thirty-nine volcanic fields, the intermediate Mogollon-Datil, and Marysvale volcanic fields, and the distal Trans-Pecos, Great Basin, and Sierra Madre Occidental volcanic fields (McIntosh and Chapin, 2004; Lipman, 2007). The nearest potential source of subpopulation A3 is the local Laramide intrusions to the north of the Sangre de Cristo Mountains (Cunningham et al., 1994) (Fig. 3-1B).

Major sources of subpopulations B1 (500–75 Ma) and B3 (1300–550 Ma) include the Cordilleran magmatism in the western USA (~250–75 Ma), Appalachian magmatism in the eastern USA (500–250 Ma), and the Grenville orogeny (1300–900 Ma) (Dalziel, 1997) (Fig. 3-1A). These sources are far away from our study area. Zircons of these subpopulations were recycled from Paleozoic-Mesozoic sedimentary rocks in the study area (e.g., Bush et al., 2016) (Fig. 3-6). Local source of subpopulation B2 (550–550 Ma) is the McClure granite complex (~510 Ma) in the north part of the Wet Mountains (Rasmussen and Foreman, 2017) (Fig. 3-1B), providing a direct source for this zircon population.

Zircons of population C (1500–1300 Ma) were formed by the anorogenic trans-Laurentian magmatism (Bickford et al., 2015 and references therein). Zircons of Population D (1800–1500 Ma) were formed during the Yavapai-Mazatzal orogeny (Hoffman, 1988). The basement rocks in the region are of these ages, and zircon grains of these ages were recycled into Phanerozoic sedimentary rocks by exhumation of basement rocks by the Cambrian-Mississippian Transcontinental Arch (e.g., Sloss, 1988), the Pennsylvanian-early Permian Ancestral Rocky Mountain orogeny (e.g., Kluth, 1986), and the latest Cretaceous-early Paleogene Laramide orogeny (Kelley and Chapin, 2004). The Wet Mountains, Sangre de Cristo Range, Sawatch and Mosquito ranges all have Yavapai-Mazatzal basement (Fig. 3-1B). The Paleozoic-lower Cenozoic sedimentary rocks in the southern Rockies also contain zircons of these two populations (Fig. 3-6). Large bodies of plutonic rocks of population C in the study area include the San Isabel Batholith in the Wet Mountains (Cullers et al., 1992), the southern Sawatch Range near Salida, and the southern Mosquito Range to the west of the South Park (Kellogg et al., 2017; Moscati et al., 2017) (Fig. 3-1B). Therefore, zircons of these populations were recycled from the Paleozoic-lower Cenozoic strata or directly from the Laramide uplifts.

The ultimate sources of zircons of population E (>1800 Ma) include the Archean Wyoming-Heane-Rae craton (>2500 Ma), the Penokean-Trans-Hudson orogens and Great Falls tectonic zone (2000–1800 Ma) (Hoffman, 1988; Whitmeyer and

Karlstrom, 2007). The closest exposure of this basement rocks are the Laramide uplifts in Wyoming (Frost et al., 2000). These sources are far from the study area, and zircons of this population are most likely recycled from the Paleozoic-lower Cenozoic strata (Fig. 3-6).

3.5 Discussion

3.5.1 Chronostratigraphy

Depositional ages of sedimentary rocks can be approximated from maximum depositional ages of detrital zircon when synchronous magmatic activity was frequent and intense (e.g., Fan et al., 2015, 2018; Rowley and Fan, 2016; Smith et al., 2017). The maximum depositional ages in this study improve the chronostratigraphy of the latest Eocene-earliest Oligocene strata because of intense synchronous volcanism in central Colorado (McIntosh and Chapin, 2004). The Dry Union Formation was estimated to be Miocene-Pliocene based on fragments of vertebrate fossils (Van Alstine and Lewis, 1960; Van Alstine, 1971), geochemical correlation of two ash beds near the top of the formation to volcanic ashes in Yellowstone (Hubbard et al., 2001), and whole rock $^{40}Ar/^{39}Ar$ dating of the two ash beds (Morgan and Cosca, 2017). The maximum depositional age of latest Eocene-early Oligocene in this study extends the age of the Dry Union Formation to the latest Eocene.

The maximum depositional ages of the Farisita Conglomerate are older than previously estimated depositional ages. While the Farisita Conglomerate is equivalent to the Huerfano Formation that was constrained to be Eocene based on mammal fossils in several localities (Scott and Taylor, 1975), the sample of the lowest stratigraphic position in the Farisita Conglomerate yields an maximum depositional age of 66.3±0.3 Ma (Table 2-1). Early to middle Eocene is a period of tectonic quiescence and magmatism of this period is restricted to small intrusions in the Colorado Mineral Belt (Chapin et al., 2004; Roberts et al., 2012). This local volcanism may be not intense enough to send ash into the study site in the Wet Mountain Valley based on the lack of zircons of early-middle Eocene age. Moreover, the youngest cluster of zircon grains in the Farisita Conglomerate is not euhedral and make only a small fraction (<3%), thus unlikely sourced from air-fall ash. Therefore, the early Eocene depositional age of the Farisita Conglomerate constrained by mammal fossils is better than the maximum depositional age constrained by detrital zircon.

3.5.2 The high Wet Mountains and southward drainage pattern during the Eocene

The distributions of detrital zircon ages in the Farisita Conglomerate, characterized by dominant population D (1800–1500 Ma) and subordinate subpopulation B2 (550–500 Ma) and population C (1500–1300 Ma) (Figs. 2-4, 2-5), suggest that the grains were derived primarily from the basement rocks in the Wet Mountains during the Eocene. Although both the Sangre de Cristo Range and Wet Mountains have Proterozoic basement, the major local source of subpopulation B2 is the McClure granite complex (~510 Ma) in the northern Wet Mountains (Fig.

3-1B). Mesozoic and Paleozoic sedimentary rocks are exposed on the eastern flank of the Sangre de Cristo Range (Fig. 3-1B), and the rocks have zircons of B1 (1200–900 Ma), and B3 (500–75 Ma) subpopulations (Bush et al., 2016) (Fig. 3-6). The lack of zircons of these subpopulations in our samples suggests that the Sangre de Cristo Range was not a major sediment source during the Eocene. Therefore, the Wet Mountains was the major topographic feature surrounding the Wet Mountain Valley during the Eocene. The Sangre de Cristo Range was encompassed by the San Luis uplift. The uplift was exhumed during the late Paleozoic Ancestral Rocky Mountain orogeny, and was re-exhumed during the Laramide deformation (Lindsey, 2010). The exhumation of the Sangre de Cristo Range was further constrained to occur during the early stage (latest Cretaceous-Paleocene) of the Laramide deformation based on a sediment provenance study in the Raton Basin (Bush et al., 2016). Our interpretation that the Wet Mountains was the major regional topographic feature during the Eocene may suggest that exhumation of the Laramide ranges in the southern Rockies was temporally diachronous. This inference is consistent with the previous interpretation that the San Luis uplift, encompassing the Sangre de Cristo Range, was not a dominant topographic feature during the Eocene, based on the relationship between sedimentation and deformation (Hoy and Ridgway, 2002).

Based on paleocurrent measurement and the absence of B1 and B3 subpopulations in the Eocene Huerfano, Cuchara, and Poison Canyon Formations in the Huerfano Basin (Fig. 3-6), it is inferred that a paleoriver drained from north to south in the Wet Mountain Valley during the Eocene (Rasmussen and Foreman, 2017). The age distribution of our samples in the Farisita Conglomerate in the Wet Mountain Valley is very similar to those in the Huerfano Basin to the south (Fig. 3-6), supporting the interpretation of a southward-flowing river during the Eocene. Our sample age distribution is also similar to that of the Eocene Farisita Conglomerate in the subsurface of the Raton Basin further to the south (Bush et al., 2016) (Fig. 3-6), suggesting that the paleodrainage in the Wet Mountain Valley, Huerfano Basin, and Raton Basin was connected during the Eocene.

Based on the interpretation that the major sediment source during the early Eocene was the Wet Mountains but not the San Luis uplift, we infer that an ancient river, likely the paleo-Arkansas River, flowed in the Wet Mountain Valley as an axial river in front of the Wet Mountains (Fig. 3-7A). The presence of early Paleocene zircons (75–50 Ma, A3 subpopulation) in the lower Farisita Conglomerate (Gardner-5) suggests that the upper stream of the paleodrainage extended to the north of the Sangre de Cristo Range, where local Laramide intrusion occurred during the latest Cretaceous-earliest Eocene (Cunningham et al., 1994) (Fig. 3-7A). The upper stream of the paleodrainage may have gradually migrated southward and the Laramide intrusion was excluded from the drainage during the deposition of the middle and upper Farisita Conglomerate because of the lack of A3 subpopulation (Fig. 3-4). The fraction of subpopulation B2 (550–500 Ma) also decreases from the lower to the upper Farisita Conglomerate. Without major changes in the distributions of detrital zircon ages, we attribute this trend to a depositional switch between trunk stream and local point source of the alluvial fan.

3.5.3 Change of drainage pattern after filling basins by the early Oligocene

The latest Eocene-earliest Oligocene Devils Hole Formation on the Greenhorn Mountain contains 4% of subpopulations B1 and B3 (Fig. 3-5). Because the Mesozoic and Paleozoic sedimentary rocks on the Wet Mountains had been removed before the deposition of the Farisita Conglomerate in the Eocene, these grains in the Devils Hole Formation cannot be derived from the Wet Mountains. These grains were most likely derived from the Sangre de Cristo Range (Fig. 3-7B), on which the sedimentary rocks cover should have been thicker during the latest Eocene-earliest Oligocene than today. Because Greenhorn Mountain is the highest peak of the Wet Mountains, sediment transport from the Sangre de Cristo Range requires that the Wet Mountain Valley and Huerfano Basin to be filled up by sedimentation by the late Eocene.

Our interpretation of basin aggradation in the Wet Mountain Valley and the Huerfano Basin during the Eocene is supported by the presence of ash-flow of the Fish Canyon Tuff (27 Ma) at multiple highland localities, including the northern Wet Mountains, the Echo Park and Fear Canyon across the modern Arkansas Valley, and the Rosita Volcanic Field to the south of the Valley (Epis and Chapin, 1974; McIntosh and Chapin, 2004) (Fig. 3-1B). The tuff was erupted from the La

Garita caldera in the San Juan volcanic field, and it is widespread for being one of the largest eruptions of the field (Steven and Lipman, 1976). Ash on highland suggests that the basin was filled up to reduce the local relief. The age of the ash suggests that the basin aggradation had lasted at least until the late Oligocene (ca. ~27 Ma).

The lack of zircons of subpopulation B2 (550-550 Ma) in the Devils Hole Formation suggests that the north-to-south flowing paleo-Arkansas River may have changed its course during aggradation of the Wet Mountain Valley (Fig. 3-7B). After the modern Arkansas River flows southward in the upper Arkansas River valley, it does not continuously flow southward following the northern Rio Grande Rift to the west of the Sangre de Cristo Range. Instead, the modern River turns sharply to east at Salida and flows into the lower valley to the north of the Wet Mountains (Fig. 3-1B). This eastward drainage pattern must have been developed during the late Eocene-Oligocene when the low-relief topography was achieved by basin aggradation before opening of the northern Rio Grande Rift. A recent study in the adjacent Great Plains in southwestern Kansas discovered at least 85-m-thick uppermost Eocene-Oligocene strata (36.4-27.4 Ma) that unconformably overlies the Upper Cretaceous (Smith et al., 2017). The early Oligocene deposition on the Great Plains is coincident with the aggradation of the Wet Mountain Valley, likely reflecting syndepositional incision of the lower valley by the paleoriver. The latest Eocene-Oligocene strata in the Great Plains also contain abundant zircons of populations C and D (Fig. 3-6), suggesting that the drainage contains Proterozoic basement. The presence of Paleocene and Grenvillian zircons in the Great Plains and lack of such grains in our latest Eocene-Oligocene samples in the southern Rockies (Fig. 3-6) may suggest downstream increase of sediment recycling from Phanerozoic sedimentary rocks.

3.5.4 Miocene dissection of the low-relief paleosurface and establishment of the Arkansas River drainage

The low-relief surface formed by basin aggradation was dissected by Miocene extension. The two Miocene samples, 69Airport-1 in the Wet Mountain Valley and Badger Creek-1 in the South Park Basin have different age distributions. 69Airport-1 has a major peak at ~27 Ma and the dominant basement population is D (1800-1600 Ma), while Badger Creek-1 has a major peak at ~35 Ma and the dominant basement population is C (1500-1300 Ma). These differences suggest that the sediment sources in the two basins are different. The ~27 Ma peak reflects recycling of upper Oligocene strata containing the Fish Canyon Tuff, while the ~35 Ma peak reflects recycling of the latest Eocene-early Oligocene strata, which has abundant syndepositional tuff from the San Juan volcanic field. The presence of both peaks in the two samples suggests Miocene erosion of the late Eocene-Oligocene strata deposited during basin aggradation. The sample in the South Park Basin (~17 Ma) to the northwest is older than the sample in the Wet Mountain Valley (~11 Ma) to the southeast, while the dominant source unit in the middle

Cenozoic strata in the South Park Basin is older than the southeast, suggesting unroofing of sedimentary cover was faster in the northwest than the southeast. The faster unroofing in the northwest may be a result of uplift induced by mantle upwelling beneath the Colorado Plateau to the west of the study area (Moucha et al., 2008). The magnitude of uplift should decrease eastward as the area becomes farther away from the Colorado Plateau. The dominant basement population, C or D, in the two samples also reflects erosion of local basement. Near the South Park Basin, the local source containing 1500-1300 Ma basement is the southern Mosquito Range to the west of the Basin (Kellogg et al., 2017) (Fig. 3-1B). Thus, we infer that the Miocene sediment source of the South Park Basin was primarily the Mosquito Range. The dominant D population in the Wet Mountain Valley suggests that the primary sediment sources could be both the Wet Mountains and the Sangre de Cristo Range. One recent low temperature thermochronology study has suggested that extension associated with the Rift occurred between 25 and 10 Ma, after the Oligocene ignimbrite flare-up (Ricketts et al., 2016). Another study, focused on the upper Arkansas River valley, has suggested that the extension initiated between 22 and 18 Ma (Abbey and Niemi, 2018). Our interpretation of sediment provenance derived from local source unroofing broadly coincide with the thermochronology results, suggesting that the Miocene opening of the northern Rio Grande Rift formed the modern upper Arkansas River valley and connected the lower and upper Valleys to form the modern Arkansas River valley.

3.6 Conclusions

We study detrital zircon U-Pb ages of early Eocene-Miocene sedimentary rocks in south-central Colorado and use their maximum depositional ages and provenance information constrain the landscape and paleodrainage evolution in the southern Rockies. Maximum depositional ages derived from the groups of youngest zircons improve the absolute ages of the latest Eocene-Oligocene strata because of the presence of abundant air-fall zircons derived from intense synchronous volcanism. The detrital zircons contain major populations of 75–11 Ma, 1500–1300 Ma, and 1800–1500 Ma, and minor populations of 1300–950 Ma and 2709–1800 Ma. We conclude that the landscape and paleodrainage pattern in the southern Rockies experienced three distinctive stages including that (1) during the early Eocene, the Wet Mountains was the dominant local topographic feature, and a southward river, likely the paleo-Arkansas River, connected the Wet Mountain Valley with the Huerfano and Raton Basins to the south; (2) during the Eocene-early Oligocene, the Wet Mountain Valley and the Huerfano Basin experienced basin aggradation to form a low-relief surface, and subsequent river erosion on the low-relief surface carved the eastward lower Arkansas River valley; and (3) during the Miocene, the opening of the Rio Grande Rift dissected the low-relief surface and formed the upper Arkansas River valley, and the upper valley was connected with the lower Valley to establish the modern drainage pattern of the Arkansas

River in the southern Rockies. The study highlights that the middle-Cenozoic landscape in the southern Rockies was mostly resulted from tectonics.

Acknowledgement

This research was supported by National Science Foundation [grant number EAR-1454802]. We would like to thank Emma Gains for her help in the field, and Dr. Lin Li and Hepeng Tian for their help in the lab. We also thank Dr. Paul Link and editor Dr. Jasper Knight for their constructive comments.

References

Abbey, A.L., Niemi, N.A., 2018. Low-temperature thermochronometric constraints on fault initiation and growth in the northern Rio Grande rift, upper Arkansas River valley, Colorado, USA. Geology 46, 627–630.

Bickford, M.E., Van Schmus, W.R., Karlstrom, K.E., Mueller, P.A., Kamenov, G.D., 2015. Mesoproterozoic-trans-Laurentian magmatism: A synthesis of continent-wide age distributions, new SIMS U-Pb ages, zircon saturation temperatures, and Hf and Nd isotopic compositions. Precambrian Research 265, 286–312.

Bonnet, S., 2009. Shrinking and splitting of drainage basins in orogenic landscapes from the migration of themain drainage divide. Nature Geoscience 2, 766–771.

Bush, M.A., Horton, B.K., Murphy, M.A., Stockli, D.F., 2016. Detrital record of initial basement exhumation along the Laramide deformation front, southern

Rocky Mountains. Tectonics 35, 2117–2130.

Castelltort, S., Goren, L., Willett, S.D., Champagnac, J.D., Herman, F., Braun, J., 2012. River drainage patterns in the New Zealand Alps primarily controlled by plate tectonic strain. Nature Geoscience 5, 744–748.

Cather, S.M., Chapin, C.E., Kelley, S.A., 2012. Diachronous episodes of Cenozoic erosion in southwestern North America and their relationship to surface uplift, paleoclimate, paleodrainage, and paleoaltimetry. Geosphere 8, 1177–1206.

Chapin, C.E., Kelley, S.A., Cather, S.M., 2014. The Rocky Mountain Front, southwestern USA. Geosphere 10, 1043–1060.

Chapin, C.E., Wilks, M., Mcintosh, W.C., 2004. Space-time patterns of Late Cretaceous to present magmatism in New Mexico—comparison with Andean volcanism and potential for future volcanism. New Mexico Bureau of Geology and Mineral Resources, Bulletin 160, 13–40.

Coblentz, D., Chase, C.G., Karlstrom, K.E., Van Wijk, J., 2011. Topography, the geoid, and compensation mechanisms for the southern Rocky Mountains. Geochemistry, Geophysics, Geosystems 12, Q04002.

Copeland, P., Murphy, M.A., Dupre, W.R., Lapen, T.J., 2011. Oligocene Laramide deformation in southern New Mexico and its implications for Farallon plate geodynamics. Geosphere 7, 1209–1219.

Cosca, M.A., Thompson, R.A., Lee, J.P., Turner, K.J., Neymark, L.A., Premo, W.R., 2014. $^{40}Ar/^{39}Ar$ geochronology, isotope geochemistry (Sr, Nd, Pb), and petrology of alkaline lavas near Yampa, Colorado: Migration of alkaline volcanism and evolution of the northern Rio Grande rift. Geosphere 10, 374–400.

Cullers, R.L., Griffin, T., Bickford, M.E., Anderson, J.L., 1992. Origin and chemical evolution of the 1360 Ma San Isabel Batholith, Wet Mountains, Colorado: a mid-crustal granite of anorogenic affinities. Geological Society of America Bulletin 104, 316–328.

Cunningham, C.G., Naeser, C.W., Marvin, R.F., Luedke, R.G., Wallace, A.R., 1994. Ages of Selected Intrusive Rocks ana Associated Ore Deposits in the Colorado Mineral Belt. U.S. Geological Survey Bulletin 2109, 1–37.

Dalziel, I.W.D., 1997. Neoproterozoic-paleozoic geography and tectonics: Review, hypothesis, environmental speculation. Bulletin of the Geological Society of America 109, 16–42.

Dick, R., Nish, M., 1966. The Cenozoic history of the Wet Mountain Valley, Colorado. University of Michigan, Ph.D dissertation. 120 p.

Dickinson, W.R., Gehrels, G.E., 2009. U-Pb ages of detrital zircons in Jurassic eolian and associated sandstones of the Colorado plateau: Evidence for transcontinental dispersal and intraregional recycling of sediment. Bulletin of the Geological Society of America 121, 408–433.

Donahue, M.M.S., 2016. Episodic uplift of the Rocky Mountains: evidence from U-Pb detrital zircon geochronology and low-temperature thermochronology with a chapter on using mobile technology for geoscience and education. The University of New Mexico, Albuquerque. Earth & Planetary Sciences Ph.D dissertation. 188 p.

Eaton, G.P., 1987. Topography and origin of the southern Rocky Mountains and Alvarado Ridge. Geological Society, London, Special Publications 28, 355–369.

Eaton, G.P., 2009. Epeirogeny in the Southern Rocky Mountains region: Evidence and origin. Geosphere 5, 408–408.

Epis, R.C., Chapin, C.E., 1974. Stratigraphic Nomenclature of the Thirtynine Mile Volcanic Field, Central Colorado. Geological Survey Bulletin 1395–C, 32 p.

Epis, R.C., Scott, G.R., Taylor, R.B., Chapin, C.E., 1976. Cenozoic volcanic, tectonic, and geomorphic features of central Colorado. CSM Professional Contributions 8, 323–338.

Epis, R.C., Scott, G.R., Taylor, R.B., Chapin, C.E., 1980. Summary of Cenozoic geomorphic, volcanic, and tectonic features of central Colorado and adjoining areas. Colorado Geology. Rocky Mountain Association of Geologist-1980 Symposium. 135–156.

Fan, M., Brown, E., Li, L., 2018. Cenozoic drainage evolution of the Rio Grande paleoriver recorded in detrital zircons in South Texas. International Geology Review. online, 1–15.

Fan, M., Mankin, A., Chamberlain, K., 2015. Provenance and depositional ages of

Late Paleogene fluvial sedimentary rocks in the central Rocky Mountains, USA. Journal of Sedimentary Research 85, 1416–1430.

Frost, B.R., Chamberlain, K.R., Swapp, S., Frost, C.D., Hulsebosch, T.P., 2000. Late Archean structural and metamorphic history of the Wind River Range: Evidence for a long-lived active margin on the Archean Wyoming craton. Bulletin of the Geological Society of America 112, 564–578.

Gehrels, G., 2012. Detrital Zircon U-Pb Geochronology: Current Methods and New Opportunities, in: Busby, C., Azor, A. (Eds.), Tectonics of Sedimentary Basins: Recent Advances. Blackwell Publishing Ltd., New Jersey, pp. 45–62.

Gregory, K.M., Chase, C.G., 1994. Tectonic and climatic significance of a late Eocene low-relief, high-level geomorphic surface, Colorado. Journal of Geophysical Research 99, 141–160.

Gregory, K.M., McIntosh, W.C., 1996. Paleoclimate and paleoelevation of the Oligocene Pitch-Pinnacle flora, Sawatch Range, Colorado. GSA Bulletin 108, 545–561.

Hansen, S.M., Dueker, K.G., Stachnik, J.C., Aster, R.C., Karlstrom, K.E., 2013. A rootless rockies - Support and lithospheric structure of the Colorado Rocky Mountains inferred from CREST and TA seismic data. Geochemistry, Geophysics, Geosystems 14, 2670–2695.

Hoffman, P.F., 1988. United plates of America , the birth of craton: Early Proterozoic assembly and growth of Laurentia. Annual Review of Earth and

Planetary Sciences 16, 543–603.

Hoy, R.G., Ridgway, K.D., 2002. Syndepositional thrust-related deformation and sedimentation in an Ancestral Rocky Mountains basin, Central Colorado trough, Colorado, USA. Bulletin of the Geological Society of America 114, 804–828.

Hubbard, M.S., Oviatt, C.G., Kelley, S.A., Perkins, M.E., Hodges, K. V., Robbins, R., 2001. Oligocene-Miocene basin formation and modification in the northern Rio Grande rift; constraints from $^{40}Ar/^{39}Ar$, fission track, and tephrochronology. Geological Society of America Abstracts with Programs 33, A-257.

Johnson, R.B., 1959. Geology of the Huerfano Park Area Huerfano and Custer Counties Colorado. U.S. Geological Survey Bulletin 1071–D, 40p.

Karlstrom, K.E., Coblentz, D., Dueker, K., Ouimet, W., Kirby, E., Van Wijk, J., Schmandt, B., Kelley, S., Lazear, G., Crossey, L.J., Crow, R., Aslan, A., Darling, A., Aster, R., MacCarthy, J., Hansen, S.M., Stachnik, J., Stockli, D.F., Garcia, R. V., Hoffman, M., McKeon, R., Feldman, J., Heizler, M., Donahue, M.S., 2012. Mantle-driven dynamic uplift of the Rocky Mountains and Colorado Plateau and its surface response: Toward a unified hypothesis. Lithosphere 4, 3–22.

Kelley, S. a, Chapin, C.E., 2004. Denudation history and internal structure of the Front Range and Wet Mountains , Colorado , based on apatite - fission - track thermochronology. New Mexico Bureau of Geology and Mineral Resources Bulletin 1, 41–78.

Kellogg, K.S., 1999. Neogene basins of the northern Rio Grande rift: Partitioning and asymmetry inherited from Laramide and older uplifts. Tectonophysics 305, 141–152.

Kellogg, K.S., Shroba, R.R., Ruleman, C.A., Bohannon, R.G., William C. McIntosh, Premo, W.R., Cosca, M.A., Moscati, R.J., Brandt, T.R., 2017. Geologic Map of the Upper Arkansas River Valley Region , North-Central Colorado (No. 3382). US Geological Survey.

Kluth, C.F., 1986. Plate tectonics of the Ancestral Rocky Mountains: Part III. Middle Rocky Mountians, in: Paleotectonics and Sedimentation in the Rocky Mountian Region, United States: American Association of Petroleum Geologists Memoir 41. pp. 353–369.

Landman, R.L., Flowers, R.M., 2013. (U-Th)/He thermochronologic constraints on the evolution of the northern Rio Grande Rift, Gore Range, Colorado, and implications for rift propagation models. Geosphere 9, 170–187.

Lazear, G., Karlstrom, K., Aslan, A., Kelley, S., 2013. Denudation and flexural isostatic response of the Colorado Plateau and southern Rocky Mountains region since 10 Ma. Geosphere 9, 792–814.

Leonard, E.M., 2002. Geomorphic and tectonic forcing of late Cenozoic warping of the Colorado piedmont. Geology 30, 595–598.

Lindsey, D.A., 2010. The Geologic Story of Colorado's Sangre de Cristo Range. US Department of the Interior, US Geological Survey, Circular 1349. 24 p.

Link, P.K., Fanning, C.M., Beranek, L.P., 2005. Reliability and longitudinal change of detrital-zircon age spectra in the Snake River system, Idaho and Wyoming: An example of reproducing the bumpy barcode. Sedimentary Geology 182, 101–142.

Lipman, P.W., 2007. Incremental assembly and prolonged consolidation of Cordilleran magma chambers: Evidence from the Southern Rocky Mountain volcanic field. Geosphere 3, 42–70.

Ludwig, K.R., Mundil, R., 2002. Extracting reliable U-Pb ages and errors from complex populations of zircons from Phanerozoic tuffs. Goldschmidt Conference Abstracts A463.

Maughan, E.K., 1988. Geology and petroleum potential, Colorado Park Basin Province, North-central Colorado, United State Geological Survey Open-File Report 88-450 E.

McIntosh, W.C., Chapin, C.E., 2004. Geochronology of the central Colorado volcanic field. New Mexico Bureau of Geology & Mineral Resources, Bulletin 160, 205–237.

McMillan, M.E., Heller, P.L., Wing, S.L., 2006. History and causes of post-Laramide relief in the Rocky Mountain orogenic plateau. Bulletin of the Geological Society of America 118, 393–405.

Morgan, L.E., Cosca, M.., 2017. Argon data for Poncha Pass Map: U.S. Geological Survey data release. https://doi.org/10.5066/F7PV6J8X.

Moscati, R.J., Premo, W.R., DeWitt, E.H., Wooden, J.L., 2017. U-Pb ages and geochemistry of zircon from Proterozoic plutons of the Sawatch and Mosquito ranges, Colorado, U.S.A.—Implications for crustal growth of the central Colorado Province. Rocky Mountain Geology 52, 17–106.

Moucha, R., Forte, A.M., Rowley, D.B., Mitrovica, J.X., Simmons, N.A., Grand, S.P., 2008. Mantle convection and the recent evolution of the Colorado Plateau and the Rio Grande Rift valley. Geology 36, 439–442.

Pelletier, J.D., 2009. The impact of snowmelt on the late Cenozoic landscape of the southern Rocky Mountains, USA. GSA Today 19, 4–11.

Perkins, M.E., Nash, B.P., 2002. Explosive silicic volcanism of the Yellowstone hotspot: The ash fall tuff record. Bulletin of the Geological Society of America 114, 367–381.

Prothero, D.R., Emry, R.J., 2004. The Chadronian, Orellan, and Whitneyan North American Land Mammal Ages, in: Woodburne, M.O. (Ed.), Late Cretaceous and Cenozoic Mammals of North America: Biostratigraphy and Geochronology. Columbia University Press, New York, pp. 156–168.

Rasmussen, D.M., Foreman, B.Z., 2017. Provenance of lower Paleogene strata in the Huerfano Basin: Implications for uplift of the Wet Mountains, Colorado, U.S.S. Journal of Sedimentary Research 87, 579–593.

Ricketts, J.W., Kelley, S.A., Karlstrom, K.E., Schmandt, B., Donahue, M.S., van Wijk, J., 2016. Synchronous opening of the Rio Grande rift along its entire length at 25-10 Ma supported by apatite (U-Th)/He and fission-track thermochronology, and evaluation of possible driving mechanisms. Bulletin of the Geological Society of America 128, 397–424.

Roberts, G.G., White, N.J., Crosby, A.G., Martin-Brandis, G.L., 2012. An uplift history of the Colorado Plateau and its surroundings from inverse modeling of longitudinal river profiles. Tectonics 31, 4.

Robinson, P., 1966. Fossil mammals of the Huerfano Formation, Eocene, of Colorado. Peabody Museum of Natural History Yale University Bulletin 21.

Robinson, P., Gunnell, G.F., Walsh, S.L., Clyde, W.C., Storer, J.E., Stucky, R.K., Forehlich, D.J., Ferrusquia-Villafranca, I., McKenna, M.C., 2004. Wasatchian through Duchesnean biochronology, in: Woodburne, M.O. (Ed.), Late Cretaceous and Cenozoic Mammals of North America: Biostratigraphy and Geochronology. Columbia University Press, pp. 106–155.

Rosenberg, R., Kirby, E., Aslan, A., Karlstrom, K., Heizler, M., Ouimet, W., 2014. Late Miocene erosion and evolution of topography along the western slope of the Colorado Rockies. Geosphere 10, 641–663.

Rowley, J., Fan, M., 2016. Middle Cenozoic diachronous shift to eolian deposition in the central Rocky Mountains: Timing, provenance, and significance for paleoclimate, tectonics, and paleogeography. Geosphere 12, 1795–1812.

Roy, M., Kelley, S., Pazzaglia, F., Cather, S., House, M., 2004. Middle Tertiary buoyancy modification and its relationship to rock exhumation, cooling, and subsequent extension at the eastern margin of the Colorado Plateau. Geology 32, 925–928.

Scott, G.R., Taylor, R.B., 1975. Post-Paleocene Tertiary Rocks and Quaternary Volcanic Ash of the Wet Mountain Valley, Colorado (No. 868). United States Government Printing Office.

Sims, P.K., Bankey, V., Finn, C.A., 2001. Preliminary Precambrian basement map of Colorado-A geologic interpretation of an aeromagnetic anomaly map. US Geological Survey Open-File Report 01-0364.

Sloss, L. l., 1988. Tectonic evolution of the craton in Phanerozoic time, in: Sedimentary Cover-North American Craton, U.S., Geological Society of America. pp. 25–51.

Smith, J.J., Ludvigson, G.A., Layzell, A., Möller, A., Harlow, R.H., Turner, E., Platt, B., Petronis, M., 2017. Discovery of Paleogene deposits of the Central High Plains Aquifer in the western Great Plains, U.S.A. Journal of Sedimentary Research 87, 880–896.

Stark, J.T., Johnson, J.H., Behre, C.H., Powers, W.E., Howland, A.L., Gould, D.B., 1949. Geology and Origin of South Park, Colorado. Geological Society of America. 188 p.

Steven, T.A., Lipman, P.W., 1976. Calderas of the San Juan Volcanic Field, Southwestern Colorado. USGS Professional Paper 958, 35 p.

Tomlinson, D.W., Copeland, P., Murphy, M.A., Lapen, T.J., 2013. Oligocne shortening in the Little Burro Mountains of southwest New Mexico. Rocky Mountain Geology 48, 169–183.

Tweto, O., 1961. Late Cenozoic events of the Leadville Distric and upper Arkansas Valley, Colorado. US Geological Survey Professional Paper 424, B133-135.

Van Alstine, R.E., 1971. Allochthonous Paleozoic blocks in the Tertiary San Luis-Upper Arkansas graben , Colorado. New Mexico Geological Society 22nd Annual Fall Field Conference Guidebook. 169–177.

Van Alstine, R.E., Lewis, G.E., 1960. Pliocene sediments near Salida, Chaffee County, Colorado. Sort papers in the geological sciences: US. Geological Survey Professoional Paer 400, B245.

Vermeesch, P., 2004. How many grains are needed for a provenance study? Earth and Planetary Science Letters 224, 441–451.

Vermeesch, P., Resentini, A., Garzanti, E., 2016. An R package for statistical provenance analysis. Sedimentary Geology 336, 14–25.

Whitmeyer, S.J., Karlstrom, K.E., 2007. Tectonic model for the Proterozoic growth of North America. Geosphere 3, 220–259.

Wolfe, J.A., Forest, C.E., Molnar, P., 1998. Paleobotanical evidence of Eocene and Oligocene paleoaltitudes in midlatitude western North America. Bulletin of the Geological Society of America 110, 664–678.

Figures and tables

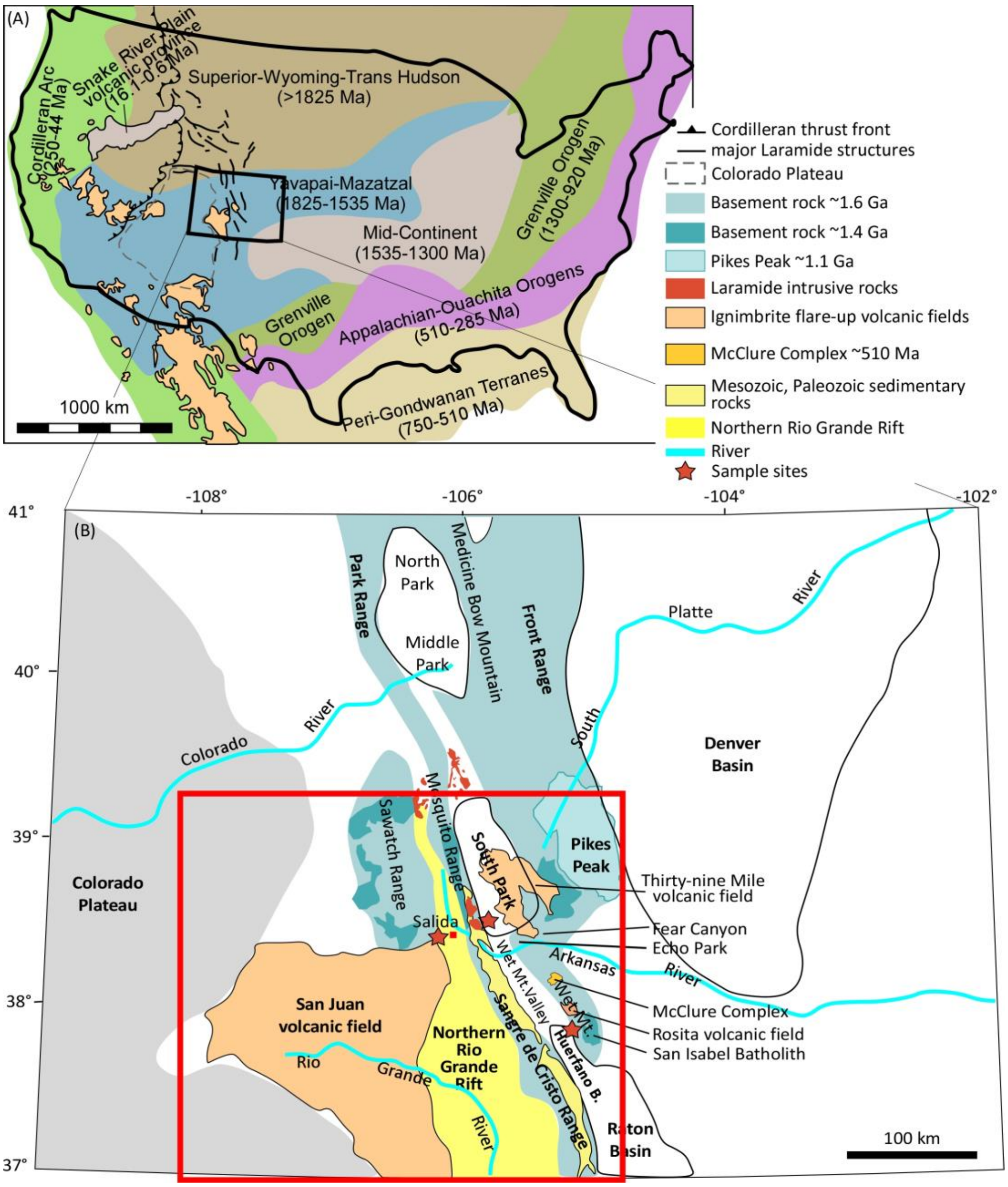

Figure 3-1 (A) Major zircon provinces in North America (after Dickinson and Gehrels, 2009) and location of the study area in the southern Rockies. (B) Simplified geologic map of the study area in south-central Colorado. The red rectangle indicates the map area in Figure 5.

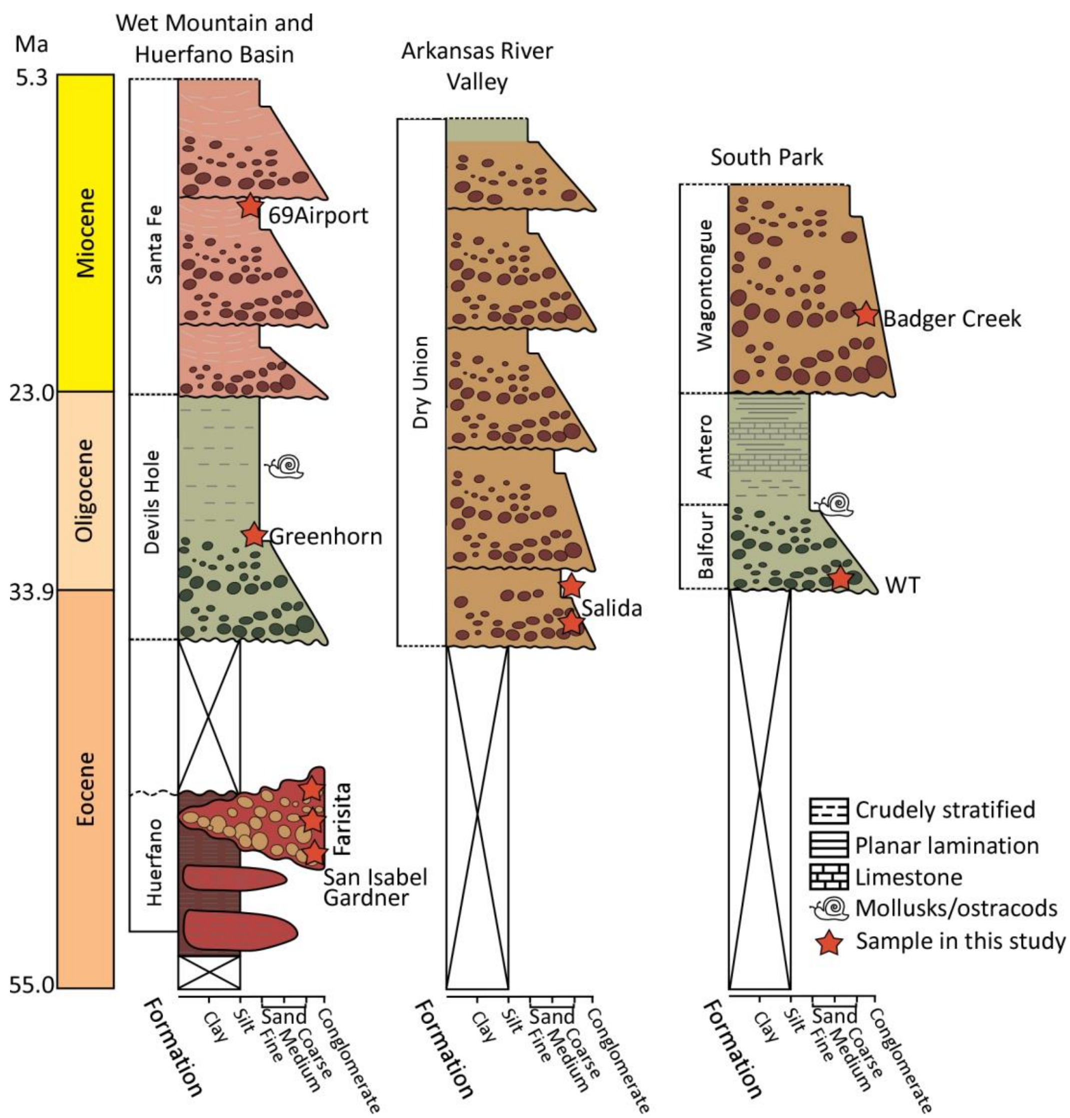

Figure 3-2 Simplified stratigraphic columns of the studied strata (modified after Scott and Taylor (1975), and Stark et al. (1949)). Time scale follows the Geological Time Scale 2012.

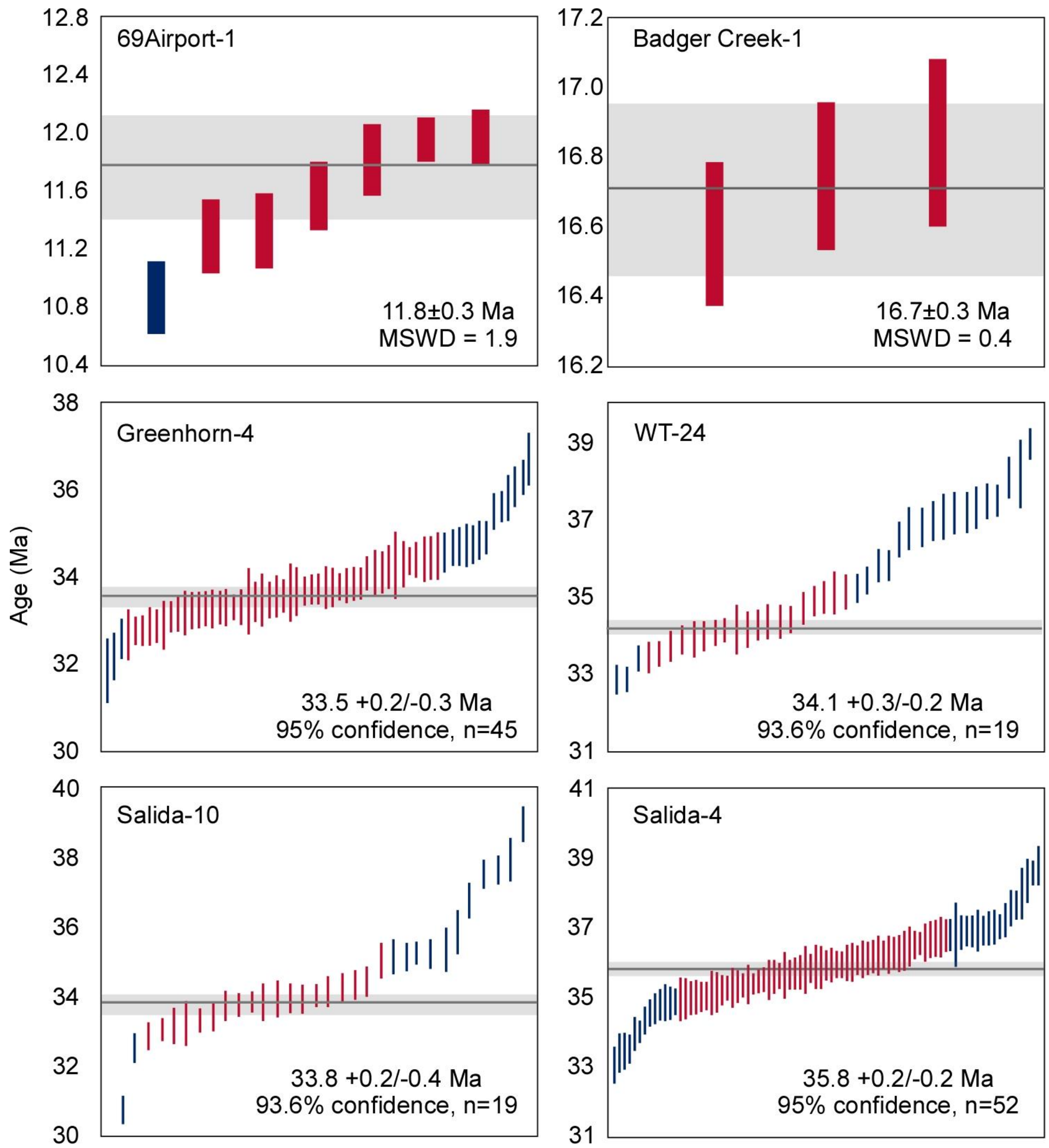

Figure 3-3 Maximum depositional ages of the Oligocene and Miocene samples. Bars represent 1σ internal error. MSWD=mean square of weighted deviation. Airport 69-1 and Bagder Creek-1 are calculated in weighted mean ages, and Greenhorn-4, WT-24, Salida-10 and -4 are calculated using TuffZirc algorithm (Ludwig and Mundil, 2002).

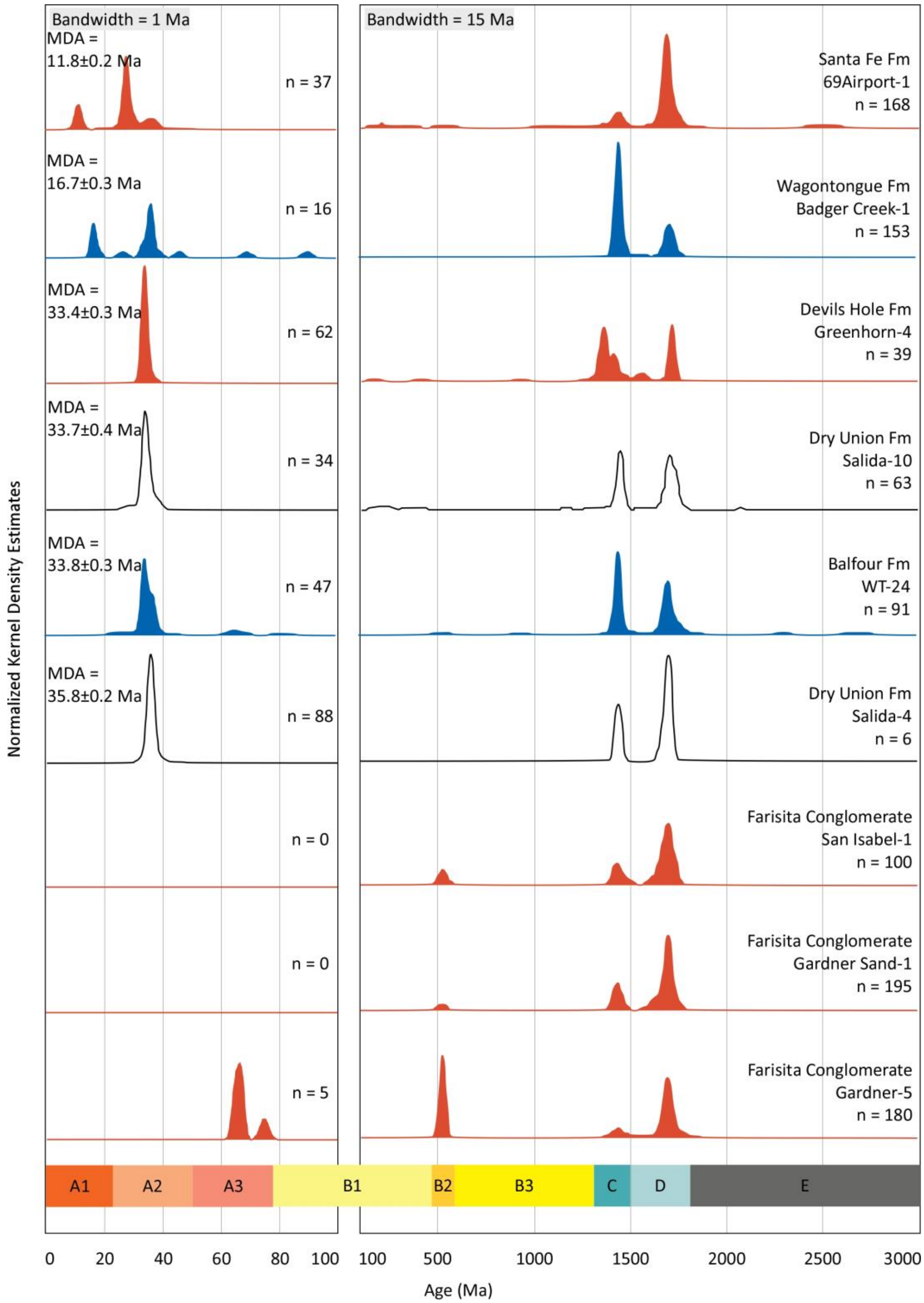

Bandwidth = 1 Ma
Bandwidth = 15 Ma
MDA =
11.8±0.2 Ma
n = 37
Santa Fe Fm
69Airport-1
n = 168
MDA =
16.7±0.3 Ma
n = 16
Wagontongue Fm
Badger Creek-1
n = 153
MDA =
33.4±0.3 Ma
n = 62
Devils Hole Fm
Greenhorn-4
n = 39
MDA =
33.7±0.4 Ma
n = 34
Dry Union Fm
Salida-10
n = 63
MDA =
33.8±0.3 Ma
n = 47
Balfour Fm
WT-24
n = 91
MDA =
35.8±0.2 Ma
n = 88
Dry Union Fm
Salida-4
n = 6
n = 0
Farisita Conglomerate
San Isabel-1
n = 100
n = 0
Farisita Conglomerate
Gardner Sand-1
n = 195
n = 5
Farisita Conglomerate
Gardner-5
n = 180
A1
A2
A3
B1
B2
B3
C
D
E
Normalized Kernel Density Estimates
0
20
40
60
80
100
100
500
1000
1500
2000
2500
3000
Age (Ma)

Figure 3-4 Normalized detrital zircon U-Pb age distributions of the studied samples. Kernel density estimates were conducted using R program following Vermeesch et al. (2016). A1-E represents populations and subpopulations defined by cluster of ages. See text for details of the populations and subpopulations. Curves in orange color represent samples from the Wet Mountain Valley, Huerfano Park, and Greenhorn Mountain. Curves in black color represent samples from the Arkansas Valley near Salida, CO. Curves in blue color represent samples from the South Park Basin. MDA=maximum depositional age. See Figure 5 for name and potential sources of each population and subpopulation.

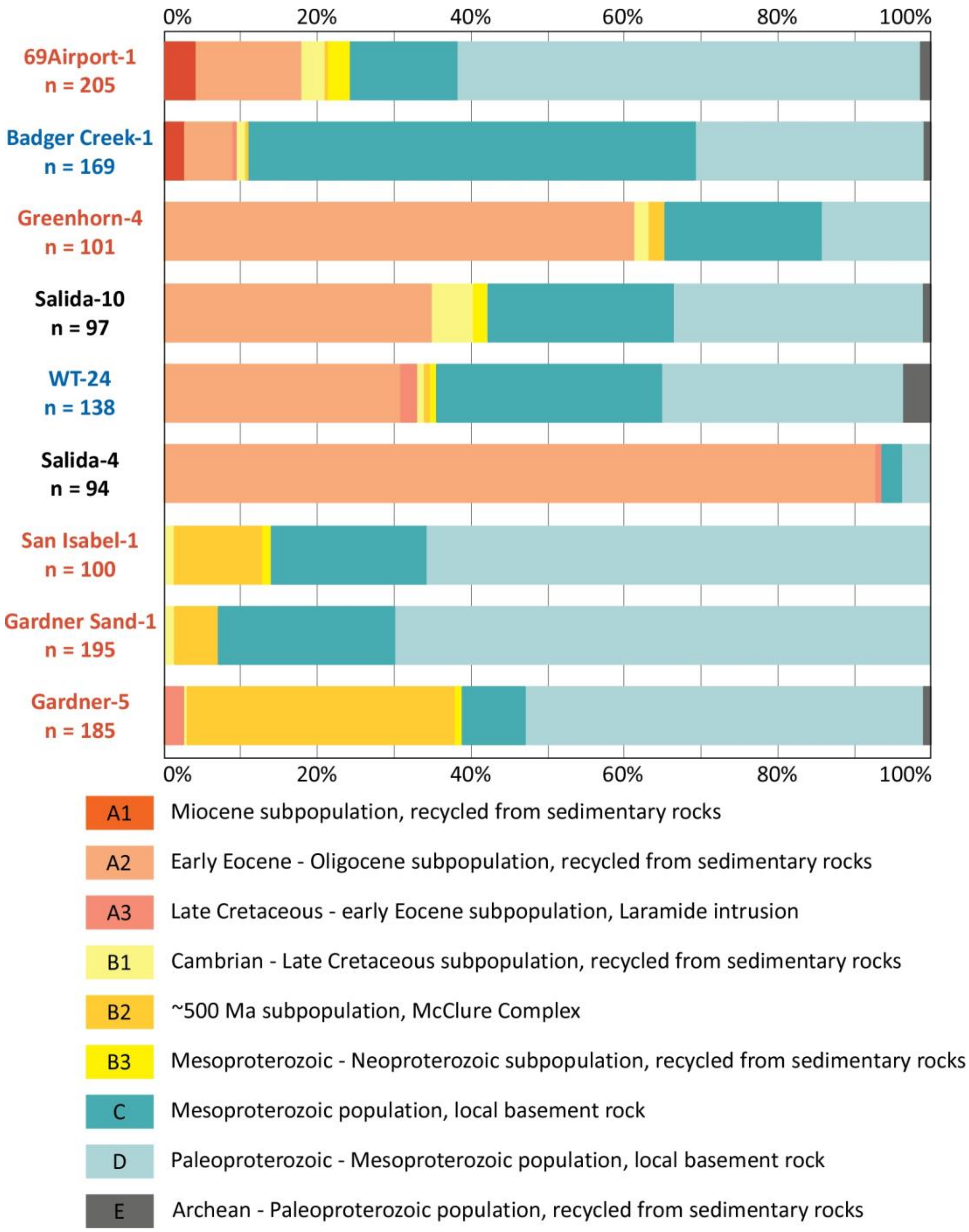

Figure 3-5 Relative abundance of defined zircon populations and subpopulations in each sample.

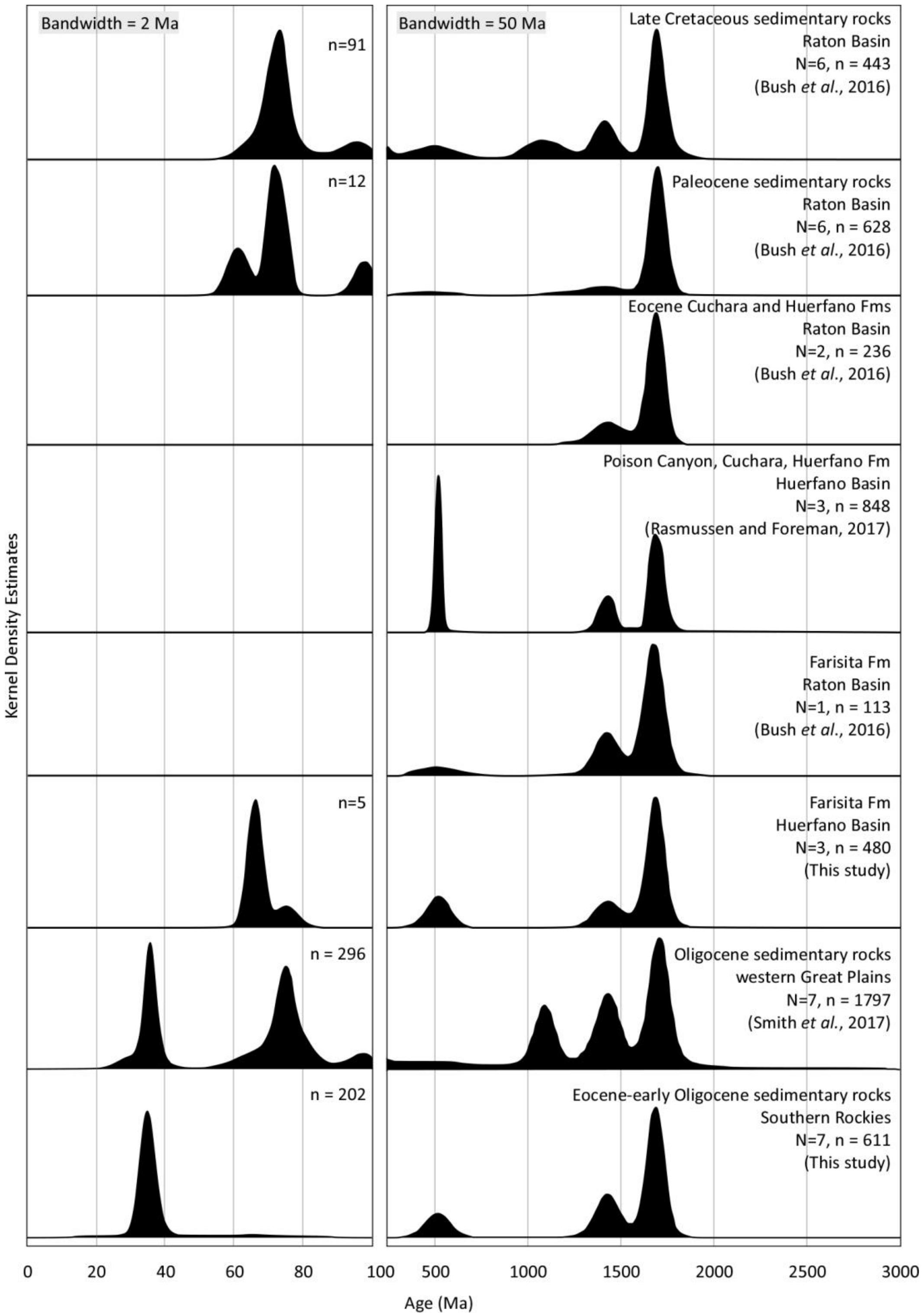
Bandwidth = 2 Ma
Bandwidth = 50 Ma
n=91
Late Cretaceous sedimentary rocks
Raton Basin
N=6, n = 443
(Bush et al., 2016)
n=12
Paleocene sedimentary rocks
Raton Basin
N=6, n = 628
(Bush et al., 2016)
Eocene Cuchara and Huerfano Fms
Raton Basin
N=2, n = 236
(Bush et al., 2016)
Poison Canyon, Cuchara, Huerfano Fm
Huerfano Basin
N=3, n = 848
(Rasmussen and Foreman, 2017)
Farisita Fm
Raton Basin
N=1, n = 113
(Bush et al., 2016)
n=5
Farisita Fm
Huerfano Basin
N=3, n = 480
(This study)
n = 296
Oligocene sedimentary rocks
western Great Plains
N=7, n = 1797
(Smith et al., 2017)
n = 202
Eocene-early Oligocene sedimentary rocks
Southern Rockies
N=7, n = 611
(This study)
Kernel Density Estimates
0
20
40
60
80
100
500
1000
1500
2000
2500
3000
Age (Ma)

Figure 3-6 Comparison of detrital zircon U-Pb age distributions of the latest Cretaceous-Oligocene strata in the southern Rockies and the Oligocene strata on the western Great Plains. N=number of samples combined. n=number of zircon grains.

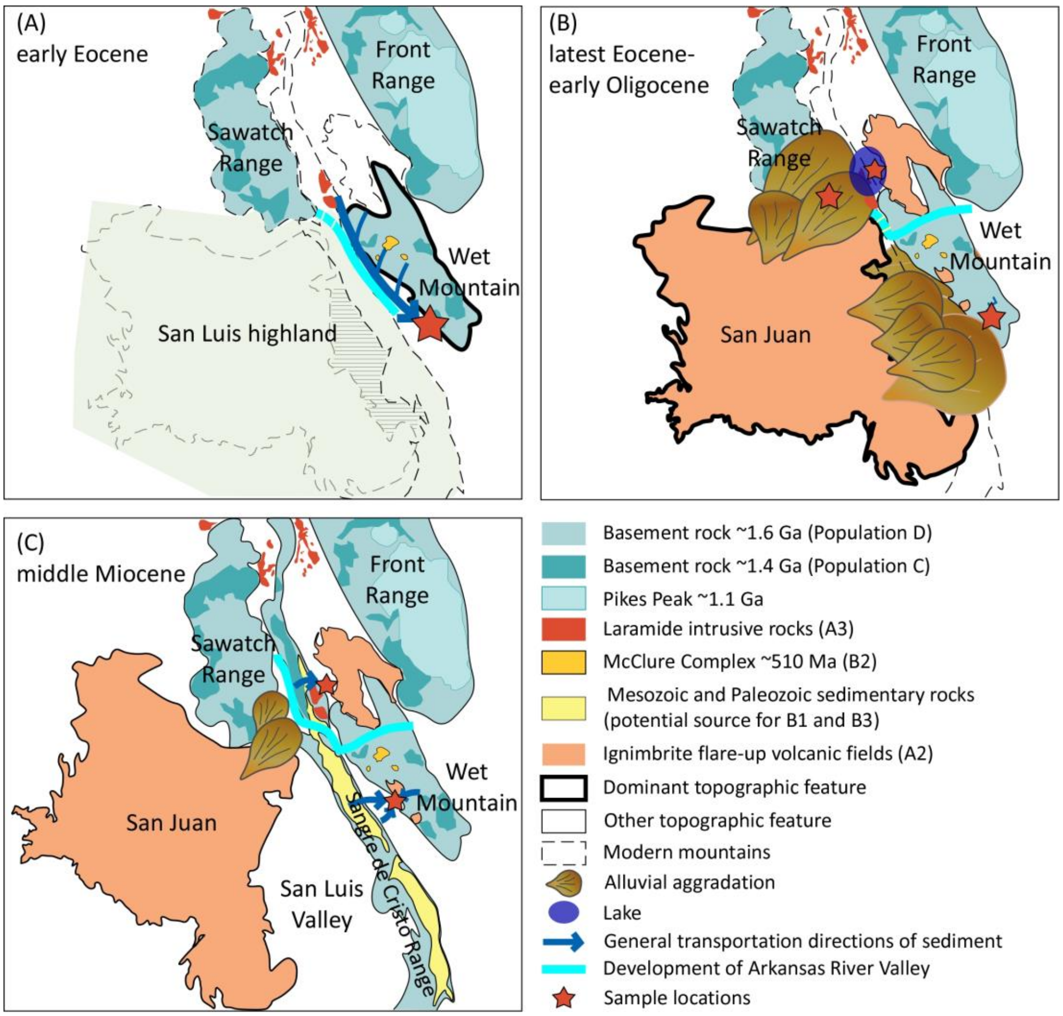

Figure 3-7 Evolution of landscape and paleodrainage in the southern Rockies during the late Eocene-middle Miocene. Basement map is modified from Sims et al. (2001) and Kellogg et al. (2017).

Table 3-1 Maximum depositional age and other age constraints of the studied strata

Sample location	Formation	Sample name and coordinate	Maximum depositional age (Ma)	Expected age	Sample site description	Depositional environment
Wet Mountain Valley	Santa Fe	69Airport-1 (37.985804, -105.308601)	11.8±0.2	Miocene-Pliocene (Scott and Taylor, 1975)	Orange red, crudely stratified, poorly sorted, interbedded pebble to cobble conglomerate and medium- to coarse-grained sandstone	Alluvial (Scott and Taylor, 1975)
	Devils Hole	Greenhorn-4 (37.894197, -105.041446)	33.4±0.3	Late Eocene-Oligocene (Scott and Taylor, 1975)	~150 m thick, grey, stratified, poorly sorted, fine- to medium-grained muddy sandstone. Contains some mollusk shell fragments.	Alluvial debris flow and lahar (Scott and Taylor, 1975)
	Conglomerate	San Isabel-1 (37.898103, -105.227803)	N.A	Eocene (Scott and Taylor, 1975)	Poorly sorted, well rounded, cobble to boulder conglomerate. Clasts are predominantly granite and gneiss. Lower part is brown, crudely stratified, clast-supported, and upper part is brownish orange, cross-stratified, matrix-supported. Samples are matrix of the conglomerate.	Alluvial (Johnson, 1959; Scott and Taylor, 1975; Rasmussen and Foreman, 2017)
		Gardner Sand-1 (37.841211 -105.131695)	N.A			
		Gardner-5 (37.854933 -105.316049)	N.A			
Salida	Dry Union	Salida-10 (38.511804, -106.023809)	33.7±0.4	Miocene-Pliocene (Van Alstine and	~120 m thick, interbedded dark grey, cross-stratified, matrix-supported	Alluvial (Scott and Taylor, 1975)

				Lewis, 1960; Hubbard et al., 2001)	conglomerate, medium-grained sandstone, and paleosol. Outcrop contains white ash beds. Sample was collected from a pumice-bearing sandstone in the lower part. Two ash beds near the top were previously dated to be 11-8 Ma.	
	Dry Union	Salida-4 (38.666607, -106.100006)	35.8±0.2		~100 m thick, yellowish brown, poorly sorted, medium- to coarse-grained sandstone interbedded with conglomerate. Sample is the matrix of the conglomerate near the top of the exposure	
South Park	Wagon tongue	Badger Creek-1 (38.750948 -105.851845)	16.7±0.3	Miocene-Pliocene (Stark et al., 1949)	~5 m thick, black, crudely stratified, poorly sorted, pebble to cobble conglomerate and medium-grained sandstone	Alluvial (Stark et al., 1949)
	Balfour	WT-24 (38.807301 -105.777202)	33.8±0.3	Oligocene (Stark et al., 1949)	3 m thick, light grey, crudely stratified, tuffaceous conglomerate and medium- to coarse-grained sandstone. Clasts are exclusively tuffaceous mudstone.	Lacustrine (Stark et al., 1949)

N.A.=not applicable

Table 3-2 Zircon data presented in this chapter

											Age		Age		Age			
Spot #	U	206Pb	U/Th	206Pb*	± (1σ)	207Pb*	± (1σ)	206Pb*	± (1σ)	error	206Pb*	±	207Pb*	±	206Pb*	±	Best age	±
	(ppm)	204Pb		207Pb*	(%)	235U*	(%)	238U	(%)	corr.	238U*	(Ma)	235U	(Ma)	207Pb*	(Ma)	(Ma)	(Ma)
69 Airport-1	263	1255	1.6	18.8482	7.8	0.0123	8.2	0.0017	2.3	0.28	10.9	0.3	12.5	1.0	330.2	177.7	10.9	0.3
69 Airport-1	149	1944	1.4	22.2316	5.2	0.0109	5.7	0.0018	2.3	0.40	11.3	0.3	11.0	0.6	NA	NA	11.3	0.3
69 Airport-1	3303	4098	0.5	9.4300	13.3	0.0257	13.5	0.0018	2.4	0.17	11.3	0.3	25.8	3.4	1731.7	245.1	11.3	0.3
69 Airport-1	120	12317	2.4	18.4157	6.3	0.0134	6.6	0.0018	2.0	0.30	11.6	0.2	13.6	0.9	382.6	141.0	11.6	0.2
69 Airport-1	126	2148	1.8	14.7600	8.7	0.0171	9.0	0.0018	2.1	0.24	11.8	0.2	17.3	1.5	860.0	181.2	11.8	0.2
69 Airport-1	154	4202	2.3	19.9208	5.5	0.0128	5.7	0.0019	1.3	0.23	12.0	0.2	13.0	0.7	203.2	128.5	12.0	0.2
69 Airport-1	172	752	1.8	23.1477	14.2	0.0111	14.3	0.0019	1.7	0.12	12.0	0.2	11.2	1.6	NA	NA	12.0	0.2
69 Airport-1	131	1859	1.0	15.9790	7.8	0.0307	8.0	0.0036	1.6	0.20	22.9	0.4	30.7	2.4	693.2	167.3	22.9	0.4
69 Airport-1	114	880	1.4	29.0112	4.7	0.0194	4.9	0.0041	1.5	0.31	26.3	0.4	19.5	0.9	NA	NA	26.3	0.4
69 Airport-1	765	6477	0.6	21.5533	3.1	0.0265	3.4	0.0041	1.3	0.38	26.6	0.3	26.5	0.9	17.2	75.4	26.6	0.3
69 Airport-1	113	497	1.2	58.8579	20.1	0.0098	20.2	0.0042	1.7	0.08	26.9	0.5	9.9	2.0	NA	NA	26.9	0.5
69 Airport-1	164	1473	1.9	25.2470	3.9	0.0229	4.2	0.0042	1.5	0.36	27.0	0.4	23.0	0.9	NA	NA	27.0	0.4
69 Airport-1	148	3311	1.2	20.0750	4.9	0.0293	5.1	0.0043	1.7	0.32	27.4	0.5	29.3	1.5	185.2	113.5	27.4	0.5
69 Airport-1	107	637	1.4	38.4502	20.4	0.0153	20.5	0.0043	1.9	0.09	27.4	0.5	15.4	3.1	NA	NA	27.4	0.5
69 Airport-1	724	4398	3.1	22.4175	4.3	0.0264	4.4	0.0043	1.2	0.27	27.6	0.3	26.4	1.2	NA	NA	27.6	0.3
69 Airport-1	145	6675	1.9	21.2366	3.8	0.0281	4.0	0.0043	1.3	0.33	27.8	0.4	28.1	1.1	52.7	90.0	27.8	0.4
69 Airport-1	742	3947	1.8	22.4225	1.7	0.0268	2.1	0.0044	1.3	0.60	28.0	0.4	26.8	0.6	NA	NA	28.0	0.4
69 Airport-1	303	77723	1.7	20.9010	2.6	0.0288	2.7	0.0044	1.0	0.37	28.1	0.3	28.8	0.8	90.5	60.6	28.1	0.3
69 Airport-1	388	4476	1.3	22.1638	2.5	0.0271	2.9	0.0044	1.5	0.50	28.1	0.4	27.2	0.8	NA	NA	28.1	0.4
69 Airport-1	357	133918	1.6	20.4239	2.4	0.0295	2.8	0.0044	1.4	0.50	28.1	0.4	29.5	0.8	145.0	56.3	28.1	0.4
69 Airport-1	182	3302	1.1	21.8083	3.5	0.0278	3.9	0.0044	1.5	0.39	28.3	0.4	27.8	1.1	NA	NA	28.3	0.4
69 Airport-1	739	28766	1.8	21.2832	1.6	0.0285	2.0	0.0044	1.3	0.63	28.4	0.4	28.6	0.6	47.5	37.5	28.4	0.4
69 Airport-1	643	39403	3.2	20.6972	1.7	0.0295	2.1	0.0044	1.3	0.62	28.5	0.4	29.5	0.6	113.7	39.2	28.5	0.4
69 Airport-1	282	1735	2.7	24.9013	2.6	0.0245	2.9	0.0044	1.3	0.44	28.5	0.4	24.6	0.7	NA	NA	28.5	0.4
69 Airport-1	237	1059	1.2	26.9977	10.7	0.0228	10.8	0.0045	1.4	0.13	28.7	0.4	22.9	2.4	NA	NA	28.7	0.4

69 Airport-1	123	1891	2.3	27.4030	8.6	0.0232	8.7	0.0046	1.6	0.18	29.6	0.5	23.2	2.0	NA	NA	29.6	0.5
69 Airport-1	162	2155	2.0	24.8335	3.5	0.0257	3.7	0.0046	1.4	0.36	29.8	0.4	25.8	1.0	NA	NA	29.8	0.4
69 Airport-1	1537	20308	0.5	21.0178	1.2	0.0309	1.6	0.0047	1.0	0.62	30.3	0.3	30.9	0.5	77.3	29.6	30.3	0.3
69 Airport-1	748	15411	1.6	21.2254	1.6	0.0306	2.0	0.0047	1.1	0.58	30.3	0.3	30.6	0.6	53.9	37.8	30.3	0.3
69 Airport-1	174	7414	2.9	21.1395	3.4	0.0322	3.6	0.0049	1.3	0.35	31.8	0.4	32.2	1.1	63.6	80.4	31.8	0.4
69 Airport-1	270	923	1.0	6.3723	23.4	0.1132	23.4	0.0052	1.6	0.07	33.6	0.5	108.9	24.2	2422.1	402.7	33.6	0.5
69 Airport-1	218	8043	2.9	21.5807	2.6	0.0352	4.4	0.0055	3.6	0.81	35.4	1.3	35.1	1.5	14.2	62.3	35.4	1.3
69 Airport-1	527	13032	1.5	18.6441	2.7	0.0408	2.9	0.0055	1.1	0.36	35.5	0.4	40.7	1.2	354.8	61.8	35.5	0.4
69 Airport-1	285	1483	1.0	26.5327	13.8	0.0301	13.9	0.0058	1.3	0.09	37.2	0.5	30.1	4.1	NA	NA	37.2	0.5
69 Airport-1	145	606	2.8	5.8339	9.0	0.1380	9.6	0.0058	3.3	0.34	37.5	1.2	131.3	11.8	2570.7	150.7	37.5	1.2
69 Airport-1	99	1990	1.2	10.9228	12.4	0.0747	12.5	0.0059	1.7	0.13	38.0	0.6	73.1	8.8	1457.3	236.4	38.0	0.6
69 Airport-1	1165	29227	1.8	21.1603	1.0	0.0470	1.6	0.0072	1.3	0.77	46.3	0.6	46.6	0.7	61.3	24.8	46.3	0.6
69 Airport-1	160	26660	0.9	18.2274	2.9	0.1808	3.0	0.0239	1.0	0.32	152.3	1.5	168.8	4.7	405.6	64.1	152.3	1.5
69 Airport-1	691	311871	1.0	19.8282	1.0	0.1753	1.5	0.0252	1.0	0.70	160.6	1.6	164.0	2.2	214.0	24.1	160.6	1.6
69 Airport-1	384	51548	1.1	19.9480	1.1	0.1812	1.6	0.0262	1.2	0.73	166.9	1.9	169.1	2.5	200.0	25.2	166.9	1.9
69 Airport-1	383	4778	1.2	15.7741	3.5	0.2300	3.8	0.0263	1.3	0.36	167.5	2.2	210.2	7.2	720.6	74.8	167.5	2.2
69 Airport-1	305	67470	2.3	19.3594	1.0	0.2622	1.6	0.0368	1.2	0.76	233.2	2.7	236.5	3.3	269.1	23.6	233.2	2.7
69 Airport-1	946	10839	17.7	9.5732	0.8	0.6367	1.4	0.0442	1.2	0.83	279.0	3.1	500.3	5.5	1704.0	14.4	279.0	3.1
69 Airport-1	613	60072	1.6	17.2317	0.6	0.6633	1.3	0.0829	1.1	0.87	513.6	5.5	516.6	5.2	530.1	14.0	513.6	5.5
69 Airport-1	24	15360	0.8	13.5034	1.1	1.8145	1.7	0.1778	1.3	0.76	1054.9	12.8	1050.7	11.3	1042.1	22.8	1042.1	22.8
69 Airport-1	347	410593	2.1	13.3382	0.7	1.8926	1.2	0.1832	1.0	0.84	1084.2	10.5	1078.5	8.3	1066.9	13.7	1066.9	13.7
69 Airport-1	220	60817	1.6	13.2388	0.5	1.8838	1.1	0.1810	0.9	0.87	1072.2	9.2	1075.4	7.1	1081.9	10.7	1081.9	10.7
69 Airport-1	335	83529	2.4	12.8291	0.7	2.0975	1.4	0.1952	1.2	0.86	1149.7	13.0	1148.0	9.9	1144.7	14.7	1144.7	14.7
69 Airport-1	216	96406	3.8	12.6640	0.7	2.2129	1.4	0.2033	1.1	0.84	1193.2	12.4	1185.1	9.4	1170.4	14.5	1170.4	14.5
69 Airport-1	201	40693	2.6	12.6327	0.7	2.1560	1.4	0.1976	1.2	0.88	1162.5	13.0	1167.0	9.7	1175.3	13.4	1175.3	13.4
69 Airport-1	123	76338	2.4	11.6051	0.7	2.7291	1.3	0.2298	1.1	0.83	1333.5	13.1	1336.4	9.8	1341.1	14.2	1341.1	14.2
69 Airport-1	40	49907	1.4	11.5510	0.9	2.6711	1.4	0.2239	1.0	0.75	1302.3	12.0	1320.5	10.0	1350.1	17.4	1350.1	17.4
69 Airport-1	70	16569	1.9	11.5359	0.8	2.8085	1.3	0.2351	1.0	0.78	1361.1	12.6	1357.8	9.9	1352.7	15.9	1352.7	15.9
69 Airport-1	126	118204	2.3	11.4235	0.8	2.8440	1.2	0.2357	0.9	0.76	1364.5	11.5	1367.2	9.3	1371.5	15.5	1371.5	15.5
69 Airport-1	469	118253	4.1	11.3985	0.5	2.9711	1.1	0.2457	1.0	0.90	1416.4	12.5	1400.2	8.3	1375.7	9.2	1375.7	9.2
69 Airport-1	755	2084144	3.9	11.2592	0.6	3.0533	1.5	0.2494	1.3	0.90	1435.6	17.0	1421.1	11.3	1399.4	12.4	1399.4	12.4

69 Airport-1	152	23343	0.7	11.1710	1.1	2.8368	1.7	0.2299	1.2	0.74	1334.2	14.9	1365.3	12.6	1414.4	21.7	1414.4	21.7
69 Airport-1	110	40041	1.6	11.1680	0.8	3.1195	1.3	0.2528	1.1	0.80	1452.8	13.8	1437.5	10.3	1414.9	15.5	1414.9	15.5
69 Airport-1	217	172389	4.1	11.1522	0.7	3.1079	1.2	0.2515	1.0	0.83	1446.1	13.2	1434.6	9.5	1417.6	13.3	1417.6	13.3
69 Airport-1	409	186397	0.8	11.1398	0.6	3.1080	1.3	0.2512	1.2	0.89	1444.7	15.3	1434.7	10.3	1419.8	11.9	1419.8	11.9
69 Airport-1	521	190353	2.0	11.1224	0.6	3.0980	1.2	0.2500	1.1	0.86	1438.6	13.8	1432.2	9.6	1422.7	12.2	1422.7	12.2
69 Airport-1	265	70993	1.0	11.1174	0.5	3.1369	1.1	0.2530	1.0	0.89	1454.1	12.9	1441.8	8.6	1423.6	9.6	1423.6	9.6
69 Airport-1	131	67259	2.0	11.0690	0.8	3.1210	1.2	0.2507	0.9	0.76	1441.9	11.5	1437.9	9.0	1431.9	14.6	1431.9	14.6
69 Airport-1	113	20952	2.0	11.0589	0.7	3.1360	1.2	0.2516	1.0	0.82	1446.9	12.4	1441.6	9.0	1433.7	12.7	1433.7	12.7
69 Airport-1	2319	76010	59.5	11.0519	0.7	2.9122	1.1	0.2335	0.8	0.77	1353.0	10.2	1385.1	8.2	1434.9	13.4	1434.9	13.4
69 Airport-1	618	285383	1.4	11.0318	0.7	3.0140	1.4	0.2413	1.3	0.89	1393.2	16.2	1411.2	11.0	1438.3	12.4	1438.3	12.4
69 Airport-1	139	48672	1.7	11.0039	0.5	3.1118	1.0	0.2485	0.9	0.87	1430.5	11.6	1435.6	8.0	1443.2	9.6	1443.2	9.6
69 Airport-1	905	615814	1.2	10.9957	0.7	3.0563	1.3	0.2438	1.1	0.84	1406.6	13.6	1421.8	9.8	1444.6	13.1	1444.6	13.1
69 Airport-1	174	69479	1.8	10.9828	0.6	3.1362	1.4	0.2499	1.2	0.90	1438.1	16.0	1441.6	10.6	1446.8	11.2	1446.8	11.2
69 Airport-1	137	160575	1.2	10.9789	0.5	3.0626	1.2	0.2440	1.1	0.90	1407.3	13.8	1423.4	9.2	1447.5	9.9	1447.5	9.9
69 Airport-1	1147	213595	6.3	10.9717	0.7	3.0009	1.3	0.2389	1.1	0.84	1381.0	14.0	1407.9	10.2	1448.8	13.7	1448.8	13.7
69 Airport-1	252	144290	1.1	10.9704	0.7	3.0786	1.4	0.2451	1.2	0.87	1412.9	15.2	1427.4	10.6	1449.0	13.2	1449.0	13.2
69 Airport-1	319	62082	0.8	10.9689	0.9	3.1939	1.6	0.2542	1.3	0.82	1460.1	16.8	1455.7	12.2	1449.2	17.3	1449.2	17.3
69 Airport-1	130	51879	1.2	10.9276	0.6	3.1067	1.3	0.2463	1.1	0.87	1419.5	14.0	1434.3	9.7	1456.4	11.8	1456.4	11.8
69 Airport-1	1202	65825	126.5	10.9129	0.6	2.9881	1.3	0.2366	1.1	0.87	1369.0	13.7	1404.6	9.7	1459.0	12.0	1459.0	12.0
69 Airport-1	159	1396748	1.9	10.8485	0.5	3.0712	1.2	0.2418	1.1	0.91	1395.8	13.9	1425.5	9.4	1470.2	9.7	1470.2	9.7
69 Airport-1	197	157425	1.6	10.8046	0.6	3.2125	1.4	0.2519	1.2	0.90	1448.0	15.9	1460.2	10.6	1477.9	11.2	1477.9	11.2
69 Airport-1	321	53617	1.3	10.7930	0.5	2.8691	1.3	0.2247	1.2	0.91	1306.6	14.4	1373.8	10.0	1480.0	10.3	1480.0	10.3
69 Airport-1	1751	23669	5.9	10.5767	0.5	3.0266	0.9	0.2323	0.8	0.83	1346.4	9.5	1414.3	7.2	1518.2	10.1	1518.2	10.1
69 Airport-1	824	189394	73.3	10.4766	0.7	3.3887	1.3	0.2576	1.1	0.86	1477.5	14.7	1501.8	10.1	1536.1	12.3	1536.1	12.3
69 Airport-1	343	11304	6.1	10.1846	1.0	3.2493	1.4	0.2401	1.0	0.72	1387.3	13.0	1469.0	11.3	1589.2	18.9	1589.2	18.9
69 Airport-1	484	258124	2.3	10.1290	0.6	3.8832	1.2	0.2854	1.1	0.89	1618.5	16.0	1610.2	10.1	1599.4	10.5	1599.4	10.5
69 Airport-1	55	28072	2.1	10.1029	0.7	3.8533	1.2	0.2825	1.0	0.83	1603.8	13.8	1604.0	9.4	1604.2	12.1	1604.2	12.1
69 Airport-1	167	30962	1.7	10.0034	0.7	3.9416	1.2	0.2861	1.0	0.81	1622.0	14.2	1622.3	10.0	1622.6	13.5	1622.6	13.5
69 Airport-1	1615	194035	2.6	9.9573	0.5	3.1493	1.4	0.2275	1.3	0.92	1321.6	15.0	1444.8	10.5	1631.2	9.7	1631.2	9.7
69 Airport-1	432	1822575	1.0	9.8910	0.5	4.1775	1.2	0.2998	1.1	0.91	1690.4	16.0	1669.6	9.7	1643.6	9.1	1643.6	9.1
69 Airport-1	442	8965900	31.3	9.8897	0.7	4.0441	1.6	0.2902	1.4	0.90	1642.5	20.4	1643.1	12.7	1643.9	12.7	1643.9	12.7

69 Airport-1	637	77616	1.9	9.8732	0.7	3.7064	1.5	0.2655	1.2	0.86	1518.0	16.9	1572.7	11.6	1647.0	13.7	1647.0	13.7
69 Airport-1	551	6373522	4.8	9.8604	0.7	4.1650	1.3	0.2980	1.1	0.84	1681.3	16.7	1667.2	11.0	1649.4	13.5	1649.4	13.5
69 Airport-1	547	283221	2.7	9.8263	0.7	4.3339	1.3	0.3090	1.1	0.85	1735.8	16.7	1699.8	10.7	1655.8	12.8	1655.8	12.8
69 Airport-1	405	107139	1.4	9.8172	0.5	4.2120	1.5	0.3000	1.4	0.93	1691.4	20.9	1676.4	12.4	1657.5	10.0	1657.5	10.0
69 Airport-1	348	343370	1.7	9.8167	0.7	4.1968	1.2	0.2989	1.0	0.84	1686.0	14.9	1673.4	9.8	1657.6	12.1	1657.6	12.1
69 Airport-1	72	37569	2.5	9.8165	0.7	4.1112	1.2	0.2928	1.0	0.82	1655.6	14.7	1656.5	9.9	1657.6	12.7	1657.6	12.7
69 Airport-1	144	113612	3.3	9.8163	0.9	4.0326	1.6	0.2872	1.3	0.83	1627.7	18.8	1640.8	12.7	1657.7	16.0	1657.7	16.0
69 Airport-1	535	760118	1.6	9.8122	0.9	4.1867	1.9	0.2981	1.7	0.88	1681.8	24.6	1671.4	15.4	1658.4	16.2	1658.4	16.2
69 Airport-1	304	69069	5.3	9.7881	0.7	4.2554	1.3	0.3022	1.1	0.85	1702.3	16.0	1684.8	10.4	1663.0	12.3	1663.0	12.3
69 Airport-1	662	334928	1.4	9.7766	0.7	4.1639	1.3	0.2954	1.1	0.84	1668.3	15.7	1666.9	10.3	1665.2	12.5	1665.2	12.5
69 Airport-1	200	50805	3.1	9.7731	0.5	4.3954	1.1	0.3117	1.0	0.90	1749.0	15.1	1711.5	9.0	1665.8	8.9	1665.8	8.9
69 Airport-1	90	70135	2.1	9.7661	0.7	4.1810	1.2	0.2963	1.0	0.81	1672.8	14.3	1670.3	9.8	1667.2	13.0	1667.2	13.0
69 Airport-1	309	393418	2.7	9.7606	0.7	4.1914	1.4	0.2968	1.2	0.86	1675.6	17.3	1672.3	11.2	1668.2	13.0	1668.2	13.0
69 Airport-1	496	5655960	3.2	9.7545	0.6	4.2904	1.1	0.3037	0.9	0.85	1709.4	14.0	1691.5	9.0	1669.4	10.7	1669.4	10.7
69 Airport-1	159	98898	2.7	9.7543	0.6	4.1766	1.1	0.2956	1.0	0.86	1669.5	14.1	1669.4	9.2	1669.4	10.7	1669.4	10.7
69 Airport-1	411	39764	2.7	9.7459	0.6	4.0086	1.4	0.2835	1.3	0.90	1608.8	17.8	1635.9	11.3	1671.0	11.2	1671.0	11.2
69 Airport-1	299	119538	4.6	9.7367	0.6	4.2672	1.1	0.3015	1.0	0.87	1698.6	15.0	1687.1	9.4	1672.7	10.3	1672.7	10.3
69 Airport-1	448	181930	3.6	9.7363	0.6	4.3186	1.5	0.3051	1.4	0.91	1716.5	20.7	1696.9	12.4	1672.8	11.5	1672.8	11.5
69 Airport-1	625	52570	4.3	9.7320	0.7	3.4475	1.5	0.2434	1.3	0.87	1404.6	16.6	1515.3	11.9	1673.6	13.8	1673.6	13.8
69 Airport-1	59	23618	1.1	9.7252	0.7	4.0585	1.4	0.2864	1.2	0.87	1623.4	17.2	1646.0	11.3	1674.9	12.7	1674.9	12.7
69 Airport-1	129	595132	2.5	9.7246	0.7	4.1438	1.2	0.2924	1.0	0.80	1653.4	14.1	1663.0	9.9	1675.0	13.6	1675.0	13.6
69 Airport-1	54	83310	6.7	9.7235	0.8	4.1991	1.3	0.2963	1.0	0.78	1672.7	15.1	1673.8	10.8	1675.2	15.1	1675.2	15.1
69 Airport-1	478	188429	2.1	9.7226	0.6	4.2135	1.1	0.2972	0.9	0.83	1677.6	14.0	1676.7	9.3	1675.4	11.5	1675.4	11.5
69 Airport-1	267	268947	2.0	9.7174	0.6	4.1692	1.4	0.2940	1.2	0.90	1661.3	17.8	1668.0	11.1	1676.4	11.2	1676.4	11.2
69 Airport-1	259	243201	5.7	9.7158	0.5	4.2763	1.3	0.3015	1.2	0.90	1698.6	17.3	1688.8	10.6	1676.7	10.2	1676.7	10.2
69 Airport-1	104	62589	1.9	9.7135	0.6	4.0769	1.1	0.2873	1.0	0.87	1628.2	14.1	1649.7	9.2	1677.1	10.3	1677.1	10.3
69 Airport-1	341	196927	9.8	9.7128	0.6	4.2048	1.2	0.2963	1.1	0.88	1673.1	15.9	1674.9	10.0	1677.3	10.6	1677.3	10.6
69 Airport-1	399	203163	4.5	9.7057	0.8	4.2924	1.7	0.3023	1.5	0.88	1702.6	22.0	1691.9	13.7	1678.6	14.4	1678.6	14.4
69 Airport-1	182	103533	4.6	9.7001	0.6	4.2223	1.3	0.2972	1.2	0.88	1677.3	17.3	1678.4	10.9	1679.7	11.7	1679.7	11.7
69 Airport-1	299	61128	5.0	9.6989	0.6	4.3029	1.2	0.3028	1.1	0.87	1705.2	15.8	1693.9	10.0	1679.9	11.1	1679.9	11.1
69 Airport-1	158	224938	11.7	9.6947	0.6	4.2227	1.1	0.2970	0.9	0.82	1676.6	13.1	1678.5	8.9	1680.7	11.6	1680.7	11.6

69 Airport-1	268	215388	3.8	9.6895	0.5	4.2475	1.4	0.2986	1.3	0.93	1684.5	19.6	1683.2	11.7	1681.7	9.9	1681.7	9.9
69 Airport-1	105	36034	1.5	9.6867	0.7	4.2139	1.3	0.2962	1.1	0.84	1672.3	16.1	1676.7	10.6	1682.2	12.8	1682.2	12.8
69 Airport-1	87	191507	1.9	9.6799	0.9	4.1253	1.5	0.2897	1.1	0.77	1640.2	16.2	1659.3	11.9	1683.5	17.2	1683.5	17.2
69 Airport-1	338	317389	2.3	9.6715	0.7	4.2877	1.4	0.3009	1.2	0.87	1695.7	17.8	1691.0	11.3	1685.2	12.3	1685.2	12.3
69 Airport-1	226	78584	3.0	9.6712	0.7	3.8628	1.4	0.2711	1.2	0.86	1546.2	16.0	1605.9	10.9	1685.2	12.8	1685.2	12.8
69 Airport-1	82	69431	2.0	9.6701	0.7	4.2560	1.3	0.2986	1.0	0.82	1684.5	15.4	1684.9	10.4	1685.4	13.3	1685.4	13.3
69 Airport-1	173	47159	4.9	9.6675	0.5	4.2605	1.4	0.2989	1.3	0.93	1685.6	19.5	1685.8	11.7	1685.9	9.9	1685.9	9.9
69 Airport-1	237	73131	2.2	9.6642	0.7	4.2244	1.5	0.2962	1.3	0.88	1672.6	19.0	1678.8	12.0	1686.5	12.8	1686.5	12.8
69 Airport-1	659	60635	2.0	9.6563	0.6	3.4252	1.5	0.2400	1.4	0.92	1386.6	17.7	1510.2	12.2	1688.0	11.5	1688.0	11.5
69 Airport-1	84	52580	2.6	9.6504	0.6	4.1473	1.3	0.2904	1.2	0.88	1643.5	16.9	1663.7	10.8	1689.2	11.4	1689.2	11.4
69 Airport-1	61	26313	2.8	9.6501	0.6	4.2863	1.2	0.3001	1.0	0.87	1691.9	15.1	1690.7	9.6	1689.2	10.8	1689.2	10.8
69 Airport-1	689	100155	3.2	9.6439	0.7	4.0518	1.4	0.2835	1.3	0.89	1609.1	17.9	1644.7	11.5	1690.4	12.2	1690.4	12.2
69 Airport-1	178	38932	4.4	9.6424	0.6	4.1942	1.4	0.2934	1.3	0.91	1658.7	19.0	1672.9	11.7	1690.7	11.0	1690.7	11.0
69 Airport-1	61	47019	1.3	9.6421	0.6	4.4159	1.7	0.3089	1.5	0.92	1735.5	23.2	1715.3	13.7	1690.8	11.6	1690.8	11.6
69 Airport-1	250	635514	5.8	9.6409	0.7	4.1926	1.3	0.2933	1.0	0.81	1657.9	14.8	1672.6	10.3	1691.0	13.7	1691.0	13.7
69 Airport-1	118	309629	2.3	9.6405	0.6	4.3809	1.3	0.3064	1.2	0.88	1723.2	17.8	1708.7	11.0	1691.1	11.6	1691.1	11.6
69 Airport-1	176	276093	2.1	9.6389	1.0	4.2170	1.5	0.2949	1.2	0.78	1666.1	17.6	1677.3	12.7	1691.4	18.0	1691.4	18.0
69 Airport-1	142	57735	2.9	9.6384	0.7	4.4285	1.3	0.3097	1.1	0.85	1739.3	16.3	1717.7	10.4	1691.5	12.1	1691.5	12.1
69 Airport-1	64	122803	2.4	9.6376	0.7	4.2118	1.3	0.2945	1.1	0.85	1664.1	16.1	1676.3	10.6	1691.6	12.7	1691.6	12.7
69 Airport-1	346	724842	5.4	9.6349	0.5	4.3367	1.2	0.3032	1.1	0.92	1707.0	16.6	1700.4	9.9	1692.1	8.7	1692.1	8.7
69 Airport-1	58	418196	6.4	9.6348	0.7	4.1817	1.2	0.2923	1.0	0.83	1653.2	15.0	1670.4	10.2	1692.2	12.7	1692.2	12.7
69 Airport-1	150	4403095	2.0	9.6338	0.8	4.3708	1.2	0.3055	1.0	0.79	1718.6	14.6	1706.8	10.2	1692.3	14.1	1692.3	14.1
69 Airport-1	958	163238	4.2	9.6327	0.7	4.1395	1.3	0.2893	1.1	0.86	1638.2	15.7	1662.1	10.4	1692.6	12.1	1692.6	12.1
69 Airport-1	124	62826	2.6	9.6316	0.7	4.2808	1.3	0.2992	1.1	0.85	1687.2	16.8	1689.7	11.0	1692.8	12.9	1692.8	12.9
69 Airport-1	281	244926	9.4	9.6310	0.6	4.3178	1.1	0.3017	1.0	0.86	1699.9	14.6	1696.8	9.3	1692.9	10.7	1692.9	10.7
69 Airport-1	813	61005	2.5	9.6306	0.7	3.7560	1.8	0.2625	1.7	0.91	1502.4	22.1	1583.4	14.5	1693.0	13.7	1693.0	13.7
69 Airport-1	677	99788	4.0	9.6293	0.7	4.1350	1.3	0.2889	1.1	0.86	1636.1	16.4	1661.2	10.8	1693.2	12.3	1693.2	12.3
69 Airport-1	92	91260	1.8	9.6263	0.6	4.2668	1.2	0.2980	1.0	0.85	1681.5	15.1	1687.0	9.8	1693.8	11.5	1693.8	11.5
69 Airport-1	317	77644	3.5	9.6261	0.5	4.5239	1.4	0.3160	1.3	0.93	1770.0	20.7	1735.4	11.9	1693.8	9.5	1693.8	9.5
69 Airport-1	173	72659	2.6	9.6253	0.6	4.2603	1.5	0.2975	1.4	0.91	1679.1	20.1	1685.7	12.2	1694.0	11.1	1694.0	11.1
69 Airport-1	69	39662	3.5	9.6221	0.8	4.2792	1.5	0.2988	1.2	0.83	1685.1	18.0	1689.4	12.1	1694.6	15.3	1694.6	15.3

69 Airport-1	174	1328471	7.8	9.6220	0.4	4.2723	1.1	0.2983	1.0	0.92	1682.8	15.4	1688.0	9.2	1694.6	7.9	1694.6	7.9
69 Airport-1	229	87664	3.4	9.6179	0.9	4.2644	1.4	0.2976	1.1	0.76	1679.4	15.6	1686.5	11.5	1695.4	16.8	1695.4	16.8
69 Airport-1	161	38976	5.8	9.6160	0.7	4.2600	1.2	0.2972	0.9	0.80	1677.6	14.0	1685.7	9.8	1695.8	13.2	1695.8	13.2
69 Airport-1	55	35992	2.8	9.6150	0.7	4.4757	1.3	0.3122	1.1	0.85	1751.8	17.2	1726.5	11.0	1696.0	12.9	1696.0	12.9
69 Airport-1	353	57561872	2.7	9.6146	0.6	4.1839	1.3	0.2919	1.2	0.87	1650.9	17.1	1670.9	11.0	1696.0	12.0	1696.0	12.0
69 Airport-1	282	77879	1.8	9.6104	0.6	4.3229	1.6	0.3014	1.4	0.92	1698.5	21.6	1697.7	13.0	1696.8	11.6	1696.8	11.6
69 Airport-1	118	60953	2.4	9.6026	0.7	4.2276	1.3	0.2946	1.1	0.85	1664.3	16.2	1679.4	10.7	1698.3	12.9	1698.3	12.9
69 Airport-1	429	64120	5.0	9.6018	0.7	3.7674	2.1	0.2625	2.0	0.94	1502.5	26.6	1585.8	16.9	1698.5	12.7	1698.5	12.7
69 Airport-1	211	76246	3.6	9.6002	0.9	4.1947	1.5	0.2922	1.2	0.79	1652.5	17.1	1673.0	12.2	1698.8	16.7	1698.8	16.7
69 Airport-1	1363	165361	2.4	9.5963	0.6	3.9567	1.2	0.2755	1.1	0.89	1568.7	15.3	1625.4	10.0	1699.5	10.3	1699.5	10.3
69 Airport-1	74	46207	2.7	9.5912	0.7	4.3316	1.3	0.3014	1.1	0.85	1698.5	16.8	1699.4	11.0	1700.5	13.1	1700.5	13.1
69 Airport-1	102	22962	3.3	9.5882	0.7	4.3922	1.3	0.3056	1.1	0.82	1718.9	16.3	1710.9	10.8	1701.1	13.6	1701.1	13.6
69 Airport-1	53	177964	2.5	9.5735	1.0	4.2083	1.6	0.2923	1.2	0.75	1653.2	17.2	1675.6	12.9	1703.9	19.1	1703.9	19.1
69 Airport-1	103	38093	4.5	9.5735	0.7	4.2769	1.3	0.2971	1.1	0.83	1676.8	16.3	1688.9	10.9	1703.9	13.5	1703.9	13.5
69 Airport-1	1702	16204	13.4	9.5728	0.7	3.4288	1.5	0.2382	1.3	0.89	1377.1	16.2	1511.0	11.5	1704.1	12.1	1704.1	12.1
69 Airport-1	242	62377	4.3	9.5718	0.8	4.1907	1.4	0.2910	1.2	0.83	1646.8	17.4	1672.2	11.9	1704.3	15.0	1704.3	15.0
69 Airport-1	77	77732	2.6	9.5715	0.6	4.5089	1.1	0.3131	1.0	0.87	1756.2	15.2	1732.6	9.4	1704.3	10.2	1704.3	10.2
69 Airport-1	341	79269	0.9	9.5577	0.5	4.2260	1.3	0.2931	1.2	0.93	1656.8	18.1	1679.1	10.9	1707.0	9.0	1707.0	9.0
69 Airport-1	103	64320	3.1	9.5546	0.7	4.2760	1.3	0.2964	1.1	0.83	1673.6	16.2	1688.7	10.9	1707.6	13.5	1707.6	13.5
69 Airport-1	148	81739	3.9	9.5535	0.6	4.2895	1.6	0.2973	1.5	0.93	1678.1	21.8	1691.4	13.1	1707.8	11.1	1707.8	11.1
69 Airport-1	245	154489	3.5	9.5497	0.6	4.4880	1.2	0.3110	1.0	0.85	1745.5	15.5	1728.7	9.9	1708.5	11.6	1708.5	11.6
69 Airport-1	362	2832236	1.6	9.5402	0.6	4.2460	1.5	0.2939	1.4	0.93	1661.1	20.7	1683.0	12.5	1710.3	10.4	1710.3	10.4
69 Airport-1	820	61226	4.5	9.5346	0.8	4.0692	1.3	0.2815	1.1	0.83	1599.0	15.6	1648.1	10.9	1711.4	13.9	1711.4	13.9
69 Airport-1	342	123506	2.9	9.5343	0.5	4.4213	1.1	0.3059	1.0	0.89	1720.3	14.5	1716.3	8.9	1711.5	9.1	1711.5	9.1
69 Airport-1	33	53065	3.2	9.5337	0.8	4.3446	1.4	0.3005	1.1	0.83	1694.0	16.8	1701.9	11.2	1711.6	13.8	1711.6	13.8
69 Airport-1	106	43531	3.9	9.5308	0.8	4.3951	1.5	0.3039	1.2	0.84	1710.8	18.4	1711.4	12.1	1712.1	14.8	1712.1	14.8
69 Airport-1	81	47464	2.5	9.5217	0.7	4.3137	1.2	0.2980	1.0	0.84	1681.5	15.4	1696.0	10.2	1713.9	12.2	1713.9	12.2
69 Airport-1	220	64835	3.4	9.5178	0.5	4.4487	1.2	0.3072	1.1	0.91	1727.0	16.4	1721.5	9.9	1714.7	9.3	1714.7	9.3
69 Airport-1	97	9853	1.3	9.5131	2.6	3.8172	2.8	0.2635	1.1	0.39	1507.7	14.7	1596.4	22.7	1715.6	47.8	1715.6	47.8
69 Airport-1	457	457296	1.9	9.5081	0.6	4.4777	1.4	0.3089	1.3	0.91	1735.4	19.7	1726.8	11.8	1716.5	10.7	1716.5	10.7
69 Airport-1	87	53349	4.4	9.5052	0.7	4.3635	1.1	0.3009	0.9	0.77	1696.0	13.0	1705.5	9.4	1717.1	13.4	1717.1	13.4

69 Airport-1	204	130664	2.6	9.5036	0.5	4.4784	1.0	0.3088	0.8	0.83	1734.9	12.2	1727.0	8.0	1717.4	9.9	1717.4	9.9
69 Airport-1	75	120190	2.3	9.5032	0.6	4.3238	1.0	0.2981	0.7	0.75	1682.1	10.8	1697.9	8.0	1717.5	11.9	1717.5	11.9
69 Airport-1	85	236699	3.5	9.4967	0.6	4.2936	1.2	0.2959	1.1	0.88	1670.7	15.9	1692.1	10.1	1718.7	10.9	1718.7	10.9
69 Airport-1	137	43296	1.9	9.4963	0.6	4.4408	1.2	0.3060	1.0	0.85	1720.9	14.9	1720.0	9.7	1718.8	11.3	1718.8	11.3
69 Airport-1	156	85748	2.9	9.4504	0.6	4.5224	1.3	0.3101	1.1	0.86	1741.2	16.6	1735.1	10.5	1727.7	11.9	1727.7	11.9
69 Airport-1	70	48724	8.2	9.4407	0.7	4.4334	1.2	0.3037	0.9	0.80	1709.6	13.8	1718.6	9.6	1729.6	12.9	1729.6	12.9
69 Airport-1	195	196958	2.5	9.4240	0.7	4.5317	1.2	0.3099	0.9	0.79	1740.1	14.2	1736.8	9.8	1732.9	13.4	1732.9	13.4
69 Airport-1	155	41010	2.9	9.4216	0.7	4.4321	1.3	0.3030	1.1	0.84	1706.1	16.0	1718.4	10.4	1733.3	12.4	1733.3	12.4
69 Airport-1	177	165860	4.2	9.4044	0.7	4.5547	1.3	0.3108	1.1	0.86	1744.6	17.2	1741.0	10.9	1736.7	12.3	1736.7	12.3
69 Airport-1	63	29940	2.7	9.3958	0.9	4.4221	1.7	0.3015	1.4	0.84	1698.6	21.0	1716.5	13.9	1738.3	16.9	1738.3	16.9
69 Airport-1	123	76895	3.9	9.3957	0.6	4.5578	1.4	0.3107	1.2	0.89	1744.3	18.5	1741.6	11.3	1738.4	11.4	1738.4	11.4
69 Airport-1	840	24310	2.2	9.3630	0.8	3.8654	1.7	0.2626	1.5	0.88	1503.1	19.5	1606.5	13.4	1744.8	14.5	1744.8	14.5
69 Airport-1	981	139402	1.9	9.3434	0.5	4.3878	1.0	0.2975	0.9	0.86	1678.7	13.2	1710.0	8.6	1748.6	9.8	1748.6	9.8
69 Airport-1	301	63708	1.6	9.3390	0.6	4.5202	1.3	0.3063	1.2	0.89	1722.5	18.0	1734.7	11.1	1749.5	11.1	1749.5	11.1
69 Airport-1	110	238562	3.5	9.3326	0.6	4.6568	1.2	0.3153	1.1	0.86	1766.9	16.5	1759.5	10.4	1750.7	11.6	1750.7	11.6
69 Airport-1	166	24214	4.8	9.3009	0.7	4.3871	1.2	0.2961	1.0	0.83	1671.8	15.2	1709.9	10.3	1756.9	12.7	1756.9	12.7
69 Airport-1	173	124044	3.0	9.2974	0.5	4.5676	1.0	0.3081	0.8	0.85	1731.5	12.6	1743.4	8.1	1757.6	9.2	1757.6	9.2
69 Airport-1	1140	41056	2.6	9.2971	0.6	4.1353	1.0	0.2790	0.8	0.82	1586.1	11.8	1661.3	8.4	1757.7	10.7	1757.7	10.7
69 Airport-1	64	15236	2.4	9.2870	1.0	4.3471	1.5	0.2929	1.2	0.77	1656.2	17.3	1702.3	12.6	1759.7	17.8	1759.7	17.8
69 Airport-1	1549	26696	4.5	9.2770	0.7	4.0625	1.5	0.2735	1.4	0.89	1558.3	18.9	1646.8	12.6	1761.6	13.1	1761.6	13.1
69 Airport-1	112	20157	1.4	9.2360	1.1	4.3979	1.4	0.2947	0.9	0.63	1665.1	12.7	1711.9	11.5	1769.7	19.7	1769.7	19.7
69 Airport-1	132	29278	3.3	9.1494	0.7	4.6369	1.3	0.3078	1.0	0.80	1730.0	15.2	1755.9	10.4	1786.9	13.6	1786.9	13.6
69 Airport-1	287	8453	2.5	8.9563	1.0	4.5689	1.6	0.2969	1.3	0.81	1676.0	19.3	1743.6	13.5	1825.7	17.5	1825.7	17.5
69 Airport-1	102	68069	1.2	6.0853	0.7	9.1095	1.2	0.4022	1.0	0.82	2179.2	17.7	2349.1	10.7	2500.0	11.4	2500.0	11.4
69 Airport-1	327	221944	1.3	5.9019	0.7	11.7493	1.4	0.5031	1.2	0.86	2627.3	25.7	2584.6	12.9	2551.4	11.7	2551.4	11.7
BaggerCreek1	170	6022	1.1	15.2684	5.5	0.0232	5.6	0.0026	1.2	0.22	16.6	0.2	23.3	1.3	789.3	115.1	16.6	0.2
BaggerCreek1	660	11557	1.4	22.1495	2.5	0.0162	2.8	0.0026	1.3	0.45	16.7	0.2	16.3	0.5	NA	NA	16.7	0.2
BaggerCreek1	528	6723	1.2	20.5569	2.2	0.0175	2.6	0.0026	1.4	0.54	16.8	0.2	17.7	0.5	129.7	51.8	16.8	0.2
BaggerCreek1	150	2174	1.6	22.6076	6.2	0.0174	6.6	0.0029	2.3	0.36	18.4	0.4	17.5	1.1	NA	NA	18.4	0.4
BaggerCreek1	902	11388	1.7	21.9883	1.3	0.0261	1.8	0.0042	1.2	0.68	26.8	0.3	26.2	0.5	NA	NA	26.8	0.3

BaggerCreek1	152	7391	1.1	20.5847	2.8	0.0349	3.0	0.0052	1.3	0.41	33.5	0.4	34.8	1.0	126.6	65.2	33.5	0.4
BaggerCreek1	807	9850	1.6	20.8138	2.1	0.0354	2.4	0.0054	1.1	0.47	34.4	0.4	35.4	0.8	100.5	50.3	34.4	0.4
BaggerCreek1	226	15006	1.0	21.0036	2.1	0.0367	2.5	0.0056	1.3	0.53	35.9	0.5	36.6	0.9	78.9	49.5	35.9	0.5
BaggerCreek1	172	57549	1.6	20.6330	2.2	0.0374	2.6	0.0056	1.5	0.55	36.0	0.5	37.3	1.0	121.1	51.4	36.0	0.5
BaggerCreek1	95	6288	1.0	22.1226	3.5	0.0354	4.0	0.0057	1.8	0.46	36.5	0.7	35.3	1.4	NA	NA	36.5	0.7
BaggerCreek1	55	70731	1.1	20.5084	3.8	0.0384	4.2	0.0057	1.7	0.41	36.7	0.6	38.2	1.6	135.3	89.3	36.7	0.6
BaggerCreek1	245	14754	1.0	20.9380	1.6	0.0381	2.2	0.0058	1.5	0.69	37.2	0.6	38.0	0.8	86.4	37.8	37.2	0.6
BaggerCreek1	122	2772	1.0	15.0594	8.4	0.0556	8.5	0.0061	1.4	0.16	39.1	0.5	55.0	4.5	818.2	175.1	39.1	0.5
BaggerCreek1	76	1699	1.1	4.4098	25.9	0.2246	26.1	0.0072	3.0	0.12	46.2	1.4	205.7	48.6	3028.7	423.5	46.2	1.4
BaggerCreek1	43	3539	1.1	21.3296	3.7	0.0699	4.1	0.0108	1.8	0.43	69.3	1.2	68.6	2.7	42.2	89.4	69.3	1.2
BaggerCreek1	665	39309	2.3	20.7558	0.9	0.0935	1.2	0.0141	0.8	0.67	90.1	0.7	90.8	1.1	107.1	21.4	90.1	0.7
BaggerCreek1	1053	308793	1.3	19.7456	0.5	0.2436	1.1	0.0349	1.0	0.91	221.2	2.2	221.4	2.2	223.7	10.7	221.2	2.2
BaggerCreek1	72	49819	3.2	16.9679	1.3	0.6631	2.0	0.0816	1.5	0.75	505.9	7.2	516.5	8.0	563.7	28.6	505.9	7.2
BaggerCreek1	91	95649	2.2	11.2409	0.7	3.1169	1.3	0.2542	1.1	0.85	1460.2	14.2	1436.9	9.9	1402.5	13.2	1402.5	13.2
BaggerCreek1	155	117874	2.5	11.2046	0.6	3.0586	1.5	0.2487	1.3	0.92	1431.6	17.3	1422.4	11.2	1408.7	11.2	1408.7	11.2
BaggerCreek1	63	67350	1.6	11.1814	0.9	3.1152	1.5	0.2527	1.3	0.83	1452.6	16.6	1436.5	11.9	1412.6	16.5	1412.6	16.5
BaggerCreek1	170	119719	1.9	11.1761	0.6	3.0934	1.2	0.2509	1.0	0.86	1442.9	13.4	1431.1	9.3	1413.5	12.0	1413.5	12.0
BaggerCreek1	287	723925	0.9	11.1623	0.6	3.0209	1.4	0.2447	1.2	0.89	1410.9	15.6	1412.9	10.6	1415.9	12.0	1415.9	12.0
BaggerCreek1	189	117564	5.8	11.1623	0.8	3.0109	1.4	0.2439	1.2	0.84	1406.7	15.0	1410.4	10.7	1415.9	14.5	1415.9	14.5
BaggerCreek1	101	241214	1.8	11.1622	0.8	3.1198	1.5	0.2527	1.2	0.85	1452.3	16.2	1437.6	11.3	1415.9	14.8	1415.9	14.8
BaggerCreek1	141	380764	1.3	11.1469	0.6	3.0485	1.2	0.2466	1.0	0.84	1420.7	12.6	1419.9	9.0	1418.5	12.4	1418.5	12.4
BaggerCreek1	119	1712203	2.0	11.1457	0.7	3.1000	1.2	0.2507	1.0	0.85	1442.1	13.4	1432.7	9.4	1418.7	12.5	1418.7	12.5
BaggerCreek1	50	18690	2.4	11.1380	0.6	3.0579	1.3	0.2471	1.1	0.86	1423.6	14.1	1422.2	9.8	1420.1	12.4	1420.1	12.4
BaggerCreek1	117	68903	2.9	11.1360	0.7	3.1002	1.1	0.2505	0.8	0.76	1441.1	10.9	1432.7	8.5	1420.4	13.8	1420.4	13.8
BaggerCreek1	134	116117	1.9	11.1256	0.6	3.0811	1.1	0.2487	0.9	0.85	1431.9	11.5	1428.0	8.1	1422.2	10.6	1422.2	10.6
BaggerCreek1	91	94734	1.7	11.1195	0.6	3.0828	1.3	0.2487	1.1	0.89	1431.9	14.5	1428.4	9.7	1423.2	11.2	1423.2	11.2
BaggerCreek1	99	104352	1.4	11.1153	0.5	3.1862	1.2	0.2570	1.1	0.89	1474.3	14.1	1453.8	9.3	1424.0	10.4	1424.0	10.4
BaggerCreek1	126	286348	1.6	11.1132	0.8	3.0261	1.5	0.2440	1.2	0.84	1407.5	15.4	1414.2	11.1	1424.3	15.2	1424.3	15.2
BaggerCreek1	88	101998	1.7	11.1097	0.7	3.0663	1.3	0.2472	1.1	0.84	1423.9	13.6	1424.3	9.7	1424.9	13.1	1424.9	13.1
BaggerCreek1	105	147745	1.7	11.1093	0.6	3.1692	1.1	0.2555	0.9	0.84	1466.6	11.5	1449.7	8.1	1425.0	11.0	1425.0	11.0
BaggerCreek1	155	69959	1.7	11.1080	0.7	3.0246	1.3	0.2438	1.2	0.86	1406.3	14.6	1413.8	10.2	1425.2	12.8	1425.2	12.8

BaggerCreek1	77	101921	1.9	11.0987	0.8	3.1051	1.4	0.2501	1.1	0.82	1438.7	14.7	1433.9	10.6	1426.8	15.0	1426.8	15.0
BaggerCreek1	217	2860793	4.1	11.0986	0.8	3.0611	1.6	0.2465	1.4	0.87	1420.5	17.7	1423.0	12.3	1426.8	15.3	1426.8	15.3
BaggerCreek1	178	94468	2.0	11.0930	0.7	3.0340	1.2	0.2442	1.0	0.82	1408.5	12.6	1416.2	9.3	1427.8	13.4	1427.8	13.4
BaggerCreek1	47	38653	1.8	11.0908	0.8	3.0398	1.5	0.2446	1.2	0.84	1410.7	15.6	1417.7	11.1	1428.2	14.8	1428.2	14.8
BaggerCreek1	97	56075	1.8	11.0836	0.6	3.0433	1.5	0.2447	1.4	0.91	1411.3	17.7	1418.6	11.7	1429.4	11.9	1429.4	11.9
BaggerCreek1	86	845650	1.1	11.0699	0.7	3.0759	1.1	0.2471	0.8	0.75	1423.3	10.6	1426.7	8.5	1431.8	14.1	1431.8	14.1
BaggerCreek1	155	96353	2.3	11.0689	0.6	3.0337	1.5	0.2437	1.4	0.92	1405.6	17.7	1416.1	11.6	1431.9	11.4	1431.9	11.4
BaggerCreek1	70	3191719	1.2	11.0619	0.7	3.1158	1.4	0.2501	1.2	0.84	1438.9	15.0	1436.6	10.6	1433.2	14.1	1433.2	14.1
BaggerCreek1	63	136661	2.2	11.0606	0.7	3.1919	1.3	0.2562	1.1	0.85	1470.2	14.6	1455.2	10.1	1433.4	12.9	1433.4	12.9
BaggerCreek1	66	160640	1.1	11.0591	0.8	3.0212	1.2	0.2424	0.9	0.72	1399.3	10.8	1413.0	9.1	1433.6	15.9	1433.6	15.9
BaggerCreek1	113	62411	2.0	11.0569	0.5	3.0073	1.2	0.2413	1.1	0.91	1393.3	13.6	1409.5	9.1	1434.0	9.6	1434.0	9.6
BaggerCreek1	49	38763	2.0	11.0563	0.6	3.1421	1.1	0.2521	0.9	0.83	1449.1	11.9	1443.1	8.5	1434.1	11.9	1434.1	11.9
BaggerCreek1	74	41642	1.5	11.0526	0.7	3.0332	1.3	0.2433	1.1	0.85	1403.6	13.3	1416.0	9.5	1434.7	12.7	1434.7	12.7
BaggerCreek1	211	116852	2.4	11.0472	0.8	3.0359	1.4	0.2433	1.1	0.81	1404.1	13.9	1416.7	10.4	1435.7	15.2	1435.7	15.2
BaggerCreek1	251	1446404	2.5	11.0444	0.6	3.1096	1.3	0.2492	1.1	0.87	1434.3	14.4	1435.1	9.9	1436.2	12.3	1436.2	12.3
BaggerCreek1	58	105584	1.9	11.0439	1.0	3.1330	1.7	0.2511	1.4	0.81	1443.9	17.7	1440.8	13.0	1436.3	18.8	1436.3	18.8
BaggerCreek1	71	53548	1.6	11.0437	0.5	3.1505	1.1	0.2525	1.0	0.88	1451.1	13.0	1445.1	8.8	1436.3	10.5	1436.3	10.5
BaggerCreek1	91	52785	1.7	11.0435	0.7	3.0619	1.6	0.2453	1.4	0.89	1414.4	17.8	1423.2	12.0	1436.3	13.4	1436.3	13.4
BaggerCreek1	104	365402	1.7	11.0422	0.7	3.0634	1.4	0.2454	1.2	0.86	1414.9	15.6	1423.6	11.0	1436.6	14.1	1436.6	14.1
BaggerCreek1	175	383798	2.6	11.0416	0.5	3.0270	1.4	0.2425	1.3	0.93	1399.8	16.7	1414.5	10.9	1436.7	10.2	1436.7	10.2
BaggerCreek1	63	133811	1.9	11.0412	0.8	3.0931	1.5	0.2478	1.3	0.86	1427.1	16.2	1431.0	11.3	1436.7	14.4	1436.7	14.4
BaggerCreek1	97	74110	1.5	11.0403	0.6	3.0570	1.5	0.2449	1.4	0.91	1412.1	17.6	1422.0	11.6	1436.9	12.1	1436.9	12.1
BaggerCreek1	32	18757	2.3	11.0381	0.9	3.1269	1.5	0.2504	1.2	0.82	1440.7	15.9	1439.3	11.6	1437.3	16.6	1437.3	16.6
BaggerCreek1	150	103150	2.1	11.0366	0.6	3.0581	1.2	0.2449	1.0	0.86	1412.1	12.8	1422.3	9.0	1437.5	11.4	1437.5	11.4
BaggerCreek1	115	149775	1.7	11.0362	0.6	3.0594	1.3	0.2450	1.1	0.86	1412.6	13.7	1422.6	9.7	1437.6	12.3	1437.6	12.3
BaggerCreek1	121	602931	1.7	11.0303	0.5	3.1531	1.1	0.2524	1.0	0.88	1450.6	12.6	1445.8	8.6	1438.6	10.2	1438.6	10.2
BaggerCreek1	102	244021	1.9	11.0296	0.6	3.0981	1.2	0.2479	1.0	0.84	1427.8	12.7	1432.2	9.1	1438.7	12.3	1438.7	12.3
BaggerCreek1	123	183496	2.8	11.0293	0.8	3.0745	1.4	0.2460	1.1	0.81	1418.0	14.6	1426.4	10.9	1438.8	16.0	1438.8	16.0
BaggerCreek1	92	162275	1.9	11.0286	0.6	2.9929	1.1	0.2395	0.9	0.83	1384.1	11.7	1405.8	8.6	1438.9	12.1	1438.9	12.1
BaggerCreek1	284	107074	5.6	11.0271	0.6	3.1459	1.2	0.2517	1.1	0.88	1447.3	14.0	1444.0	9.5	1439.2	11.3	1439.2	11.3
BaggerCreek1	68	179958	1.8	11.0229	0.7	3.1332	1.6	0.2506	1.5	0.89	1441.5	18.9	1440.9	12.6	1439.9	14.0	1439.9	14.0

BaggerCreek1	86	92391	1.5	11.0226	0.9	3.1657	1.5	0.2532	1.3	0.83	1454.9	16.8	1448.8	11.9	1439.9	16.4	1439.9	16.4
BaggerCreek1	110	417121	2.4	11.0220	0.5	3.2643	1.2	0.2611	1.0	0.89	1495.3	13.9	1472.6	9.1	1440.0	10.3	1440.0	10.3
BaggerCreek1	88	156528	2.4	11.0220	0.8	3.1328	1.2	0.2505	0.9	0.77	1441.3	11.9	1440.8	9.3	1440.1	14.7	1440.1	14.7
BaggerCreek1	60	36789	2.0	11.0194	0.7	3.0703	1.3	0.2455	1.1	0.84	1415.2	14.2	1425.3	10.2	1440.5	13.7	1440.5	13.7
BaggerCreek1	99	91688	1.9	11.0180	0.7	3.1202	1.4	0.2494	1.2	0.85	1435.6	15.1	1437.7	10.6	1440.7	13.9	1440.7	13.9
BaggerCreek1	153	113179	1.8	11.0157	0.5	3.0646	1.2	0.2450	1.1	0.89	1412.4	13.4	1423.9	9.1	1441.1	10.5	1441.1	10.5
BaggerCreek1	64	415176	1.8	11.0141	0.7	3.1074	1.3	0.2483	1.1	0.86	1429.9	14.2	1434.5	9.9	1441.4	12.6	1441.4	12.6
BaggerCreek1	64	81522	1.6	11.0121	0.6	3.0902	1.1	0.2469	0.9	0.83	1422.5	12.0	1430.3	8.7	1441.8	11.9	1441.8	11.9
BaggerCreek1	75	84958	1.8	11.0115	0.7	3.1248	1.1	0.2497	0.9	0.81	1436.7	11.7	1438.8	8.6	1441.9	12.4	1441.9	12.4
BaggerCreek1	70	59679	1.8	11.0051	0.8	3.0630	1.4	0.2446	1.1	0.80	1410.5	14.2	1423.5	10.7	1443.0	15.8	1443.0	15.8
BaggerCreek1	103	285810	1.7	11.0007	0.6	3.1572	1.1	0.2520	0.9	0.82	1448.8	11.8	1446.8	8.5	1443.7	12.0	1443.7	12.0
BaggerCreek1	104	108241	1.2	11.0006	0.7	3.1330	1.4	0.2501	1.2	0.85	1438.9	15.1	1440.8	10.5	1443.7	13.6	1443.7	13.6
BaggerCreek1	148	92980	1.8	10.9965	0.6	3.1318	1.0	0.2499	0.9	0.84	1437.9	11.4	1440.5	8.1	1444.5	10.8	1444.5	10.8
BaggerCreek1	128	167761	1.2	10.9918	0.7	3.1160	1.6	0.2485	1.4	0.88	1430.8	17.8	1436.7	12.0	1445.3	13.9	1445.3	13.9
BaggerCreek1	190	1635280	2.0	10.9886	0.6	3.1751	1.2	0.2532	1.1	0.88	1454.7	13.8	1451.1	9.3	1445.8	10.9	1445.8	10.9
BaggerCreek1	318	1801779	1.3	10.9884	0.8	3.0928	1.4	0.2466	1.1	0.83	1420.9	14.3	1430.9	10.4	1445.9	14.6	1445.9	14.6
BaggerCreek1	109	317455	2.3	10.9879	0.6	3.0622	1.3	0.2441	1.1	0.89	1408.2	14.5	1423.3	9.8	1446.0	11.2	1446.0	11.2
BaggerCreek1	69	631469	1.5	10.9833	1.0	3.1798	1.5	0.2534	1.2	0.78	1456.0	15.5	1452.3	11.8	1446.7	18.2	1446.7	18.2
BaggerCreek1	102	92523	2.0	10.9816	0.6	3.0395	1.3	0.2422	1.2	0.89	1398.1	14.7	1417.6	10.1	1447.0	11.7	1447.0	11.7
BaggerCreek1	86	147556	1.4	10.9813	0.7	3.0414	1.4	0.2423	1.2	0.86	1398.8	15.3	1418.1	10.9	1447.1	14.1	1447.1	14.1
BaggerCreek1	108	563503	1.2	10.9780	0.7	3.0899	1.0	0.2461	0.8	0.77	1418.5	10.3	1430.2	8.0	1447.7	12.6	1447.7	12.6
BaggerCreek1	189	333275	4.9	10.9780	0.6	3.0715	1.5	0.2447	1.4	0.92	1410.9	17.6	1425.6	11.5	1447.7	11.0	1447.7	11.0
BaggerCreek1	100	799369	1.5	10.9758	0.8	3.0618	1.4	0.2438	1.1	0.82	1406.6	14.5	1423.2	10.7	1448.0	15.3	1448.0	15.3
BaggerCreek1	133	137839	1.4	10.9754	0.7	3.0951	1.3	0.2465	1.1	0.84	1420.3	13.5	1431.5	9.7	1448.1	13.1	1448.1	13.1
BaggerCreek1	114	1404279	2.3	10.9746	0.7	3.0849	1.1	0.2457	0.9	0.78	1416.0	11.1	1428.9	8.6	1448.3	13.5	1448.3	13.5
BaggerCreek1	63	71413	1.5	10.9712	0.8	3.0308	1.2	0.2413	0.8	0.73	1393.3	10.6	1415.4	8.9	1448.8	15.2	1448.8	15.2
BaggerCreek1	110	119507	1.6	10.9707	0.6	3.0983	1.3	0.2466	1.2	0.90	1421.1	15.3	1432.3	10.2	1448.9	10.9	1448.9	10.9
BaggerCreek1	67	104587	1.8	10.9673	0.7	3.2066	1.4	0.2552	1.2	0.85	1465.1	15.9	1458.7	11.0	1449.5	14.2	1449.5	14.2
BaggerCreek1	80	105030	2.1	10.9673	0.6	3.1024	1.1	0.2469	0.9	0.85	1422.4	11.9	1433.3	8.5	1449.5	11.2	1449.5	11.2
BaggerCreek1	113	75974	1.2	10.9633	0.6	3.1921	1.1	0.2539	0.9	0.81	1458.7	11.3	1455.3	8.2	1450.2	12.0	1450.2	12.0
BaggerCreek1	158	95199	1.1	10.9597	0.6	3.0609	1.1	0.2434	1.0	0.84	1404.4	12.0	1423.0	8.6	1450.8	11.5	1450.8	11.5

BaggerCreek1	78	53002	2.1	10.9540	0.8	3.1514	1.5	0.2505	1.3	0.86	1440.9	16.8	1445.3	11.6	1451.8	14.5	1451.8	14.5
BaggerCreek1	110	255648	1.9	10.9537	0.6	3.1386	1.2	0.2495	1.1	0.88	1435.7	13.8	1442.2	9.4	1451.9	11.2	1451.9	11.2
BaggerCreek1	200	105831	1.8	10.9528	0.8	3.1161	1.5	0.2476	1.3	0.85	1426.3	16.4	1436.7	11.5	1452.0	14.8	1452.0	14.8
BaggerCreek1	82	203611	1.9	10.9458	0.8	3.0420	1.4	0.2416	1.2	0.83	1395.0	14.8	1418.2	10.9	1453.3	15.3	1453.3	15.3
BaggerCreek1	111	162915	1.8	10.9438	0.6	3.0603	1.2	0.2430	1.0	0.87	1402.3	13.0	1422.8	9.1	1453.6	11.3	1453.6	11.3
BaggerCreek1	86	197001	1.9	10.9273	0.7	3.1807	1.2	0.2522	1.0	0.82	1449.8	13.0	1452.5	9.4	1456.5	13.3	1456.5	13.3
BaggerCreek1	100	83899	2.3	10.9187	0.6	3.1050	1.2	0.2460	1.1	0.88	1417.8	13.9	1433.9	9.5	1458.0	11.0	1458.0	11.0
BaggerCreek1	103	137252	3.4	10.9172	0.6	3.1263	1.1	0.2476	0.9	0.83	1426.3	11.6	1439.2	8.4	1458.2	11.7	1458.2	11.7
BaggerCreek1	135	120072	2.0	10.9068	0.6	3.0945	1.1	0.2449	0.9	0.82	1412.1	11.8	1431.3	8.7	1460.1	12.3	1460.1	12.3
BaggerCreek1	163	325904	1.5	10.8904	0.7	3.1263	1.1	0.2470	0.9	0.80	1423.2	11.2	1439.2	8.4	1462.9	12.5	1462.9	12.5
BaggerCreek1	76	203423	1.7	10.8872	0.6	3.1744	1.1	0.2508	0.9	0.85	1442.4	11.7	1450.9	8.2	1463.5	10.8	1463.5	10.8
BaggerCreek1	41	132772	2.2	10.8823	0.8	3.0518	1.3	0.2410	1.0	0.78	1391.7	12.4	1420.7	9.7	1464.3	15.0	1464.3	15.0
BaggerCreek1	192	623228	2.4	10.8818	0.8	3.1657	1.2	0.2500	0.9	0.76	1438.2	11.9	1448.8	9.4	1464.4	15.2	1464.4	15.2
BaggerCreek1	367	84759	1.4	10.8759	0.9	3.2503	1.6	0.2565	1.3	0.82	1471.9	16.8	1469.2	12.1	1465.4	17.1	1465.4	17.1
BaggerCreek1	193	142005	2.2	10.8616	0.7	3.0138	1.4	0.2375	1.3	0.87	1373.8	15.5	1411.1	11.1	1467.9	13.8	1467.9	13.8
BaggerCreek1	103	216832	1.6	10.8131	0.7	3.0111	1.3	0.2362	1.1	0.85	1367.1	13.9	1410.4	10.2	1476.4	13.4	1476.4	13.4
BaggerCreek1	78	127607	1.9	10.8062	0.8	2.9784	1.5	0.2335	1.2	0.84	1353.0	15.2	1402.1	11.3	1477.6	15.2	1477.6	15.2
BaggerCreek1	70	27219	1.7	10.7775	1.2	3.2177	1.6	0.2516	1.1	0.69	1446.8	14.2	1461.4	12.4	1482.7	22.0	1482.7	22.0
BaggerCreek1	47	76184	1.6	10.6786	1.0	3.1357	1.4	0.2430	1.0	0.71	1402.1	12.6	1441.5	10.9	1500.1	18.8	1500.1	18.8
BaggerCreek1	83	91518	1.1	10.6733	0.6	3.2301	1.1	0.2502	1.0	0.84	1439.3	12.3	1464.4	8.8	1501.1	11.7	1501.1	11.7
BaggerCreek1	69	35841	2.2	10.4597	1.3	3.3505	1.5	0.2543	0.9	0.58	1460.5	11.5	1492.9	12.0	1539.2	23.6	1539.2	23.6
BaggerCreek1	321	101768	5.2	10.4098	0.7	3.5374	1.4	0.2672	1.2	0.88	1526.5	16.5	1535.6	10.9	1548.2	12.3	1548.2	12.3
BaggerCreek1	67	32776	1.2	10.3718	1.0	3.2985	1.6	0.2482	1.3	0.78	1429.3	16.2	1480.7	12.6	1555.0	18.8	1555.0	18.8
BaggerCreek1	81	27776	1.8	10.3200	0.9	3.1856	1.4	0.2385	1.0	0.75	1379.1	13.0	1453.7	10.9	1564.4	17.5	1564.4	17.5
BaggerCreek1	643	132638	2.0	10.0686	0.6	3.1786	1.3	0.2322	1.1	0.87	1346.1	13.5	1452.0	9.8	1610.5	11.6	1610.5	11.6
BaggerCreek1	267	458416	3.9	9.8627	0.6	3.9709	1.2	0.2842	1.1	0.88	1612.3	15.5	1628.3	10.1	1648.9	11.1	1648.9	11.1
BaggerCreek1	359	139591	2.8	9.7682	0.5	4.1878	1.1	0.2968	1.0	0.89	1675.5	14.8	1671.6	9.3	1666.8	9.6	1666.8	9.6
BaggerCreek1	213	193895	3.3	9.7568	0.7	4.1962	1.3	0.2971	1.1	0.85	1676.7	16.8	1673.3	11.0	1668.9	13.3	1668.9	13.3
BaggerCreek1	247	111242	2.0	9.7336	0.6	4.2904	1.2	0.3030	1.0	0.87	1706.2	15.4	1691.5	9.7	1673.3	10.6	1673.3	10.6
BaggerCreek1	194	250590	2.8	9.7222	0.7	4.3146	1.3	0.3044	1.1	0.86	1712.9	16.9	1696.2	10.8	1675.5	12.2	1675.5	12.2
BaggerCreek1	340	155826	2.8	9.6868	0.6	4.1885	1.3	0.2944	1.1	0.87	1663.4	16.0	1671.8	10.3	1682.2	11.5	1682.2	11.5

BaggerCreek1	180	130385	2.3	9.6847	0.6	4.0750	1.3	0.2864	1.2	0.89	1623.3	16.5	1649.3	10.6	1682.6	10.9	1682.6	10.9
BaggerCreek1	190	213275	2.8	9.6611	0.7	4.3173	1.3	0.3026	1.1	0.85	1704.4	16.9	1696.7	10.9	1687.1	12.7	1687.1	12.7
BaggerCreek1	114	4020246	3.0	9.6611	0.8	4.3334	1.4	0.3038	1.1	0.82	1709.9	16.6	1699.7	11.2	1687.1	14.5	1687.1	14.5
BaggerCreek1	342	231228	5.1	9.6512	0.7	4.0869	1.4	0.2862	1.2	0.85	1622.5	16.7	1651.7	11.2	1689.0	13.5	1689.0	13.5
BaggerCreek1	528	161553	3.2	9.6385	0.6	3.8020	1.3	0.2659	1.1	0.89	1519.9	15.5	1593.2	10.3	1691.5	10.7	1691.5	10.7
BaggerCreek1	203	374509	1.8	9.6297	0.7	4.1715	1.4	0.2915	1.2	0.86	1648.9	17.8	1668.4	11.6	1693.1	13.2	1693.1	13.2
BaggerCreek1	111	76020	2.5	9.6264	0.5	4.4159	1.1	0.3084	1.0	0.87	1733.0	14.8	1715.3	9.2	1693.8	10.1	1693.8	10.1
BaggerCreek1	312	309661	4.4	9.6221	0.6	4.3820	1.2	0.3059	1.0	0.87	1720.7	15.5	1709.0	9.8	1694.6	11.0	1694.6	11.0
BaggerCreek1	91	147225	2.0	9.6172	0.7	4.3468	1.3	0.3033	1.1	0.85	1707.8	17.2	1702.3	11.1	1695.5	13.0	1695.5	13.0
BaggerCreek1	138	169848	1.2	9.6099	0.7	4.0754	1.7	0.2842	1.5	0.91	1612.3	21.6	1649.4	13.5	1696.9	12.7	1696.9	12.7
BaggerCreek1	537	453006	3.2	9.5967	0.6	3.9872	1.2	0.2776	1.1	0.87	1579.5	15.2	1631.6	10.1	1699.5	11.1	1699.5	11.1
BaggerCreek1	131	327104	2.2	9.5966	0.5	4.4891	1.2	0.3126	1.0	0.89	1753.4	15.8	1729.0	9.6	1699.5	9.8	1699.5	9.8
BaggerCreek1	346	298163	2.9	9.5759	0.8	4.2107	1.3	0.2926	1.1	0.78	1654.3	15.3	1676.1	11.0	1703.5	15.4	1703.5	15.4
BaggerCreek1	198	248062	2.0	9.5741	0.8	4.3849	1.4	0.3046	1.2	0.84	1714.1	18.1	1709.5	11.9	1703.8	14.4	1703.8	14.4
BaggerCreek1	247	151836	2.3	9.5723	0.6	4.4649	1.3	0.3101	1.1	0.87	1741.2	16.7	1724.5	10.4	1704.1	11.5	1704.1	11.5
BaggerCreek1	406	134940	1.7	9.5669	1.0	3.6664	1.9	0.2545	1.6	0.85	1461.7	20.5	1564.1	14.8	1705.2	18.2	1705.2	18.2
BaggerCreek1	139	65611	2.5	9.5606	0.7	4.4415	1.6	0.3081	1.5	0.90	1731.4	22.1	1720.1	13.4	1706.4	12.9	1706.4	12.9
BaggerCreek1	114	388062	2.4	9.5557	0.7	4.3138	1.4	0.2991	1.2	0.88	1686.8	18.1	1696.0	11.4	1707.4	12.0	1707.4	12.0
BaggerCreek1	275	105325	11.1	9.5442	0.9	4.3309	1.5	0.2999	1.3	0.82	1690.9	18.8	1699.3	12.7	1709.6	16.1	1709.6	16.1
BaggerCreek1	802	1977089	2.9	9.5401	0.7	3.5266	1.7	0.2441	1.5	0.90	1408.1	19.2	1533.2	13.3	1710.4	13.3	1710.4	13.3
BaggerCreek1	133	264815	3.0	9.5397	0.7	4.5190	1.5	0.3128	1.4	0.90	1754.5	21.1	1734.5	12.7	1710.4	12.5	1710.4	12.5
BaggerCreek1	89	799517	1.7	9.5327	0.6	4.2442	1.4	0.2936	1.3	0.89	1659.3	18.4	1682.6	11.6	1711.8	11.8	1711.8	11.8
BaggerCreek1	232	606119	3.8	9.5262	0.6	4.3306	1.4	0.2993	1.3	0.90	1688.0	19.2	1699.2	11.9	1713.0	11.8	1713.0	11.8
BaggerCreek1	431	295010	2.8	9.5237	0.8	4.3220	1.2	0.2987	0.9	0.77	1684.7	13.7	1697.6	9.8	1713.5	13.9	1713.5	13.9
BaggerCreek1	257	2449356	2.4	9.5201	0.8	4.4164	1.5	0.3051	1.3	0.86	1716.4	19.3	1715.4	12.3	1714.2	14.1	1714.2	14.1
BaggerCreek1	420	711833	13.4	9.5192	0.9	4.2069	1.4	0.2906	1.2	0.81	1644.4	16.9	1675.4	11.9	1714.4	15.8	1714.4	15.8
BaggerCreek1	111	153641	2.2	9.5178	0.7	3.8346	1.4	0.2648	1.2	0.86	1514.5	15.7	1600.0	10.9	1714.6	12.8	1714.6	12.8
BaggerCreek1	338	137487	3.9	9.5174	0.6	4.3091	1.2	0.2976	1.0	0.83	1679.3	14.2	1695.1	9.5	1714.7	11.8	1714.7	11.8
BaggerCreek1	119	705936	2.2	9.4707	0.8	4.3757	1.2	0.3007	0.9	0.77	1694.7	13.9	1707.8	10.0	1723.8	14.1	1723.8	14.1
BaggerCreek1	131	80827	2.4	9.4622	0.7	4.3080	1.4	0.2958	1.1	0.84	1670.3	16.8	1694.9	11.2	1725.4	13.4	1725.4	13.4
BaggerCreek1	444	65379	8.9	9.4558	1.0	3.9408	2.2	0.2704	2.0	0.88	1542.7	27.1	1622.1	18.1	1726.7	19.2	1726.7	19.2

BaggerCreek1	92	106150	2.6	9.4506	0.8	4.6168	1.3	0.3166	1.0	0.78	1773.0	15.3	1752.3	10.6	1727.7	14.5	1727.7	14.5
BaggerCreek1	629	284915	4.5	9.4359	0.6	4.0855	1.1	0.2797	0.9	0.80	1589.9	12.0	1651.4	8.7	1730.5	11.9	1730.5	11.9
BaggerCreek1	539	723955	4.0	9.4084	0.8	4.2667	1.4	0.2913	1.1	0.81	1647.9	16.1	1687.0	11.2	1735.9	14.5	1735.9	14.5
BaggerCreek1	693	308604	3.2	9.3939	0.6	3.8157	1.3	0.2601	1.1	0.87	1490.3	14.6	1596.1	10.1	1738.7	11.4	1738.7	11.4
BaggerCreek1	759	595050	1.8	9.3843	0.6	4.0737	1.2	0.2774	1.0	0.84	1578.1	13.7	1649.0	9.5	1740.6	11.5	1740.6	11.5
BaggerCreek1	648	81069	1.2	9.3034	0.5	3.7383	1.1	0.2523	0.9	0.87	1450.6	12.3	1579.6	8.7	1756.4	9.7	1756.4	9.7
BaggerCreek1	394	21755	3.8	9.2191	0.8	4.1681	1.6	0.2788	1.4	0.87	1585.4	19.3	1667.8	13.0	1773.1	14.4	1773.1	14.4
BaggerCreek1	251	56645	2.5	8.2723	0.6	4.9615	1.1	0.2978	1.0	0.85	1680.4	14.2	1812.8	9.5	1968.5	10.7	1968.5	10.7
BaggerCreek1	233	25556	0.7	5.3694	0.7	10.8539	1.7	0.4229	1.5	0.92	2273.5	29.4	2510.7	15.5	2708.5	10.8	2708.5	10.8
Gardner 5	869	46320	11.4	21.1117	0.9	0.0656	1.4	0.0101	1.2	0.80	64.5	0.7	64.5	0.9	66.7	20.6	64.5	0.7
Gardner 5	113	26479	0.9	16.6779	3.6	0.0841	3.7	0.0102	1.1	0.30	65.3	0.7	82.0	2.9	601.1	77.2	65.3	0.7
Gardner 5	293	5026	2.1	22.1207	1.5	0.0648	1.9	0.0104	1.1	0.60	66.7	0.8	63.8	1.2	NA	NA	66.7	0.8
Gardner 5	70	1455	1.5	22.8816	4.5	0.0630	4.7	0.0105	1.3	0.28	67.1	0.9	62.1	2.8	NA	NA	67.1	0.9
Gardner 5	267	11162	1.4	21.4212	1.5	0.0751	2.0	0.0117	1.3	0.64	74.8	0.9	73.5	1.4	32.0	36.4	74.8	0.9
Gardner 5	988	1148	3.5	6.8132	0.9	1.0917	1.4	0.0540	1.1	0.77	338.8	3.5	749.3	7.3	2307.9	15.3	338.8	3.5
Gardner 5	573	36319	3.4	16.7771	0.6	0.6679	1.2	0.0813	1.0	0.86	503.9	5.1	519.5	4.9	588.3	13.6	503.9	5.1
Gardner 5	106	63481	4.8	16.8599	0.8	0.6713	1.4	0.0821	1.1	0.81	508.8	5.5	521.5	5.7	577.7	18.1	508.8	5.5
Gardner 5	127	133361	1.8	17.0992	0.8	0.6648	1.1	0.0825	0.8	0.66	510.9	3.7	517.6	4.6	546.9	18.5	510.9	3.7
Gardner 5	102	12568	1.8	17.3374	0.9	0.6574	1.2	0.0827	0.8	0.65	512.2	3.8	513.0	4.8	516.6	19.8	512.2	3.8
Gardner 5	140	27166	3.2	17.3508	0.9	0.6586	1.3	0.0829	1.0	0.75	513.5	5.0	513.8	5.4	514.9	19.8	513.5	5.0
Gardner 5	156	19253	4.2	17.3882	0.8	0.6573	1.2	0.0829	1.0	0.80	513.5	4.9	512.9	5.0	510.2	16.5	513.5	4.9
Gardner 5	149	67534	1.9	17.0871	0.9	0.6689	1.3	0.0829	0.9	0.68	513.6	4.4	520.1	5.3	548.5	20.7	513.6	4.4
Gardner 5	206	29524	3.7	17.3427	0.8	0.6598	1.2	0.0830	0.9	0.75	514.1	4.5	514.5	4.9	515.9	17.7	514.1	4.5
Gardner 5	83	16925	2.8	17.3284	0.8	0.6607	1.5	0.0831	1.2	0.81	514.5	5.9	515.1	5.9	517.7	18.6	514.5	5.9
Gardner 5	115	101004	2.8	17.1110	0.7	0.6702	1.3	0.0832	1.0	0.83	515.2	5.2	520.8	5.2	545.4	15.6	515.2	5.2
Gardner 5	240	52174	4.1	17.4130	0.8	0.6586	1.6	0.0832	1.4	0.88	515.3	6.9	513.8	6.4	507.1	16.6	515.3	6.9
Gardner 5	186	88419	2.8	17.0379	0.8	0.6738	1.3	0.0833	1.1	0.79	515.8	5.3	523.0	5.5	554.8	17.8	515.8	5.3
Gardner 5	246	26122	3.7	17.3955	0.6	0.6606	1.4	0.0834	1.2	0.88	516.3	5.9	515.0	5.5	509.3	14.0	516.3	5.9
Gardner 5	50	85891	2.8	17.1226	1.3	0.6716	1.7	0.0834	1.1	0.63	516.6	5.4	521.7	7.0	544.0	29.0	516.6	5.4
Gardner 5	167	79450	3.3	17.2100	0.8	0.6682	1.3	0.0834	1.1	0.79	516.6	5.2	519.6	5.4	532.8	17.7	516.6	5.2

Gardner 5	243	71794	1.9	17.2633	0.9	0.6662	1.4	0.0835	1.1	0.76	516.7	5.2	518.4	5.6	526.0	19.6	516.7	5.2
Gardner 5	92	39520	2.1	17.1600	1.0	0.6707	1.5	0.0835	1.1	0.73	517.0	5.5	521.1	6.1	539.2	22.3	517.0	5.5
Gardner 5	76	16991	3.8	17.4312	1.0	0.6608	1.5	0.0836	1.0	0.70	517.5	5.1	515.1	5.9	504.8	23.1	517.5	5.1
Gardner 5	247	32040	2.6	17.2003	0.8	0.6700	1.4	0.0836	1.2	0.84	517.7	5.7	520.7	5.6	534.1	16.5	517.7	5.7
Gardner 5	112	15655	2.2	17.2388	0.8	0.6686	1.2	0.0836	0.9	0.77	517.7	4.7	519.9	5.0	529.2	17.0	517.7	4.7
Gardner 5	363	98315	3.9	17.2771	0.6	0.6677	1.0	0.0837	0.8	0.79	518.2	4.1	519.3	4.2	524.2	13.9	518.2	4.1
Gardner 5	94	21251	3.9	17.1945	0.9	0.6710	1.3	0.0837	0.9	0.68	518.3	4.3	521.3	5.2	534.8	20.6	518.3	4.3
Gardner 5	114	41194	2.6	17.2052	0.7	0.6706	1.1	0.0837	0.8	0.72	518.3	3.8	521.1	4.3	533.4	16.2	518.3	3.8
Gardner 5	173	49291	2.2	17.3831	0.9	0.6641	1.5	0.0838	1.2	0.81	518.5	6.1	517.1	6.0	510.9	19.0	518.5	6.1
Gardner 5	120	131437	2.5	17.2178	0.8	0.6712	1.5	0.0838	1.4	0.87	519.1	6.7	521.4	6.3	531.8	16.6	519.1	6.7
Gardner 5	179	14331	3.4	17.3412	0.6	0.6667	1.3	0.0839	1.1	0.88	519.2	5.5	518.7	5.1	516.1	13.4	519.2	5.5
Gardner 5	114	278760	2.2	17.0945	0.8	0.6767	1.3	0.0839	1.0	0.76	519.6	4.9	524.8	5.3	547.5	18.2	519.6	4.9
Gardner 5	378	50090	2.9	17.2666	0.7	0.6711	1.2	0.0841	1.0	0.82	520.4	5.0	521.4	5.0	525.6	15.2	520.4	5.0
Gardner 5	488	115638	2.5	17.0850	0.6	0.6787	1.1	0.0841	0.9	0.85	520.8	4.6	526.0	4.4	548.7	12.4	520.8	4.6
Gardner 5	381	196154	6.2	17.2333	0.5	0.6731	1.1	0.0842	0.9	0.88	521.0	4.6	522.6	4.3	529.9	11.2	521.0	4.6
Gardner 5	118	165403	2.4	17.0906	0.9	0.6790	1.4	0.0842	1.0	0.77	521.1	5.2	526.2	5.6	548.0	19.2	521.1	5.2
Gardner 5	200	176207	1.8	17.1602	0.7	0.6767	1.4	0.0843	1.2	0.84	521.5	5.8	524.8	5.6	539.2	16.4	521.5	5.8
Gardner 5	283	69558	2.8	17.0814	0.7	0.6802	1.3	0.0843	1.1	0.87	521.8	5.7	526.9	5.4	549.2	14.3	521.8	5.7
Gardner 5	107	214832	4.6	16.8672	0.9	0.6890	1.4	0.0843	1.1	0.78	521.9	5.4	532.2	5.8	576.7	19.0	521.9	5.4
Gardner 5	235	50305	2.5	17.2526	0.8	0.6741	1.3	0.0844	1.1	0.81	522.3	5.4	523.2	5.4	527.4	17.1	522.3	5.4
Gardner 5	405	123008	4.0	17.0692	0.5	0.6816	1.0	0.0844	0.8	0.84	522.5	4.1	527.8	4.0	550.8	11.5	522.5	4.1
Gardner 5	62	23615	4.0	17.0086	1.1	0.6841	1.5	0.0844	1.1	0.70	522.5	5.4	529.2	6.4	558.5	23.9	522.5	5.4
Gardner 5	129	41434	3.7	17.4270	0.7	0.6679	1.3	0.0845	1.0	0.81	522.6	5.2	519.4	5.2	505.3	16.4	522.6	5.2
Gardner 5	242	151796	3.7	17.2141	0.6	0.6764	1.4	0.0845	1.2	0.90	522.8	6.2	524.6	5.6	532.3	13.3	522.8	6.2
Gardner 5	181	98101	3.0	17.3102	0.8	0.6727	1.3	0.0845	1.0	0.78	522.9	5.0	522.4	5.2	520.0	17.6	522.9	5.0
Gardner 5	384	77952	5.6	17.0894	0.7	0.6815	1.2	0.0845	0.9	0.81	522.9	4.8	527.7	4.8	548.2	15.1	522.9	4.8
Gardner 5	237	110670	2.3	17.2396	0.7	0.6760	1.3	0.0846	1.1	0.85	523.3	5.7	524.4	5.5	529.0	15.2	523.3	5.7
Gardner 5	419	184528	1.5	17.3949	0.6	0.6703	1.2	0.0846	1.0	0.85	523.6	5.1	520.9	4.9	509.3	14.0	523.6	5.1
Gardner 5	303	676497	3.2	17.0650	0.7	0.6843	1.2	0.0847	1.0	0.81	524.3	5.1	529.4	5.1	551.3	15.9	524.3	5.1
Gardner 5	89	34966	2.7	17.3273	0.5	0.6745	1.2	0.0848	1.1	0.89	524.8	5.3	523.5	4.8	517.9	11.9	524.8	5.3
Gardner 5	178	81453	3.6	17.2941	0.8	0.6766	1.1	0.0849	0.8	0.74	525.3	4.2	524.7	4.6	522.1	16.8	525.3	4.2

Gardner 5	123	64360	3.1	17.3580	0.7	0.6742	1.1	0.0849	0.8	0.76	525.4	4.2	523.2	4.5	514.0	15.7	525.4	4.2
Gardner 5	184	92927	3.6	16.9585	0.9	0.6902	1.2	0.0849	0.8	0.66	525.4	4.0	532.9	4.9	564.9	19.5	525.4	4.0
Gardner 5	151	83736	2.9	17.3298	0.8	0.6754	1.2	0.0849	0.8	0.72	525.5	4.3	524.0	4.8	517.6	17.9	525.5	4.3
Gardner 5	445	65516	4.3	17.2198	0.7	0.6799	1.0	0.0850	0.8	0.77	525.6	4.0	526.7	4.3	531.6	14.4	525.6	4.0
Gardner 5	158	75869	3.6	17.3440	0.8	0.6753	1.2	0.0850	0.9	0.73	525.8	4.4	523.9	4.9	515.8	17.8	525.8	4.4
Gardner 5	126	19803	4.5	17.3953	0.9	0.6733	1.3	0.0850	0.9	0.69	525.8	4.5	522.7	5.3	509.3	20.8	525.8	4.5
Gardner 5	506	61565	3.5	17.3613	0.7	0.6748	1.1	0.0850	0.8	0.78	525.9	4.2	523.6	4.4	513.6	14.9	525.9	4.2
Gardner 5	346	61400	5.8	17.2900	0.6	0.6785	1.2	0.0851	1.1	0.88	526.6	5.3	525.9	4.9	522.6	12.7	526.6	5.3
Gardner 5	238	57739	2.6	17.2221	0.6	0.6812	1.3	0.0851	1.1	0.87	526.6	5.6	527.5	5.2	531.3	13.9	526.6	5.6
Gardner 5	204	71281	2.5	17.0947	0.7	0.6879	1.2	0.0853	0.9	0.80	527.9	4.8	531.6	4.9	547.5	15.6	527.9	4.8
Gardner 5	319	68175	2.8	17.3037	0.6	0.6798	1.2	0.0853	1.0	0.84	528.0	5.1	526.6	4.9	520.9	14.1	528.0	5.1
Gardner 5	184	61638	2.5	17.4101	0.8	0.6765	1.2	0.0855	0.9	0.75	528.6	4.7	524.7	5.0	507.5	17.8	528.6	4.7
Gardner 5	267	46287	3.0	17.4125	0.6	0.6772	1.0	0.0856	0.8	0.81	529.2	4.1	525.1	4.1	507.1	13.0	529.2	4.1
Gardner 5	131	813652	3.1	16.6347	0.8	0.7111	1.2	0.0858	0.9	0.74	530.8	4.7	545.4	5.3	606.8	18.1	530.8	4.7
Gardner 5	121	11481	4.3	17.2711	0.8	0.6862	1.7	0.0860	1.5	0.88	531.8	7.9	530.5	7.2	525.0	18.2	531.8	7.9
Gardner 5	334	80695	4.9	17.2302	0.8	0.6884	1.3	0.0861	1.1	0.82	532.2	5.6	531.8	5.5	530.2	16.5	532.2	5.6
Gardner 5	132	54121	2.1	17.2386	0.9	0.6882	1.4	0.0861	1.1	0.76	532.3	5.6	531.7	6.0	529.2	20.6	532.3	5.6
Gardner 5	74	58939	1.6	16.6824	0.9	0.7784	1.5	0.0942	1.2	0.79	580.4	6.5	584.6	6.6	600.6	19.6	580.4	6.5
Gardner 5	83	35610	3.0	13.7158	0.8	1.7111	1.4	0.1703	1.1	0.81	1013.7	10.5	1012.7	8.8	1010.5	16.2	1010.5	16.2
Gardner 5	55	22535	3.9	13.0152	1.1	1.9578	1.5	0.1849	1.1	0.71	1093.6	10.7	1101.1	10.1	1116.0	21.3	1116.0	21.3
Gardner 5	136	103992	3.8	11.2286	0.7	3.0151	1.3	0.2456	1.1	0.84	1416.0	13.9	1411.4	10.0	1404.6	13.8	1404.6	13.8
Gardner 5	76	251474	1.5	11.2271	0.8	3.1317	1.6	0.2551	1.4	0.88	1464.8	19.0	1440.5	12.6	1404.8	14.8	1404.8	14.8
Gardner 5	435	192019	2.1	11.2164	0.5	3.0446	1.2	0.2478	1.1	0.90	1427.0	14.1	1418.9	9.4	1406.7	10.4	1406.7	10.4
Gardner 5	171	115958	1.1	11.2096	0.6	3.0804	1.1	0.2505	0.9	0.82	1441.3	11.2	1427.8	8.1	1407.8	11.4	1407.8	11.4
Gardner 5	136	179113	3.8	11.1496	0.6	3.0315	1.3	0.2452	1.2	0.90	1413.9	15.3	1415.6	10.2	1418.1	11.2	1418.1	11.2
Gardner 5	207	157785	4.5	11.1308	0.6	3.0630	1.2	0.2474	1.0	0.85	1424.9	12.8	1423.5	9.0	1421.3	11.7	1421.3	11.7
Gardner 5	507	1426213	5.5	11.1053	0.6	3.0224	1.0	0.2435	0.8	0.80	1405.1	10.2	1413.3	7.6	1425.7	11.3	1425.7	11.3
Gardner 5	156	382779	1.8	11.1014	0.7	3.1687	1.1	0.2552	0.9	0.77	1465.4	11.4	1449.6	8.7	1426.4	13.7	1426.4	13.7
Gardner 5	139	594002	2.0	11.0923	0.7	3.0681	1.2	0.2469	1.0	0.82	1422.7	12.6	1424.8	9.2	1427.9	13.0	1427.9	13.0
Gardner 5	303	82682	2.2	11.0858	0.7	3.0825	1.3	0.2479	1.1	0.85	1427.9	14.4	1428.4	10.1	1429.0	13.1	1429.0	13.1
Gardner 5	233	198751	3.3	11.0699	0.6	3.0422	1.3	0.2444	1.1	0.88	1409.3	14.4	1418.3	9.9	1431.8	12.0	1431.8	12.0

Gardner 5	290	297939	1.6	11.0584	0.6	3.1366	1.1	0.2517	0.9	0.82	1447.1	11.4	1441.7	8.3	1433.8	11.8	1433.8	11.8
Gardner 5	557	85237	6.4	10.9723	0.7	3.0482	1.4	0.2427	1.2	0.88	1400.6	15.2	1419.8	10.5	1448.7	12.5	1448.7	12.5
Gardner 5	686	718646	8.3	10.9251	0.5	3.0816	1.0	0.2443	0.8	0.86	1408.9	10.6	1428.1	7.5	1456.9	9.5	1456.9	9.5
Gardner 5	35	54017	1.7	10.9085	0.7	3.1545	1.0	0.2497	0.7	0.71	1436.8	9.3	1446.1	7.8	1459.7	13.5	1459.7	13.5
Gardner 5	125	146149	2.8	10.9066	0.6	3.0505	1.2	0.2414	1.1	0.87	1394.0	13.6	1420.4	9.5	1460.1	11.7	1460.1	11.7
Gardner 5	166	429345	2.2	10.6240	0.7	3.3364	1.8	0.2572	1.6	0.91	1475.4	21.4	1489.6	13.9	1509.8	13.7	1509.8	13.7
Gardner 5	118	106435	1.2	10.5634	0.6	3.2471	1.2	0.2489	1.1	0.87	1432.7	13.8	1468.5	9.6	1520.6	11.4	1520.6	11.4
Gardner 5	111	77552	1.5	10.3293	0.6	3.3434	1.2	0.2506	1.0	0.88	1441.5	13.3	1491.3	9.2	1562.7	10.7	1562.7	10.7
Gardner 5	44	142603	5.2	10.0966	0.6	3.9010	1.3	0.2858	1.2	0.89	1620.4	16.7	1613.9	10.6	1605.3	11.2	1605.3	11.2
Gardner 5	88	365553	3.4	9.9954	0.7	3.9287	1.2	0.2849	1.0	0.83	1616.1	14.6	1619.6	10.0	1624.1	12.8	1624.1	12.8
Gardner 5	48	62433	2.9	9.9103	0.8	3.9471	1.2	0.2838	0.9	0.73	1610.6	12.3	1623.4	9.6	1640.0	15.0	1640.0	15.0
Gardner 5	199	134431	3.9	9.8938	0.8	4.1048	1.3	0.2947	1.0	0.81	1664.9	15.4	1655.3	10.6	1643.1	14.3	1643.1	14.3
Gardner 5	18	32473	2.4	9.8690	0.8	4.0094	1.2	0.2871	0.9	0.75	1627.0	12.6	1636.1	9.5	1647.8	14.3	1647.8	14.3
Gardner 5	405	134793	5.7	9.8580	0.6	4.2681	1.1	0.3053	0.9	0.83	1717.5	13.4	1687.2	8.8	1649.8	11.2	1649.8	11.2
Gardner 5	80	40523	17.1	9.8559	0.7	4.0594	1.3	0.2903	1.1	0.84	1643.0	15.7	1646.2	10.6	1650.2	13.2	1650.2	13.2
Gardner 5	84	308202	2.3	9.8479	0.8	4.0712	1.5	0.2909	1.2	0.84	1646.0	18.1	1648.5	12.0	1651.7	14.7	1651.7	14.7
Gardner 5	51	42107	3.2	9.8461	1.0	4.1662	1.4	0.2976	1.0	0.70	1679.6	14.5	1667.4	11.5	1652.0	18.6	1652.0	18.6
Gardner 5	209	90935	2.6	9.8358	0.6	4.1217	1.0	0.2941	0.9	0.84	1662.2	12.5	1658.6	8.4	1654.0	10.4	1654.0	10.4
Gardner 5	445	2140316	5.6	9.8325	0.6	4.1797	1.1	0.2982	0.9	0.83	1682.3	13.9	1670.1	9.3	1654.6	11.9	1654.6	11.9
Gardner 5	400	220659	3.1	9.8099	0.6	4.2498	1.2	0.3025	1.1	0.87	1703.7	16.2	1683.7	10.2	1658.9	11.5	1658.9	11.5
Gardner 5	225	167695	3.8	9.8002	0.6	4.2959	1.1	0.3055	1.0	0.85	1718.4	14.6	1692.6	9.4	1660.7	11.3	1660.7	11.3
Gardner 5	289	49526	1.5	9.7970	0.5	4.0349	1.3	0.2868	1.2	0.92	1625.6	17.1	1641.3	10.5	1661.3	9.2	1661.3	9.2
Gardner 5	177	100255	2.6	9.7869	0.6	4.1823	1.0	0.2970	0.8	0.83	1676.4	12.2	1670.5	8.2	1663.2	10.3	1663.2	10.3
Gardner 5	230	87243	5.1	9.7673	0.6	4.2509	1.2	0.3013	1.1	0.88	1697.6	16.2	1683.9	10.1	1666.9	10.7	1666.9	10.7
Gardner 5	132	463657	3.1	9.7652	0.6	4.1914	1.1	0.2970	0.9	0.83	1676.3	13.6	1672.3	9.1	1667.3	11.3	1667.3	11.3
Gardner 5	70	88486	2.1	9.7588	0.7	4.0311	1.2	0.2854	1.0	0.83	1618.7	14.7	1640.5	10.1	1668.5	13.0	1668.5	13.0
Gardner 5	321	111786	8.8	9.7471	0.8	4.1783	1.4	0.2955	1.1	0.83	1669.0	16.8	1669.8	11.2	1670.8	14.0	1670.8	14.0
Gardner 5	109	79808	1.8	9.7438	0.6	4.1794	1.1	0.2955	1.0	0.87	1668.9	14.6	1670.0	9.3	1671.4	10.3	1671.4	10.3
Gardner 5	98	147422	4.3	9.7415	0.7	4.2578	1.1	0.3010	0.9	0.80	1696.0	13.0	1685.3	9.0	1671.8	12.3	1671.8	12.3
Gardner 5	118	67895	1.7	9.7406	0.7	4.2943	1.1	0.3035	0.9	0.77	1708.6	12.9	1692.3	9.2	1672.0	13.2	1672.0	13.2
Gardner 5	127	160695	1.7	9.7353	0.5	4.2346	0.9	0.2991	0.8	0.84	1687.0	11.6	1680.8	7.7	1673.0	9.4	1673.0	9.4

Gardner 5	89	62778	3.6	9.7312	0.7	4.3662	1.2	0.3083	0.9	0.80	1732.3	14.2	1706.0	9.7	1673.8	13.0	1673.8	13.0
Gardner 5	112	123542	2.2	9.7262	0.5	4.2871	1.1	0.3025	1.0	0.89	1703.9	14.7	1690.9	9.0	1674.7	9.1	1674.7	9.1
Gardner 5	141	87245	1.4	9.7260	0.5	4.1395	0.9	0.2921	0.8	0.83	1652.1	11.4	1662.1	7.7	1674.8	9.6	1674.8	9.6
Gardner 5	121	56716	2.5	9.7217	0.6	4.1934	1.0	0.2958	0.8	0.79	1670.4	11.9	1672.7	8.4	1675.6	11.5	1675.6	11.5
Gardner 5	217	70006	3.2	9.7216	0.5	4.3003	1.3	0.3033	1.2	0.91	1707.8	18.1	1693.4	10.9	1675.6	10.0	1675.6	10.0
Gardner 5	56	107751	1.7	9.7198	0.7	4.0824	1.2	0.2879	1.0	0.80	1631.1	13.8	1650.8	9.8	1675.9	13.2	1675.9	13.2
Gardner 5	387	443105	2.5	9.7147	0.6	4.1649	1.2	0.2936	1.0	0.85	1659.4	14.8	1667.1	9.8	1676.9	11.8	1676.9	11.8
Gardner 5	277	176877	3.8	9.7088	0.7	4.2239	1.3	0.2976	1.1	0.85	1679.2	16.3	1678.7	10.6	1678.0	12.4	1678.0	12.4
Gardner 5	143	259002	5.1	9.7068	0.6	4.2875	0.9	0.3020	0.8	0.80	1701.1	11.2	1691.0	7.7	1678.4	10.4	1678.4	10.4
Gardner 5	24	11002	2.5	9.7051	0.9	4.2284	1.3	0.2978	0.8	0.66	1680.2	12.4	1679.5	10.4	1678.7	17.5	1678.7	17.5
Gardner 5	28	11810	2.1	9.7009	0.7	4.3268	1.3	0.3046	1.2	0.86	1713.9	17.4	1698.5	11.1	1679.5	12.9	1679.5	12.9
Gardner 5	213	249447	3.4	9.6928	0.7	4.2314	1.4	0.2976	1.2	0.88	1679.3	18.4	1680.1	11.6	1681.1	12.1	1681.1	12.1
Gardner 5	147	5806450	3.5	9.6885	0.6	4.3466	1.3	0.3056	1.2	0.89	1718.8	18.1	1702.3	11.1	1681.9	11.3	1681.9	11.3
Gardner 5	248	143270	4.0	9.6854	0.7	4.2848	1.5	0.3011	1.3	0.87	1696.8	19.1	1690.4	12.2	1682.5	13.5	1682.5	13.5
Gardner 5	266	182388	1.5	9.6850	0.7	4.1212	1.3	0.2896	1.1	0.82	1639.6	15.4	1658.5	10.6	1682.6	13.8	1682.6	13.8
Gardner 5	262	160294	2.1	9.6840	0.8	4.2225	1.3	0.2967	1.0	0.81	1674.9	15.5	1678.4	10.6	1682.8	13.9	1682.8	13.9
Gardner 5	74	688123	2.4	9.6799	0.6	4.1814	1.1	0.2937	1.0	0.85	1659.9	14.0	1670.4	9.2	1683.5	10.9	1683.5	10.9
Gardner 5	79	229683	2.4	9.6781	0.7	4.2401	1.2	0.2978	0.9	0.78	1680.2	13.6	1681.8	9.7	1683.9	13.8	1683.9	13.8
Gardner 5	179	63849	3.7	9.6738	0.5	4.2169	1.1	0.2960	0.9	0.87	1671.4	13.7	1677.3	8.8	1684.7	9.9	1684.7	9.9
Gardner 5	154	6574208	3.0	9.6638	0.5	4.3599	1.0	0.3057	0.9	0.85	1719.6	13.1	1704.8	8.5	1686.6	10.0	1686.6	10.0
Gardner 5	71	127242	3.6	9.6630	0.6	4.0921	1.2	0.2869	1.1	0.86	1626.1	15.1	1652.7	10.0	1686.8	11.5	1686.8	11.5
Gardner 5	91	225637	4.0	9.6625	0.6	4.3419	1.1	0.3044	1.0	0.87	1713.1	14.9	1701.4	9.4	1686.9	10.3	1686.9	10.3
Gardner 5	77	67789	2.4	9.6521	0.6	4.2553	1.2	0.2980	1.0	0.88	1681.5	15.3	1684.8	9.6	1688.9	10.3	1688.9	10.3
Gardner 5	216	386989	3.3	9.6502	0.7	4.3383	1.4	0.3038	1.2	0.86	1710.0	17.8	1700.7	11.3	1689.2	12.8	1689.2	12.8
Gardner 5	411	139231	5.3	9.6481	0.6	4.2721	1.3	0.2991	1.2	0.87	1686.7	17.2	1688.0	10.9	1689.6	11.9	1689.6	11.9
Gardner 5	41	33527	2.1	9.6407	0.8	4.2893	1.1	0.3000	0.8	0.72	1691.5	11.7	1691.3	9.0	1691.0	14.1	1691.0	14.1
Gardner 5	47	87263	2.2	9.6374	0.7	4.0713	1.4	0.2847	1.2	0.85	1615.0	16.7	1648.6	11.2	1691.7	13.1	1691.7	13.1
Gardner 5	33	11758	2.0	9.6316	0.9	4.2099	1.4	0.2942	1.1	0.78	1662.5	16.6	1676.0	11.8	1692.8	16.5	1692.8	16.5
Gardner 5	135	70835	1.9	9.6300	0.7	4.2120	1.2	0.2943	1.0	0.83	1663.0	14.3	1676.4	9.6	1693.1	12.0	1693.1	12.0
Gardner 5	145	76990	4.4	9.6268	0.5	4.3749	1.1	0.3056	0.9	0.86	1719.0	14.0	1707.6	8.9	1693.7	10.0	1693.7	10.0
Gardner 5	125	74301	2.4	9.6244	0.7	4.2377	1.0	0.2959	0.8	0.75	1671.1	11.4	1681.3	8.5	1694.1	12.5	1694.1	12.5

Gardner 5	114	50652	1.7	9.6204	0.7	4.1398	1.3	0.2890	1.1	0.86	1636.4	15.8	1662.2	10.4	1694.9	12.1	1694.9	12.1
Gardner 5	503	39499	3.7	9.6172	0.9	3.9287	1.4	0.2741	1.1	0.77	1561.8	14.7	1619.6	11.1	1695.5	16.0	1695.5	16.0
Gardner 5	255	507190	2.4	9.6157	0.7	4.3259	1.2	0.3018	1.0	0.83	1700.3	14.2	1698.3	9.5	1695.8	12.0	1695.8	12.0
Gardner 5	86	52595	1.7	9.6051	0.5	4.3232	1.2	0.3013	1.1	0.91	1697.8	15.7	1697.8	9.6	1697.9	8.8	1697.9	8.8
Gardner 5	116	276651	2.6	9.6009	0.6	4.1115	1.2	0.2864	1.1	0.87	1623.6	15.3	1656.6	9.9	1698.7	10.9	1698.7	10.9
Gardner 5	56	124962	3.1	9.5993	0.7	4.3151	1.3	0.3006	1.1	0.87	1694.0	17.1	1696.2	10.9	1699.0	12.1	1699.0	12.1
Gardner 5	83	40710	3.2	9.5988	0.6	4.3947	1.2	0.3061	1.0	0.88	1721.4	15.8	1711.3	9.9	1699.1	10.6	1699.1	10.6
Gardner 5	315	29135	4.3	9.5988	0.5	4.0434	1.2	0.2816	1.1	0.90	1599.5	15.9	1643.0	10.1	1699.1	9.8	1699.1	9.8
Gardner 5	79	56512	2.0	9.5903	0.5	4.2839	1.0	0.2981	0.8	0.84	1681.9	12.2	1690.3	8.1	1700.7	9.8	1700.7	9.8
Gardner 5	43	37606	2.2	9.5893	0.6	4.2842	1.2	0.2981	1.0	0.86	1681.8	15.3	1690.3	9.8	1700.9	11.1	1700.9	11.1
Gardner 5	200	151768	3.2	9.5885	0.6	4.3456	1.1	0.3023	0.9	0.80	1702.9	13.0	1702.1	8.9	1701.0	11.8	1701.0	11.8
Gardner 5	477	153068	5.6	9.5798	0.7	4.1042	1.2	0.2853	0.9	0.78	1617.9	13.1	1655.1	9.6	1702.7	13.5	1702.7	13.5
Gardner 5	233	74085	2.9	9.5757	0.6	4.1228	1.2	0.2865	1.1	0.88	1623.8	15.6	1658.8	10.0	1703.5	10.7	1703.5	10.7
Gardner 5	264	202237	3.4	9.5721	0.7	4.3766	1.3	0.3040	1.1	0.84	1711.0	16.8	1707.9	10.9	1704.2	13.0	1704.2	13.0
Gardner 5	107	83845	1.8	9.5716	0.5	4.3992	1.1	0.3055	1.0	0.88	1718.7	14.8	1712.2	9.2	1704.3	9.7	1704.3	9.7
Gardner 5	31	67421	4.2	9.5674	0.8	4.4141	1.6	0.3064	1.4	0.86	1723.1	21.3	1715.0	13.5	1705.1	15.2	1705.1	15.2
Gardner 5	88	682649	2.2	9.5552	0.6	4.3317	1.1	0.3003	0.9	0.82	1692.9	13.1	1699.4	8.9	1707.4	11.4	1707.4	11.4
Gardner 5	473	704165	3.5	9.5463	0.8	4.1164	1.3	0.2851	1.0	0.80	1617.2	14.7	1657.6	10.6	1709.2	14.5	1709.2	14.5
Gardner 5	82	97770	1.5	9.5453	0.7	4.3714	1.3	0.3028	1.1	0.84	1705.0	15.8	1706.9	10.3	1709.3	12.4	1709.3	12.4
Gardner 5	76	585039	1.4	9.5444	0.7	4.2112	1.5	0.2916	1.3	0.87	1649.7	19.0	1676.2	12.3	1709.5	13.7	1709.5	13.7
Gardner 5	126	424561	1.9	9.5442	0.5	4.3764	1.0	0.3031	0.9	0.85	1706.5	13.1	1707.9	8.5	1709.6	10.0	1709.6	10.0
Gardner 5	68	39797	2.4	9.5370	0.6	4.3914	1.3	0.3039	1.1	0.88	1710.5	16.8	1710.7	10.5	1711.0	10.9	1711.0	10.9
Gardner 5	60	58396	2.7	9.5331	0.6	4.3063	1.2	0.2979	1.1	0.87	1680.7	15.9	1694.6	10.2	1711.7	11.3	1711.7	11.3
Gardner 5	103	67550	2.6	9.5245	0.6	4.2920	1.2	0.2966	1.1	0.89	1674.5	16.0	1691.8	10.0	1713.4	10.1	1713.4	10.1
Gardner 5	484	73878	3.2	9.5143	0.7	4.0683	1.1	0.2808	0.8	0.73	1595.6	11.1	1648.0	8.8	1715.3	13.6	1715.3	13.6
Gardner 5	337	739440	3.0	9.5038	0.8	4.4201	1.5	0.3048	1.2	0.83	1715.1	18.5	1716.1	12.2	1717.4	15.1	1717.4	15.1
Gardner 5	34	66008	1.8	9.4917	0.7	4.3334	1.4	0.2984	1.2	0.87	1683.6	17.8	1699.7	11.4	1719.7	12.6	1719.7	12.6
Gardner 5	277	154755	2.4	9.4632	0.5	4.5631	1.3	0.3133	1.2	0.91	1757.0	17.8	1742.6	10.6	1725.2	9.5	1725.2	9.5
Gardner 5	170	106453	4.2	9.4316	0.7	4.5036	1.2	0.3082	1.1	0.85	1731.8	16.0	1731.6	10.3	1731.4	12.0	1731.4	12.0
Gardner 5	66	29148	2.2	9.4197	0.7	4.4429	1.3	0.3037	1.1	0.84	1709.5	16.9	1720.4	11.2	1733.7	13.6	1733.7	13.6
Gardner 5	110	78626	2.8	9.4103	0.7	4.5189	1.3	0.3085	1.1	0.86	1733.6	16.4	1734.5	10.5	1735.5	12.0	1735.5	12.0

Gardner 5	117	300952	4.0	9.4055	0.6	4.5360	1.3	0.3096	1.1	0.89	1738.5	17.2	1737.6	10.6	1736.4	10.8	1736.4	10.8
Gardner 5	20	18764	9.9	9.4049	0.8	4.5433	1.3	0.3100	1.0	0.81	1740.9	15.8	1738.9	10.7	1736.6	13.9	1736.6	13.9
Gardner 5	172	175747	1.8	9.3486	0.6	4.6365	1.0	0.3145	0.8	0.81	1762.8	12.3	1755.9	8.2	1747.6	10.6	1747.6	10.6
Gardner 5	43	16308	1.6	9.2884	1.5	4.4266	1.8	0.2983	1.0	0.54	1683.0	14.5	1717.3	15.0	1759.4	27.8	1759.4	27.8
Gardner 5	139	111541	7.4	9.2615	0.7	4.7157	1.4	0.3169	1.2	0.87	1774.6	18.4	1770.0	11.5	1764.7	12.6	1764.7	12.6
Gardner 5	76	18818	1.7	9.1777	0.8	4.3617	1.3	0.2905	1.0	0.78	1643.8	14.2	1705.1	10.4	1781.3	14.3	1781.3	14.3
Gardner 5	73	15508	1.9	9.1662	0.8	4.5199	1.2	0.3006	0.9	0.76	1694.3	14.0	1734.6	10.2	1783.6	14.4	1783.6	14.4
Gardner 5	136	12447	4.8	9.0411	1.2	4.4430	1.7	0.2915	1.2	0.71	1648.8	17.3	1720.4	14.0	1808.6	21.7	1808.6	21.7
Gardner 5	352	7695	2.0	8.7263	1.8	4.8112	2.1	0.3046	0.9	0.46	1714.2	14.3	1786.9	17.3	1872.7	32.9	1872.7	32.9
GardnerSand1	2208	15957	3.4	14.8536	0.6	0.4285	1.6	0.0462	1.5	0.93	291.0	4.2	362.1	4.8	846.9	11.8	291.0	4.2
GardnerSand1	1157	44792	5.5	16.5235	0.9	0.5279	1.4	0.0633	1.0	0.76	395.6	4.0	430.4	4.8	621.3	19.3	395.6	4.0
GardnerSand1	111	31002	2.8	17.3025	0.8	0.6512	1.1	0.0818	0.8	0.72	506.6	3.9	509.2	4.5	521.0	17.1	506.6	3.9
GardnerSand1	41	18607	2.2	16.4970	1.4	0.6874	1.7	0.0823	1.0	0.56	509.7	4.7	531.2	7.0	624.7	30.2	509.7	4.7
GardnerSand1	644	495322	1.4	17.2632	0.6	0.6595	1.2	0.0826	1.0	0.84	511.7	4.9	514.3	4.8	526.1	14.2	511.7	4.9
GardnerSand1	61	7214	1.9	17.4138	1.0	0.6557	1.4	0.0828	1.0	0.71	513.1	5.1	512.0	5.8	506.9	22.3	513.1	5.1
GardnerSand1	220	89405	3.0	17.4196	0.7	0.6558	1.3	0.0829	1.1	0.82	513.3	5.3	512.0	5.2	506.2	16.3	513.3	5.3
GardnerSand1	602	333439	3.0	17.2207	0.6	0.6649	1.3	0.0831	1.1	0.87	514.5	5.5	517.6	5.2	531.5	13.8	514.5	5.5
GardnerSand1	94	30410	1.7	17.1579	1.3	0.6705	1.8	0.0835	1.2	0.67	516.9	6.0	521.0	7.3	539.4	28.9	516.9	6.0
GardnerSand1	74	101994	2.8	17.1652	0.9	0.6736	1.4	0.0839	1.0	0.73	519.3	4.9	522.9	5.6	538.5	20.5	519.3	4.9
GardnerSand1	127	130100	4.5	17.2369	0.8	0.6712	1.4	0.0839	1.1	0.81	519.6	5.6	521.4	5.7	529.4	18.2	519.6	5.6
GardnerSand1	60	188268630	2.2	17.1861	1.1	0.6732	1.4	0.0839	0.9	0.65	519.6	4.7	522.7	5.9	535.9	24.0	519.6	4.7
GardnerSand1	124	18368	3.9	17.4179	0.9	0.6707	1.2	0.0848	0.9	0.72	524.5	4.4	521.2	5.0	506.4	18.7	524.5	4.4
GardnerSand1	82	34796	1.7	17.3581	1.1	0.6766	1.5	0.0852	0.9	0.63	527.2	4.7	524.7	6.0	514.0	25.1	527.2	4.7
GardnerSand1	479	437353	3.4	11.3982	0.7	2.9876	1.1	0.2471	0.8	0.78	1423.4	10.7	1404.5	8.1	1375.8	12.8	1375.8	12.8
GardnerSand1	655	116961	11.0	11.3477	0.6	2.4001	1.2	0.1976	1.1	0.89	1162.5	11.6	1242.6	8.8	1384.3	10.9	1384.3	10.9
GardnerSand1	282	137695	3.0	11.2888	0.6	3.0187	1.1	0.2473	0.9	0.86	1424.3	11.9	1412.4	8.3	1394.3	10.8	1394.3	10.8
GardnerSand1	407	286167	2.6	11.2870	0.5	3.0404	1.3	0.2490	1.2	0.92	1433.3	15.4	1417.8	9.9	1394.6	9.5	1394.6	9.5
GardnerSand1	415	251379	5.4	11.2616	0.6	3.0134	1.2	0.2462	1.0	0.85	1419.0	12.5	1411.0	8.9	1398.9	11.9	1398.9	11.9
GardnerSand1	110	164567	2.8	11.2543	0.7	2.9672	1.3	0.2423	1.1	0.84	1398.7	14.0	1399.3	10.0	1400.2	13.6	1400.2	13.6
GardnerSand1	389	170340	5.4	11.2465	0.6	3.0469	1.3	0.2486	1.1	0.90	1431.4	14.7	1419.5	9.7	1401.5	10.6	1401.5	10.6

GardnerSand1	152	263494	2.2	11.2185	0.6	3.0434	1.1	0.2477	0.9	0.83	1426.8	11.2	1418.6	8.0	1406.3	11.3	1406.3	11.3
GardnerSand1	420	266819	1.3	11.1974	0.8	2.9136	1.5	0.2367	1.3	0.85	1369.6	15.6	1385.5	11.3	1409.9	15.1	1409.9	15.1
GardnerSand1	274	116682	3.9	11.1933	0.5	3.0926	1.2	0.2512	1.1	0.91	1444.5	14.6	1430.8	9.5	1410.6	9.6	1410.6	9.6
GardnerSand1	158	305636	1.1	11.1813	0.5	3.0303	1.2	0.2458	1.1	0.89	1417.0	13.5	1415.3	9.0	1412.6	10.2	1412.6	10.2
GardnerSand1	281	4512924	3.5	11.1747	0.6	3.0473	1.2	0.2471	1.1	0.89	1423.4	14.2	1419.6	9.5	1413.8	10.7	1413.8	10.7
GardnerSand1	539	623934	6.4	11.1740	0.5	3.0157	1.1	0.2445	1.0	0.91	1410.1	13.2	1411.6	8.7	1413.9	9.3	1413.9	9.3
GardnerSand1	290	315381	91.6	11.1690	0.6	3.1194	1.3	0.2528	1.2	0.88	1452.9	15.3	1437.5	10.2	1414.7	12.0	1414.7	12.0
GardnerSand1	437	450054	3.9	11.1682	0.6	3.0669	1.4	0.2485	1.3	0.92	1430.9	16.9	1424.5	11.0	1414.9	10.8	1414.9	10.8
GardnerSand1	135	108690	1.2	11.1490	0.6	3.1370	1.2	0.2538	1.0	0.86	1457.9	13.2	1441.8	9.0	1418.2	11.4	1418.2	11.4
GardnerSand1	168	378445	4.0	11.1406	0.7	3.0619	1.4	0.2475	1.1	0.84	1425.6	14.6	1423.2	10.4	1419.6	14.2	1419.6	14.2
GardnerSand1	108	82265	3.6	11.1318	0.6	3.0289	1.0	0.2446	0.8	0.80	1410.8	9.9	1414.9	7.4	1421.1	11.1	1421.1	11.1
GardnerSand1	182	90774	5.1	11.1318	0.8	2.9764	1.4	0.2404	1.2	0.84	1388.8	14.8	1401.6	10.7	1421.1	14.5	1421.1	14.5
GardnerSand1	319	150797	8.9	11.1298	0.7	3.1669	1.3	0.2557	1.1	0.85	1468.0	14.8	1449.1	10.2	1421.5	13.1	1421.5	13.1
GardnerSand1	298	598683	4.9	11.1268	0.8	3.0657	1.2	0.2475	1.0	0.78	1425.6	12.5	1424.2	9.6	1422.0	14.9	1422.0	14.9
GardnerSand1	361	863166	227.6	11.1220	0.7	3.0463	1.7	0.2458	1.6	0.92	1416.9	19.8	1419.3	13.0	1422.8	12.9	1422.8	12.9
GardnerSand1	196	258043	1.9	11.1053	0.7	3.0550	1.4	0.2462	1.2	0.85	1418.7	15.3	1421.5	10.8	1425.7	14.3	1425.7	14.3
GardnerSand1	251	647428	2.3	11.1041	0.6	3.0633	1.2	0.2468	1.0	0.86	1422.0	12.7	1423.6	8.9	1425.9	11.5	1425.9	11.5
GardnerSand1	162	3326256	354.1	11.1008	0.5	3.0969	1.2	0.2494	1.0	0.89	1435.6	13.4	1431.9	8.9	1426.5	10.1	1426.5	10.1
GardnerSand1	291	185581	5.5	11.0921	0.7	3.0584	1.0	0.2461	0.8	0.74	1418.6	9.9	1422.3	8.0	1427.9	13.4	1427.9	13.4
GardnerSand1	696	5336250	4.4	11.0858	0.6	3.0061	1.2	0.2418	1.0	0.86	1396.1	12.6	1409.2	8.9	1429.0	11.2	1429.0	11.2
GardnerSand1	217	119732	1.2	11.0832	0.7	3.0776	1.2	0.2475	1.0	0.84	1425.5	13.1	1427.1	9.3	1429.5	12.4	1429.5	12.4
GardnerSand1	259	209246	18.9	11.0711	0.7	3.0536	1.3	0.2453	1.1	0.85	1414.2	13.6	1421.1	9.7	1431.6	12.8	1431.6	12.8
GardnerSand1	678	449072	184.3	11.0678	0.7	3.0128	1.2	0.2419	1.0	0.84	1396.8	12.9	1410.9	9.3	1432.1	12.6	1432.1	12.6
GardnerSand1	130	205742	1.7	11.0624	0.7	3.2383	1.4	0.2599	1.1	0.84	1489.5	15.1	1466.4	10.6	1433.1	14.3	1433.1	14.3
GardnerSand1	104	71399	2.3	11.0325	0.6	2.9996	1.2	0.2401	1.1	0.85	1387.3	13.3	1407.5	9.5	1438.2	12.3	1438.2	12.3
GardnerSand1	219	512397	5.5	11.0181	0.7	3.0831	1.2	0.2465	1.0	0.84	1420.3	12.9	1428.5	9.3	1440.7	12.4	1440.7	12.4
GardnerSand1	86	78907	1.8	11.0095	0.7	3.0297	1.2	0.2420	1.0	0.83	1397.2	12.8	1415.1	9.4	1442.2	12.9	1442.2	12.9
GardnerSand1	1426	275741	32.1	11.0009	0.5	2.8657	1.3	0.2287	1.2	0.91	1327.9	14.1	1372.9	9.7	1443.7	10.4	1443.7	10.4
GardnerSand1	982	2003449	11.6	10.9707	0.5	3.0120	1.0	0.2398	0.8	0.86	1385.5	10.5	1410.7	7.5	1448.9	9.4	1448.9	9.4
GardnerSand1	167	134198	139.0	10.9697	0.7	3.0695	1.3	0.2443	1.1	0.85	1409.1	13.6	1425.1	9.7	1449.1	12.6	1449.1	12.6
GardnerSand1	38	194109	6.2	10.9574	0.7	2.8207	1.3	0.2243	1.0	0.82	1304.4	12.3	1361.1	9.5	1451.2	14.0	1451.2	14.0

GardnerSand1	1031	362642	145.0	10.9554	0.5	3.0110	1.1	0.2393	1.0	0.89	1383.3	12.6	1410.4	8.7	1451.6	10.0	1451.6	10.0
GardnerSand1	776	164304	6.8	10.9524	0.5	2.9408	1.2	0.2337	1.1	0.91	1353.9	12.9	1392.5	8.8	1452.1	9.3	1452.1	9.3
GardnerSand1	127	187092	2.0	10.9481	0.8	3.0906	1.2	0.2455	1.0	0.77	1415.3	12.1	1430.4	9.5	1452.9	15.1	1452.9	15.1
GardnerSand1	29	380748	57.4	10.9405	1.0	3.2818	1.6	0.2605	1.2	0.78	1492.5	16.6	1476.7	12.4	1454.2	18.9	1454.2	18.9
GardnerSand1	88	517323	1.3	10.9292	0.9	3.1079	1.4	0.2465	1.1	0.78	1420.2	14.1	1434.7	10.9	1456.1	16.8	1456.1	16.8
GardnerSand1	97	203413	1.9	10.9080	0.6	3.1034	1.0	0.2456	0.8	0.81	1415.9	10.3	1433.5	7.7	1459.8	11.1	1459.8	11.1
GardnerSand1	1263	440380	9.3	10.9060	0.7	2.9360	1.3	0.2323	1.1	0.84	1346.7	13.6	1391.2	10.1	1460.2	13.6	1460.2	13.6
GardnerSand1	1765	520314	110.0	10.6122	0.6	2.9348	1.4	0.2260	1.2	0.90	1313.4	14.6	1390.9	10.4	1511.9	11.5	1511.9	11.5
GardnerSand1	258	4555563	2.5	10.5564	0.7	3.4051	1.3	0.2608	1.1	0.84	1494.0	14.9	1505.6	10.4	1521.9	13.6	1521.9	13.6
GardnerSand1	116	80668	1.5	10.5350	0.6	3.1826	1.1	0.2433	0.9	0.82	1403.7	11.5	1453.0	8.6	1525.7	12.1	1525.7	12.1
GardnerSand1	51	59709	3.8	10.4093	0.7	3.4407	1.4	0.2599	1.2	0.86	1489.2	16.4	1513.7	11.3	1548.3	13.8	1548.3	13.8
GardnerSand1	875	401294	15.1	10.3096	0.6	3.0371	1.2	0.2272	1.0	0.86	1319.7	12.2	1417.0	9.1	1566.3	11.3	1566.3	11.3
GardnerSand1	214	138822	12.3	10.2757	0.6	3.6318	1.3	0.2708	1.1	0.88	1544.8	15.1	1556.5	10.0	1572.5	11.3	1572.5	11.3
GardnerSand1	284	109254	1.2	10.1889	0.6	3.8936	1.0	0.2878	0.8	0.82	1630.8	11.9	1612.3	8.1	1588.4	10.6	1588.4	10.6
GardnerSand1	178	107033	2.7	10.1751	0.7	3.5000	1.2	0.2584	1.0	0.81	1481.7	12.9	1527.2	9.5	1590.9	13.2	1590.9	13.2
GardnerSand1	336	233825	1.7	10.1579	0.6	3.7616	1.2	0.2772	1.0	0.86	1577.5	14.6	1584.6	9.8	1594.1	11.8	1594.1	11.8
GardnerSand1	558	215134	20.0	10.1221	0.7	3.5604	1.2	0.2615	1.0	0.83	1497.5	13.3	1540.7	9.5	1600.6	12.6	1600.6	12.6
GardnerSand1	82	116475	2.4	10.1204	0.7	3.8307	1.2	0.2813	1.0	0.81	1597.9	14.1	1599.2	9.9	1601.0	13.3	1601.0	13.3
GardnerSand1	306	3578252	68.9	10.0936	0.5	3.8974	1.3	0.2854	1.2	0.91	1618.7	16.8	1613.1	10.4	1605.9	9.8	1605.9	9.8
GardnerSand1	312	511320	5.6	10.0480	0.6	3.8643	1.3	0.2817	1.2	0.90	1600.1	16.7	1606.3	10.6	1614.3	10.9	1614.3	10.9
GardnerSand1	385	348204	13.3	10.0478	0.6	4.0905	1.3	0.2982	1.2	0.89	1682.5	17.5	1652.4	10.8	1614.4	11.0	1614.4	11.0
GardnerSand1	247	136088	7.1	10.0360	0.8	3.8680	1.5	0.2817	1.3	0.86	1599.8	18.4	1607.0	12.1	1616.6	14.1	1616.6	14.1
GardnerSand1	144	93641	3.8	10.0239	0.6	3.8112	1.3	0.2772	1.1	0.88	1577.2	16.0	1595.1	10.4	1618.8	11.2	1618.8	11.2
GardnerSand1	406	241428	18.9	10.0236	0.7	3.5721	1.3	0.2598	1.1	0.86	1488.8	14.5	1543.4	10.1	1618.9	12.1	1618.9	12.1
GardnerSand1	564	413464	8.5	10.0110	0.7	3.7547	1.1	0.2727	0.9	0.81	1554.6	12.7	1583.1	9.1	1621.2	12.3	1621.2	12.3
GardnerSand1	123	244968	2.4	10.0061	0.8	3.7732	1.3	0.2739	1.0	0.80	1560.8	14.5	1587.1	10.5	1622.1	14.6	1622.1	14.6
GardnerSand1	264	456254	2.4	10.0010	0.9	4.1163	1.5	0.2987	1.2	0.82	1684.9	18.5	1657.5	12.4	1623.1	16.2	1623.1	16.2
GardnerSand1	31	81399	7.2	9.9889	0.7	3.7136	1.2	0.2692	0.9	0.79	1536.5	12.5	1574.3	9.3	1625.3	13.3	1625.3	13.3
GardnerSand1	370	537349	8.9	9.9715	0.7	3.8130	1.3	0.2759	1.2	0.87	1570.6	16.2	1595.5	10.8	1628.6	12.4	1628.6	12.4
GardnerSand1	109	104665	2.9	9.9614	0.6	3.5807	1.4	0.2588	1.3	0.89	1483.8	16.7	1545.3	11.3	1630.5	12.0	1630.5	12.0
GardnerSand1	356	360853	9.3	9.9431	0.5	3.5623	1.4	0.2570	1.3	0.95	1474.5	17.3	1541.2	11.0	1633.9	8.4	1633.9	8.4

GardnerSand1	88	95435	6.0	9.9129	0.6	3.9299	1.2	0.2827	1.1	0.86	1604.8	14.9	1619.9	9.9	1639.5	11.7	1639.5	11.7
GardnerSand1	284	329112	31.8	9.8693	0.8	4.0159	1.4	0.2876	1.2	0.84	1629.4	16.7	1637.4	11.3	1647.7	14.0	1647.7	14.0
GardnerSand1	699	11321713	11.1	9.8445	0.6	4.0133	1.1	0.2867	1.0	0.87	1624.9	14.1	1636.9	9.2	1652.4	10.4	1652.4	10.4
GardnerSand1	1194	329184	21.7	9.8399	0.6	3.2347	2.2	0.2309	2.2	0.97	1339.5	26.2	1465.5	17.4	1653.2	10.7	1653.2	10.7
GardnerSand1	235	98973	2.9	9.8395	0.5	4.2178	1.3	0.3011	1.2	0.92	1696.9	18.1	1677.5	10.9	1653.3	9.8	1653.3	9.8
GardnerSand1	374	197238	4.4	9.8385	0.5	4.1489	1.0	0.2962	0.9	0.88	1672.3	13.5	1664.0	8.5	1653.5	9.0	1653.5	9.0
GardnerSand1	146	332902	2.5	9.8321	0.7	3.7446	1.4	0.2671	1.2	0.86	1526.3	16.2	1581.0	11.1	1654.7	13.0	1654.7	13.0
GardnerSand1	586	115911	17.8	9.8312	0.6	3.5546	2.7	0.2536	2.6	0.97	1456.8	34.5	1539.5	21.5	1654.9	11.8	1654.9	11.8
GardnerSand1	135	109739	11.1	9.8263	0.7	4.1309	1.2	0.2945	1.0	0.83	1664.1	14.7	1660.4	9.8	1655.8	12.3	1655.8	12.3
GardnerSand1	268	2919092	2.5	9.8140	0.6	4.1281	1.2	0.2940	1.0	0.87	1661.3	14.6	1659.9	9.4	1658.1	10.6	1658.1	10.6
GardnerSand1	95	196994	5.7	9.8103	0.6	4.2249	1.2	0.3007	1.0	0.86	1695.0	15.6	1678.9	10.0	1658.8	11.6	1658.8	11.6
GardnerSand1	394	207789	10.0	9.7978	0.8	4.1262	1.5	0.2933	1.3	0.86	1658.2	18.5	1659.5	12.0	1661.2	13.9	1661.2	13.9
GardnerSand1	400	113492	1.5	9.7854	0.7	3.6467	1.4	0.2589	1.2	0.85	1484.3	15.5	1559.8	11.0	1663.5	13.5	1663.5	13.5
GardnerSand1	204	1404631	22.7	9.7814	0.8	4.0157	1.5	0.2850	1.2	0.82	1616.5	17.0	1637.4	11.8	1664.3	15.6	1664.3	15.6
GardnerSand1	580	725522	3.7	9.7788	0.5	4.1749	1.0	0.2962	0.9	0.85	1672.5	12.7	1669.1	8.3	1664.8	10.1	1664.8	10.1
GardnerSand1	556	735293	3.8	9.7762	0.7	4.0782	1.1	0.2893	0.8	0.76	1637.9	11.7	1649.9	8.7	1665.2	12.8	1665.2	12.8
GardnerSand1	87	50051	3.7	9.7739	0.7	4.2710	1.2	0.3029	1.0	0.82	1705.6	15.4	1687.8	10.3	1665.7	13.2	1665.7	13.2
GardnerSand1	124	113619	2.0	9.7660	0.6	4.1727	1.2	0.2957	1.0	0.85	1669.9	14.9	1668.7	9.8	1667.2	11.7	1667.2	11.7
GardnerSand1	334	215160	3.5	9.7612	0.6	4.2539	1.3	0.3013	1.1	0.89	1697.7	16.7	1684.5	10.4	1668.1	10.7	1668.1	10.7
GardnerSand1	100	69061	1.9	9.7519	0.7	4.1829	1.4	0.2960	1.2	0.84	1671.3	17.0	1670.7	11.2	1669.8	13.7	1669.8	13.7
GardnerSand1	16	7578	2.8	9.7473	0.9	4.1354	1.4	0.2925	1.1	0.78	1653.9	16.3	1661.3	11.7	1670.7	16.5	1670.7	16.5
GardnerSand1	132	247071	1.9	9.7459	0.6	4.0720	1.4	0.2880	1.3	0.92	1631.3	18.3	1648.7	11.3	1671.0	10.2	1671.0	10.2
GardnerSand1	188	608159	2.4	9.7419	0.6	4.3255	1.3	0.3058	1.1	0.86	1719.8	16.3	1698.2	10.3	1671.7	11.8	1671.7	11.8
GardnerSand1	18	10492	3.1	9.7397	0.9	4.2293	1.4	0.2989	1.0	0.74	1685.8	15.0	1679.7	11.3	1672.2	17.2	1672.2	17.2
GardnerSand1	248	163327	3.4	9.7392	0.6	4.2777	1.2	0.3023	1.1	0.89	1702.6	16.3	1689.1	10.1	1672.3	10.5	1672.3	10.5
GardnerSand1	42	54736	2.6	9.7300	0.6	4.2367	1.4	0.2991	1.3	0.90	1686.9	19.2	1681.2	11.8	1674.0	11.4	1674.0	11.4
GardnerSand1	334	382032	5.5	9.7283	0.8	3.8040	1.7	0.2685	1.5	0.88	1533.3	20.0	1593.6	13.3	1674.3	14.4	1674.3	14.4
GardnerSand1	262	2283764	2.4	9.7248	0.7	4.2332	1.6	0.2987	1.5	0.90	1684.9	21.8	1680.5	13.5	1675.0	13.4	1675.0	13.4
GardnerSand1	149	106987	2.3	9.7122	1.0	4.1119	2.6	0.2898	2.4	0.93	1640.4	34.6	1656.7	21.1	1677.4	17.8	1677.4	17.8
GardnerSand1	282	430798	3.7	9.7038	0.5	4.1683	1.2	0.2935	1.1	0.92	1658.9	16.6	1667.8	10.1	1679.0	8.8	1679.0	8.8
GardnerSand1	354	130094	5.6	9.6981	0.6	3.5928	1.7	0.2528	1.6	0.94	1453.0	20.6	1547.9	13.4	1680.1	11.0	1680.1	11.0

GardnerSand1	587	461047	28.5	9.6969	0.7	3.8166	1.1	0.2685	0.9	0.78	1533.3	12.2	1596.2	9.2	1680.3	13.3	1680.3	13.3
GardnerSand1	50	41087	3.3	9.6936	0.7	4.2311	1.2	0.2976	1.0	0.81	1679.4	14.8	1680.1	10.1	1680.9	13.4	1680.9	13.4
GardnerSand1	638	397588	6.3	9.6933	0.6	4.1323	1.3	0.2906	1.2	0.90	1644.7	17.7	1660.7	11.0	1681.0	10.7	1681.0	10.7
GardnerSand1	125	55810	2.3	9.6917	0.7	4.0844	1.4	0.2872	1.2	0.86	1627.6	17.2	1651.2	11.3	1681.3	13.1	1681.3	13.1
GardnerSand1	202	224742	3.5	9.6917	0.6	4.2445	1.2	0.2985	1.1	0.88	1683.8	16.1	1682.7	10.1	1681.3	10.7	1681.3	10.7
GardnerSand1	81	95679	1.8	9.6897	0.7	4.1445	1.3	0.2914	1.0	0.83	1648.5	15.1	1663.1	10.3	1681.7	13.1	1681.7	13.1
GardnerSand1	149	222172	7.7	9.6858	0.8	4.3830	1.3	0.3080	1.1	0.80	1731.0	16.2	1709.1	11.0	1682.4	14.7	1682.4	14.7
GardnerSand1	42	23943	4.3	9.6840	0.8	4.2084	1.3	0.2957	1.0	0.78	1670.0	14.8	1675.7	10.5	1682.8	14.6	1682.8	14.6
GardnerSand1	36	63204	3.4	9.6787	0.9	4.0612	1.5	0.2852	1.2	0.80	1617.5	16.8	1646.6	11.9	1683.8	16.1	1683.8	16.1
GardnerSand1	33	93395	3.7	9.6713	0.7	4.1583	1.3	0.2918	1.0	0.82	1650.5	15.2	1665.8	10.4	1685.2	13.2	1685.2	13.2
GardnerSand1	46	758758	14.4	9.6685	1.0	4.1155	1.8	0.2887	1.5	0.83	1635.1	22.0	1657.4	15.0	1685.7	18.7	1685.7	18.7
GardnerSand1	107	147583	2.5	9.6672	0.6	4.3151	1.3	0.3027	1.1	0.89	1704.6	17.2	1696.2	10.6	1686.0	10.9	1686.0	10.9
GardnerSand1	41	50105	2.2	9.6665	0.8	4.1101	1.4	0.2883	1.1	0.82	1632.9	16.2	1656.3	11.2	1686.1	14.5	1686.1	14.5
GardnerSand1	61	76357	2.9	9.6635	0.8	4.2619	1.2	0.2988	0.8	0.70	1685.5	12.2	1686.0	9.6	1686.7	15.4	1686.7	15.4
GardnerSand1	117	200256	2.6	9.6635	0.6	3.9309	1.3	0.2756	1.2	0.89	1569.3	16.1	1620.1	10.5	1686.7	11.0	1686.7	11.0
GardnerSand1	41	257174	4.5	9.6606	0.6	4.3888	1.3	0.3076	1.1	0.87	1729.1	17.3	1710.2	10.8	1687.2	11.7	1687.2	11.7
GardnerSand1	216	575400	8.7	9.6598	0.7	4.2954	1.4	0.3011	1.2	0.86	1696.6	17.9	1692.5	11.6	1687.4	13.4	1687.4	13.4
GardnerSand1	586	571055	3.0	9.6593	0.5	4.1335	1.2	0.2897	1.1	0.89	1640.0	15.3	1660.9	9.7	1687.5	9.9	1687.5	9.9
GardnerSand1	92	72500	2.1	9.6590	0.7	4.3140	1.3	0.3023	1.1	0.84	1702.9	16.3	1696.0	10.6	1687.5	12.9	1687.5	12.9
GardnerSand1	112	2805268	2.3	9.6579	0.6	4.2926	1.4	0.3008	1.3	0.90	1695.3	19.3	1691.9	11.8	1687.7	11.5	1687.7	11.5
GardnerSand1	213	98203	15.8	9.6518	0.5	4.2227	1.1	0.2957	1.0	0.88	1670.1	14.3	1678.4	9.1	1688.9	9.6	1688.9	9.6
GardnerSand1	68	6167002	5.1	9.6514	0.6	4.2358	1.2	0.2966	1.1	0.86	1674.6	15.5	1681.0	10.0	1689.0	11.3	1689.0	11.3
GardnerSand1	169	131102	2.9	9.6481	0.5	3.9592	1.3	0.2772	1.2	0.91	1577.1	16.3	1625.9	10.4	1689.6	10.0	1689.6	10.0
GardnerSand1	585	251637	8.1	9.6438	0.5	4.0430	1.2	0.2829	1.1	0.90	1606.0	15.8	1642.9	10.0	1690.4	9.8	1690.4	9.8
GardnerSand1	375	274028	9.7	9.6414	0.8	4.2008	1.7	0.2939	1.5	0.89	1660.9	21.8	1674.2	13.7	1690.9	14.0	1690.9	14.0
GardnerSand1	125	185977	2.6	9.6407	0.5	4.1913	1.0	0.2932	0.9	0.86	1657.4	12.9	1672.3	8.5	1691.0	9.8	1691.0	9.8
GardnerSand1	486	173622	6.2	9.6360	0.7	3.5666	1.7	0.2494	1.5	0.91	1435.2	19.9	1542.1	13.5	1691.9	13.1	1691.9	13.1
GardnerSand1	67	61256	3.1	9.6349	0.5	4.4078	1.1	0.3081	0.9	0.87	1731.6	14.1	1713.8	8.8	1692.1	9.5	1692.1	9.5
GardnerSand1	211	107139	3.1	9.6347	0.8	4.1838	1.3	0.2925	1.0	0.77	1653.9	14.2	1670.9	10.4	1692.2	15.0	1692.2	15.0
GardnerSand1	69	510723	2.2	9.6327	0.6	4.2362	1.5	0.2961	1.3	0.90	1671.9	19.2	1681.1	11.9	1692.6	11.9	1692.6	11.9
GardnerSand1	616	235253	3.3	9.6299	0.8	4.0416	1.5	0.2824	1.2	0.83	1603.4	17.5	1642.6	12.2	1693.1	15.5	1693.1	15.5

GardnerSand1	168	177186	16.3	9.6266	0.6	4.2469	1.1	0.2966	0.9	0.85	1674.6	13.4	1683.1	8.8	1693.7	10.5	1693.7	10.5
GardnerSand1	68	159760	3.9	9.6212	0.8	4.1253	1.4	0.2880	1.2	0.83	1631.5	17.0	1659.3	11.6	1694.8	14.4	1694.8	14.4
GardnerSand1	109	94359	2.8	9.6149	0.5	3.9367	1.0	0.2746	0.9	0.86	1564.3	12.4	1621.3	8.4	1696.0	9.7	1696.0	9.7
GardnerSand1	46	2229085	2.7	9.6148	0.7	4.1677	1.2	0.2908	1.0	0.80	1645.3	13.8	1667.7	9.8	1696.0	13.2	1696.0	13.2
GardnerSand1	37	114685	3.2	9.6141	0.7	4.2982	1.5	0.2998	1.3	0.87	1690.5	19.1	1693.0	12.1	1696.1	13.1	1696.1	13.1
GardnerSand1	212	378120	1.8	9.6097	0.6	4.1951	1.3	0.2925	1.2	0.87	1654.1	16.8	1673.1	10.8	1697.0	11.9	1697.0	11.9
GardnerSand1	329	127228	2.5	9.6070	0.6	4.2813	1.2	0.2984	1.0	0.85	1683.5	15.0	1689.8	9.8	1697.5	11.5	1697.5	11.5
GardnerSand1	172	158444	4.8	9.6046	0.8	4.1901	1.2	0.2920	1.0	0.78	1651.6	14.1	1672.1	10.2	1697.9	14.4	1697.9	14.4
GardnerSand1	165	129258	3.5	9.6038	0.6	4.2241	1.1	0.2944	0.9	0.82	1663.2	12.9	1678.7	8.8	1698.1	11.3	1698.1	11.3
GardnerSand1	77	100056	2.3	9.6026	0.8	4.1225	1.4	0.2872	1.2	0.84	1627.7	17.1	1658.8	11.5	1698.3	14.0	1698.3	14.0
GardnerSand1	49	36346	3.0	9.6000	0.7	4.2655	1.2	0.2971	1.0	0.82	1677.0	14.7	1686.7	10.0	1698.8	12.7	1698.8	12.7
GardnerSand1	172	90941	3.9	9.5993	0.7	4.3360	1.2	0.3020	1.0	0.82	1701.3	14.6	1700.2	9.8	1699.0	12.4	1699.0	12.4
GardnerSand1	85	70465	3.9	9.5988	0.8	4.3300	1.3	0.3016	1.1	0.81	1699.1	16.3	1699.1	11.0	1699.1	14.3	1699.1	14.3
GardnerSand1	58	241891	2.9	9.5983	0.8	4.2742	1.3	0.2977	1.0	0.78	1679.8	14.7	1688.4	10.5	1699.2	14.6	1699.2	14.6
GardnerSand1	36	319601	1.9	9.5956	0.9	4.1304	1.7	0.2876	1.4	0.85	1629.4	20.5	1660.3	13.6	1699.7	16.0	1699.7	16.0
GardnerSand1	148	656104	3.6	9.5871	0.6	4.2875	1.4	0.2983	1.2	0.89	1682.6	18.5	1691.0	11.5	1701.3	11.7	1701.3	11.7
GardnerSand1	852	307234	157.0	9.5865	0.6	3.9737	1.1	0.2764	1.0	0.87	1573.2	13.5	1628.8	9.1	1701.4	10.2	1701.4	10.2
GardnerSand1	159	119663	23.1	9.5789	0.7	4.3488	1.5	0.3023	1.3	0.88	1702.5	19.5	1702.7	12.2	1702.9	12.8	1702.9	12.8
GardnerSand1	77	280138	2.1	9.5777	0.8	4.4634	1.2	0.3102	0.9	0.74	1741.6	13.3	1724.2	9.7	1703.1	14.3	1703.1	14.3
GardnerSand1	72	99456	1.7	9.5724	0.6	4.2748	1.3	0.2969	1.2	0.90	1676.0	17.4	1688.5	10.9	1704.1	10.8	1704.1	10.8
GardnerSand1	356	206482	3.1	9.5678	0.6	4.2896	1.6	0.2978	1.5	0.93	1680.4	21.5	1691.4	12.9	1705.0	10.9	1705.0	10.9
GardnerSand1	130	176238	1.8	9.5589	0.6	4.2345	1.0	0.2937	0.8	0.82	1660.0	12.0	1680.7	8.1	1706.7	10.3	1706.7	10.3
GardnerSand1	63	49369	3.7	9.5579	0.7	4.3092	1.4	0.2988	1.2	0.85	1685.6	17.2	1695.1	11.2	1706.9	13.0	1706.9	13.0
GardnerSand1	77	1388253	2.4	9.5498	0.7	4.2070	1.5	0.2915	1.3	0.89	1649.1	19.2	1675.4	12.2	1708.5	12.4	1708.5	12.4
GardnerSand1	1024	5020365	20.7	9.5446	0.6	3.9659	1.0	0.2747	0.8	0.83	1564.4	11.5	1627.2	8.1	1709.5	10.2	1709.5	10.2
GardnerSand1	39	211556	2.7	9.5445	0.8	4.2739	1.4	0.2960	1.1	0.82	1671.4	16.7	1688.4	11.4	1709.5	14.5	1709.5	14.5
GardnerSand1	50	3951203	2.2	9.5383	1.0	4.4270	1.5	0.3064	1.1	0.75	1722.9	16.6	1717.4	12.1	1710.7	17.8	1710.7	17.8
GardnerSand1	702	72588	3.7	9.5348	0.6	3.5180	1.5	0.2434	1.4	0.93	1404.3	17.4	1531.3	11.7	1711.4	10.3	1711.4	10.3
GardnerSand1	308	99574	4.1	9.5325	0.5	3.5564	1.8	0.2460	1.7	0.96	1417.7	21.8	1539.9	14.2	1711.8	9.2	1711.8	9.2
GardnerSand1	290	165045	2.8	9.5198	0.6	4.4714	1.3	0.3089	1.1	0.87	1735.1	17.3	1725.7	10.8	1714.3	11.7	1714.3	11.7
GardnerSand1	118	108412	5.2	9.5178	0.7	4.1971	1.2	0.2899	1.0	0.84	1640.8	15.0	1673.5	10.1	1714.7	12.1	1714.7	12.1

GardnerSand1	282	107073	4.7	9.5020	0.6	4.0589	1.1	0.2798	0.9	0.86	1590.6	13.3	1646.1	8.9	1717.7	10.3	1717.7	10.3
GardnerSand1	141	49045	3.9	9.4874	0.7	4.2404	1.4	0.2919	1.2	0.87	1651.0	17.3	1681.9	11.2	1720.5	12.1	1720.5	12.1
GardnerSand1	46	181520	2.6	9.4740	0.8	4.2578	1.2	0.2927	0.9	0.78	1654.9	13.6	1685.2	9.8	1723.1	13.9	1723.1	13.9
GardnerSand1	93	73821	2.1	9.4731	1.1	4.1689	1.6	0.2865	1.2	0.73	1624.2	17.0	1667.9	13.3	1723.3	20.3	1723.3	20.3
GardnerSand1	174	314903	4.5	9.4656	0.7	4.3678	1.0	0.3000	0.8	0.73	1691.3	11.2	1706.3	8.5	1724.8	12.8	1724.8	12.8
GardnerSand1	152	280409	4.5	9.4411	0.5	4.3950	1.3	0.3011	1.2	0.92	1696.6	17.4	1711.4	10.5	1729.5	9.0	1729.5	9.0
GardnerSand1	177	151898	6.1	9.4394	0.8	4.5003	1.5	0.3082	1.3	0.86	1732.0	19.7	1731.0	12.5	1729.9	13.9	1729.9	13.9
GardnerSand1	99	175443	3.2	9.4346	0.7	4.2714	1.2	0.2924	1.0	0.83	1653.5	14.4	1687.9	9.8	1730.8	12.1	1730.8	12.1
GardnerSand1	30	146878	1.9	9.4273	0.8	4.3884	1.3	0.3002	1.0	0.77	1692.2	14.9	1710.2	10.7	1732.2	15.1	1732.2	15.1
GardnerSand1	566	433141	2.7	9.4246	0.8	4.3507	1.3	0.2975	1.0	0.77	1679.0	15.3	1703.0	11.0	1732.7	15.5	1732.7	15.5
GardnerSand1	92	337961	3.1	9.4152	0.5	4.3264	1.0	0.2956	0.9	0.89	1669.3	13.4	1698.4	8.4	1734.6	8.4	1734.6	8.4
GardnerSand1	209	194027	5.2	9.4087	0.6	4.4008	1.4	0.3004	1.2	0.89	1693.5	18.4	1712.5	11.5	1735.8	11.6	1735.8	11.6
GardnerSand1	81	43977	9.8	9.3735	0.8	4.6269	1.3	0.3147	1.1	0.83	1763.7	17.1	1754.1	11.2	1742.7	13.9	1742.7	13.9
GardnerSand1	24	26103	10.1	9.3584	0.9	4.5653	1.5	0.3100	1.2	0.80	1740.7	18.4	1743.0	12.6	1745.6	16.7	1745.6	16.7
GardnerSand1	79	62534	7.1	9.3503	0.7	4.6069	1.2	0.3126	1.0	0.83	1753.3	15.5	1750.5	10.2	1747.2	12.5	1747.2	12.5
GardnerSand1	156	109692	4.5	9.3336	0.6	4.5316	1.1	0.3069	0.9	0.81	1725.4	13.6	1736.8	9.2	1750.5	11.8	1750.5	11.8
GardnerSand1	76	69672	4.4	9.2989	0.6	4.6053	1.3	0.3107	1.1	0.87	1744.3	16.8	1750.2	10.6	1757.3	11.4	1757.3	11.4
GardnerSand1	70	299690	7.8	9.2557	0.6	4.4916	1.3	0.3016	1.2	0.88	1699.5	17.6	1729.4	11.1	1765.8	11.5	1765.8	11.5
GardnerSand1	131	132183	10.7	9.2482	0.6	4.4900	1.0	0.3013	0.8	0.80	1697.7	12.2	1729.1	8.5	1767.3	11.3	1767.3	11.3
Greenhorn4	466	44407	1.0	19.8474	3.2	0.0343	3.9	0.0049	2.3	0.59	31.8	0.7	34.3	1.3	211.7	73.5	31.8	0.7
Greenhorn4	89	691	2.6	41.5411	3.7	0.0166	4.0	0.0050	1.7	0.42	32.1	0.5	16.7	0.7	NA	NA	32.1	0.5
Greenhorn4	353	5460	1.2	21.9611	2.2	0.0317	2.6	0.0051	1.4	0.54	32.5	0.5	31.7	0.8	NA	NA	32.5	0.5
Greenhorn4	69	1631	1.4	24.5846	7.2	0.0284	7.5	0.0051	1.8	0.23	32.6	0.6	28.5	2.1	NA	NA	32.6	0.6
Greenhorn4	1384	25939	0.9	20.9920	1.4	0.0334	1.7	0.0051	1.0	0.59	32.7	0.3	33.4	0.6	80.2	32.4	32.7	0.3
Greenhorn4	285	17868	1.3	20.9557	2.0	0.0335	2.2	0.0051	1.0	0.45	32.7	0.3	33.4	0.7	84.3	47.2	32.7	0.3
Greenhorn4	351	5678	1.6	22.6833	2.1	0.0310	2.4	0.0051	1.3	0.53	32.8	0.4	31.0	0.7	NA	NA	32.8	0.4
Greenhorn4	104	505	1.2	40.3996	3.2	0.0174	3.4	0.0051	1.1	0.33	32.8	0.4	17.5	0.6	NA	NA	32.8	0.4
Greenhorn4	142	1188	1.7	29.4151	19.2	0.0239	19.3	0.0051	1.6	0.08	32.8	0.5	24.0	4.6	NA	NA	32.8	0.5
Greenhorn4	410	4908	1.8	20.7647	2.4	0.0341	2.6	0.0051	1.0	0.40	33.0	0.3	34.0	0.9	106.0	55.9	33.0	0.3
Greenhorn4	213	178956	1.3	20.4465	2.5	0.0347	2.8	0.0051	1.2	0.43	33.1	0.4	34.6	0.9	142.4	59.1	33.1	0.4

Greenhorn4	95	6526	2.2	22.5731	4.8	0.0314	5.0	0.0052	1.5	0.30	33.1	0.5	31.4	1.6	NA	NA	33.1	0.5
Greenhorn4	162	1031	1.9	30.9424	3.9	0.0230	4.1	0.0052	1.2	0.30	33.2	0.4	23.1	0.9	NA	NA	33.2	0.4
Greenhorn4	469	8374	1.6	21.1836	1.6	0.0336	2.0	0.0052	1.2	0.62	33.2	0.4	33.5	0.7	58.7	37.4	33.2	0.4
Greenhorn4	104	1366	1.3	25.4851	6.3	0.0279	6.4	0.0052	1.2	0.18	33.2	0.4	28.0	1.8	NA	NA	33.2	0.4
Greenhorn4	118	6252	1.4	20.5886	3.8	0.0346	4.0	0.0052	1.3	0.32	33.2	0.4	34.5	1.4	126.1	89.4	33.2	0.4
Greenhorn4	183	2093	1.3	25.2599	3.6	0.0282	3.8	0.0052	1.1	0.30	33.2	0.4	28.2	1.0	NA	NA	33.2	0.4
Greenhorn4	683	7215	1.2	22.1065	1.4	0.0322	1.9	0.0052	1.2	0.65	33.2	0.4	32.2	0.6	NA	NA	33.2	0.4
Greenhorn4	565	48505	1.4	20.9362	1.4	0.0340	1.6	0.0052	0.8	0.52	33.2	0.3	34.0	0.5	86.6	32.1	33.2	0.3
Greenhorn4	439	4653	1.9	22.5009	4.1	0.0317	4.2	0.0052	1.2	0.28	33.3	0.4	31.7	1.3	NA	NA	33.3	0.4
Greenhorn4	34	816	2.7	31.0453	9.1	0.0231	9.4	0.0052	2.2	0.24	33.4	0.7	23.1	2.1	NA	NA	33.4	0.7
Greenhorn4	394	6332	1.9	21.8193	2.1	0.0328	2.5	0.0052	1.3	0.53	33.4	0.4	32.8	0.8	NA	NA	33.4	0.4
Greenhorn4	68	815	1.7	32.1266	30.5	0.0223	30.6	0.0052	1.8	0.06	33.4	0.6	22.4	6.8	NA	NA	33.4	0.6
Greenhorn4	132	1672	1.4	23.1558	6.6	0.0309	6.7	0.0052	1.2	0.18	33.4	0.4	30.9	2.0	NA	NA	33.4	0.4
Greenhorn4	211	11246	1.7	21.0377	1.9	0.0341	2.3	0.0052	1.4	0.60	33.5	0.5	34.1	0.8	75.1	44.4	33.5	0.5
Greenhorn4	180	3359	1.8	21.9872	5.7	0.0327	5.8	0.0052	1.1	0.19	33.5	0.4	32.6	1.8	NA	NA	33.5	0.4
Greenhorn4	40	425	2.5	20.5399	10.7	0.0351	10.8	0.0052	1.9	0.18	33.6	0.6	35.0	3.7	131.7	251.4	33.6	0.6
Greenhorn4	105	6674	3.1	20.1193	3.6	0.0358	3.9	0.0052	1.6	0.42	33.6	0.5	35.7	1.4	180.1	83.1	33.6	0.5
Greenhorn4	496	23481	1.2	19.9931	1.5	0.0360	1.7	0.0052	0.9	0.55	33.6	0.3	36.0	0.6	194.8	33.8	33.6	0.3
Greenhorn4	1882	22767	2.3	19.7946	0.9	0.0365	1.3	0.0052	0.9	0.72	33.7	0.3	36.4	0.5	217.9	21.0	33.7	0.3
Greenhorn4	567	26502	0.9	20.4180	1.9	0.0354	2.1	0.0052	1.0	0.47	33.7	0.3	35.3	0.7	145.7	44.4	33.7	0.3
Greenhorn4	152	1306	4.7	28.0372	7.6	0.0258	7.8	0.0052	1.4	0.18	33.7	0.5	25.8	2.0	NA	NA	33.7	0.5
Greenhorn4	159	3087	4.1	20.3312	2.3	0.0355	2.6	0.0052	1.3	0.49	33.7	0.4	35.5	0.9	155.7	53.4	33.7	0.4
Greenhorn4	1466	31921	2.1	20.9712	1.1	0.0345	1.4	0.0052	0.9	0.63	33.7	0.3	34.4	0.5	82.6	25.3	33.7	0.3
Greenhorn4	169	3273	1.3	21.8116	2.9	0.0332	3.1	0.0052	1.2	0.38	33.7	0.4	33.1	1.0	NA	NA	33.7	0.4
Greenhorn4	927	18689	1.4	21.1554	1.1	0.0342	1.6	0.0053	1.1	0.72	33.8	0.4	34.2	0.5	61.8	25.8	33.8	0.4
Greenhorn4	309	6265	0.8	20.7317	2.1	0.0349	2.4	0.0053	1.1	0.44	33.8	0.4	34.9	0.8	109.8	50.4	33.8	0.4
Greenhorn4	179	6734	1.8	20.7054	3.0	0.0352	3.2	0.0053	1.1	0.35	34.0	0.4	35.2	1.1	112.8	70.1	34.0	0.4
Greenhorn4	170	6404	1.1	18.7170	2.6	0.0390	3.0	0.0053	1.5	0.51	34.0	0.5	38.8	1.1	346.0	57.7	34.0	0.5
Greenhorn4	191	8005	0.9	22.2349	2.6	0.0328	2.9	0.0053	1.4	0.46	34.1	0.5	32.8	0.9	NA	NA	34.1	0.5
Greenhorn4	183	3094	1.8	24.2464	3.4	0.0302	3.7	0.0053	1.4	0.38	34.2	0.5	30.2	1.1	NA	NA	34.2	0.5
Greenhorn4	352	9567	1.0	21.1515	2.4	0.0347	3.3	0.0053	2.2	0.67	34.2	0.8	34.6	1.1	62.3	57.6	34.2	0.8

Greenhorn4	64	2136	2.4	22.3366	5.4	0.0329	5.6	0.0053	1.5	0.27	34.2	0.5	32.8	1.8	NA	NA	34.2	0.5
Greenhorn4	549	11796	1.4	21.2426	1.8	0.0346	2.0	0.0053	0.9	0.45	34.3	0.3	34.6	0.7	52.0	41.9	34.3	0.3
Greenhorn4	125	7628	1.2	22.2207	3.1	0.0331	3.3	0.0053	1.1	0.35	34.3	0.4	33.1	1.1	NA	NA	34.3	0.4
Greenhorn4	76	1463	1.4	23.0146	12.4	0.0320	12.5	0.0053	1.5	0.12	34.4	0.5	32.0	3.9	NA	NA	34.4	0.5
Greenhorn4	119	1033	1.3	28.1749	3.6	0.0262	3.8	0.0053	1.4	0.36	34.4	0.5	26.2	1.0	NA	NA	34.4	0.5
Greenhorn4	59	1080	3.1	20.3690	4.2	0.0362	4.5	0.0054	1.5	0.34	34.4	0.5	36.1	1.6	151.3	98.7	34.4	0.5
Greenhorn4	62	3581	1.3	18.9578	4.1	0.0390	4.3	0.0054	1.3	0.30	34.5	0.4	38.9	1.6	317.0	93.9	34.5	0.4
Greenhorn4	172	11419	1.4	20.5132	2.2	0.0362	2.4	0.0054	1.2	0.47	34.6	0.4	36.1	0.9	134.7	50.7	34.6	0.4
Greenhorn4	73	617	3.0	36.8324	4.8	0.0202	5.0	0.0054	1.2	0.25	34.7	0.4	20.3	1.0	NA	NA	34.7	0.4
Greenhorn4	88	1970	2.7	21.9934	4.0	0.0338	4.2	0.0054	1.4	0.33	34.7	0.5	33.7	1.4	NA	NA	34.7	0.5
Greenhorn4	526	5386	1.9	22.0903	1.6	0.0337	2.0	0.0054	1.2	0.61	34.7	0.4	33.6	0.7	NA	NA	34.7	0.4
Greenhorn4	286	26138	1.3	20.4843	2.0	0.0364	2.4	0.0054	1.2	0.53	34.8	0.4	36.3	0.8	138.1	46.8	34.8	0.4
Greenhorn4	1518	5588	0.5	15.3396	1.9	0.0487	2.2	0.0054	1.1	0.49	34.8	0.4	48.3	1.0	779.6	40.2	34.8	0.4
Greenhorn4	279	1812	2.1	16.0894	4.5	0.0472	4.6	0.0055	1.2	0.25	35.4	0.4	46.9	2.1	678.4	95.5	35.4	0.4
Greenhorn4	708	62765	1.9	20.0458	1.5	0.0380	1.8	0.0055	1.0	0.54	35.6	0.3	37.9	0.7	188.6	34.9	35.6	0.3
Greenhorn4	48	14000	0.8	14.8391	4.2	0.0517	4.5	0.0056	1.4	0.32	35.8	0.5	51.1	2.2	848.9	88.3	35.8	0.5
Greenhorn4	152	2710	2.7	23.1510	2.3	0.0334	2.6	0.0056	1.2	0.47	36.0	0.4	33.3	0.8	NA	NA	36.0	0.4
Greenhorn4	679	10895	4.9	22.0712	1.6	0.0352	1.9	0.0056	1.1	0.57	36.2	0.4	35.1	0.7	NA	NA	36.2	0.4
Greenhorn4	57	8435	3.0	12.5373	3.8	0.0627	4.1	0.0057	1.6	0.39	36.7	0.6	61.7	2.5	1190.2	74.6	36.7	0.6
Greenhorn4	184	529	1.1	5.3278	25.2	0.1609	25.4	0.0062	3.2	0.13	40.0	1.3	151.5	35.7	2721.4	422.1	40.0	1.3
Greenhorn4	181	274622	2.0	19.4733	1.3	0.1890	1.7	0.0267	1.1	0.66	169.9	1.9	175.7	2.8	255.7	29.9	169.9	1.9
Greenhorn4	85	56838	4.3	17.9244	0.9	0.5006	1.5	0.0651	1.2	0.79	406.6	4.6	412.1	5.1	443.0	20.5	406.6	4.6
Greenhorn4	571	753530	1.6	14.2740	0.6	1.5322	1.3	0.1587	1.2	0.88	949.5	10.3	943.4	8.1	929.1	12.6	929.1	12.6
Greenhorn4	127	149882	1.9	12.0049	0.6	2.5313	1.1	0.2205	0.9	0.82	1284.5	10.0	1281.1	7.7	1275.4	11.7	1275.4	11.7
Greenhorn4	113	74069	5.8	11.7171	0.7	2.5373	1.2	0.2157	0.9	0.80	1259.2	10.7	1282.8	8.5	1322.5	13.5	1322.5	13.5
Greenhorn4	59	20366	2.0	11.6473	0.6	2.7387	1.2	0.2315	1.0	0.86	1342.1	12.4	1339.0	8.9	1334.1	11.9	1334.1	11.9
Greenhorn4	342	10825069	2.2	11.6350	0.7	2.7436	1.4	0.2316	1.2	0.88	1343.0	14.8	1340.4	10.3	1336.1	12.6	1336.1	12.6
Greenhorn4	175	5694938	2.9	11.6098	0.6	2.6780	1.4	0.2256	1.3	0.92	1311.4	15.6	1322.4	10.6	1340.3	11.1	1340.3	11.1
Greenhorn4	116	63559	1.1	11.5525	0.7	2.4327	1.1	0.2039	0.9	0.77	1196.3	9.5	1252.3	8.1	1349.9	13.8	1349.9	13.8
Greenhorn4	329	117700	2.1	11.5501	0.5	2.7210	1.2	0.2280	1.1	0.90	1324.2	13.2	1334.2	9.2	1350.3	10.6	1350.3	10.6
Greenhorn4	155	159285	3.7	11.5216	0.7	2.6430	1.2	0.2210	1.0	0.81	1286.9	11.4	1312.7	8.9	1355.0	13.6	1355.0	13.6

Greenhorn4	139	210304	2.6	11.5173	0.6	2.7209	1.3	0.2274	1.1	0.87	1320.7	13.7	1334.2	9.8	1355.8	12.5	1355.8	12.5
Greenhorn4	86	62547	1.5	11.4916	0.7	2.7672	1.2	0.2307	1.0	0.84	1338.3	12.6	1346.7	9.3	1360.1	12.9	1360.1	12.9
Greenhorn4	112	47823	1.9	11.4850	0.5	2.5703	1.2	0.2142	1.1	0.90	1251.1	12.3	1292.2	8.7	1361.2	10.0	1361.2	10.0
Greenhorn4	116	59840	6.6	11.4673	0.7	2.6738	1.5	0.2225	1.3	0.88	1294.9	15.5	1321.3	11.1	1364.2	13.6	1364.2	13.6
Greenhorn4	131	77251	2.3	11.4253	0.6	2.7688	1.2	0.2295	1.0	0.86	1332.0	12.1	1347.2	8.7	1371.2	11.6	1371.2	11.6
Greenhorn4	40	29925	2.3	11.3944	0.9	2.8154	1.4	0.2328	1.1	0.80	1349.0	13.8	1359.6	10.7	1376.4	16.5	1376.4	16.5
Greenhorn4	363	186819	5.0	11.3029	0.6	2.8825	1.2	0.2364	1.0	0.83	1367.9	11.9	1377.3	8.8	1391.9	12.4	1391.9	12.4
Greenhorn4	291	89014	1.3	11.2292	0.7	3.0092	1.5	0.2452	1.3	0.90	1413.6	16.8	1410.0	11.3	1404.5	12.6	1404.5	12.6
Greenhorn4	47	20939	2.8	11.2234	0.8	2.7350	1.2	0.2227	0.9	0.74	1296.3	10.0	1338.0	8.6	1405.5	15.1	1405.5	15.1
Greenhorn4	917	961719	41.1	11.2050	0.7	2.5874	1.3	0.2104	1.1	0.83	1230.7	12.2	1297.1	9.6	1408.6	14.0	1408.6	14.0
Greenhorn4	59	15163	1.7	11.1839	1.1	2.9485	1.7	0.2393	1.3	0.76	1382.9	16.3	1394.5	13.1	1412.2	21.7	1412.2	21.7
Greenhorn4	437	92586	23.7	11.1302	0.7	2.6564	1.3	0.2145	1.1	0.84	1252.9	12.8	1316.4	9.9	1421.4	13.8	1421.4	13.8
Greenhorn4	198	28280	1.9	10.9687	1.4	2.7942	2.6	0.2224	2.2	0.85	1294.5	26.0	1354.0	19.6	1449.3	26.5	1449.3	26.5
Greenhorn4	2042	280701	7.5	10.8502	0.5	2.9659	1.1	0.2335	0.9	0.87	1352.8	11.5	1398.9	8.2	1469.9	10.0	1469.9	10.0
Greenhorn4	29	11619	2.0	10.5488	1.4	3.1161	1.6	0.2385	0.9	0.54	1378.9	11.1	1436.7	12.6	1523.2	25.9	1523.2	25.9
Greenhorn4	265	37840	18.3	10.3775	0.6	2.9885	1.3	0.2250	1.2	0.88	1308.4	13.8	1404.7	10.1	1554.0	11.8	1554.0	11.8
Greenhorn4	455	220871	8.1	10.3102	0.7	3.7774	1.4	0.2826	1.2	0.88	1604.4	17.5	1587.9	11.3	1566.2	12.6	1566.2	12.6
Greenhorn4	33	36143	1.5	9.7986	0.8	4.2279	1.2	0.3006	0.9	0.74	1694.2	13.6	1679.5	10.2	1661.0	15.6	1661.0	15.6
Greenhorn4	488	517602	2.2	9.6087	0.7	4.1594	1.2	0.2900	1.0	0.83	1641.5	14.4	1666.1	9.8	1697.2	12.3	1697.2	12.3
Greenhorn4	46	62472	5.6	9.6021	0.8	4.1163	1.4	0.2868	1.1	0.82	1625.5	16.3	1657.5	11.3	1698.4	14.5	1698.4	14.5
Greenhorn4	604	368735	4.6	9.5739	0.6	4.1991	1.1	0.2917	0.9	0.84	1650.0	13.5	1673.9	9.1	1703.8	11.1	1703.8	11.1
Greenhorn4	102	96519	1.5	9.5713	0.6	4.3648	1.2	0.3031	1.0	0.84	1706.8	15.0	1705.7	9.8	1704.3	11.8	1704.3	11.8
Greenhorn4	192	77599	5.1	9.5560	0.6	4.4560	0.8	0.3090	0.6	0.75	1735.6	9.7	1722.8	7.0	1707.3	10.2	1707.3	10.2
Greenhorn4	308	52993	4.6	9.5543	0.6	3.9497	1.2	0.2738	1.0	0.87	1560.1	14.0	1623.9	9.4	1707.6	10.6	1707.6	10.6
Greenhorn4	809	49877	14.9	9.5307	0.5	3.6394	1.0	0.2517	0.8	0.84	1447.1	10.8	1558.2	7.9	1712.2	9.9	1712.2	9.9
Greenhorn4	236	564650	4.6	9.5166	0.6	4.3931	0.9	0.3033	0.8	0.81	1707.9	11.5	1711.0	7.8	1714.9	10.2	1714.9	10.2
Greenhorn4	606	103913	5.4	9.4979	0.6	4.2752	0.9	0.2946	0.7	0.75	1664.6	10.0	1688.6	7.5	1718.5	11.1	1718.5	11.1
Greenhorn4	49	121433	4.6	9.4973	0.8	4.3513	1.2	0.2999	0.9	0.74	1690.6	12.8	1703.1	9.7	1718.6	14.6	1718.6	14.6
Salida 4	245	46889	0.7	20.1483	2.3	0.0352	2.8	0.0051	1.6	0.57	33.1	0.5	35.1	0.9	176.8	53.0	33.1	0.5
Salida 4	417	29754	0.6	21.9172	2.3	0.0327	2.8	0.0052	1.6	0.57	33.4	0.5	32.6	0.9	NA	NA	33.4	0.5

Salida 4	236	21676	0.9	15.2939	2.4	0.0468	2.8	0.0052	1.5	0.54	33.4	0.5	46.5	1.3	785.8	49.4	33.4	0.5
Salida 4	760	10349	0.9	21.8318	2.0	0.0329	2.3	0.0052	1.3	0.54	33.5	0.4	32.9	0.8	NA	NA	33.5	0.4
Salida 4	188	4650	0.9	24.7524	3.7	0.0294	4.0	0.0053	1.3	0.34	33.9	0.5	29.4	1.2	NA	NA	33.9	0.5
Salida 4	967	10256	0.6	20.5453	1.8	0.0355	2.0	0.0053	0.9	0.44	34.0	0.3	35.4	0.7	131.1	42.4	34.0	0.3
Salida 4	1052	61325	1.4	21.1479	1.0	0.0348	1.5	0.0053	1.1	0.72	34.3	0.4	34.7	0.5	62.6	24.4	34.3	0.4
Salida 4	1332	55889	1.6	21.4665	1.2	0.0345	1.6	0.0054	1.1	0.68	34.5	0.4	34.4	0.6	26.9	28.7	34.5	0.4
Salida 4	665	25370	0.8	20.2299	1.6	0.0368	2.0	0.0054	1.2	0.60	34.7	0.4	36.6	0.7	167.3	37.6	34.7	0.4
Salida 4	947	24275	2.0	18.9060	2.7	0.0394	3.0	0.0054	1.2	0.42	34.8	0.4	39.3	1.1	323.2	61.3	34.8	0.4
Salida 4	226	3073	0.7	21.5884	3.6	0.0346	3.9	0.0054	1.5	0.38	34.8	0.5	34.5	1.3	13.3	86.3	34.8	0.5
Salida 4	337	40038	1.9	21.0772	2.6	0.0354	2.9	0.0054	1.3	0.45	34.8	0.5	35.3	1.0	70.6	61.5	34.8	0.5
Salida 4	321	7781	0.9	22.0347	1.6	0.0339	1.9	0.0054	1.0	0.54	34.9	0.4	33.9	0.6	NA	NA	34.9	0.4
Salida 4	181	1540	1.2	18.9225	10.8	0.0396	10.9	0.0054	1.7	0.16	34.9	0.6	39.4	4.2	321.3	245.7	34.9	0.6
Salida 4	357	8581	0.7	15.4021	4.9	0.0486	5.2	0.0054	1.6	0.31	34.9	0.6	48.2	2.4	771.0	103.5	34.9	0.6
Salida 4	155	4158	1.4	20.9748	4.8	0.0357	5.0	0.0054	1.4	0.27	34.9	0.5	35.6	1.7	82.2	113.2	34.9	0.5
Salida 4	233	11506	0.9	20.9575	2.6	0.0358	3.0	0.0054	1.3	0.44	35.0	0.5	35.7	1.0	84.1	62.7	35.0	0.5
Salida 4	196	5042	0.9	21.7198	2.9	0.0346	3.1	0.0054	1.2	0.37	35.0	0.4	34.5	1.1	NA	NA	35.0	0.4
Salida 4	513	18276	1.3	19.8030	2.3	0.0379	2.6	0.0054	1.1	0.43	35.0	0.4	37.8	1.0	217.0	53.8	35.0	0.4
Salida 4	169	2127	0.9	25.1084	3.6	0.0300	4.0	0.0055	1.8	0.44	35.1	0.6	30.0	1.2	NA	NA	35.1	0.6
Salida 4	361	5937	0.5	22.1806	2.7	0.0339	3.1	0.0055	1.6	0.51	35.1	0.6	33.9	1.0	NA	NA	35.1	0.6
Salida 4	1828	42376	1.0	20.3641	1.3	0.0370	1.7	0.0055	1.2	0.67	35.2	0.4	36.9	0.6	151.9	29.6	35.2	0.4
Salida 4	663	28343	1.5	21.5529	1.4	0.0351	1.7	0.0055	1.0	0.57	35.3	0.3	35.0	0.6	17.3	33.8	35.3	0.3
Salida 4	131	51455	1.0	21.0887	2.6	0.0359	3.0	0.0055	1.5	0.50	35.3	0.5	35.8	1.1	69.3	63.0	35.3	0.5
Salida 4	569	125572	1.3	21.4058	1.5	0.0353	2.0	0.0055	1.4	0.69	35.3	0.5	35.3	0.7	33.7	34.7	35.3	0.5
Salida 4	1687	21275	0.7	21.5010	1.0	0.0352	1.4	0.0055	0.9	0.63	35.3	0.3	35.2	0.5	23.1	25.1	35.3	0.3
Salida 4	234	4731	0.6	16.7567	4.2	0.0452	4.5	0.0055	1.6	0.36	35.4	0.6	44.9	2.0	591.0	91.6	35.4	0.6
Salida 4	1653	19970	1.8	21.7017	1.4	0.0349	1.6	0.0055	0.8	0.49	35.4	0.3	34.9	0.6	NA	NA	35.4	0.3
Salida 4	1588	11787	2.6	19.3819	2.0	0.0392	2.2	0.0055	0.9	0.43	35.4	0.3	39.0	0.8	266.5	45.2	35.4	0.3
Salida 4	1859	109374	2.5	21.3059	0.9	0.0357	1.3	0.0055	1.0	0.72	35.5	0.3	35.6	0.5	44.9	22.2	35.5	0.3
Salida 4	192	4578	0.9	21.9930	3.0	0.0346	3.4	0.0055	1.5	0.46	35.5	0.5	34.5	1.1	NA	NA	35.5	0.5
Salida 4	142	2645	1.1	12.6399	5.5	0.0604	5.7	0.0055	1.3	0.23	35.6	0.5	59.5	3.3	1174.2	109.1	35.6	0.5
Salida 4	82	67564	1.1	20.1158	4.1	0.0379	4.2	0.0055	1.1	0.25	35.6	0.4	37.8	1.6	180.5	94.5	35.6	0.4

Salida 4	89	3859	0.8	23.3159	4.1	0.0328	4.5	0.0055	1.9	0.42	35.6	0.7	32.7	1.4	NA	NA	35.6	0.7
Salida 4	418	51361	1.0	21.2190	2.0	0.0360	2.3	0.0055	1.2	0.52	35.6	0.4	35.9	0.8	54.7	47.6	35.6	0.4
Salida 4	354	25493	1.1	19.5130	2.5	0.0392	2.7	0.0055	1.2	0.44	35.6	0.4	39.0	1.0	251.0	56.4	35.6	0.4
Salida 4	459	10974	0.5	20.1493	2.4	0.0380	2.7	0.0056	1.3	0.49	35.7	0.5	37.8	1.0	176.6	55.3	35.7	0.5
Salida 4	276	110203	0.8	21.5105	2.2	0.0357	2.8	0.0056	1.8	0.65	35.8	0.6	35.6	1.0	22.0	51.6	35.8	0.6
Salida 4	577	881562	1.1	20.5997	1.9	0.0373	2.2	0.0056	1.1	0.50	35.8	0.4	37.2	0.8	124.8	44.8	35.8	0.4
Salida 4	135	1634	1.3	27.1594	3.3	0.0283	3.7	0.0056	1.7	0.46	35.8	0.6	28.3	1.0	NA	NA	35.8	0.6
Salida 4	295	61319	1.0	16.0347	5.0	0.0479	5.3	0.0056	1.7	0.32	35.8	0.6	47.5	2.5	685.7	107.5	35.8	0.6
Salida 4	2160	140378	2.9	21.3598	0.8	0.0360	1.4	0.0056	1.2	0.82	35.9	0.4	35.9	0.5	38.8	19.0	35.9	0.4
Salida 4	214	5497	0.8	23.1339	2.9	0.0333	3.2	0.0056	1.3	0.41	35.9	0.5	33.2	1.0	NA	NA	35.9	0.5
Salida 4	874	8659	0.6	22.6766	1.4	0.0340	1.8	0.0056	1.1	0.60	35.9	0.4	33.9	0.6	NA	NA	35.9	0.4
Salida 4	620	8317	1.2	21.5020	1.7	0.0358	2.0	0.0056	1.0	0.51	35.9	0.4	35.7	0.7	22.9	40.4	35.9	0.4
Salida 4	204	4835	1.1	17.6002	2.9	0.0438	3.3	0.0056	1.4	0.43	36.0	0.5	43.6	1.4	483.5	65.0	36.0	0.5
Salida 4	162	2247	0.9	25.0649	4.6	0.0308	4.8	0.0056	1.5	0.31	36.0	0.5	30.8	1.5	NA	NA	36.0	0.5
Salida 4	929	35655	0.7	20.3543	1.1	0.0379	1.6	0.0056	1.1	0.69	36.0	0.4	37.8	0.6	153.0	26.4	36.0	0.4
Salida 4	221	14997	0.8	21.3341	2.8	0.0362	3.2	0.0056	1.5	0.46	36.1	0.5	36.1	1.1	41.8	67.2	36.1	0.5
Salida 4	189	3407	0.8	23.6705	6.0	0.0327	6.1	0.0056	1.3	0.21	36.1	0.5	32.7	2.0	NA	NA	36.1	0.5
Salida 4	156	5581	1.0	23.3038	2.8	0.0333	3.1	0.0056	1.2	0.40	36.1	0.4	33.2	1.0	NA	NA	36.1	0.4
Salida 4	148	12649	1.1	18.4286	4.3	0.0421	4.6	0.0056	1.6	0.34	36.2	0.6	41.9	1.9	381.0	97.6	36.2	0.6
Salida 4	575	21240	1.7	21.0336	1.3	0.0369	1.7	0.0056	1.1	0.63	36.2	0.4	36.8	0.6	75.5	31.2	36.2	0.4
Salida 4	92	3335	1.1	21.0745	5.7	0.0368	5.9	0.0056	1.5	0.26	36.2	0.5	36.7	2.1	71.0	136.4	36.2	0.5
Salida 4	104	136449	1.0	19.2618	3.6	0.0403	3.8	0.0056	1.2	0.32	36.2	0.4	40.2	1.5	280.8	83.5	36.2	0.4
Salida 4	127	1280	1.1	28.0612	4.2	0.0277	4.5	0.0056	1.4	0.31	36.2	0.5	27.7	1.2	NA	NA	36.2	0.5
Salida 4	277	16821	0.7	21.3149	2.1	0.0365	2.5	0.0057	1.5	0.57	36.3	0.5	36.4	0.9	43.9	49.5	36.3	0.5
Salida 4	109	2718	1.1	24.7777	3.3	0.0315	3.6	0.0057	1.4	0.40	36.4	0.5	31.5	1.1	NA	NA	36.4	0.5
Salida 4	1764	26999	0.4	18.6896	1.9	0.0419	2.1	0.0057	1.0	0.45	36.5	0.3	41.6	0.9	349.3	42.5	36.5	0.3
Salida 4	1915	1599477	0.7	21.1584	0.9	0.0370	1.3	0.0057	0.9	0.67	36.5	0.3	36.9	0.5	61.5	22.4	36.5	0.3
Salida 4	111	2064	0.9	25.1231	7.9	0.0312	8.1	0.0057	1.5	0.18	36.6	0.5	31.2	2.5	NA	NA	36.6	0.5
Salida 4	140	1737	0.8	15.4296	6.3	0.0509	6.4	0.0057	1.3	0.21	36.6	0.5	50.4	3.2	767.3	132.8	36.6	0.5
Salida 4	296	4580	1.0	22.7368	2.2	0.0346	2.5	0.0057	1.3	0.53	36.7	0.5	34.5	0.9	NA	NA	36.7	0.5
Salida 4	109	17855	1.1	22.8344	3.7	0.0345	4.0	0.0057	1.6	0.39	36.7	0.6	34.4	1.4	NA	NA	36.7	0.6

Salida 4	143	9350	0.9	21.0049	3.1	0.0375	3.3	0.0057	1.2	0.37	36.7	0.4	37.4	1.2	78.8	73.1	36.7	0.4
Salida 4	167	91423	1.1	20.6719	3.2	0.0381	3.4	0.0057	1.2	0.35	36.7	0.4	38.0	1.3	116.6	75.2	36.7	0.4
Salida 4	164	3714	1.3	10.9911	9.6	0.0718	9.9	0.0057	2.4	0.24	36.8	0.9	70.4	6.7	1445.4	183.6	36.8	0.9
Salida 4	128	9704	1.2	20.7668	3.3	0.0380	3.5	0.0057	1.4	0.39	36.8	0.5	37.9	1.3	105.8	77.1	36.8	0.5
Salida 4	543	5579	1.3	14.3464	4.6	0.0551	4.8	0.0057	1.2	0.24	36.9	0.4	54.5	2.5	918.8	95.2	36.9	0.4
Salida 4	163	4834	1.0	22.9801	4.9	0.0344	5.1	0.0057	1.2	0.23	36.9	0.4	34.3	1.7	NA	NA	36.9	0.4
Salida 4	90	6198	1.1	24.4878	3.7	0.0323	4.0	0.0057	1.6	0.40	36.9	0.6	32.3	1.3	NA	NA	36.9	0.6
Salida 4	123	12108	1.0	21.5597	2.9	0.0367	3.1	0.0057	1.1	0.36	36.9	0.4	36.6	1.1	16.5	69.9	36.9	0.4
Salida 4	291	11627	0.7	21.4062	2.1	0.0370	2.5	0.0057	1.3	0.52	36.9	0.5	36.9	0.9	33.7	51.1	36.9	0.5
Salida 4	277	7600	0.8	21.8256	2.5	0.0363	2.8	0.0058	1.3	0.47	37.0	0.5	36.2	1.0	NA	NA	37.0	0.5
Salida 4	188	6868	0.8	24.2189	2.3	0.0327	2.5	0.0058	0.9	0.37	37.0	0.3	32.7	0.8	NA	NA	37.0	0.3
Salida 4	161	9321	1.0	13.7697	4.9	0.0579	5.1	0.0058	1.2	0.24	37.2	0.5	57.1	2.8	1002.6	99.7	37.2	0.5
Salida 4	257	28176	0.6	21.3866	2.1	0.0376	2.5	0.0058	1.4	0.54	37.5	0.5	37.5	0.9	35.8	50.8	37.5	0.5
Salida 4	168	6821	1.1	23.5616	2.6	0.0342	2.8	0.0059	1.0	0.37	37.6	0.4	34.2	0.9	NA	NA	37.6	0.4
Salida 4	235	1553	1.1	6.2961	5.8	0.1292	6.1	0.0059	1.9	0.31	37.9	0.7	123.4	7.1	2442.5	98.4	37.9	0.7
Salida 4	388	9682	0.7	21.1549	2.3	0.0388	2.8	0.0060	1.6	0.56	38.3	0.6	38.7	1.1	61.9	55.6	38.3	0.6
Salida 4	2917	108521	1.4	21.5220	1.0	0.0384	1.3	0.0060	0.9	0.67	38.5	0.3	38.2	0.5	20.7	22.8	38.5	0.3
Salida 4	281	1619	3.9	6.4712	22.5	0.1278	22.9	0.0060	4.2	0.18	38.6	1.6	122.1	26.4	2395.9	389.0	38.6	1.6
Salida 4	218	1887	1.4	16.3024	6.4	0.0509	6.5	0.0060	1.4	0.21	38.7	0.5	50.4	3.2	650.3	136.6	38.7	0.5
Salida 4	193	7851	1.2	6.2912	18.7	0.1414	18.9	0.0065	2.4	0.13	41.5	1.0	134.3	23.7	2443.8	319.5	41.5	1.0
Salida 4	247	12067	1.4	21.6836	2.7	0.0414	3.2	0.0065	1.8	0.54	41.8	0.7	41.2	1.3	2.7	65.4	41.8	0.7
Salida 4	113	3747	0.9	7.0746	14.0	0.1299	14.3	0.0067	2.9	0.20	42.8	1.2	124.0	16.7	2243.1	243.2	42.8	1.2
Salida 4	155	3336	0.9	6.1074	14.6	0.1709	15.0	0.0076	3.4	0.22	48.6	1.6	160.2	22.2	2493.9	247.5	48.6	1.6
Salida 4	127	806	1.1	2.8266	7.3	0.4254	8.7	0.0087	4.6	0.53	56.0	2.6	359.9	26.3	3722.7	111.6	56.0	2.6
Salida 4	92	143258	1.4	11.0930	0.8	2.9881	1.5	0.2405	1.2	0.82	1389.3	15.2	1404.6	11.2	1427.8	16.1	1427.8	16.1
Salida 4	519	247275	1.7	11.0611	0.5	2.4661	1.8	0.1979	1.7	0.95	1164.1	17.9	1262.1	12.7	1433.3	10.1	1433.3	10.1
Salida 4	477	152839	2.0	9.7954	0.5	4.0005	1.3	0.2843	1.2	0.93	1613.1	17.8	1634.3	10.8	1661.6	8.9	1661.6	8.9
Salida 4	134	178801	1.6	9.6785	0.8	4.2933	1.3	0.3015	1.0	0.75	1698.8	14.4	1692.1	10.6	1683.8	15.6	1683.8	15.6
Salida 4	69	44974	4.8	9.6188	0.7	4.2630	1.3	0.2975	1.1	0.84	1679.0	16.2	1686.3	10.7	1695.2	13.1	1695.2	13.1
Salida 4	292	2196945	3.5	9.6156	0.6	4.3112	1.3	0.3008	1.2	0.90	1695.2	18.2	1695.5	11.1	1695.8	10.6	1695.8	10.6

Salida 10	301	3914	1.4	17.9297	5.0	0.0338	5.1	0.0044	1.1	0.21	28.3	0.3	33.7	1.7	442.4	112.0	28.3	0.3
Salida 10	613	25186	1.5	20.0173	1.8	0.0304	2.3	0.0044	1.3	0.60	28.4	0.4	30.4	0.7	192.0	42.1	28.4	0.4
Salida 10	1404	10519	0.6	21.5455	1.1	0.0305	1.7	0.0048	1.2	0.74	30.7	0.4	30.5	0.5	18.1	26.6	30.7	0.4
Salida 10	141	812	1.1	29.8594	4.6	0.0233	4.7	0.0050	1.1	0.24	32.5	0.4	23.4	1.1	NA	NA	32.5	0.4
Salida 10	503	14524	0.9	20.4814	1.8	0.0343	2.1	0.0051	1.2	0.56	32.8	0.4	34.3	0.7	138.4	41.2	32.8	0.4
Salida 10	284	959	0.8	29.8544	5.8	0.0237	5.8	0.0051	1.0	0.17	33.0	0.3	23.8	1.4	NA	NA	33.0	0.3
Salida 10	139	1116	1.1	28.7315	14.9	0.0247	15.0	0.0051	1.4	0.09	33.1	0.5	24.8	3.7	NA	NA	33.1	0.5
Salida 10	553	21466	1.4	20.5608	1.6	0.0347	2.3	0.0052	1.7	0.72	33.2	0.6	34.6	0.8	129.3	38.4	33.2	0.6
Salida 10	1147	37570	0.9	19.2637	1.5	0.0371	1.7	0.0052	0.8	0.48	33.3	0.3	36.9	0.6	280.5	33.7	33.3	0.3
Salida 10	456	26281	0.7	19.7112	1.9	0.0363	2.3	0.0052	1.3	0.56	33.4	0.4	36.2	0.8	227.7	43.1	33.4	0.4
Salida 10	1471	6979	1.7	16.4449	1.7	0.0439	1.9	0.0052	1.0	0.52	33.7	0.3	43.6	0.8	631.6	35.7	33.7	0.3
Salida 10	1832	54714	2.6	19.6763	1.2	0.0367	1.7	0.0052	1.2	0.73	33.7	0.4	36.6	0.6	231.8	27.0	33.7	0.4
Salida 10	146	1120	0.9	26.5807	18.4	0.0273	18.4	0.0053	1.3	0.07	33.8	0.5	27.3	5.0	NA	NA	33.8	0.5
Salida 10	487	3444937	1.6	19.8062	1.8	0.0366	2.0	0.0053	1.0	0.48	33.8	0.3	36.5	0.7	216.6	40.9	33.8	0.3
Salida 10	69	6071	1.0	17.8839	4.8	0.0406	5.0	0.0053	1.3	0.27	33.9	0.4	40.4	2.0	448.1	106.9	33.9	0.4
Salida 10	556	8111	1.1	20.9565	1.6	0.0347	2.0	0.0053	1.2	0.60	33.9	0.4	34.6	0.7	84.2	38.0	33.9	0.4
Salida 10	439	2641	0.8	23.2691	2.0	0.0313	2.5	0.0053	1.5	0.62	33.9	0.5	31.3	0.8	NA	NA	33.9	0.5
Salida 10	571	42510	1.3	20.7339	1.5	0.0352	1.7	0.0053	0.8	0.48	34.0	0.3	35.1	0.6	109.6	34.4	34.0	0.3
Salida 10	411	12352	0.7	20.5126	2.2	0.0357	2.4	0.0053	1.1	0.45	34.1	0.4	35.6	0.8	134.8	50.7	34.1	0.4
Salida 10	599	26741	1.2	20.2177	1.8	0.0363	2.1	0.0053	1.1	0.51	34.2	0.4	36.2	0.7	168.7	41.9	34.2	0.4
Salida 10	550	8516	0.9	21.4794	1.7	0.0342	2.1	0.0053	1.2	0.58	34.3	0.4	34.1	0.7	25.5	41.6	34.3	0.4
Salida 10	858	5647	0.8	20.6439	2.0	0.0357	2.3	0.0053	1.2	0.50	34.4	0.4	35.6	0.8	119.8	47.0	34.4	0.4
Salida 10	116	2669	0.6	20.1341	3.7	0.0372	3.9	0.0054	1.3	0.34	35.0	0.5	37.1	1.4	178.4	85.6	35.0	0.5
Salida 10	573	4209	1.3	22.4804	1.5	0.0335	1.9	0.0055	1.0	0.56	35.1	0.4	33.4	0.6	NA	NA	35.1	0.4
Salida 10	131	2163	0.9	20.1508	4.1	0.0373	4.4	0.0055	1.5	0.34	35.1	0.5	37.2	1.6	176.5	96.8	35.1	0.5
Salida 10	174	2014	1.0	24.2677	3.0	0.0311	3.2	0.0055	1.1	0.33	35.2	0.4	31.1	1.0	NA	NA	35.2	0.4
Salida 10	630	13967	1.1	21.1073	1.3	0.0358	1.5	0.0055	0.8	0.54	35.2	0.3	35.7	0.5	67.2	30.9	35.2	0.3
Salida 10	276	5524	0.9	21.0669	4.1	0.0359	4.4	0.0055	1.6	0.37	35.3	0.6	35.8	1.6	71.8	97.1	35.3	0.6
Salida 10	333	218731	0.6	21.1989	1.9	0.0363	2.5	0.0056	1.6	0.64	35.8	0.6	36.2	0.9	56.9	46.3	35.8	0.6
Salida 10	450	2402	1.0	22.6665	1.8	0.0348	2.3	0.0057	1.4	0.62	36.7	0.5	34.7	0.8	NA	NA	36.7	0.5
Salida 10	315	5716	1.0	21.2179	2.1	0.0379	2.4	0.0058	1.1	0.45	37.5	0.4	37.8	0.9	54.8	50.8	37.5	0.4

Salida 10	200	4220	1.0	22.5173	4.8	0.0358	4.9	0.0058	1.2	0.24	37.6	0.4	35.7	1.7	NA	NA	37.6	0.4
Salida 10	300	72385	0.8	20.3374	2.0	0.0399	2.6	0.0059	1.5	0.60	37.9	0.6	39.8	1.0	155.0	47.8	37.9	0.6
Salida 10	389	2301	0.9	6.6621	4.8	0.1253	5.0	0.0061	1.2	0.24	38.9	0.5	119.8	5.6	2346.3	82.4	38.9	0.5
Salida 10	218	42322	1.9	19.9684	1.3	0.1840	1.6	0.0267	0.9	0.57	169.6	1.6	171.5	2.6	197.6	31.2	169.6	1.6
Salida 10	770	32438	0.9	20.0408	0.6	0.2342	1.1	0.0340	0.9	0.83	215.8	1.9	213.6	2.1	189.2	14.1	215.8	1.9
Salida 10	925	67039	3.2	19.6593	0.8	0.2459	1.3	0.0351	1.1	0.79	222.2	2.3	223.2	2.7	233.8	18.7	222.2	2.3
Salida 10	515	24249	6.5	18.6413	0.8	0.3911	1.1	0.0529	0.8	0.72	332.3	2.6	335.2	3.2	355.2	17.5	332.3	2.6
Salida 10	556	88220	2.0	17.9663	0.8	0.5154	1.4	0.0672	1.2	0.84	419.2	4.9	422.0	5.0	437.8	17.4	419.2	4.9
Salida 10	308	191945	2.2	12.7276	0.7	2.2058	1.2	0.2037	1.0	0.82	1195.2	10.9	1182.9	8.5	1160.4	13.9	1160.4	13.9
Salida 10	54	395885	1.9	11.9445	0.7	2.5141	1.3	0.2179	1.1	0.85	1270.7	12.4	1276.1	9.1	1285.2	12.7	1285.2	12.7
Salida 10	232	2912131	1.8	11.3963	0.7	2.7955	1.1	0.2312	0.9	0.79	1340.6	10.9	1354.3	8.6	1376.1	13.6	1376.1	13.6
Salida 10	462	143413	10.0	11.3362	0.6	3.0213	1.5	0.2485	1.4	0.92	1430.8	18.2	1413.0	11.8	1386.3	11.9	1386.3	11.9
Salida 10	218	130632	3.2	11.1891	0.7	3.0187	1.3	0.2451	1.1	0.85	1413.1	13.4	1412.4	9.5	1411.3	12.8	1411.3	12.8
Salida 10	330	80380	2.1	11.1044	0.6	3.1112	1.4	0.2507	1.2	0.90	1442.0	15.9	1435.5	10.5	1425.8	11.5	1425.8	11.5
Salida 10	84	37395	2.1	11.0939	0.8	3.0891	1.5	0.2487	1.3	0.84	1431.6	16.2	1430.0	11.5	1427.6	15.6	1427.6	15.6
Salida 10	195	107813	2.1	11.0768	0.7	3.0260	1.2	0.2432	1.0	0.82	1403.3	12.3	1414.2	9.1	1430.6	13.0	1430.6	13.0
Salida 10	3510	627332	6.1	11.0536	0.6	2.7784	1.3	0.2228	1.1	0.87	1296.9	12.8	1349.8	9.4	1434.6	11.9	1434.6	11.9
Salida 10	147	52020	1.2	11.0471	0.6	3.1781	1.4	0.2547	1.2	0.89	1462.9	16.0	1451.9	10.6	1435.7	11.8	1435.7	11.8
Salida 10	242	105018	1.3	11.0466	0.5	3.1661	1.2	0.2538	1.1	0.91	1457.9	13.8	1448.9	9.0	1435.8	9.1	1435.8	9.1
Salida 10	283	106820	1.5	11.0462	0.6	3.0685	1.2	0.2459	1.1	0.85	1417.5	13.5	1424.9	9.5	1435.9	12.4	1435.9	12.4
Salida 10	207	52429	1.8	11.0363	0.8	3.1657	1.4	0.2535	1.1	0.79	1456.5	14.2	1448.8	10.6	1437.6	16.1	1437.6	16.1
Salida 10	66	24550	1.1	11.0258	0.8	3.1154	1.3	0.2492	1.0	0.76	1434.5	12.4	1436.5	9.8	1439.4	15.8	1439.4	15.8
Salida 10	227	67275	1.0	11.0077	0.6	3.1031	1.3	0.2478	1.1	0.87	1427.3	14.3	1433.5	9.8	1442.5	12.1	1442.5	12.1
Salida 10	67	49893	1.1	11.0061	0.6	3.2647	1.3	0.2607	1.1	0.87	1493.5	14.6	1472.7	9.8	1442.8	11.9	1442.8	11.9
Salida 10	107	89484	0.8	10.9836	0.6	3.1508	1.1	0.2511	0.9	0.82	1444.2	12.0	1445.2	8.7	1446.7	12.2	1446.7	12.2
Salida 10	76	37702	0.7	10.9814	0.8	3.2731	1.4	0.2608	1.2	0.81	1493.9	15.5	1474.7	11.1	1447.1	16.0	1447.1	16.0
Salida 10	121	63406	1.5	10.9799	0.7	3.1212	1.3	0.2487	1.1	0.85	1431.6	14.4	1437.9	10.1	1447.3	13.3	1447.3	13.3
Salida 10	108	118599	1.1	10.9413	0.5	3.1916	1.2	0.2534	1.1	0.89	1455.9	14.0	1455.1	9.3	1454.0	10.3	1454.0	10.3
Salida 10	91	72740	1.9	10.9278	0.7	3.2836	1.2	0.2604	0.9	0.77	1491.7	11.9	1477.2	9.0	1456.4	13.9	1456.4	13.9
Salida 10	75	26119	1.1	10.9217	0.7	3.2267	1.3	0.2557	1.1	0.83	1467.8	14.3	1463.6	10.2	1457.4	14.2	1457.4	14.2
Salida 10	179	127553	1.0	10.9148	0.6	3.3381	1.2	0.2644	1.0	0.88	1512.1	13.9	1490.0	9.2	1458.6	10.7	1458.6	10.7

Salida 10	127	100513	1.7	10.9062	0.6	3.2525	1.1	0.2574	0.9	0.84	1476.4	12.3	1469.8	8.7	1460.2	11.6	1460.2	11.6
Salida 10	110	403145	1.4	10.4564	0.8	3.4748	1.3	0.2636	1.0	0.75	1508.4	13.0	1521.5	10.1	1539.8	15.9	1539.8	15.9
Salida 10	1177	391693	2.4	9.9486	0.6	3.8377	1.2	0.2770	1.0	0.86	1576.4	14.0	1600.7	9.3	1632.8	10.8	1632.8	10.8
Salida 10	418	592590	1.5	9.8404	0.5	4.2226	1.1	0.3015	0.9	0.88	1698.7	14.0	1678.4	8.7	1653.1	9.2	1653.1	9.2
Salida 10	409	66293	2.0	9.7778	0.6	4.2872	1.2	0.3042	1.0	0.85	1711.9	15.5	1690.9	9.9	1664.9	11.6	1664.9	11.6
Salida 10	395	111218	2.6	9.7744	0.6	4.2453	1.1	0.3011	1.0	0.86	1696.7	14.2	1682.8	9.1	1665.6	10.5	1665.6	10.5
Salida 10	392	1140145	3.7	9.7599	0.7	4.2765	1.3	0.3028	1.1	0.84	1705.4	16.9	1688.8	11.1	1668.3	13.7	1668.3	13.7
Salida 10	1963	113953	2.3	9.6992	0.5	3.7940	1.2	0.2670	1.1	0.91	1525.6	15.3	1591.5	9.9	1679.9	9.6	1679.9	9.6
Salida 10	290	392255	3.2	9.6988	0.5	4.2623	1.2	0.2999	1.1	0.90	1691.1	16.7	1686.1	10.3	1679.9	10.0	1679.9	10.0
Salida 10	579	192091	3.2	9.6901	0.5	4.3947	1.5	0.3090	1.4	0.94	1735.7	21.9	1711.3	12.7	1681.6	9.7	1681.6	9.7
Salida 10	1017	150062	3.4	9.6626	0.6	3.6451	1.4	0.2556	1.3	0.91	1467.1	16.8	1559.4	11.2	1686.8	10.5	1686.8	10.5
Salida 10	525	464626	2.0	9.6546	0.6	4.4770	1.3	0.3136	1.1	0.89	1758.5	17.4	1726.7	10.5	1688.4	10.7	1688.4	10.7
Salida 10	557	96867	1.8	9.6295	0.7	4.4650	1.2	0.3120	1.0	0.81	1750.4	14.7	1724.5	9.9	1693.2	13.0	1693.2	13.0
Salida 10	1649	188305	1.7	9.6226	0.4	3.7196	1.0	0.2597	0.9	0.91	1488.3	12.0	1575.6	7.9	1694.5	7.4	1694.5	7.4
Salida 10	330	592302	1.8	9.6058	0.6	4.3185	1.3	0.3010	1.1	0.87	1696.2	16.5	1696.9	10.4	1697.7	11.3	1697.7	11.3
Salida 10	360	3684079	2.5	9.6041	0.4	4.4698	1.1	0.3115	1.0	0.92	1748.0	16.0	1725.4	9.4	1698.0	8.3	1698.0	8.3
Salida 10	257	129762	3.0	9.6030	0.5	4.4934	1.0	0.3131	0.9	0.85	1755.9	13.1	1729.7	8.3	1698.3	9.6	1698.3	9.6
Salida 10	830	482672	2.6	9.6029	0.6	3.8125	1.4	0.2656	1.2	0.89	1518.7	16.7	1595.4	11.1	1698.3	11.4	1698.3	11.4
Salida 10	1191	327607	3.6	9.5937	0.6	4.2959	1.2	0.2990	1.1	0.87	1686.6	16.1	1692.6	10.2	1700.0	11.1	1700.0	11.1
Salida 10	601	50610	1.9	9.5820	0.7	4.4961	1.2	0.3126	1.0	0.82	1753.5	15.0	1730.3	9.9	1702.3	12.5	1702.3	12.5
Salida 10	469	103556	1.9	9.5722	0.6	4.4063	1.4	0.3060	1.3	0.90	1721.2	19.6	1713.5	12.0	1704.2	11.8	1704.2	11.8
Salida 10	698	65681	1.7	9.5192	0.7	4.1756	1.2	0.2884	1.0	0.85	1633.6	15.1	1669.2	10.1	1714.4	12.0	1714.4	12.0
Salida 10	378	2275066	1.7	9.5061	0.8	4.4989	1.5	0.3103	1.3	0.84	1742.2	19.7	1730.8	12.7	1716.9	15.1	1716.9	15.1
Salida 10	775	274397	1.3	9.5036	0.7	4.2789	1.1	0.2951	0.8	0.78	1666.8	12.5	1689.3	8.9	1717.4	12.3	1717.4	12.3
Salida 10	683	195440	1.7	9.5008	0.7	4.4117	1.4	0.3041	1.2	0.87	1711.7	18.0	1714.5	11.5	1717.9	12.7	1717.9	12.7
Salida 10	192	116472	2.9	9.4649	0.6	4.5438	1.2	0.3121	1.0	0.85	1750.8	15.5	1739.0	9.8	1724.9	11.2	1724.9	11.2
Salida 10	153	222893	2.9	9.4541	0.5	4.5222	1.3	0.3102	1.2	0.92	1741.8	17.7	1735.1	10.4	1727.0	8.9	1727.0	8.9
Salida 10	358	215783	1.8	9.4453	0.6	4.6124	1.5	0.3161	1.4	0.91	1770.7	21.3	1751.5	12.6	1728.7	11.6	1728.7	11.6
Salida 10	150	68293	2.6	9.4352	0.5	4.4667	1.4	0.3058	1.2	0.92	1719.9	18.8	1724.8	11.3	1730.7	10.0	1730.7	10.0
Salida 10	753	4448191	1.9	9.4341	0.7	4.2524	1.1	0.2911	0.9	0.80	1646.9	13.3	1684.2	9.4	1730.9	12.6	1730.9	12.6
Salida 10	839	255376	1.0	9.4239	0.5	4.3335	1.0	0.2963	0.9	0.88	1673.0	13.5	1699.8	8.6	1732.9	9.1	1732.9	9.1

Salida 10	182	332033	2.4	9.3890	0.5	4.4938	1.0	0.3061	0.9	0.89	1721.7	13.8	1729.8	8.5	1739.7	8.7	1739.7	8.7
Salida 10	966	284820	16.3	9.3321	0.7	4.2587	1.2	0.2884	0.9	0.78	1633.3	13.0	1685.4	9.5	1750.8	13.3	1750.8	13.3
Salida 10	427	19194	2.0	9.2700	1.4	4.5724	1.8	0.3075	1.3	0.68	1728.6	19.0	1744.3	15.3	1763.0	24.7	1763.0	24.7
Salida 10	111	70725	1.2	7.8345	0.5	6.7607	1.1	0.3843	1.0	0.88	2096.4	17.5	2080.6	9.9	2065.0	9.5	2065.0	9.5
SanIsabel1	2941	12009	8.8	10.8646	0.6	0.7213	1.2	0.0569	1.0	0.85	356.5	3.5	551.4	5.1	1467.4	11.8	356.5	3.5
SanIsabel1	100	11266	3.5	17.4024	1.5	0.6396	1.8	0.0808	1.0	0.57	500.6	4.9	502.0	7.1	508.4	32.3	500.6	4.9
SanIsabel1	156	61073	1.1	17.0887	0.9	0.6575	1.3	0.0815	0.9	0.70	505.2	4.5	513.1	5.3	548.3	20.7	505.2	4.5
SanIsabel1	580	277197	2.0	16.9831	0.6	0.6692	1.2	0.0825	1.0	0.87	510.8	5.0	520.3	4.8	561.8	12.8	510.8	5.0
SanIsabel1	291	90562	0.4	17.1313	0.7	0.6659	1.2	0.0828	0.9	0.80	512.6	4.5	518.2	4.7	542.8	15.2	512.6	4.5
SanIsabel1	110	67496	1.2	17.3201	0.9	0.6696	1.3	0.0842	1.0	0.74	520.9	4.9	520.5	5.3	518.8	19.3	520.9	4.9
SanIsabel1	344	276906	2.8	17.0682	0.8	0.6810	1.2	0.0843	0.9	0.75	521.9	4.4	527.3	4.8	550.9	16.8	521.9	4.4
SanIsabel1	77	14183	2.2	17.3216	0.9	0.6713	1.3	0.0844	1.0	0.72	522.2	4.8	521.5	5.5	518.6	20.4	522.2	4.8
SanIsabel1	335	283960	1.8	17.3929	0.6	0.6722	1.2	0.0848	1.0	0.86	524.9	5.1	522.1	4.8	509.6	13.2	524.9	5.1
SanIsabel1	125	53163	3.3	17.0545	0.8	0.6945	1.3	0.0859	1.0	0.77	531.5	5.2	535.5	5.5	552.6	18.3	531.5	5.2
SanIsabel1	14	6197	1.2	17.3712	2.1	0.6842	2.6	0.0862	1.5	0.57	533.3	7.5	529.3	10.6	512.4	46.6	533.3	7.5
SanIsabel1	22	35782	2.2	16.6917	1.6	0.7208	1.9	0.0873	1.1	0.58	539.6	5.8	551.2	8.2	599.4	34.1	539.6	5.8
SanIsabel1	45	32934	1.2	16.5873	1.6	0.7884	2.1	0.0949	1.3	0.65	584.4	7.5	590.3	9.2	612.9	33.7	584.4	7.5
SanIsabel1	237	80305	1.8	13.1511	0.6	1.9526	1.2	0.1863	1.0	0.86	1101.4	10.3	1099.3	8.0	1095.2	12.3	1095.2	12.3
SanIsabel1	381	295916	2.2	11.4417	0.6	2.8444	1.2	0.2361	1.0	0.87	1366.6	12.3	1367.3	8.7	1368.5	11.1	1368.5	11.1
SanIsabel1	620	2057534	43.9	11.2398	0.6	2.9869	1.1	0.2436	1.0	0.84	1405.3	12.0	1404.3	8.6	1402.6	11.7	1402.6	11.7
SanIsabel1	344	239084	2.4	11.2145	0.7	2.8980	1.6	0.2358	1.5	0.89	1364.9	18.0	1381.4	12.4	1407.0	14.1	1407.0	14.1
SanIsabel1	585	2570813	3.4	11.1847	0.7	3.0835	1.3	0.2502	1.1	0.84	1439.7	14.2	1428.6	10.0	1412.1	13.4	1412.1	13.4
SanIsabel1	371	368891	43.7	11.1825	0.5	2.9726	1.3	0.2412	1.2	0.92	1392.9	14.6	1400.6	9.6	1412.4	9.3	1412.4	9.3
SanIsabel1	381	895220	2.1	11.1793	0.6	3.0501	1.1	0.2474	0.9	0.85	1425.1	11.8	1420.3	8.2	1413.0	10.7	1413.0	10.7
SanIsabel1	92	542123	1.2	11.1481	0.8	3.1828	1.3	0.2575	1.1	0.80	1476.8	13.9	1453.0	10.2	1418.3	15.1	1418.3	15.1
SanIsabel1	153	221575	1.3	11.1455	0.5	3.1401	1.1	0.2539	0.9	0.89	1458.8	12.3	1442.6	8.2	1418.8	9.3	1418.8	9.3
SanIsabel1	52	30787	9.0	11.1385	0.7	3.0512	1.5	0.2466	1.3	0.88	1420.9	17.2	1420.5	11.7	1420.0	13.6	1420.0	13.6
SanIsabel1	806	1399394	9.5	11.1139	0.6	2.9005	1.2	0.2339	1.0	0.87	1354.9	12.3	1382.0	8.8	1424.2	11.0	1424.2	11.0
SanIsabel1	218	252396	2.1	11.1048	0.7	3.1874	1.2	0.2568	1.0	0.83	1473.6	13.6	1454.1	9.7	1425.8	13.4	1425.8	13.4
SanIsabel1	115	237202	1.3	11.0598	0.6	3.1194	1.1	0.2503	0.9	0.84	1440.2	11.6	1437.5	8.2	1433.5	11.0	1433.5	11.0

SanIsabel1	210	285458	2.3	11.0402	0.6	3.0670	1.4	0.2457	1.3	0.89	1416.2	15.9	1424.5	10.8	1436.9	12.4	1436.9	12.4
SanIsabel1	217	153748	2.3	11.0300	0.6	3.1459	1.1	0.2518	1.0	0.86	1447.6	12.9	1444.0	8.8	1438.7	11.0	1438.7	11.0
SanIsabel1	105	84511	1.0	10.9862	0.7	2.9936	1.1	0.2386	0.9	0.78	1379.6	10.8	1406.0	8.4	1446.2	13.1	1446.2	13.1
SanIsabel1	862	461245	11.0	10.9734	0.5	3.0488	1.2	0.2428	1.1	0.91	1401.0	13.3	1419.9	8.8	1448.5	8.9	1448.5	8.9
SanIsabel1	877	8693665	33.6	10.8831	0.6	3.0114	1.3	0.2378	1.1	0.88	1375.2	13.7	1410.5	9.6	1464.2	11.3	1464.2	11.3
SanIsabel1	878	418888	32.5	10.8650	0.5	3.0477	1.1	0.2403	0.9	0.88	1388.1	11.7	1419.7	8.1	1467.3	9.7	1467.3	9.7
SanIsabel1	40	78990	6.3	10.7892	0.7	3.4068	1.2	0.2667	1.0	0.82	1524.1	13.7	1506.0	9.8	1480.6	13.6	1480.6	13.6
SanIsabel1	936	110492	24.0	10.7752	0.8	3.0253	1.3	0.2365	1.1	0.82	1368.6	13.5	1414.0	10.2	1483.1	14.5	1483.1	14.5
SanIsabel1	78	212607	8.3	10.6492	0.7	3.3045	1.1	0.2553	0.9	0.80	1465.9	11.7	1482.1	8.7	1505.3	12.8	1505.3	12.8
SanIsabel1	270	244905	6.4	10.1038	0.8	3.8583	1.6	0.2829	1.4	0.87	1605.7	19.3	1605.0	12.6	1604.0	14.4	1604.0	14.4
SanIsabel1	133	110807	1.2	10.1020	0.6	3.7789	1.1	0.2770	1.0	0.88	1576.2	14.0	1588.3	9.2	1604.4	10.3	1604.4	10.3
SanIsabel1	513	1282881	7.1	10.0989	0.6	3.8549	1.3	0.2825	1.1	0.87	1603.8	16.3	1604.3	10.6	1604.9	11.9	1604.9	11.9
SanIsabel1	235	304526	2.4	10.0963	0.6	3.5938	1.3	0.2633	1.2	0.88	1506.6	15.6	1548.2	10.5	1605.4	11.9	1605.4	11.9
SanIsabel1	223	196448	15.9	10.0606	0.6	3.9933	1.4	0.2915	1.2	0.89	1649.0	17.5	1632.8	11.0	1612.0	11.5	1612.0	11.5
SanIsabel1	398	271493	2.0	9.9591	0.6	4.0242	1.0	0.2908	0.8	0.81	1645.5	12.2	1639.1	8.4	1630.9	11.3	1630.9	11.3
SanIsabel1	70	28410	2.6	9.9535	0.6	4.0230	1.5	0.2905	1.4	0.91	1644.3	19.7	1638.9	12.1	1631.9	11.6	1631.9	11.6
SanIsabel1	117	309349	2.5	9.9146	0.6	4.0336	1.1	0.2902	0.9	0.85	1642.4	13.1	1641.0	8.7	1639.2	10.4	1639.2	10.4
SanIsabel1	362	493846	2.0	9.9010	0.5	4.1485	1.3	0.2980	1.2	0.92	1681.5	17.7	1663.9	10.6	1641.7	9.1	1641.7	9.1
SanIsabel1	482	2685694	4.1	9.9009	0.7	4.1537	1.3	0.2984	1.1	0.86	1683.4	16.5	1664.9	10.6	1641.8	12.5	1641.8	12.5
SanIsabel1	314	251779	3.5	9.8991	0.5	4.1117	1.5	0.2953	1.4	0.94	1668.1	20.0	1656.6	11.9	1642.1	9.6	1642.1	9.6
SanIsabel1	57	28138	5.0	9.8898	0.6	4.1663	1.1	0.2990	0.9	0.84	1686.2	13.5	1667.4	8.8	1643.9	10.7	1643.9	10.7
SanIsabel1	67	209534	3.3	9.8395	0.9	4.1640	1.5	0.2973	1.2	0.78	1677.8	17.7	1667.0	12.5	1653.3	17.6	1653.3	17.6
SanIsabel1	174	2774382	2.8	9.8258	0.7	4.2786	1.4	0.3050	1.3	0.87	1716.2	18.9	1689.2	11.8	1655.9	13.2	1655.9	13.2
SanIsabel1	359	102562	2.3	9.8254	0.8	4.1933	1.5	0.2989	1.3	0.86	1686.1	19.8	1672.7	12.7	1655.9	14.6	1655.9	14.6
SanIsabel1	210	188655	3.9	9.8232	0.5	4.2937	1.2	0.3060	1.0	0.89	1721.2	15.8	1692.2	9.7	1656.4	10.0	1656.4	10.0
SanIsabel1	439	973844	0.9	9.7988	0.7	4.2199	1.4	0.3000	1.1	0.84	1691.4	16.9	1677.9	11.1	1661.0	13.6	1661.0	13.6
SanIsabel1	283	229437	21.5	9.7938	0.6	4.1457	1.4	0.2946	1.3	0.91	1664.5	18.7	1663.4	11.4	1661.9	10.6	1661.9	10.6
SanIsabel1	277	136781	2.5	9.7892	0.5	3.9222	1.5	0.2786	1.4	0.95	1584.3	19.7	1618.3	12.0	1662.8	9.0	1662.8	9.0
SanIsabel1	122	221050	2.5	9.7861	0.7	4.1996	1.1	0.2982	0.9	0.82	1682.4	13.9	1673.9	9.4	1663.4	12.2	1663.4	12.2
SanIsabel1	215	206379	3.7	9.7735	0.6	4.1862	1.2	0.2969	1.0	0.87	1675.7	15.2	1671.3	9.7	1665.8	10.6	1665.8	10.6
SanIsabel1	85	8599961	5.9	9.7722	0.8	4.0864	1.4	0.2897	1.1	0.82	1640.2	16.4	1651.6	11.3	1666.0	14.7	1666.0	14.7

SanIsabel1	119	868681	1.9	9.7643	0.6	4.0362	1.4	0.2860	1.2	0.89	1621.3	17.9	1641.5	11.4	1667.5	11.9	1667.5	11.9
SanIsabel1	487	8045881	2.3	9.7459	0.6	4.1970	1.1	0.2968	0.9	0.83	1675.4	13.8	1673.4	9.3	1671.0	11.7	1671.0	11.7
SanIsabel1	174	200259	3.2	9.7311	0.7	4.0827	1.5	0.2883	1.3	0.89	1632.9	18.9	1650.9	12.0	1673.8	12.2	1673.8	12.2
SanIsabel1	109	153319	4.8	9.7277	0.6	4.2056	1.2	0.2968	1.1	0.89	1675.6	15.7	1675.1	9.9	1674.4	10.3	1674.4	10.3
SanIsabel1	76	363356	2.7	9.7226	0.7	4.2828	1.4	0.3021	1.2	0.88	1701.9	18.1	1690.1	11.4	1675.4	12.3	1675.4	12.3
SanIsabel1	194	123212	1.7	9.7110	0.6	4.1366	1.0	0.2915	0.8	0.78	1648.9	11.3	1661.6	8.1	1677.6	11.5	1677.6	11.5
SanIsabel1	95	92113	1.5	9.7026	0.7	4.3285	1.3	0.3047	1.1	0.83	1714.7	16.5	1698.8	10.9	1679.2	13.8	1679.2	13.8
SanIsabel1	272	175608	1.9	9.6949	0.5	4.2987	1.0	0.3024	0.9	0.89	1703.1	13.9	1693.1	8.6	1680.7	8.8	1680.7	8.8
SanIsabel1	752	191444	1.7	9.6917	0.7	3.8805	1.6	0.2729	1.4	0.90	1555.4	19.5	1609.6	12.7	1681.3	12.8	1681.3	12.8
SanIsabel1	114	115322	5.2	9.6905	0.5	4.1612	1.2	0.2926	1.1	0.89	1654.4	15.6	1666.4	9.8	1681.5	10.0	1681.5	10.0
SanIsabel1	81	360689	2.4	9.6814	0.7	4.2764	1.2	0.3004	1.0	0.84	1693.3	15.4	1688.8	10.1	1683.3	12.2	1683.3	12.2
SanIsabel1	131	86985	3.9	9.6582	0.6	4.3683	1.2	0.3061	1.0	0.85	1721.6	15.8	1706.4	10.1	1687.7	11.8	1687.7	11.8
SanIsabel1	460	1469379	2.8	9.6539	0.7	4.4094	1.1	0.3089	0.9	0.78	1735.1	13.2	1714.1	9.1	1688.5	12.6	1688.5	12.6
SanIsabel1	56	34530	1.9	9.6523	0.8	3.9780	1.1	0.2786	0.7	0.68	1584.3	10.1	1629.7	8.6	1688.8	14.2	1688.8	14.2
SanIsabel1	140	532536	2.4	9.6482	0.5	4.2191	1.1	0.2954	1.0	0.90	1668.3	14.5	1677.7	9.0	1689.6	8.7	1689.6	8.7
SanIsabel1	770	83445	28.8	9.6475	0.5	3.6977	1.0	0.2588	0.9	0.87	1483.9	11.9	1570.9	8.3	1689.7	9.5	1689.7	9.5
SanIsabel1	213	335343	3.1	9.6449	0.6	4.1106	1.3	0.2877	1.2	0.90	1629.9	16.9	1656.4	10.6	1690.2	10.3	1690.2	10.3
SanIsabel1	229	194040	4.0	9.6448	0.6	4.2351	1.4	0.2964	1.2	0.90	1673.3	17.9	1680.9	11.1	1690.2	11.0	1690.2	11.0
SanIsabel1	118	748262	1.5	9.6342	0.5	4.0755	1.1	0.2849	0.9	0.87	1616.0	13.1	1649.4	8.7	1692.3	9.8	1692.3	9.8
SanIsabel1	47	33610	2.5	9.6340	0.8	4.2910	1.2	0.3000	1.0	0.78	1691.1	14.1	1691.6	10.0	1692.3	14.0	1692.3	14.0
SanIsabel1	86	87426	4.7	9.6190	0.7	4.3519	1.3	0.3037	1.1	0.85	1709.8	16.0	1703.3	10.3	1695.2	12.1	1695.2	12.1
SanIsabel1	62	40905	1.6	9.6143	0.6	4.4037	1.5	0.3072	1.3	0.91	1726.9	20.4	1713.0	12.2	1696.1	11.2	1696.1	11.2
SanIsabel1	100	215477	4.3	9.6006	0.4	4.1977	1.1	0.2924	1.0	0.91	1653.6	14.6	1673.6	9.0	1698.7	8.3	1698.7	8.3
SanIsabel1	269	807681	3.4	9.5978	0.6	4.3587	1.3	0.3035	1.2	0.89	1708.8	17.9	1704.5	11.1	1699.3	11.3	1699.3	11.3
SanIsabel1	607	221860	10.2	9.5933	0.6	4.0485	1.1	0.2818	0.9	0.85	1600.4	12.9	1644.0	8.7	1700.1	10.3	1700.1	10.3
SanIsabel1	72	278303	1.8	9.5926	0.7	4.3184	1.2	0.3006	1.0	0.82	1694.1	15.1	1696.9	10.2	1700.3	12.9	1700.3	12.9
SanIsabel1	351	403193	3.3	9.5771	0.5	4.4400	1.1	0.3085	0.9	0.86	1733.5	13.8	1719.8	8.7	1703.2	9.9	1703.2	9.9
SanIsabel1	114	175555	1.1	9.5690	0.5	4.3073	1.2	0.2991	1.1	0.90	1686.6	16.1	1694.8	10.0	1704.8	9.9	1704.8	9.9
SanIsabel1	762	160641	3.0	9.5565	0.5	3.8677	1.4	0.2682	1.3	0.92	1531.6	17.4	1607.0	11.2	1707.2	10.0	1707.2	10.0
SanIsabel1	50	486018	2.5	9.5509	0.7	4.3921	1.2	0.3044	1.0	0.81	1713.0	14.5	1710.9	9.9	1708.3	13.0	1708.3	13.0
SanIsabel1	179	130562	2.5	9.5366	0.6	4.5291	1.3	0.3134	1.2	0.89	1757.4	18.1	1736.3	11.0	1711.0	11.1	1711.0	11.1

SanIsabel1	35	70479	2.4	9.5334	0.8	4.4937	1.2	0.3108	1.0	0.77	1744.8	14.6	1729.8	10.3	1711.7	14.5	1711.7	14.5
SanIsabel1	245	743242	6.2	9.5032	0.6	4.4416	1.3	0.3063	1.2	0.89	1722.3	17.7	1720.1	10.9	1717.5	11.2	1717.5	11.2
SanIsabel1	81	126678	8.5	9.4985	0.9	4.2943	1.4	0.2960	1.2	0.80	1671.3	17.1	1692.3	11.9	1718.4	15.9	1718.4	15.9
SanIsabel1	74	50016	2.0	9.4910	0.8	4.5290	1.3	0.3119	1.0	0.78	1750.0	14.9	1736.3	10.4	1719.8	14.5	1719.8	14.5
SanIsabel1	42	49069	4.8	9.4809	0.7	4.5023	1.0	0.3097	0.7	0.72	1739.3	11.0	1731.4	8.4	1721.8	12.9	1721.8	12.9
SanIsabel1	167	224024	2.1	9.4737	0.6	4.5210	1.3	0.3108	1.2	0.90	1744.5	18.2	1734.8	11.0	1723.2	10.4	1723.2	10.4
SanIsabel1	30	45350	2.2	9.4502	1.0	4.4910	1.5	0.3079	1.2	0.76	1730.6	17.5	1729.3	12.6	1727.8	18.0	1727.8	18.0
SanIsabel1	37	254340	2.4	9.4358	0.9	4.4124	1.3	0.3021	1.0	0.73	1701.7	14.5	1714.7	11.0	1730.6	16.7	1730.6	16.7
SanIsabel1	252	37642	2.8	9.4278	0.7	3.5078	1.6	0.2400	1.4	0.91	1386.5	17.7	1529.0	12.4	1732.1	12.0	1732.1	12.0
SanIsabel1	117	274884	6.6	9.4258	0.8	4.3971	1.3	0.3007	1.1	0.82	1694.9	16.2	1711.8	11.0	1732.5	13.9	1732.5	13.9
SanIsabel1	54	131544	4.7	9.3933	0.8	4.5933	1.3	0.3131	1.1	0.81	1755.8	16.4	1748.1	11.1	1738.8	14.4	1738.8	14.4
SanIsabel1	17	30099	1.4	9.2372	1.6	4.5728	2.0	0.3065	1.1	0.55	1723.4	16.5	1744.3	16.4	1769.5	29.9	1769.5	29.9
WT-24	423	22971	2.2	23.6179	1.4	0.0236	1.8	0.0040	1.1	0.60	26.0	0.3	23.7	0.4	NA	NA	26.0	0.3
WT-24	197	3814	1.1	20.6310	3.6	0.0279	3.9	0.0042	1.5	0.38	26.9	0.4	28.0	1.1	121.3	84.0	26.9	0.4
WT-24	314	2811	2.5	22.5836	3.2	0.0279	3.4	0.0046	1.3	0.38	29.4	0.4	28.0	0.9	NA	NA	29.4	0.4
WT-24	323	64370	0.9	22.0338	1.7	0.0319	2.1	0.0051	1.2	0.56	32.8	0.4	31.9	0.7	NA	NA	32.8	0.4
WT-24	1007	4663019	0.6	21.0417	1.5	0.0334	1.8	0.0051	1.0	0.56	32.8	0.3	33.4	0.6	74.7	35.9	32.8	0.3
WT-24	548	7526	1.2	22.6282	2.0	0.0316	2.2	0.0052	1.0	0.43	33.3	0.3	31.6	0.7	NA	NA	33.3	0.3
WT-24	472	24631	1.8	21.3160	1.7	0.0335	2.1	0.0052	1.2	0.59	33.3	0.4	33.5	0.7	43.8	40.3	33.3	0.4
WT-24	949	54791	2.8	22.4041	1.0	0.0320	1.4	0.0052	0.9	0.68	33.4	0.3	32.0	0.4	NA	NA	33.4	0.3
WT-24	725	12536	2.1	22.3746	1.2	0.0323	1.6	0.0052	1.1	0.69	33.7	0.4	32.2	0.5	NA	NA	33.7	0.4
WT-24	346	18441	0.8	20.8965	2.2	0.0347	2.5	0.0053	1.1	0.44	33.8	0.4	34.6	0.8	91.1	52.8	33.8	0.4
WT-24	1104	19163	1.3	21.9377	1.2	0.0331	1.7	0.0053	1.3	0.74	33.8	0.4	33.0	0.6	NA	NA	33.8	0.4
WT-24	175	8674	1.1	22.0619	2.4	0.0330	2.7	0.0053	1.1	0.42	33.9	0.4	32.9	0.9	NA	NA	33.9	0.4
WT-24	775	65872	1.5	21.4492	1.3	0.0340	1.7	0.0053	1.0	0.60	34.0	0.3	33.9	0.6	28.9	32.1	34.0	0.3
WT-24	683	5594	1.8	21.1818	1.4	0.0345	1.7	0.0053	0.9	0.53	34.1	0.3	34.4	0.6	58.9	34.5	34.1	0.3
WT-24	38	757	0.8	29.6856	17.1	0.0246	17.2	0.0053	1.9	0.11	34.1	0.6	24.7	4.2	NA	NA	34.1	0.6
WT-24	117	5927	1.7	22.8814	2.6	0.0319	2.9	0.0053	1.4	0.47	34.1	0.5	31.9	0.9	NA	NA	34.1	0.5
WT-24	310	135152	0.9	21.8830	2.0	0.0335	2.3	0.0053	1.1	0.49	34.2	0.4	33.5	0.8	NA	NA	34.2	0.4
WT-24	162	1326	1.1	26.9749	3.5	0.0273	3.7	0.0053	1.3	0.35	34.3	0.4	27.3	1.0	NA	NA	34.3	0.4

WT-24	101	2150	1.6	25.9773	3.4	0.0283	3.6	0.0053	1.3	0.34	34.3	0.4	28.3	1.0	NA	NA	34.3	0.4
WT-24	1124	12465	3.3	22.3528	1.0	0.0329	1.5	0.0053	1.0	0.70	34.4	0.3	32.9	0.5	NA	NA	34.4	0.3
WT-24	648	5124	1.0	23.3991	1.2	0.0317	1.6	0.0054	1.1	0.70	34.6	0.4	31.7	0.5	NA	NA	34.6	0.4
WT-24	531	6210	1.4	17.0332	5.4	0.0438	5.5	0.0054	1.1	0.20	34.8	0.4	43.6	2.3	555.4	117.3	34.8	0.4
WT-24	372	14507	1.0	21.1846	2.0	0.0353	2.3	0.0054	1.1	0.50	34.9	0.4	35.3	0.8	58.5	46.8	34.9	0.4
WT-24	61	2361	1.1	23.0135	4.3	0.0326	4.6	0.0054	1.5	0.34	35.0	0.5	32.6	1.5	NA	NA	35.0	0.5
WT-24	324	22064	0.6	16.3898	5.3	0.0459	5.4	0.0055	1.2	0.23	35.1	0.4	45.5	2.4	638.8	113.7	35.1	0.4
WT-24	384	36857	1.7	20.3273	2.0	0.0371	2.3	0.0055	1.1	0.48	35.2	0.4	37.0	0.8	156.1	46.9	35.2	0.4
WT-24	206	12101	1.1	21.3675	2.9	0.0355	3.0	0.0055	1.0	0.33	35.4	0.3	35.4	1.1	38.0	68.5	35.4	0.3
WT-24	324	6580	1.3	19.2878	2.5	0.0397	2.8	0.0056	1.2	0.43	35.7	0.4	39.6	1.1	277.7	57.7	35.7	0.4
WT-24	154	2014	0.8	22.2272	3.4	0.0345	3.5	0.0056	1.1	0.31	35.8	0.4	34.4	1.2	NA	NA	35.8	0.4
WT-24	769	99820	1.6	22.4330	1.3	0.0348	1.8	0.0057	1.2	0.68	36.4	0.4	34.7	0.6	NA	NA	36.4	0.4
WT-24	261	2514	2.2	23.7770	2.4	0.0331	2.8	0.0057	1.4	0.50	36.7	0.5	33.1	0.9	NA	NA	36.7	0.5
WT-24	113	7794	0.8	21.4948	2.7	0.0366	3.1	0.0057	1.4	0.45	36.7	0.5	36.5	1.1	23.8	65.9	36.7	0.5
WT-24	289	43042	2.3	21.0684	1.8	0.0376	2.3	0.0057	1.4	0.60	36.9	0.5	37.4	0.8	71.7	43.5	36.9	0.5
WT-24	112	6662	1.1	20.6068	4.0	0.0385	4.3	0.0058	1.6	0.38	37.0	0.6	38.4	1.6	124.0	94.0	37.0	0.6
WT-24	157	1750	1.1	20.4252	4.2	0.0390	4.4	0.0058	1.4	0.32	37.1	0.5	38.8	1.7	144.8	97.5	37.1	0.5
WT-24	100	21491	0.9	22.9957	2.7	0.0346	3.1	0.0058	1.4	0.46	37.2	0.5	34.6	1.1	NA	NA	37.2	0.5
WT-24	183	2483	1.3	25.4652	6.6	0.0314	6.7	0.0058	1.5	0.22	37.2	0.5	31.3	2.1	NA	NA	37.2	0.5
WT-24	224	2311	1.0	18.5874	6.3	0.0432	6.5	0.0058	1.2	0.18	37.4	0.4	42.9	2.7	361.7	143.3	37.4	0.4
WT-24	584	3845	1.4	23.3172	1.7	0.0344	2.0	0.0058	1.1	0.53	37.4	0.4	34.4	0.7	NA	NA	37.4	0.4
WT-24	196	4715	0.9	23.5299	4.3	0.0347	4.5	0.0059	1.3	0.30	38.0	0.5	34.6	1.5	NA	NA	38.0	0.5
WT-24	49	18405	0.7	8.1230	12.3	0.1006	12.5	0.0059	2.3	0.19	38.1	0.9	97.3	11.6	2000.9	218.5	38.1	0.9
WT-24	262	2071	2.2	12.3200	10.0	0.0677	10.1	0.0061	1.0	0.10	38.9	0.4	66.5	6.5	1224.7	197.9	38.9	0.4
WT-24	225	9195	0.9	18.1991	2.9	0.0498	3.1	0.0066	1.1	0.36	42.3	0.5	49.4	1.5	409.1	64.1	42.3	0.5
WT-24	42	3066	1.8	23.7291	4.1	0.0587	4.3	0.0101	1.5	0.35	64.8	1.0	57.9	2.4	NA	NA	64.8	1.0
WT-24	79	1963	1.6	23.0495	6.2	0.0606	6.3	0.0101	1.2	0.19	65.0	0.8	59.7	3.6	NA	NA	65.0	0.8
WT-24	33	792	0.8	39.0541	4.1	0.0368	4.4	0.0104	1.4	0.32	66.8	0.9	36.7	1.6	NA	NA	66.8	0.9
WT-24	927	53418	1.5	21.1205	1.0	0.0835	1.5	0.0128	1.1	0.74	81.9	0.9	81.4	1.2	65.7	24.5	81.9	0.9
WT-24	105	20468	3.5	17.5096	0.9	0.6588	1.3	0.0837	1.0	0.74	518.2	4.9	513.9	5.4	494.9	19.6	518.2	4.9
WT-24	308	71128	1.7	14.2649	0.5	1.5113	1.2	0.1564	1.1	0.92	936.9	9.6	935.0	7.3	930.5	9.8	930.5	9.8

WT-24	450	94324	1.9	11.2893	0.6	2.9984	1.1	0.2456	0.9	0.83	1415.8	11.5	1407.2	8.3	1394.2	11.8	1394.2	11.8
WT-24	187	129504	4.6	11.1803	0.6	2.4413	1.6	0.1980	1.5	0.92	1164.8	15.8	1254.9	11.7	1412.8	12.2	1412.8	12.2
WT-24	316	139171	0.6	11.1732	0.6	3.0426	1.1	0.2467	1.0	0.86	1421.3	12.3	1418.4	8.6	1414.0	10.9	1414.0	10.9
WT-24	297	1520936	0.7	11.1708	0.6	3.1131	1.3	0.2523	1.2	0.90	1450.5	15.1	1435.9	10.0	1414.4	11.0	1414.4	11.0
WT-24	282	1643837	1.4	11.1209	0.7	2.5316	1.4	0.2043	1.2	0.86	1198.3	13.2	1281.2	10.2	1423.0	13.7	1423.0	13.7
WT-24	174	160840	1.7	11.1152	0.6	3.1907	1.3	0.2573	1.1	0.87	1476.2	14.6	1454.9	9.8	1424.0	11.7	1424.0	11.7
WT-24	222	116542	6.3	11.1048	0.7	3.0607	1.6	0.2466	1.4	0.91	1421.0	18.1	1422.9	12.0	1425.8	12.7	1425.8	12.7
WT-24	97	62711	1.3	11.1047	0.7	3.1946	1.4	0.2574	1.2	0.86	1476.5	16.3	1455.9	11.1	1425.8	14.1	1425.8	14.1
WT-24	363	90435	1.7	11.1046	0.6	2.9761	1.4	0.2398	1.2	0.89	1385.6	15.6	1401.5	10.7	1425.8	12.2	1425.8	12.2
WT-24	296	193520	1.8	11.0978	0.7	3.1317	1.5	0.2522	1.3	0.89	1449.7	17.0	1440.5	11.3	1427.0	12.9	1427.0	12.9
WT-24	287	3865247	1.7	11.0768	0.7	2.9632	1.3	0.2382	1.0	0.83	1377.1	13.0	1398.2	9.6	1430.6	13.5	1430.6	13.5
WT-24	207	2497143	40.2	11.0747	0.5	3.0986	1.3	0.2490	1.2	0.91	1433.3	14.9	1432.4	9.8	1430.9	10.4	1430.9	10.4
WT-24	158	49258	1.0	11.0690	0.6	3.0444	1.4	0.2445	1.3	0.89	1410.1	16.2	1418.8	10.9	1431.9	12.3	1431.9	12.3
WT-24	69	35745	2.3	11.0623	0.8	3.0911	1.4	0.2481	1.2	0.84	1428.7	15.0	1430.5	10.7	1433.1	14.5	1433.1	14.5
WT-24	102	32170	1.1	11.0603	0.6	3.0563	1.1	0.2453	0.9	0.83	1414.1	11.7	1421.8	8.5	1433.4	11.7	1433.4	11.7
WT-24	265	175617	2.1	11.0512	0.8	3.1100	1.4	0.2494	1.1	0.81	1435.3	14.5	1435.2	10.7	1435.0	15.5	1435.0	15.5
WT-24	148	408357	2.2	11.0510	0.7	3.0886	1.2	0.2477	1.0	0.84	1426.4	12.8	1429.9	9.2	1435.0	12.5	1435.0	12.5
WT-24	250	68424	8.2	11.0500	0.6	3.1422	1.3	0.2519	1.1	0.87	1448.4	14.6	1443.1	9.9	1435.2	12.0	1435.2	12.0
WT-24	140	70531	1.7	11.0445	0.6	3.0455	1.2	0.2441	1.0	0.85	1407.7	12.5	1419.1	8.9	1436.2	11.7	1436.2	11.7
WT-24	287	528481	4.7	11.0319	0.6	3.0238	1.3	0.2420	1.1	0.86	1397.3	13.8	1413.6	9.7	1438.3	12.3	1438.3	12.3
WT-24	201	2573673	1.5	11.0311	0.6	3.0307	1.0	0.2426	0.8	0.80	1400.1	9.6	1415.4	7.3	1438.5	11.1	1438.5	11.1
WT-24	153	119315	1.1	11.0288	0.6	3.0606	1.1	0.2449	1.0	0.84	1412.2	12.1	1422.9	8.7	1438.9	11.8	1438.9	11.8
WT-24	118	3593499	1.2	11.0256	0.6	3.0318	1.0	0.2425	0.8	0.82	1399.9	10.2	1415.7	7.5	1439.4	10.6	1439.4	10.6
WT-24	177	92726	1.2	11.0241	0.6	3.1438	1.4	0.2515	1.2	0.88	1446.0	15.4	1443.5	10.4	1439.7	12.3	1439.7	12.3
WT-24	285	1730622	4.3	11.0097	0.8	3.0699	1.4	0.2452	1.2	0.83	1413.9	15.1	1425.2	11.0	1442.2	15.1	1442.2	15.1
WT-24	180	517323	2.0	11.0089	0.7	3.1866	1.4	0.2545	1.3	0.88	1461.9	16.4	1453.9	10.9	1442.3	12.6	1442.3	12.6
WT-24	186	78451	3.7	11.0040	0.8	3.1374	1.3	0.2505	1.1	0.80	1441.0	13.8	1441.9	10.3	1443.2	15.1	1443.2	15.1
WT-24	111	96967	1.8	11.0010	0.5	3.0568	1.0	0.2440	0.8	0.86	1407.5	10.4	1421.9	7.3	1443.7	9.3	1443.7	9.3
WT-24	349	145823	1.9	10.9939	0.6	3.0932	1.3	0.2467	1.1	0.87	1421.7	14.2	1431.0	9.8	1444.9	11.8	1444.9	11.8
WT-24	128	185765	1.6	10.9894	0.7	3.1503	1.1	0.2512	0.9	0.75	1444.6	11.1	1445.1	8.8	1445.7	14.2	1445.7	14.2
WT-24	239	71581	8.4	10.9889	0.6	3.1171	1.1	0.2485	0.9	0.84	1430.9	11.9	1436.9	8.5	1445.8	11.5	1445.8	11.5

WT-24	314	137737	2.0	10.9865	1.1	3.0389	1.5	0.2422	1.0	0.65	1398.4	12.0	1417.4	11.1	1446.2	21.0	1446.2	21.0
WT-24	90	151095	1.9	10.9851	0.7	3.1266	1.5	0.2492	1.4	0.88	1434.4	17.4	1439.3	11.8	1446.4	13.9	1446.4	13.9
WT-24	147	92108	1.3	10.9758	0.8	3.2841	2.0	0.2615	1.9	0.93	1497.7	25.2	1477.3	15.8	1448.1	14.7	1448.1	14.7
WT-24	139	79631	2.1	10.9517	0.7	3.1293	1.4	0.2487	1.2	0.88	1431.6	15.4	1439.9	10.5	1452.2	12.5	1452.2	12.5
WT-24	106	94951	1.7	10.9473	0.7	3.1330	1.3	0.2489	1.1	0.83	1432.6	13.7	1440.8	9.9	1453.0	13.7	1453.0	13.7
WT-24	136	63405	1.6	10.9176	0.7	3.1465	1.1	0.2493	0.9	0.78	1434.6	11.1	1444.1	8.5	1458.2	13.0	1458.2	13.0
WT-24	52	104400	2.0	10.9172	0.6	3.2693	1.1	0.2590	1.0	0.84	1484.6	12.8	1473.8	8.9	1458.2	11.7	1458.2	11.7
WT-24	90	22566	2.5	10.9065	0.8	3.0793	1.2	0.2437	0.9	0.76	1405.8	11.7	1427.6	9.4	1460.1	15.1	1460.1	15.1
WT-24	91	82721	1.4	10.8479	0.7	3.1371	1.3	0.2469	1.1	0.85	1422.6	14.3	1441.8	10.1	1470.3	13.0	1470.3	13.0
WT-24	62	64336	2.2	10.6867	0.8	3.4017	1.3	0.2638	1.0	0.79	1509.1	13.6	1504.8	10.1	1498.7	15.1	1498.7	15.1
WT-24	112	33680	1.2	10.6784	0.9	3.0308	1.4	0.2348	1.1	0.78	1359.8	12.9	1415.4	10.3	1500.2	16.1	1500.2	16.1
WT-24	229	28207	1.2	10.5783	1.5	3.2611	2.1	0.2503	1.5	0.69	1440.1	18.8	1471.8	16.3	1518.0	28.6	1518.0	28.6
WT-24	278	74875	4.1	10.0088	0.7	3.7089	1.7	0.2693	1.6	0.91	1537.5	21.3	1573.3	13.6	1621.6	12.8	1621.6	12.8
WT-24	341	12439754	8.2	9.9302	0.5	4.2239	1.0	0.3043	0.9	0.86	1712.8	13.4	1678.7	8.5	1636.3	9.7	1636.3	9.7
WT-24	309	130861	2.6	9.8338	0.6	4.1381	1.4	0.2953	1.3	0.91	1667.8	18.6	1661.9	11.4	1654.4	10.9	1654.4	10.9
WT-24	312	155974	2.2	9.8064	0.5	4.1003	1.3	0.2918	1.2	0.91	1650.3	17.3	1654.4	10.7	1659.5	10.0	1659.5	10.0
WT-24	347	181282	2.6	9.7635	0.6	4.2902	1.1	0.3039	0.9	0.82	1710.8	13.1	1691.5	8.7	1667.7	11.2	1667.7	11.2
WT-24	447	137144	15.4	9.7503	0.5	4.2166	1.1	0.2983	1.0	0.90	1682.9	15.3	1677.3	9.4	1670.2	9.4	1670.2	9.4
WT-24	315	327600	5.0	9.7483	0.7	4.3532	1.4	0.3079	1.2	0.86	1730.4	18.7	1703.5	11.8	1670.5	13.3	1670.5	13.3
WT-24	1027	3009668	52.8	9.7347	0.6	3.4871	1.4	0.2463	1.3	0.91	1419.4	16.5	1524.3	11.2	1673.1	10.9	1673.1	10.9
WT-24	225	323624	2.9	9.7324	0.6	4.3465	1.2	0.3069	1.0	0.88	1725.6	15.9	1702.2	9.9	1673.5	10.7	1673.5	10.7
WT-24	220	202544	2.6	9.6990	0.5	4.3616	1.3	0.3069	1.2	0.91	1725.7	17.5	1705.1	10.5	1679.9	9.7	1679.9	9.7
WT-24	271	128231	6.1	9.6945	0.6	4.3475	1.4	0.3058	1.3	0.90	1720.1	19.0	1702.4	11.5	1680.8	11.0	1680.8	11.0
WT-24	331	59843	2.5	9.6920	0.8	4.4547	1.6	0.3133	1.3	0.85	1756.8	20.4	1722.6	12.9	1681.2	15.1	1681.2	15.1
WT-24	239	315630	7.6	9.6794	0.8	4.1988	1.6	0.2949	1.4	0.86	1665.9	20.3	1673.8	13.1	1683.6	15.0	1683.6	15.0
WT-24	211	60693	3.1	9.6732	0.6	4.1932	1.2	0.2943	1.1	0.89	1663.0	16.1	1672.7	10.2	1684.8	10.6	1684.8	10.6
WT-24	182	1444363	3.4	9.6713	0.5	4.3988	1.2	0.3087	1.1	0.91	1734.2	16.8	1712.1	10.1	1685.2	9.5	1685.2	9.5
WT-24	173	309658	4.6	9.6520	0.6	4.3496	1.3	0.3046	1.2	0.91	1714.2	17.7	1702.8	10.7	1688.9	10.2	1688.9	10.2
WT-24	375	134191	4.8	9.6467	0.7	4.0890	1.5	0.2862	1.4	0.88	1622.6	19.7	1652.1	12.6	1689.9	13.3	1689.9	13.3
WT-24	120	68679	4.3	9.6356	0.6	4.2874	1.0	0.2997	0.8	0.82	1690.1	12.3	1690.9	8.3	1692.0	10.5	1692.0	10.5
WT-24	93	61503	2.0	9.6162	0.6	4.4250	1.1	0.3087	0.9	0.79	1734.5	12.9	1717.0	8.9	1695.7	12.0	1695.7	12.0

WT-24	135	297213	1.9	9.6161	0.6	4.3457	1.3	0.3032	1.2	0.89	1707.2	17.7	1702.1	10.9	1695.7	11.1	1695.7	11.1
WT-24	165	74899	2.0	9.6056	0.6	4.2754	1.1	0.2980	0.9	0.85	1681.3	13.3	1688.6	8.7	1697.8	10.2	1697.8	10.2
WT-24	127	168739	1.5	9.6053	0.5	4.3419	1.4	0.3026	1.2	0.92	1704.2	18.7	1701.4	11.2	1697.8	10.1	1697.8	10.1
WT-24	193	60273	3.2	9.6012	0.8	4.2434	1.7	0.2956	1.5	0.86	1669.5	21.5	1682.5	13.9	1698.6	15.6	1698.6	15.6
WT-24	149	245690	2.1	9.6005	0.7	4.2672	1.1	0.2972	0.9	0.81	1677.6	13.5	1687.1	9.3	1698.7	12.1	1698.7	12.1
WT-24	167	1481739	2.1	9.5890	0.6	4.3074	1.4	0.2997	1.2	0.89	1689.8	17.9	1694.8	11.2	1700.9	11.6	1700.9	11.6
WT-24	47	308903	1.4	9.5781	0.8	4.2981	1.4	0.2987	1.1	0.81	1684.9	16.5	1693.0	11.3	1703.0	15.0	1703.0	15.0
WT-24	61	175229	1.4	9.5770	0.6	4.2539	1.0	0.2956	0.8	0.82	1669.5	11.6	1684.5	7.9	1703.2	10.2	1703.2	10.2
WT-24	83	75008	4.0	9.5730	0.7	4.4863	1.2	0.3116	0.9	0.78	1748.7	14.1	1728.4	9.8	1704.0	13.5	1704.0	13.5
WT-24	193	365505	2.6	9.5615	0.6	4.3434	1.3	0.3013	1.2	0.91	1697.9	17.9	1701.6	10.9	1706.2	10.2	1706.2	10.2
WT-24	167	284931	2.8	9.5478	0.5	4.2986	1.2	0.2978	1.0	0.89	1680.4	15.4	1693.1	9.6	1708.9	9.7	1708.9	9.7
WT-24	44	150222	7.7	9.5332	0.8	4.3470	1.3	0.3007	1.1	0.82	1694.7	16.0	1702.3	10.9	1711.7	13.9	1711.7	13.9
WT-24	97	635839	3.1	9.5247	0.6	4.3605	1.0	0.3014	0.8	0.78	1698.0	11.8	1704.9	8.3	1713.3	11.5	1713.3	11.5
WT-24	136	297616	4.6	9.5075	0.6	4.3888	1.3	0.3028	1.1	0.88	1705.0	16.4	1710.2	10.4	1716.7	11.1	1716.7	11.1
WT-24	101	147324	2.5	9.4870	0.6	4.2759	1.3	0.2943	1.2	0.90	1663.2	17.7	1688.7	11.0	1720.6	10.8	1720.6	10.8
WT-24	80	61397	1.9	9.4335	0.7	4.3676	1.2	0.2990	1.0	0.80	1686.1	14.6	1706.2	10.2	1731.0	13.5	1731.0	13.5
WT-24	81	12948	2.8	9.3755	0.5	4.4350	1.0	0.3017	0.9	0.85	1699.7	12.7	1718.9	8.3	1742.3	9.7	1742.3	9.7
WT-24	274	536120	8.8	9.3600	0.5	4.6941	1.2	0.3188	1.1	0.90	1783.8	17.5	1766.2	10.4	1745.3	9.9	1745.3	9.9
WT-24	61	6840086	8.2	9.3565	0.6	4.4871	1.2	0.3046	1.0	0.85	1714.2	15.7	1728.6	10.2	1746.0	11.8	1746.0	11.8
WT-24	175	544121	5.4	9.3552	0.5	4.5057	0.9	0.3058	0.8	0.82	1720.2	11.5	1732.0	7.7	1746.3	9.6	1746.3	9.6
WT-24	187	53094	6.0	9.3529	0.6	4.7328	1.3	0.3212	1.1	0.87	1795.5	17.3	1773.1	10.7	1746.7	11.6	1746.7	11.6
WT-24	691	247938	1.4	9.2407	0.5	4.4691	1.1	0.2997	1.0	0.89	1689.6	14.2	1725.3	8.9	1768.8	9.0	1768.8	9.0
WT-24	175	10165	3.0	9.0436	1.4	4.6247	1.7	0.3035	0.9	0.51	1708.5	13.0	1753.7	14.1	1808.1	26.3	1808.1	26.3
WT-24	168	12325	1.8	8.9972	0.8	4.6232	1.3	0.3018	1.0	0.79	1700.3	15.0	1753.5	10.7	1817.4	14.4	1817.4	14.4
WT-24	869	450494	9.8	6.8810	0.5	7.9620	1.1	0.3975	1.0	0.90	2157.6	18.6	2226.7	10.2	2290.9	8.4	2290.9	8.4
WT-24	237	135670	4.1	5.6256	0.5	12.0857	1.2	0.4933	1.1	0.89	2585.0	22.4	2611.1	11.1	2631.3	8.9	2631.3	8.9
WT-24	37	77213	0.9	5.3825	0.6	12.8907	1.0	0.5034	0.8	0.80	2628.6	16.9	2671.7	9.3	2704.5	9.8	2704.5	9.8

Chapter 4 Late Eocene low elevation and subsequent differential uplift of the southern Rocky Mountains

Abstract

The uplift history of the southern Rocky Mountains (Rockies) remains enigmatic because of consecutive Cenozoic deformations. Previous understanding of its surface uplift history can be classified into two schools, including that the southern Rockies has gained its modern or a higher-than-modern elevation during the Laramide Orogeny by crustal shortening and thickening, and that the southern Rockies only gained part of its modern elevation from the Laramide Orogeny and experienced Neogene uplift because of changes in lithosphere density, thermal buoyance, or both. Here we first compile modern river water stable isotope data to understand spatial patterns and their controlling factors, then apply the understanding to the late Eocene-Miocene surface water δD values reconstructed from δD values of hydrated volcanic glass samples from the high southern Rockies, its adjacent high Great Plains and near sea-level region in south Texas to constrain the surface uplift history of the southern Rockies and its adjacent high Great Plains. We find that the lowest modern river water δD has a latitudinal gradient of -3.0 ‰/degree, lower than the North America average, a lapse rate of -24.9 ‰/km along the transect of the southern Rockies and its adjacent Great Plains, and the rates are both mainly controlled by air temperature. Our reconstructed surface water δD values increase from the latest Eocene to the late Miocene in south Texas,

consistent with the records in the central Rockies and its adjacent Great Plains, reflecting gradual drying during the middle-late Cenozoic global cooling. The reconstructed latest Eocene surface water δD is comparable between the southern Rockies and its adjacent Great Plains, and the difference is large, comparable to modern difference, during the late Miocene, suggesting that the southern Rockies were low during the latest Eocene and experienced uplift during the Oligocene-middle Miocene. We then apply modern regional isotopic gradient and lapse rate to estimate the paleoelevations of the southern Rockies and its adjacent Great Plains and assess the influence of mid-late Cenozoic climate change on our reconstructions. Our quantitative paleoelevation reconstructions show that the southern Rockies were low the latest Eocene, and experienced differential uplift throughout the Oligocene and Miocene. The Arkansas River valley near the San Juan volcanic field gained nearly its modern elevation, and the South Park farther away from the field gain its partial elevation by the early Oligocene, suggesting that mid-Cenozoic crustal inflation associated with ignimbrite flare-up magmatism has caused localized uplift. The Wet Mountains gained most of its elevation by the late Miocene, likely associated with crustal thinning and thermal heating related to the opening of the Rio Grande Rift. Paleoelevation estimates of the Great Plains and the central Rockies further show along-strike variation of surface uplift process and mechanisms.

4.1 Introduction

The Rocky Mountains (Rockies) in the western USA. is the longest intracontinental belt on Earth. Its southern segment, the southern Rockies in Colorado and New Mexico, contains a system of intervening mountains and sedimentary basins (Fig. 4-1). The region is bounded by the Colorado Plateau to the west, Rio Grande Rift to the south, the Great Plains to the east, and extends to the central Rockies in northern Colorado and Wyoming. Well preserved marine sedimentary rocks of the Western Interior Seaway suggest that the region was at sea level during the Late Cretaceous (Dick and Nish, 1966). Currently, the mean elevation of the southern Rockies is ~2500 m above its adjacent Great Plains in western Kansas, Oklahoma and Texas and its local relief is greater than 1600 m (Fig. 4-1). Despite the fact that the uplift history of the southern Rockies has been studied for decades (e.g., Epis et al., 1980; Kelley and Duncan, 1984; Wolfe et al., 1998; Kelley and Chapin, 2004; McMillan et al., 2006; Eaton, 2009; Copeland et al., 2011; Cather et al., 2012; Karlstrom et al., 2012; Chapin et al., 2014; Copeland et al., 2017), the timing and tectonic processes that produced the modern topography remain ambiguous.

The poor constraint of the surface uplift history of the southern Rockies is partly caused by that multi-stage deformation has obscured the geologic record. It is generally accepted that the low-angle subduction of the Farallon plate caused the Laramide basement cored uplift and intermountain basins in both the central and southern Rockies during the latest Createaceous-Paleogene (e.g., Dickinson et al., 1988; Cather et al., 2012; Fan and Carrapa, 2014). However, the deformation may have continued into the late Oligocene in the southern Rockies, much later than in the central Rockies (Tomlinson et al., 2013; Copeland et al., 2017). While crustal shortening and thickening of the Laramide Orogeny remain as a major mechanism of surface uplift in the southern Rockies (e.g., Bird, 1998; Copeland et al., 2017), changes in llithosphere density, thermal buoyancy, mantle convection, or a comination of these mechanisms may have caused long wavelength uplift and contributed unknown amount of surface uplift during the Oligocene-Neogene (e.g., Eaton, 2009; van Wijk et al., 2010; Coblentz et al., 2011; Karlstrom et al., 2012; Hansen et al., 2013; Lazear et al., 2013; Rosenberg et al., 2014).

Current understanding of the surface uplift processes of the southern Rockies can be broadly classified into two hypotheses. One hypothesis suggests that the southern Rockies has gained most of, if not more than, its modern elevation by the late Eocene, mostly based on floral physiognomic studies (e.g., Chase and Gregory, 1992; Gregory and Chase, 1994; Gregory and McIntosh, 1996; Wolfe et al., 1998). This interpretation is also supported by results of inverse modeling of river profile and baslt vesicular paleoaltimetry, both showing that the southern Rockies and the Colorado Plateau gained 1.5 to 2 km elevation before the early Neogene and the late Neogene uplift is only up to a few hundred meters (Sahagian and Proussevitch, 2007; Roberts et al., 2012; Donahue, 2016).

The other hypothesis suggests that the southern Rockies has gained its partial modern elevation by the early Oligocene, and raised to its modern elevation, likely along with the adjacent western part of the Great Plains or the Colorado Plateau during the Neogene based on the timings of river erosion and valley incision as well as thermochoronology and pollen data (e.g., Cather et al., 2012; Landman and Flowers, 2013; Zaborac-Reed and Leopold, 2016; Leopold and Zaborac-Reed, 2019). For example, Cather et al. (2012) suggested that the near-modern surface elevations in the Front Range and adjacent Great Plains were attained throughout the Cenozoic, including the Laramide Orogeny and three subsequent episodes of surface uplift and erosion related to isostatic adjustment and mantle convection, and Rosenberg et al. (2014) suggested that the 500-1500 m of post-late Miocene river incision in northwestern Colorado may reflect long-wavelength westward tilting related to surface uplift. In addition to these tectonic mechanisms, climate-induced erosion and isostatic compensation may equally explain the late Neogene uplift (e.g., Small and Anderson, 1998; Cather et al., 2012). Our understanding to the geodynamic drivers and surface uplift process is in quest of refined paleoelevation records to make improvements.

Previous direct paleoelevation reconstruction of the southern Rockies used floral physiognomic data (Chase and Gregory, 1992; Gregory and Chase, 1994; Katheryn M. Gregory and McIntosh, 1996; Wolfe et al., 1998; Meyer, 2007) and such reconstruction is influenced significantly by atmospheric enthalpy and several other factors (Peppe et al., 2010). In the adjacent central Rockies and Colorado Plateau, recent paleoelevation reconstructions using stable isotope compositions of carbonate minerals and hydrated volcanic glass as well as carbonate clumped isotope compositions have yielded new understanding (Huntington et al., 2010; Fan et al., 2014a; Hough et al., 2014; Licht et al., 2017; Gao and Fan, 2018). However, such studies have not been conducted in the southern Rockies. Stable isotope paleoaltimetry reconstructs paleoelevation using reconstructed ancient surface water stable isotope values ($\delta^{18}O$ and δD) and the relationship between elevation and surface water $\delta^{18}O$ or δD values. In continental interiors, like the southern Rockies, it has been suggested that mixing of different atmospheric moistures and convective precipitation exert major influence on modern elevation-$\delta^{18}O$ (δD) relationship (Licht et al., 2017; Zhu et al., 2018) and the reconstructed surface water $\delta^{18}O$ is complicated by seasonal bias of carbonate precipitation and carbonate precipitation temperature (e.g., Mintz et al., 2011; Hough et al., 2014). Therefore, it is critical to examine the regional elevation-$\delta^{18}O$ (δD) relationship and its controlling factors and assess the large-scale climate pattern before using reconstructed surface water isotope values for paleoelevation reconstruction.

Here in this study, we compile and analyze the controlling factors of modern river water isotopic compositions from the near sea-level region in south Texas to the southern Rockies, then carefully evaluate the paleoclimatic conditions and apply the understanding from modern system to constrain the paleoelevation of the southern Rockies and its adjacent Great Plains for the period of late Eocene-late Miocene. Our paleoelevation estimates make use of ancient water δD values reconstruction from hydrated volcanic glass δD values, which is independent of temperature. We suggest that the southern Rockies was low (less than 1km) during the late Eocene and experienced differential uplift through early Oligocene to middle Miocene. These findings provide new insights into the uplift processes and mechanisms of the southern Rockies.

4.2 Backgrounds

4.2.1 Climate Background

At present, the southern Rockies receive more than 30% of annual precipitation during the summer, primarily brought by the North American Summer Monsoon and orographic moist convection (Higgins et al., 1997). The monsoon likely started to retreat during the Paleocene (Slattery et al., 2015). In general, the global climate experienced gradual cooling during the middle-late Eocene and drastic cooling across the Eocene-Oligocene boundary (Zachos et al., 2001). A considerable amount of studies have suggested decrease in mean annual precipitation (MAP) and mean annual temperature (MAT) in the western USA during the late Eocene-Oligocene (e.g., Zanazzi et al., 2007; Sheldon and Tabor, 2009) . Large-scale atmospheric circulation is expected to reorganize in response to this global cooling trend. For example, the position of the subtropical jet stream (e.g., Yin, 2005)and strength of the Hadley (e.g., Brierley et al., 2009; Feng and Poulsen, 2016) are known to be sensitive to zonal mean meridional temperature gradient.

4.2.2 Geological Background

During the latest Cretaceous-early Paleocene, the Western Interior Seaway regressed in association with the Laramide Orogeny caused by flat subduction of the Farallon oceanic plate beneath western North America (e.g., DeCelles, 2004; Heller and Liu, 2016). By the late Paleocene, uplift of the Black Hills in South Dakoda in the central Rockies at longitude 103°W marked the most northeastward inland interaction between the Farallon slab and the North American plate (Fan and Carrapa, 2014; Heller and Liu, 2016). The Farallon slab steepened westward subsequently and caused additional uplift in the central Rockies (Fan and Carrapa, 2014). The Laramide Orogeny caused significant amount of exhumation (Kelley and Duncan, 1984; Kelley and Chapin, 2004; Flowers et al., 2008; Ricketts et al., 2016), and formed intervening basins and mountains in the southern Rockies (e.g., Dickinson et al., 1988; Bush et al., 2016; Rasmussen and Foreman, 2017; Zhu and Fan, 2018). It has been suggested that the region experienced subsequent long-wavelength uplift (epeirogeny) during the early Oligocene and middle and late Neogene caused by lithosphere density anomalies, extra buoyancy of the mantle, dynamic mantle convection, or a combination of them (e.g., Liu and Gurnis, 2010; Coblentz et al., 2011; Roberts et al., 2012; Hansen et al., 2013; van Wijk et al., 2018). These mantle processes were related to ignimbrite flare-ups associated with foundering of the Farallon plate and opening of the Rio Grande Rift (Eaton, 2008; Ricketts et al., 2016; Copeland et al., 2017; van Wijk et al., 2018).

The uppermost Eocene-Miocene strata in the western USA all contain abundant volcanic ashes because of frequent syndepositional volcanic eruptions related to the ignimbrite flare-ups (Smith et al., 2017; Godfrey et al., 2018; Zhu and Fan, 2018). The studied geologic units in the southern Rockies are located in the Wet Mountain valley, Arkansas River valley near Salida, and South Park in south-central Colorado (Fig. 4-2). The samples were collected from the uppermost Eocene-Miocene strata with absolute ages ranging from 35.8 Ma to 9 Ma based on maximum depositional ages constrained from detrital zircon U-Pb ages of sandstones and radiometric age constraints of volcanic ashes (Table 4-1) (Scott and Taylor, 1975; Zhu and Fan, 2018). Specifically, the samples were collected from the Oligocene Devils Hole Formation deposited in distal alluvial depositional environment in the Wet Mountain valley (Scott and Taylor, 1975; Zhu and Fan, 2018), the latest Eocene-Miocene Dry Union Formation deposited in alluvial depositional environment in the Arkansas River valley (Van Alstine and Lewis, 1960; Hubbard et al., 2001; Zhu and Fan, 2018), and the.Oligocene Balfour Formation in South Park basin (Zhu and Fan, 2018). Although the Balfour Formation has been interpreted to be deposited in lacustrine depositional environment (Stark et al., 1949), our samples could be collected from its adjacent fluvial or deltaic environments because of the lack of distinctive sedimentary structures and architecture indicative of lacustrine environment.

In the Great Plains from south Texas to western Kansas, the mean elevation increases from 40 m to 900 m. In western Kanas, the uppermost Eocene strata overlie the upper Cretaceous with a disconformable contact and are only preserved among evaporite and salt dissolution structures (Smith et al., 2017). Detrital zircon maximum depositional ages place the depositional ages of the strata to 35.4 Ma (Smith et al., 2017). Rocks of this age are only found in cores and our samples were from the core HP1A in Smith et al. (2017). The strata is overlain unconformably by the Ogallala Formation of 11.7-6.3 Ma (Hallman, 2016). The Ogallala Formation is the most widely distributed Cenozoic strata in the Great Plains, and it contains fluvial, eolian strata and lenses of volcanic ash and lacustrine limestones (Ludvigson et al., 2009). Our samples of the upper most Eocene and Miocene are both from fluvial deposits (Hallman, 2016; Smith et al., 2017).

Cenozoic sedimentary rocks in south Texas contains a nearly complete sequence with depositional environment change from marine and coastal marine to fluvial environment occurred during the latest Eocene (Galloway et al., 1977; Guillemette and Yancey, 1996). Our samples were collected from the upper Eocene and lower Oligocene Manning and Catahoula formations, which contain multiple volcanic ash beds and have been dated using zircon U-Pb, sanidine $^{40}Ar/^{39}Ar$ dating methods (Heintz et al., 2015; Yancey et al., 2018) and detrital zircon U-Pb maximum depositional ages (Godfray et al., 2018). Our Miocene samples are from the Goliad Formation, which was interpreted to be deposited in fluvial depositional environment (Solis, 1981).

4.3 Methods

4.3.1 River isotope data compilation and vapor source analysis

Modern river water isotopic compositions were compiled from Copeland and Kendall (2000) to examine the controlling factors of isotopic compositions of modern surface water. The data include 152 measurements collected during 1984-1987 from 13 stations in Colorado, Kansas, Oklahoma, and Texas, with latitude ranging between 25.9°N and 39.4°N. The drainage mean elevations of the 55 samples from Colorado range from 1020 m to 3100 m, covering both the southern Rockies and its adjacent Great Plains. Elevation of samples from the low portion of the Great Plains in east-central Kansas and Oklahoma and south Texas ranges from 13 m to 488 m (Fig. 4-1). Tor this group of smples, their mean drainage elevations are similar to the elevations of sampling sites. Monthly mean temperatures and accumulative precipitation amounts of the sample collecting months were also compiled from nearby weather stations for this study.

To find vapor sources of precipitation and their proportions at the sampling sites, the Hybrid Single Particle Lagrangian Integrated Trajectory (HYSPLIT) back trajectory simulation (Draxler and Rolph, 2014) was performed every six hours for 30 days prior to the sampling dates. Each simulation back tracked the air parcel for 240 hours, which is the residence time of meteoric water in the atmosphere. This analysis only considered rain-producing trajectories. The vapor sources of rain-producing trajectories were determined by their positions of the last entrance to the contiguous United States, which include marine areas of the Gulf of Mexico and the eastern Pacific Ocean and the continental area at about latitude 50°N. The vapor source from the continental area was considered continental recycling if the trajectory remained on the continent for the 240 hours' simulation time. The numbers of trajectories from each source at each sampling site were used to estimate the mixing fraction of each vapor source. Although the number of trajectories only represents the number of raining events rather than raining amount, variations of vapor sources through the year and the seasonal dominant vapor sources can still be correctly reflected in the analysis.

4.3.2 Volcanic glass

Hydrated volcanic glass samples were separated from ash and ash-containing sandstone samples. We analyzed 37 samples, including 14 from the high southern Rockies, six from the moderately high Great Plains in western Kansas, and 17 from the near sea-level region in south Texas (Fig. 4-1). The sandstones were deposited in alluvial and fluvial depositional environments when volcanic activity was widespread in southwestern and southern USA., thus contain abundant air fall zircon and volcanic glass grains (Smith et al., 2017; Godfrey et al., 2018; Zhu and Fan, 2018). The ages of the samples range from

35.8 Ma to 6 Ma (Table 4-1). At several sites where direct age constraints are not possible, lithostratigraphic correlation is used to constrain the depositional period of the samples. Hydrated volcanic glass grains were separated from samples following procedures described by Cassel and Breecker (2017). Briefly, our samples were gently crushed with ceramic pestle and mortar, and wet sieved using tap water. The 63-125 μm grain size fractions were collected and treated with 30% hydrochloride acid for at least two minutes to ensure the complete removal of carbonate, rinsed at least five times to neutralize the pH, and wet sieved again using tap water. The resulting 63-125 μm fractions were dried in an oven at 70° C. The dried material then was separated using LST heavy liquid with density ranging between 2.30-2.35 g/cm^3, and the light fractions with hydrated volcanic glass were collected, dried and treaded with 5% hydrofluoride acid for 30-45 seconds to remove hydrous alterations on the surface of glass shards. These hydrated volcanic glass samples were inspected under microscope and samples with >98% purity were selected for analysis. The glass samples were analyzed at the Environmental Isotope Laboratory at the University of Arizona using a coupled system of Finnegan Delta V mass spectrometer and thermos Fisher TC/EA high temperature conversion elemental analyzer. Each sample was analyzed for two to three times. One in-house standard (Benzoic Acid) and two international standards (NBS-30 biotite and IAEA-CH7 Polyethylene) were analyzed with the samples to calibrate the data for any drift and offset. The results were reported in delta notation relative to VSMOW in one standard deviation (1σ).

4.4 Results and interpretations

4.4.1 Modern river water

Vapor sources

Our HYSPLIT air trajectory analysis shows that the rain vapor in the study area was mainly from four sources, including the Westerlies from the eastern Pacific, northerly moisture recycled from the northern continental region, southerly moisture directly from the Gulf of Mexico or recycled from the southwestern and southern USA that was originally from the gulfs of California and Mexico (Fig. 4-2), and recycled continental moisture. Both the southerly and northerly moistures contain recycled continental moisture from the continent of North America as well as marine moistures (Hu and Dominguez, 2015). The differences in isotopic compositions among the oceanic and the recycled continental moistures are unclear due to the long distance and long time elapsed during vapor transport.

Our analysis further shows that in both the southern Rockies and its adjacent high Great Plains, the Westerlies contributed most, 40-60%, of the annual raining events, and among the other three sources, recycled continental moisture contributed most of the the remaining raining events. The degree of mixing different moistures to surface water remained relatively stable throughout the year and across the entire region. In the low portion of the Great Plains in Nebraska, Kansas, Oklahoma and Texas, the major vapor source was significantly different. In this region, the Westerlies only accounted for 10-20% of the rain and its contribution remained stable from south the north, and the southerly moisture from the Gulf of Mexico contributed more than 90% of the raining events during spring and summer. Spring and summer precipitation in the region accounts for ~70% of the annual precipitation (Arguez et al., 2010). In winter, contribution from the southerly moisture decreased northward significantly from 75% at 25° N to 20-15% north of 32° N (Fig. 4-3), while the contribution from the continental recycled moisture increased northward from 5% to 60% of the raining events.

The predominant moisture source from the Gulf of Mexico to the low Great Plains and south Texas was caused by the existence of an extratropical low-pressure cyclone in the southern Rockies (Fig. 4-2). The cyclone was formed by the cyclonic vorticity tendency as air descends from the high southern Rockies (Wallace and Hobbs, 2006). The anticlockwise motion of the cyclone directed the moisture from the Gulf of Mexico to its east side and prevents the moisture from reaching the southern Rockies (Fig. 4-2). Because of the difference in moisture sources in the southern Rockies and the Great Plains, and because of the high content of recycled moisture in the study area, Rayleigh distillation model cannot be applied directly to the study region and explain the change of river water isotopic composition from south Texas to the southern Rockies.

Patterns of river water isotopes

Our analysis shows that the river water isotopic compositions varied very little, less than 4.1‰ for $\delta^{18}O$ and 20‰ ($\pm\sigma$) for δD, throughout the years, and the isotope values generally decrease northward from south Texas to the Great Plains and westward to the southern Rockies, following the general increased of mean elevation along the transects (Fig. 4-4). In the continental region of USA, meteoric water makes major contribution to river water and the stable isotopic composition of river water generally follows that of meteoric water (Copeland and Kendall, 2000; Dutton et al., 2005; Zhu et al., 2018). The small seasonal variation is consistent with previous observations, and the small variation was suggested to be caused by the balance of precipitation and evaporation in the watershed, the integration of multiple precipitation episodes and precipitation in the broad watershed, and the input of groundwater in river water (Copeland and Kendall, 2000; Dutton et al., 2005; Vachon et al., 2010a). The changes of isotope values with elevation suggest that the isotopic difference between the southern Rockies and its adjacent Great Plains is induced by temperature difference caused by elevation difference.

Along the transect of the southern Rockies and its adjacent Great Plains, the seasonal lapse rate of river water isotope values is -23.8, -21.8 and -24.8‰/km for δD (-3.6, -3.4, and -3.7 ‰/km for $\delta^{18}O$), in summer, winter and spring, respectively, and the mean annual lapse rate is -23.3‰/km for δD (-3.5 ‰/km for $\delta^{18}O$). The small seasonal differences are consistent with the observation that the mixing proportion of the four moisture sources remained the same in both areas throughout the years and the interpretation that the regional lapse rate is mainly a result of changing condensation temperature due to elevation difference. The mean elevation contrast is ~2.2 km and the mean annual temperature contrast is ~10°C between the two areas. The isotope-temperature ratio ($\Delta\delta D/\Delta T$) converted from the isotope lapse rate (-23.3‰/km) is 5.1‰/°C, slightly smaller than that of the global average (-5.6‰/°C; Dansgaard, 1964; Fricke and O'Neil, 1999), also suggesting that temperature is the primary controlling factor of the isotopic lapse rate. Therefore, if similar atmospheric circulation pattern existed in the geologic past, the modern isotopic lapse rates could be used to reconstruct the elevation contrast between the Rockies and its adjacent Great Plains. The small variation of lapse rate in different seasons also suggests that the air temperature change in the geologic past has little impact on paleoelevation reconstruction.

Extending the transect eastward to the low Great Plains in central Kansas, the river water lapse rates increase to -37.5, -32.5, and -39.0‰/km for δD (and -5.0, -4.3, and -5.1 ‰/km for $\delta^{18}O$) in summer, winter, and spring, respectively, and the mean annual lapse rate is -36.3‰/km for δD (-4.8 ‰/km for $\delta^{18}O$). We attribute the large lapse rate and its seasonal variations to addition of precipitation from convective storms and mixing of moisture from the Gulf of Mexico. Because of the anticlockwise motion of the extratropical cyclone, the low, eastern portion of the Great Plains receives more precipitation from convective storms and more moisture from the Gulf of Mexico than that of the western portion. Because convective storms occur in summer, and both convective precipitation and moisture rom the Gulf of Mexico have high isotope values. We use the lowest isotope values to reduce the influence of convective storms and calculate the lapse rate. The resulting lapse rate is -24.9‰/km for δD (Fig. 4-4), consistent with that of the southern Rockies and its adjacent Great Plains. This similarity further suggests that the lowest isotope values are not influenced by convective precipitation and major changes in vapor sources, and the lapse rate based on the lowest isotope values is controlled by vapor condensation temperature at various elevations. The annual variation of river water isotope values in the low portion of the Great Plains from Texas to central Kansas is up to 6.9‰ for $\delta^{18}O$ and up to 43.6‰ for δD, considerably greater than those in the southern Rockies. The isotope values are not correlated with elevations and local air temperatures, which we attribute to surface evaporation and summer convective precipitation (Allison et al., 1983; Bony et al., 2008). When such processes are weakest, in association with the northward change in vapor sources during the winter seasons, the lowest river water isotope values show a gradient of -3.0 ‰ per latitudinal degree or per 100 km for δD (Fig. 4-3A), similar to that of mean annual precipitation (-3.3 ‰ per latitudinal degree) in North America (Dutton et al., 2005). The mean winter temperature contrast between south Texas and central Kansas is ~10°C. The isotope-temperature ratio ($\Delta\delta D/\Delta T$) converted from the isotope latitudinal variation is ~4‰/°C, smaller than those of the global average and local mean annual, reflecting the influence of moisture source change on the latitudinal gradient of surface water isotope values.

4.4.2 Ancient hydrated volcanic glass

Volcanic glass hydrates when in contact with surface water and the hydration rate slows significantly with increased exposure (e.g., Cailleteau et al., 2008; Seligman et al., 2016; Cassel and Breecker, 2017). Hydration is the diffusion of water molecules into glass at the solution-glass interface and is associated with ion exchange between hydrogen ions in water and more soluble cations of Na^+, K^+, Ca^{2+}, Mg^{2+}) in glass as well as hydrolysis (e.g., Oelkers, 2001; Cailleteau et al., 2008; Cassel and Breecker, 2017). The progressive removal of mobile cations forms a microporous silica-rich layer near the exterior surface of the glass, and the layer prohibits secondary exchange between water and glass and improve long-term chemical durability of the glass (e.g., Cailleteau et al., 2008; Cassel and Breecker, 2017). The hydration process typically takes 10^3-10^4 years. Felsic pristine volcanic glass contains <0.5 wt% magmatic water while completely hydrated volcanic glass contain 2-10 wt% environmental water (Grunder et al., 2005; Cassel and Breecker, 2017) . Magmatic water has high δD values, which increases hydrated glass δD if the glass is not completely hydrated by surface water with low δD values (Friedman et al., 1993). The fractionation of hydrogen isotope between hydrated glass and environmental water is not dependent on temperature (Friedman et al., 1993), thus the δD values of ancient surface water can be calculated from hydrated volcanic glass δD values without knowing temperature.

Our studied glass samples have water contentes between 0.9 and 7.5 wt% (Fig. 4-5 and Table 4-1). Eight of the glass samples have low water content (1-2 wt%) and thus their isotope values may be influenced by magmatic water (Table 4-1). Three of the latest Eocene samples in the high southern Rockies and high Great Plains are from the group. In south Texas, the volcanic glass δD values increased from the range of -85 – -64 ‰ during the late Eocene-early Oligocene to -68‰ during the late Miocene (Table 4-1). In western Kansas, the late Miocene volcanic glass δD values are in the range of -132– -98.0 ‰. In the southern Rockies, the volcanic glass δD values are the range of -164 – -129‰ in the early Oligocene and at ~145‰ during the late Miocene. The reconstructed ancient surface water δD values follow the same trends as hydrated volcanic glass δD values (Table 4-1).

Drying in the Great Plains

The reconstructed surface water δD values in south Texas increase from the range of -51– -33‰ in the late Eocene-earliest Oligocene to -34‰ in the late Miocene, and both are lower than modern river water and precipitation δD values (Fig. 4-6). The increasing trend is consistent with those in the central Rockies and its adjacent Great Plains in Nebraska, which were attributed to drying associated with global climate cooling (Fan et al., 2014a). New data from Kansas do not have a complete record through time because the oldest only sample has low water content.

Global climate entered the icehouse stage after the earliest Oligocene and experienced stepwise cooling after the middle Miocene based on the $\delta^{18}O$ record of benthic formaminefora (Zachos et al., 2001). Climate cooling reduces atmospheric humidity which subsequently enhances subcloud evaporation as well as evaporation in terrestrial environments and increases fractions of recycled moisture in precipitation (Gat, 1996). Both processes increase precipitation isotope values. The existence of drying trend in south Texas, the Great Plains in Nebraska, and the central Rockies in Wyoming suggests that drying was a regional late Cenozoic climate feature in the western USA. The δD values of ancient surface water in the southern Rockies, however, remained between -130‰ and -94 ‰ without a clear trend, after the earliest Oligocene. The lack of drying signal in the southern Rockies may suggest that other factors have caused gradual decrease of surface water δD values, and cancled out the gradual increase induced by drying. Such factors could be surface uplift and continental drift. If continental drift has influenced the isotope record in the southern Rockies, it should also incluenced other localities where we observed increases in δD valuse. Therefore, conitental drift is unlikely the cause of removing the increasing trend.

Surface uplift of the southern Rockies

Despite that the δD values of the three latest Eocene samples from the southern Rockies and high Great Plains in Kansas may be influenced by magmatic water, their water contents are comparable suggesting that the influence of magmatic water is comparable given that they have comparable ages and the magmatic water δD values are likely the same. There is not a difference between the reconstructed late Eocene surface water δD at the two areas (Fig. 4-6), suggesting that either the late Eocene atmosphere circulation was different from that of today and the modern strong extratropical cyclone in the southern Rockies did not exist, or the vapor condensation temperatures in the two areas were not significantly different in the late Eocene. Both cases suggest that the elevation contrast between the two areas was small in the late Eocene and could not induce either the cyclone or the temperature contrast. During the late Miocene, the surface water δD difference became 48 ‰, similar to that of the modern river water (Fig. 4-6), suggesting that the cyclone climate pattern or temperature contrast between the areas was established by the late Miocene. Because we do not have samples of early Oligocene age in the Great Plains, we cannot further clarify at what time between the latest Eocene and the late Miocene the suface elevation contrast was developed sufficiently to induce the extratropical cyclone and the temperature difference.

4.5 Discussion

4.5.1 Assumptions of paleoelevation estimates

We further use the surface water isotopic differences among the southern Rockies, its adjacent high Great Plains in Kansas, and south Texas to reconstruct the paleoelevation of the southern Rockies and its adjacent Great Plains with respect to the low Great Plains along a W-E transect. Similar approach is also applied to the central Rockies and its adjacent high Great Plains in western Nebraska to reconstruct their paleoelevations using the data in Fan et al. (2014). The reconstruction first uses the modern river water δD-latitude relationship to estimate the surface water δD of the low Great Plains in central Kansas; and then uses the modern river water δD lapse rate to estimate elevation contrasts between the southern Rockies and the low Great Plains or between the high Great Plains and the low Great Plains. The calculation can be described as following equations:

$$PElev = Elev^* + \Delta\delta \times \nabla\delta_{elev}$$

$$\Delta\delta = \delta_{obs} - [\ \delta_{TXmin} + (\ Lat_{KS} - Lat_{TX}\ ) \times \nabla\delta_{Lat}\ ]$$

Where PElev and Elev* are the reconstructed paleoelevation and modern elevation of the low Great Plains, respectively (Fig. 4-8B and D); Elev* is set to be 400 m (mean modern elevation) and assumed to remain constant after the late Eocene, and it serves the datum of our paleoelevation estimates. $\nabla\delta_{elev}$ and $\nabla\delta_{Lat}$

are the modern lapse rate (-24.9‰/km) and modern latitudianl gradiant (-3.0 ‰/latitudinal degree) of surface water δD values. δ_{obs} is the reconstructed surface water δD value of the southern Rockies or the high Great Plains, and δ_{TXmin} is the minimum reconstructed surface water δD value in south Texas for each time interval (late Eocene, early Oligocene, and late Miocene). (Lat_{KS} - Lat_{TX}) is the latitudinal difference between south Texas and the low Great Plains. The derived $\Delta\delta$ represents the difference of surface water δD between the southern Rockies or the high Great Plains with respect to the low Great Plains in Kansas (Fig. 4-8A and C).

Before we conduct these recontructions, we first assess the assumptions of paleoelevation reconstructions. The assumptions include that (1) the major moisture sources of precipitation remained constant since the latest Eocene; (2) the δD latitudinal gradient remained constant since the latest Eocene; (3) the temperature influence on precipitation isotopic compositions remained constant since the latest Eocene; (4) volcanic glass was hydrated by meteoric water or river water that mainly sourced from meteoric water; and (5) the elevations of the low portion of the Great Plains and south Texas remained stable since the latest Eocene.

Atmospheric circulation model for the Paleogene (Feng et al., 2013) suggested that the high topography of the North America Cordillera in the western North America poses a barrier to cool mid-latitude air masses, allowing the northward penetration of tropical moist air across the Great Plains during the summer. Because of the existence of the high North America Cordillera in the Paleogene (e.g., DeCelles, 2004; Chamberlain et al., 2012; Feng et al., 2013), modern large-scale atmosphere circulation pattern stayed the same from the Paleogene. However, because mid-late Cenozoic global cooling should have weakened the northward march of tropical airflow, and thus the monsoon, and because cold air has small vapor capacity, southerly moisture should have decreased while recycled moisture increase in the study area since the latest Eocene. Nevertheless, the influence of reduced intensity in monsoon precipitation would mostly affect the surface water isotopic compositions of the low Great Plains during summer, and the Westerlies-dominated winter precipitation would remain steady. In our reconstruction, the high monsoon precipitation in ancient time only influences δ_{TXmin}, resulting in larger reconstructed δ_{TXmin} and thus overestimate of paleoelevation.

Despite that the Paleogene was warmer than today, the early Eocene surface water $\delta^{18}O$ latitudinal gratident in 30-50°N reconstructed from mammal fossil tooth phosphate $\delta^{18}O$ values in Big Bend in Texas, the San Juan basin in New Mexico, and Laramide basins in Wyoming, was similar to those of today in the same latitude (Fricke, 2003). A recent carbonate clumped isotope study also suggested similar-to-modern temperature gradient based on data from Big Bend and the Green River Basin in Wyoming (Kelson et al., 2018). Climate model integrated with atmostpheric moisture $\delta^{18}O$ values also showed that the influences of warm climate conditions on temperature and $\delta^{18}O$ values are uniform at low elevations in tropical and mid-latitude regions (Poulsen and Jeffery, 2011). Because water isotope latitudinal gradient is primarily driven by temperature gradient, and the change of continentality induced by shoreline retreat is negligible after the late Eocene in the study area, it is reasonable to assume that the water isotope latitudinal gradient remained constant since the latest Eocene.

Paleoclimate simulations have suggested that precipitation isotope lapse rate is lower in warm climate conditions because enhanced evaporation and vertical air and vapor convection can reduce temperature gradient (e.g., Poulsen and Jeffery, 2011; Feng and Poulsen, 2016). Temperature lapse rate is a physical property of the atmosphere, and at given surface temperature, the moist adiabatic lapse rate can be calculated (Iribarne and Godson, 1981). Early Eocene warm and extrem climate temperatures have been estimated using mammal fossil flora and tooth phosphate in the Bighorn basin in Wyoming and yielded mean annual temperatures of 19-26°C (Fricke and Wing, 2006). The temperature estimate suggests that the temperature lapse rate should be -4 to -4.3 °C/km in the early Eocene moist adiabatic condition (Iribarne and Godson, 1981). Climate simulation also showed that the temperature lapse rate during the late Paleocene-early Eocene in the western USA was -5 °C/km (Feng and Poulsen, 2016). All these estimates are smaller than modern temperature lapse rate in the western

USA (-6°C/km) and the southern Rockies (-5.5°C/km). Here we use a range of isotope lapse rate (-33.6 to -22.4 ‰/km) derived from the range of temperature lapse rate (-6 to -4 °C/km) to estimate paleoelevations given the post-Eocene climate cooling. The convertion uses the modern global temperature coeffecient for precipitation δD (-5.6 ‰/°C).

The studied glass samples were collected from fluvial-alluvial depositional environments and only the samples from the Balfour Formation in South Park may be related to lacustrine depositional environment. Here we only use the lowest δD values to reconstruct paleoelevation to eliminate the influence of any potential evaporation in surface water. The Great Plains in central Kansas and central Nebraska was tectonically stable during the Cenozic with relatively thick, high velocity lithosphere compared to the Rockies (e.g., Hansen et al., 2013). Dispite that the high (~1 km) western Great Plains was suggested to be a result of late Cenozoic uplift assoicated with a regional tillting due to eperirogeny (e.g., Eaton, 2008; van Wijk et al., 2010), the eperiogney had neglegiable influence on the elevation of the low Great Plains in central Kansas and central Nebraska. This assumption can lead to at most 400 m of overestimate of the reconstructed paleoelevations if the low Great Plains were at sea level.

4.5.2 Development of the central and southern Rockies

We first use this method to reconstruct the mean drainage elevation of the modern river sampling sites. 85% of the estimated mean drainage elevations are within ±500 m of the true mean drainage elevation (Fig. 4-7), suggesting that the reconstruction has a resolution of ±500 m with 85% of confidence. The estimates of paleoelevations of the southern and central Rockies and their adjacent high Great Plains are plotted in Figure 4-8B and D. The central Rockies were at 1600-2150 m during the latest Eocene, 1750-2350 m during the Oligocene, and 1800-2500 m during the late Miocene (Fig. 4-8D), These quatitative reconstructions support previous interpretation that the high central Rockies was developed before the latest Eocene (Fan et al., 2014a). The establishment of high elevation in the central Rockies during the late Eocene suggest that the Neogene epeirogeny contributed little to the surface uplift of the area.

The estimates of the southern Rockies show that the mean elevation was1500-2000 m during the Oligocene and 1800-2500 m during the late Miocene, lower than the modern mean elevation of 2900 m (Fig. 4-8B). Thus the southern Rockies was low during the latest Eocene and gained most of its mean topography throughout Oligocene and Miocene. Our results also show that the southern Rockies experienced differential uplift during the early Oligocene-late Miocene. The Wet Mountains gained part of its elevation by the early Oligocene, and an additional ~1900 m by the late Mocene to reach its modern elevation. The South Park gained most of its elevation by the early Oligocene, and an additional ~1000 m by the late Miocene to reach its modern elevation, while the Arkansas River valley had a paleoelevation close to its modern elevation by the early Oligocene (Fig. 4-8B).

The low elevation in the southern Rockies during the late Eocene and differential uplift during the Oligocene- Miocene suggest that several geodynamic processes may have caused surface uplift of the southern Rockies. Low elevation in the southern Rockies during the late Eocene suggests that the Laramide Orogeny, before removal of the Farallon slab, was not the major driver of surface uplift in the region. However, based on detrital zircon provenance studies, the pattern of interveneing basins and mountains has been established locally, including part of the frontal ranges and Wet Mountains by the late Eocene (Bush et al., 2016; Rasmussen and Foreman, 2017; Zhu and Fan, 2018). Thus it can be inferred that a significant amount of rock exhumation occurred during the Laramide deformation, and the low regional topography before the latest Eocene most likely a result of intense Eocene erosion that prohibited elevation gain. The Arkansas River valley gained most of its modern elevation by the early Oligocene. The valley is very close to the San Juan volcanic field (Fig. 4-1), which expereinced intense magmatism during the latest Eocene-early Oligocene (~36-27 Ma) (McIntosh and Chapin, 2004). Thus density and thermal structure changes associated with localized emplacement of batholiths and subsequent isostatic compensation adjustiment (e.g., Roy et al., 2004; Hansen et al., 2013) may have caused surface uplift of the Arkansas River valley. The South Park is closer to the volcanic field compared to the Wet Mountains, thus experience more uplift than the Wet Mountaind by the ealry Oligocene. By the late Miocene, the Wet Mountains gained its modern elevation. This localized uplift indicates a localized driver may have caused uplift. Small-scale mantle convection related to the opening of the Rio Grande Rift and convection induced by the difference in lithosphere thickness between the southern Rockies and the Great Plains (van Wijk et al., 2010; Coblentz et al., 2011) both can explain the localized uplift.

4.5.3 Developement of the high western Great Plains

Our estimates show that the western Great Plains adjacent to the southern Rockies were low during the late Eocene, and that adjacent to the central Rockies reached 1100-1400 m during the early Oligocene (Fig. 4-8B and D). The development of the high western Great Plains was long considered associated with the mid-late Cenozoic epeirogeny because the long wavelength surface expression of the topography and the regional erosional suface can be explained by its eastward tilting (e.g., McMillan et al., 2006; Eaton, 2008; Cather et al., 2012). Our findings of the development of the high western Great Plains in different times in Nebraska and Kansas suggests along strike variation in uplift mechanism. Although the lack of Oligocene-middle Miocene samples in western Kansas in our dataset does not allow constraining the specific time of major surface of the western Great Plains in Kansas, our data suggest that late Neogene (<6Ma) epeirogeny did not contribute significent surface uplift to the the region.

4.6 Conlusions

This study analyzes the spatial patterns and controling factors of modern river water isotope data compiled from a broad region covering near sea-level regions in south Texas, the Great Plains in Oklohoma and Kansas, and the southern Rockies in Colorado. Our HYSPLIT back air trajectory modeling results show that the vapors were from four sources and contienntal recycled moisture contributed significant amount. Our analyses show that the lowest modern river water δD values in the low Great Plains from south Texas to central Kansas have a latitudianl gradient of -3.0 ‰/ degree and the river water δD values in the southern Rockies and its adjacent Great Plains have a lapse rate of -24.9‰/km. Both rates are primarily controled by temperature differences, and secondarily influenced by changing abundance of recycled continental moisture. With careful assessment of the large-scale atmospheric circulation pattern and changes in temperature after the Eocene, we reconstruct the late Eocene to the late Miocene paleoelevations of the southern and central Rockies and their adjacent high Great Plains. Our estimates show that the central Rockies established its close-to-modern high elevation by the late Eocene, and its adjacent high Great Plains in western Nebraska was established by the early Oligocene, suggesting that the Neogene epeirogeny had little influence on the topogrpahy of the regions. Our estimates also showed that the southern Rockies was low during the latest Eocene, and experienced differential uplift during the Oligocene and Neogene. Latest

Eocene-early Oligocene magmatism of the San Juan volcanic field has caused surface uplift to the region close to it and its impact on topography dimishes as the study site become furthur away. The Wet Moutnains expereinced major uplift during the Miocene, likely a result of localized uplift associated with the opening of the Rio Grande Rift or difference in lithosphere thickness. The uplift of the high Great Plains adjacent to the central and southern Rockies also show along-strike variation. While the high plains adjacent to the central Rockies expereinced uplift by the early Oligocene, the one adjacent to the southern Rockies expereinced uplift during the Oligocene-middle Miocene. Uplift of the high Great Plains were not significantly influenced by the late Neogene (<6Ma) epeirogeny.

References

Allison, G.B., Barnes, C.J., Hughes, M.W., Leaney, F.W.J., 1983. Effect of climate and vegetation on oxygen-18 and deuterium profiles in soils, in: Isotopes Hydrology: Proceedings of the International Symposium on Isotope Hydrology for Water Resources Development. Int. At. Energy Agency, Vienna, Austria, pp. 105–123.

Arguez, A., Durre, I., Applequist, S., Squires, M., Vose, R., Yin, X., Bilotta, R., 2010. NOAA’s U.S. Climate Normals (1981-2010). NOAA National Centers for Environmental Information.

Bird, P., 1998. Kinematic history of the Laramide orogeny in latitudes 35°–49°N, western United States. Tectonics 17, 780.

Bony, S., Risi, C., Vimeux, F., 2008. Influence of convective processes on the isotopic composition ($\delta^{18}O$ and δD) of precipitation and water vapor in the tropics: 1. Radiative-convective equilibrium and Tropical Ocean-Global Atmosphere-Coupled Ocean-Atmosphere Response Experiment (. Journal of Geophysical Research Atmospheres 113, 1–21.

Brierley, C.M., Fedorov, a V, Liu, Z., Herbert, T.D., Lawrence, K.T., LaRiviere, J.P., 2009. Greatly expanded tropical warm pool and weakened Hadley circulation in the Early Pliocene. Science 323, 1714–1718.

Bush, M.A., Horton, B.K., Murphy, M.A., Stockli, D.F., 2016. Detrital record of initial basement exhumation along the Laramide deformation front, southern Rocky Mountains. Tectonics 35, 2117–2130.

Cailleteau, C., Angeli, F., Devreux, F., Gin, S., Jestin, J., Jollivet, P., Spalla, O., 2008. Insight into silicate-glass corrosion mechanisms. Nature materials 7, 978–983.

Cassel, E.J., Breecker, D.O., 2017. Long-term stability of hydrogen isotope ratios in hydrated volcanic glass. Geochimica et Cosmochimica Acta 200, 67–86.

Cather, S.M., Chapin, C.E., Kelley, S.A., 2012. Diachronous episodes of Cenozoic erosion in southwestern North America and their relationship to surface uplift, paleoclimate, paleodrainage, and paleoaltimetry. Geosphere 8, 1177–1206.

Chamberlain, C.P., Mix, H.T., Mulch, A., Hren, M.T., Kent-Corson, M.L., Davis, S.J., Horton, T.W., Graham, S.A., 2012. The Cenozoic climatic and topographic evolution of the western north American Cordillera. American Journal of Science 312, 213–262.

Chapin, C.E., Kelley, S.A., Cather, S.M., 2014. The Rocky Mountain Front, southwestern USA. Geosphere 10, 1043–1060.

Chase, C.G., Gregory, K.M., 1992. Tectonic significance of paleobotanically estimated climate and altitude of the late Eocene erosion surface, Colorado. Geology 20, 581–585.

Coblentz, D., Chase, C.G., Karlstrom, K.E., Wijk, J. Van, Van Wijk, J., 2011. Topography, the geoid, and compensation mechanisms for the southern Rocky Mountains. Geochemistry, Geophysics, Geosystems 12, Q04002.

Copeland, P., Currie, C.A., Lawton, T.F., Murphy, M.A., 2017. Location, location, location: The variable lifespan of the laramide orogeny. Geology 45, 223–226.

Copeland, P., Kendall, C., 2000. Stable hydrogen and oxygen isotope ratios for selected sites of the U.S. Geological Survey's NASQAN and Benchmark surface-water networks. US Geological Survey Open-File Report 00-160.

Copeland, P., Murphy, M.A., Dupre, W.R., Lapen, T.J., 2011. Oligocene Laramide deformation in southern New Mexico and its implications for Farallon plate geodynamics. Geosphere 7, 1209–1219.

Dansgaard, W., 1964. Stable isotopes in precipitation. Tellus 16, 436–468.

DeCelles, P.G., 2004. Late Jurassic to Ecocene evolution of the Cordilleran Thurst Belt and foreland basin system, western U.S.A. American Journal of Science 304, 105–168.

Dick, R., Nish, M., 1966. The Cenozoic history of the Wet Mountain Valley, Colorado. University of Michigan, Ph.D dissertation. 120 p.

Dickinson, W.R., Klute, M.A., Hayes, M.J., Janecke, S.U., Lundin, E.R., Mckittrick, M.A., Olivares, M.D., 1988. Paleogeographic and paleotectonic setting of Laramide sedimentary basins in the central Rocky. Bulletin of the Geological Society of America 100, 1023–1039.

Donahue, M.M.S., 2016. Episodic uplift of the Rocky Mountains: evidence from U-Pb detrital zircon geochronology and low-temperature thermochronology with a chapter on using mobile technology for geoscience and education. The University of New Mexico, Albuquerque. Earth & Planetary Sciences Ph.D dissertation. 188 p.

Draxler, R.R., Rolph, G.D., 2014. HYSPLIT (HYbrid Single-Particle Lagrangian Integrated Trajectory) Model access via NOAA ARL READY Website (http://www.arl.noaa.gov/HYSPLIT.php). NOAA Air Resources Laboratory, College Park, MD. NOAA Air Resources Laboratory.

Dutton, A., Wilkinson, B.H., Welker, J.M., Bowen, G.J., Lohmann, K.C., 2005. Spatial distribution and seasonal variation in 18O/16O of modern precipitation and river water across the conterminous USA. Hydrological

Processes 19, 4121–4146.

Eaton, G.P., 2008. Epeirogeny in the Southern Rocky Mountains region: Evidence and origin. Geosphere 4, 764–784.

Epis, R.C., Scott, G.R., Taylor, R.B., Chapin, C.E., 1980. Summary of Cenozoic geomorphic, volcanic, and tectonic features of central Colorado and adjoining areas. Colorado Geology. Rocky Mountain Association of Geologist-1980 Symposium. 135–156.

Fan, M., Carrapa, B., 2014. Late Cretaceous-early Eocene Laramide uplift, exhumation, and basin subsidence in Wyoming: Crustal responses to flat slab subduction. Tectonics 33, 509–529.

Fan, M., Heller, P., Allen, S.D., Hough, B.G., 2014. Middle Cenozoic uplift and concomitant drying in the central Rocky Mountains and adjacent Great Plains. Geology 42, 547–550.

Feng, R., Poulsen, C.J., 2016. Refinement of Eocene lapse rates, fossil-leaf altimetry, and North American Cordilleran surface elevation estimates. Earth and Planetary Science Letters 1, 1–12.

Feng, R., Poulsen, C.J., Werner, M., Chamberlain, C.P., Mix, H.T., Mulch, A., 2013. Early cenozoic evolution of topography, climate, and stable isotopes in precipitation in the north American cordillera. American Journal of Science 313, 613–648.

Flowers, R.M., Wernicke, B.P., Farley, K.A., 2008. Unroofing, incision, and uplift history of the southwestern Colorado Plateau from apatite (U-Th)/He thermochronometry. Bulletin of the Geological Society of America 120, 571–587.

Fricke, H.C., 2003. Investigation of early Eocene water-vapor transport and paleoelevation using oxygen isotope data from geographically widespread mammal remains. GSA Bulletin 115, 1088–1096.

Fricke, H.C., O'Neil, J.R., 1999. The correlation between 18O/16O ratios of meteoric water and surface temperature : its use in investigating terrestrial climate change over geologic time. Earth and Planetary Science Letters 170, 181–196.

Fricke, H.C., Wing, S.L., 2006. Oxygen isotope and paleobotanical estimates of temperature and 18O-latitude gradients over North America during the early Eocene. American Journal of Science 304, 612–635.

Friedman, I., Gleason, J., Sheppard, R.A., Gude, A.J., 1993. Deuterium fractionation as water diffuses into silicic volcanic ash, in: Climate Change in Continental Isotopc Records. Monogr. Ser., Vol. 78. AGU, Washington, D.C., pp. 321–323.

Galloway, W.E., Murphy, T.D., Belcher, R.C., Johnson, B.D., Sutton, S., 1977. Catahoula for- mation of the Texas Coastal Plain: depositional systems, composition, structural sevelopment, ground-water flow history, and uranium distribution, in: Bureau of Eco- Nomic Geology, the University of

Texas Report of Investigations No. 87. p. 59.

Gao, M., Fan, M., 2018. Depositional environment, sediment provenance and oxygen isotope paleoaltimetry of the early Paleogene greater Green River Basin, Southwestern Wyoming, U.S.A. American Journal of Science 318, 1018–1055.

Gat, J.R., 1996. Oxygen and hydrogen isotopes in the hydrologic cycle. Annual Review of Earth and Planetary Sciences 24, 225–262.

Godfrey, C., Fan, M., Jesmok, G., Upadhyay, D., Tripati, A., 2018. Petrography and stable isotope geochemistry of Oligocene-Miocene continental carbonates in south Texas: Implications for paleoclimate and paleoenvironment near sea-level. Sedimentary Geology 367, 69–83.

Gregory, K.M., Chase, C.G., 1994. Tectonic and climatic significance of a late Eocene low-relief, high-level geomorphic surface, Colorado. Journal of Geophysical Research 99, 141–160.

Gregory, K.M., McIntosh, W.C., 1996. Paleoclimate and paleoelevation of the Oligocene Pitch-Pinnacle flora, Sawatch Range, Colorado. Geological Society of America Bulletin 108, 545–561.

Grunder, A.L., Laporte, D., Druitt, T.H., 2005. Experimental and textural investigation of welding: Effects of compaction, sintering, and vapor-phase crystallization in the rhyolitic Rattlesnake Tuff. Journal of Volcanology and Geothermal Research 142, 89–104.

Guillemette, R.N., Yancey, T.E., 1996. Composition and provenance of volcanic glass in Late Eocene Manning Formation, east-central Texas. Gulf Coast Association of Geological Societies Transactions 46, 159166.

Hallman, J.A., 2016. Spatial and temporal patterns of Ogallala Formation deposition revealed by U-Pb zircon geochronology. University of Kansas.

Hansen, S.M., Dueker, K.G., Stachnik, J.C., Aster, R.C., Karlstrom, K.E., 2013. A rootless rockies - Support and lithospheric structure of the Colorado Rocky Mountains inferred from CREST and TA seismic data. Geochemistry, Geophysics, Geosystems 14, 2670–2695.

Heintz, M.L., Yancey, T.E., Miller, B. V, Heizler, M.T., 2015. Tephrochronology and geochemistry of Eocene and Oligocene volcanic ashes of east and central Texas. Geological Society of America Bulletin 127, 770–780.

Heller, P.L., Liu, L., 2016. Dynamic topography and vertical motion of the U.S. Rocky Mountain region prior to and during the Laramide orogeny. Geological Society of America Bulletin B31431.1.

Higgins, R.W., Yao, Y., Yarosh, E.S., Janowiak, J.E., Mo, K.C., 1997. Influence of the great plains low-level jet on summertime precipitation and moisture transport over the central United States. Journal of Climate 10, 481–507.

Hough, B.G., Fan, M., Passey, B.H., 2014. Calibration of the clumped isotope geothermometer in soil carbonate in Wyoming and Nebraska, USA: Implications for paleoelevation and paleoclimate reconstruction. Earth and

Planetary Science Letters 391, 110–120.

Hu, H., Dominguez, F., 2015. Evaluation of Oceanic and Terrestrial Sources of Moisture for the North American Monsoon Using Numerical Models and Precipitation Stable Isotopes. Journal of Hydrometeorology 16, 19–35.

Hubbard, M.S., Oviatt, C.G., Kelley, S.A., Perkins, M.E., Hodges, K. V., Robbins, R., 2001. Oligocene-Miocene basin formation and modification in the northern Rio Grande rift; constraints from 40Ar/39Ar, fission track, and tephrochronology. Geological Society of America Abstracts with Programs 33, A-257.

Huntington, K.W., Wernicke, B.P., Eiler, J.M., 2010. Influence of climate change and uplift on Colorado Plateau paleotemperatures from carbonate clumped isotope thermometry. Tectonics 29, 1–19.

Iribarne, J. V., Godson, W.L., 1981. Atomosphere Thermodynamics. D. Reidel Publishing Company, Dordrecht, the Netherlands.

Kelley, S. a, Chapin, C.E., 2004. Denudation history and internal structure of the Front Range and Wet Mountains , Colorado , based on apatite fission track thermochronology. New Mexico Bureau of Geology and Mineral Resources Bulletin 1, 41–78.

Kelley, S.A., Duncan, I.J., 1984. Tectonic history of the northern Rio Grande Rift derived from apatite fission-track geochronology. New Mexico Geological Society Guidebook, 35th Field Conference 67–73.

Kelson, J.R., Watford, D., Bataille, C., Huntington, K.W., Hyland, E., Bowen, G.J., 2018. Warm Terrestrial Subtropics During the Paleocene and Eocene: Carbonate Clumped Isotope (Δ47) Evidence From the Tornillo Basin, Texas (USA). Paleoceanography and Paleoclimatology 33, 1230–1249.

Landman, R.L., Flowers, R.M., 2013. (U-Th)/He thermochronologic constraints on the evolution of the northern Rio Grande Rift, Gore Range, Colorado, and implications for rift propagation models. Geosphere 9, 170–187.

Leopold, E.B., Zaborac-Reed, S., 2019. Pollen evidence of floristic turnover forced by cool aridity during the Oligocene in Colorado. Geosphere 15, 254–294.

Licht, A., Quade, J., Kowler, A., De Los Santos, M., Hudson, A., Schauer, A., Huntington, K., Copeland, P., Lawton, T., 2017. Impact of the north American monsoon on isotope paleoaltimeters: Implications for the paleoaltimetry of the American southwest. American Journal of Science 317, 1–33.

Liu, L., Gurnis, M., 2010. Dynamic subsidence and uplift of the Colorado Plateau. Geology 38, 663–666.

Ludvigson, G.A., Sawin, R.S., Franseen, E.K., Watney, W.L., West, R.R., Smith, J.J., 2009. Review of the stratigraphy of the Ogallala Formation and revision of Neogene ('"Tertiary"') nomenclature in Kansas: current research in earth science. Kansas Geological Survey, Bulletin 256, 1–9.

McIntosh, W.C., Chapin, C.E., 2004. Geochronology of the central Colorado volcanic field. New Mexico Bureau of Geology & Mineral Resources, Bulletin 160, 205–237.

McMillan, M.E., Heller, P.L., Wing, S.L., 2006. History and causes of post-Laramide relief in the Rocky Mountain orogenic plateau. Bulletin of the Geological Society of America 118, 393–405.

Meyer, H.W., 2007. A Review of Paleotemperature Lapse Rate Methods for Estimating Paleoelevation from Fossil Floras. Reviews in Mineralogy and Geochemistry 66, 155–171.

Mintz, J.S., Driese, S.G., Breecker, D.O., Ludvigson, G. a., 2011. Influence of Changing Hydrology on Pedogenic Calcite Precipitation in Vertisols, Dance Bayou, Brazoria County, Texas, U.S.A.: Implications for Estimating Paleoatmospheric PCO2. Journal of Sedimentary Research 81, 394–400.

Oelkers, E.H., 2001. General kinetic description of multioxide silicate mineral and glass dissolution. Geochimica et Cosmochimica Acta 65, 3703–3719.

Peppe, D.J., Royer, D.L., Wilf, P., Kowalski, E.A., 2010. Quantification of large uncertainties in fossil leaf paleoaltimetry. Tectonics 29, TC3015.

Poulsen, C.J., Jeffery, M.L., 2011. Climate change imprinting on stable isotopic compositions of high-elevation meteoric water cloaks past surface elevations of major orogens. Geology 39, 595–598.

Rasmussen, D.M., Foreman, B.Z., 2017. Provenance of lower Paleogene strata in the Huerfano Basin: Implications for uplift of the Wet Mountains, Colorado, U.S.S. Journal of Sedimentary Research 87, 579–593.

Ricketts, J.W., Kelley, S.A., Karlstrom, K.E., Schmandt, B., Donahue, M.S., van Wijk, J., 2016. Synchronous opening of the Rio Grande rift along its entire length at 25-10 Ma supported by apatite (U-Th)/He and fission-track thermochronology, and evaluation of possible driving mechanisms. Bulletin of the Geological Society of America 128, 397–424.

Roberts, G.G., White, N.J., Crosby, A.G., Martin-Brandis, G.L., 2012. An uplift history of the Colorado Plateau and its surroundings from inverse modeling of longitudinal river profiles. Tectonics 31, 4.

Rosenberg, R., Kirby, E., Aslan, A., Karlstrom, K., Heizler, M., Ouimet, W., 2014. Late Miocene erosion and evolution of topography along the western slope of the Colorado Rockies. Geosphere 10, 641–663.

Roy, M., Kelley, S., Pazzaglia, F., Cather, S., House, M., 2004. Middle Tertiary buoyancy modification and its relationship to rock exhumation, cooling, and subsequent extension at the eastern margin of the Colorado Plateau. Geology 32, 925–928.

Sahagian, D., Proussevitch, a., 2007. Paleoelevation Measurement on the Basis of Vesicular Basalts. Reviews in Mineralogy and Geochemistry 66, 195–213.

Scott, G.R., Taylor, R.B., 1975. Post-Paleocene Tertiary Rocks and Quaternary Volcanic Ash of the Wet Mountain Valley, Colorado (No. 868). United

States Government Printing Office.

Seligman, A.N., Bindeman, I.N., Watkins, J.M., Ross, A.M., 2016. Water in volcanic glass: From volcanic degassing to secondary hydration. Geochimica et Cosmochimica Acta 191, 216–238.

Sheldon, N.D., Tabor, N.J., 2009. Quantitative paleoenvironmental and paleoclimatic reconstruction using paleosols. Earth-Science Reviews 95, 1–52.

Small, E.E., Anderson, R.S., 1998. Pleistocene relief production in Laramide mountain ranges, western United States. Geology 26, 123–126.

Smith, J.J., Ludvigson, G.A., Layzell, A., Möller, A., Harlow, R.H., Turner, E., Platt, B., Petronis, M., 2017. Discovery of Paleogene deposits of the Central High Plains Aquifer in the western Great Plains, U.S.A. Journal of Sedimentary Research 87, 880–896.

Solis, R.F.I., 1981. Upper tertiary and quaternary depositional systemsin central coastal plain, Texas: regional geology of the coastal aquifer and potential liquid-waste repositories, in: Bureau of Economic Geology, University of Texas Report of Investigations No. 108. p. 89.

Stark, J.T., Johnson, J.H., Behre, C.H., Powers, W.E., Howland, A.L., Gould, D.B., 1949. Geology and Origin of South Park, Colorado, Geological Society of America Memoir 33. Geological Society of America, Baltimore, MD.

Tomlinson, D.W., Copeland, P., Murphy, M.A., Lapen, T.J., 2013. Oligocne shortening in the Little Burro Mountains of southwest New Mexico. Rocky Mountain Geology 48, 169–183.

Vachon, R.W., Welker, J.M., White, J.W.C., Vaughn, B.H., 2010. Monthly precipitation isoscapes (d18O) of the United States: Connections with surface temperatures, moisture source conditions, and air mass trajectories. Journal of Geophysical Research Atmospheres 115, 1–17.

Van Alstine, R.E., Lewis, G.E., 1960. Pliocene sediments near Salida, Chaffee County, Colorado. Sort papers in the geological sciences: US. Geological Survey Professoional Paer 400, B245.

van Wijk, J., Koning, D., Axen, G., Coblentz, D., Gragg, E., Sion, B., 2018. Tectonic subsidence, geoid analysis, and the Miocene-Pliocene unconformity in the Rio Grande rift, southwestern United States: Implications for mantle upwelling as a driving force for rift opening. Geosphere 14, 684–709.

van Wijk, J.W., Baldridge, W.S., van Hunen, J., Goes, S., Aster, R., Coblentz, D.D., Grand, S.P., Ni, J., 2010. Small-scale convection at the edge of the Colorado Plateau: Implications for topography, magmatism, and evolution of Proterozoic lithosphere. Geology 38, 611–614.

Wallace, J.M., Hobbs, P. V., 2006. Atmospheric Science: An Introductory Survey: Second Edition, Atmospheric Science: An Introductory Survey: Second Edition.

Wolfe, J.A., Forest, C.E., Molnar, P., 1998. Paleobotanical evidence of Eocene and Oligocene paleoaltitudes in midlatitude western North America. Bulletin of the Geological Society of America 110, 664–678.

Yancey, T.E., Heizler, M.T., Miller, B. V., Guillemette, R.N., 2018. Eocene–Oligocene chronostratigraphy of ignimbrite flareup volcanic ash beds on the Gulf of Mexico coastal plains. Geosphere 14, 1232–1252.

Yin, J.H., 2005. A consistent poleward shift of the storm tracks in simulations of 21st century climate. Geophysical Research Letters 32, 1–4.

Zaborac-Reed, S.J., Leopold, E.B., 2016. Determining the paleoclimate and elevation of the late Eocene Florissant flora: support from the coexistence approach. Canadian Journal of Earth Sciences 53, 565–573.

Zachos, J., Pagani, M., Sloan, L., Thomas, E., Billups, K., 2001. Trends, rhythms, and aberrations in global climate 65 Ma to present. Science 292, 686–693.

Zanazzi, A., Kohn, M.J., MacFadden, B.J., Terry, D.O., 2007. Large temperature drop across the Eocene-Oligocene transition in central North America. Nature 445, 639–642.

Zhu, L., Fan, M., 2018. Detrital zircon provenance record of middle Cenozoic landscape evolution in the southern Rockies, USA. Sedimentary Geology 378, 1–12.

Zhu, L., Fan, M., Hough, B., Li, L., 2018. Spatiotemporal distribution of river water stable isotope compositions and variability of lapse rate in the central Rocky

Mountains : Controlling factors and implications for paleoelevation reconstruction. Earth and Planetary Science Letters 496, 215–226.

Figures and tables

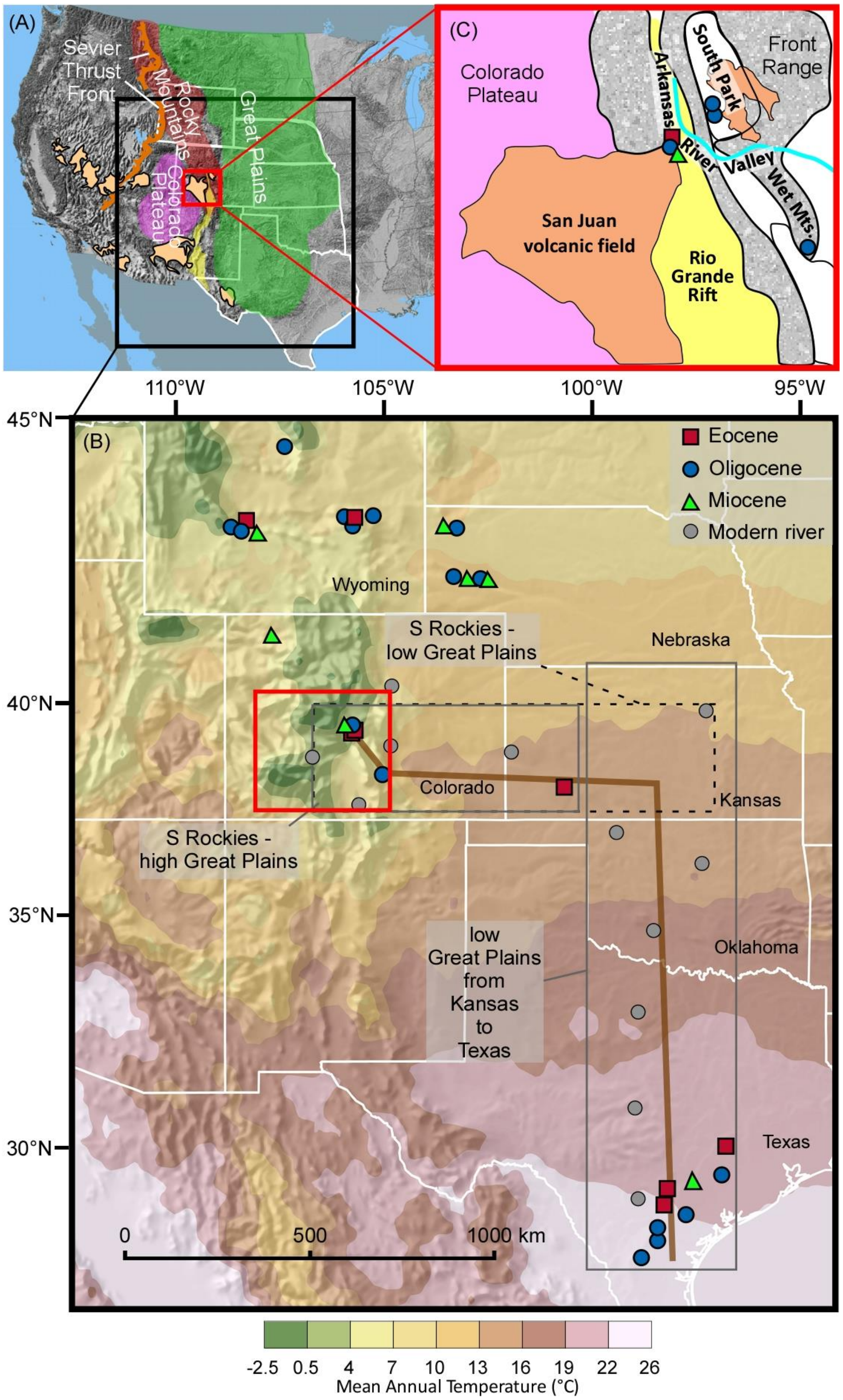

Figure 4-1 (A) Map of North America showing the locations of the Rockies, Sevier thrust front, Colorado Plateau, and the Great Plains. (B) Map showing the sampling sites in the studied area and the spatial pattern of modern mean annual temperature. The brown line represents the topographic profile in Figure 4-6. (C) Map of the southern Rockies showing sample locations in Arkansas River Valley, South Park basin, and the Wet Mountains and their spatial relationship to the San Juan volcanic field.

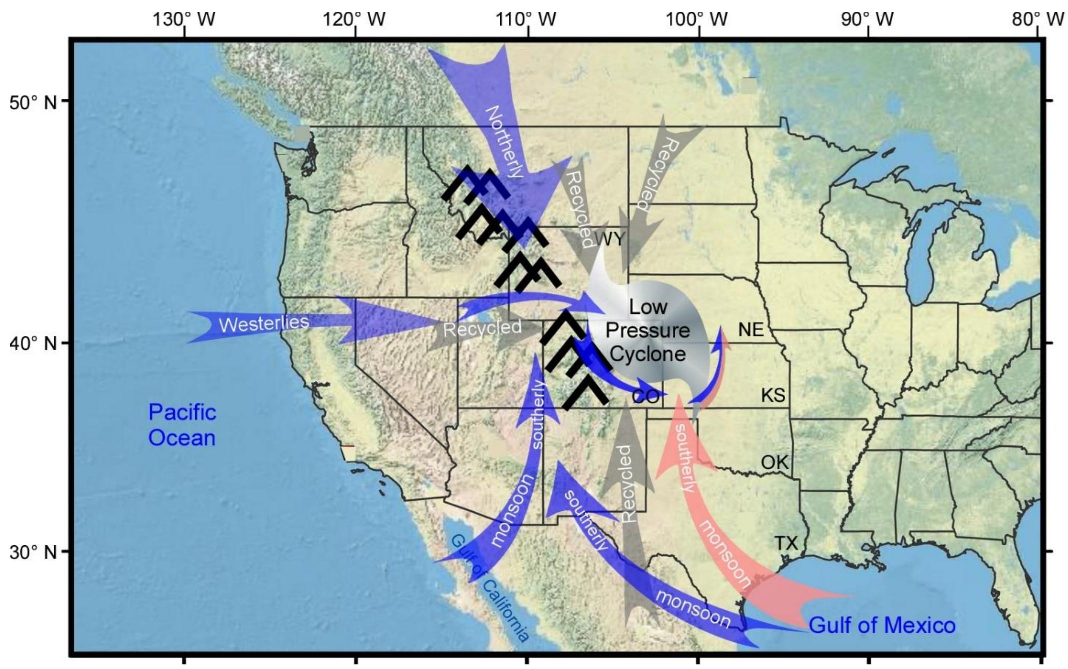

Figure 4-2 Map showing the major vapor sources in the study area and the location of the mid-latitude extratropical low-pressure cyclone. Air trajectory deflects to south as it crosses over the mountain ranges and forms the low-pressure cyclone, which directs the air trajectory from the Gulf of Mexico anticlockwise toward east to the Great Plains.

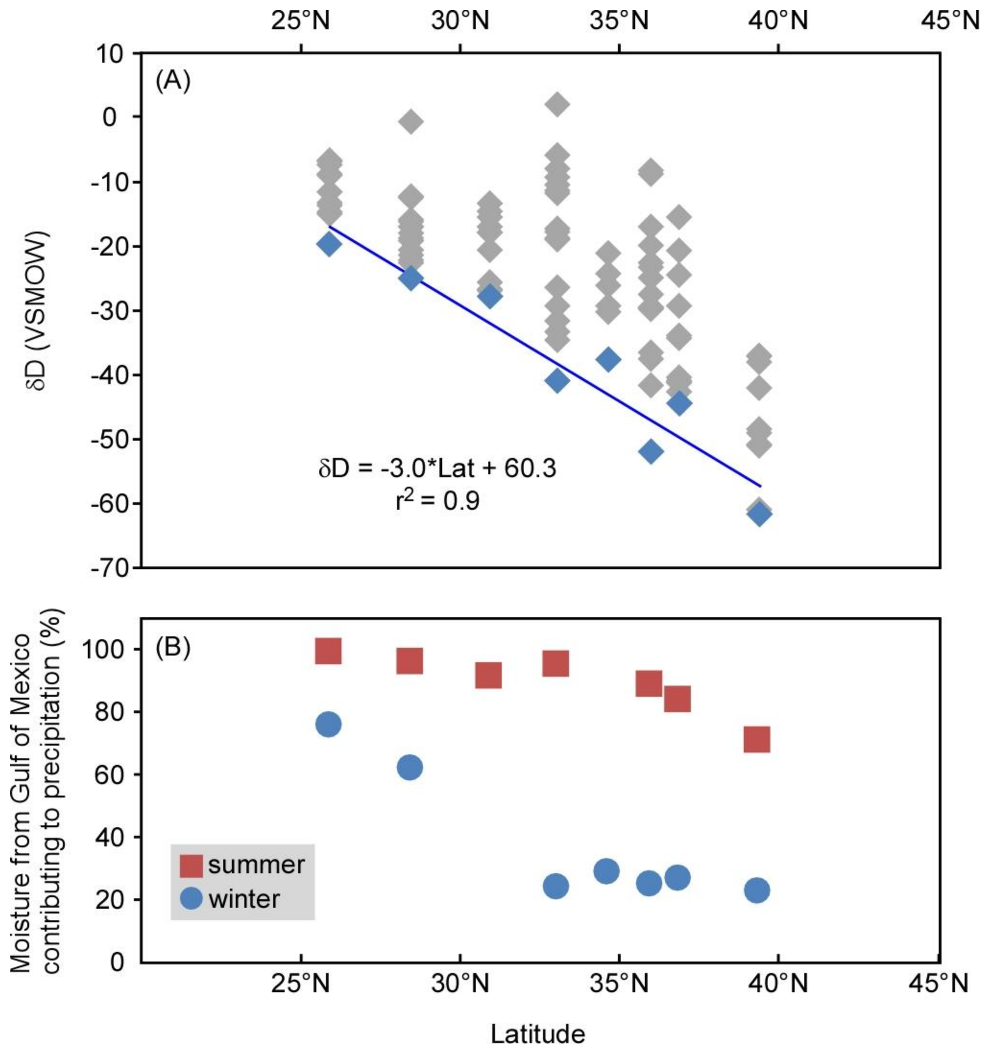

Figure 4-3 (A) Relationship between river water δD values and latitude along the S-N transect from south Texas to Kansas. River water samples were from years 1984-1987, and data were compiled from Copeland and Kendall (2000). Blue diamonds are lowest values at each sampling site. (B) Percentage of the Gulf of Mexico moisture contributed to precipitation for the summer and winter seasons of years 1984-1987. Percentage was calculated using the ratio of numbers of air trajectories from the Gulf of Mexico and numbers of all air trajectories based on our HYSPLIT results.

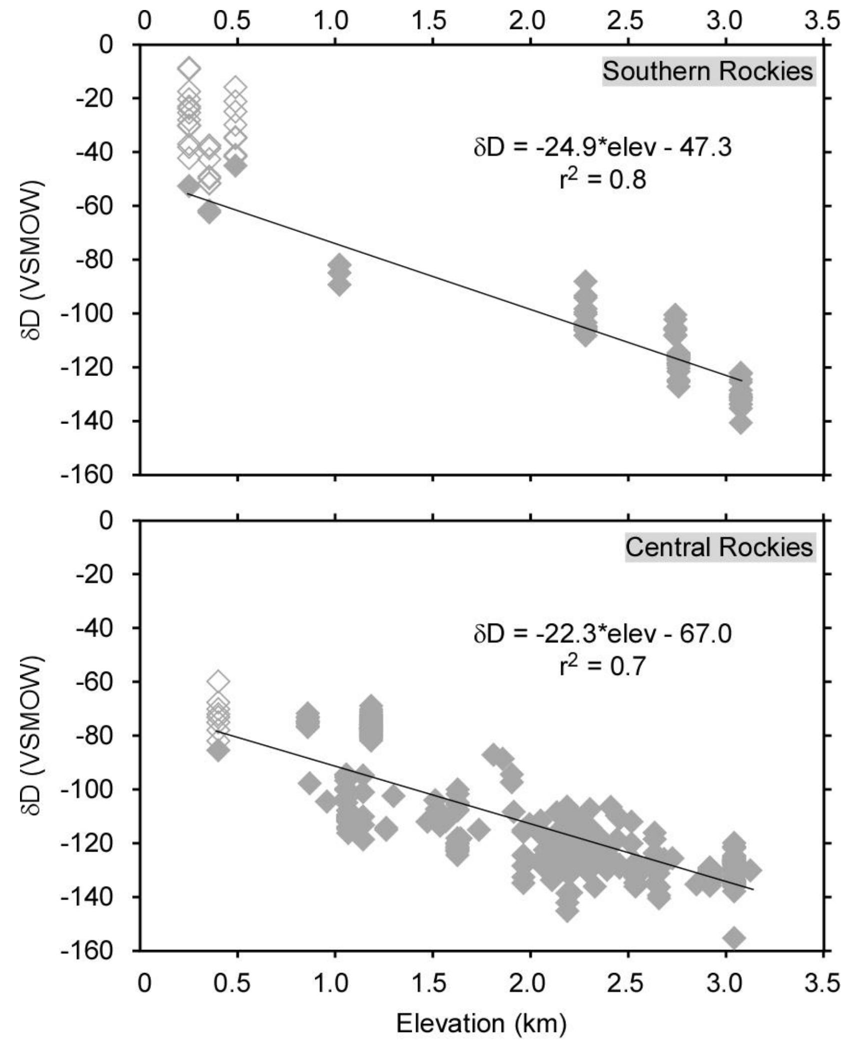

Figure 4-4 Modern river water stable isotope lapse rates in the southern and central Rockies and their adjacent Great Plains. Only the lowest isotope value of each sampling site in the low Great Plains is used to calculate the isotopic lapse rates in order to reduce the influence of the mixing of moisture from the Gulf of Mexico. Grey diamonds are used for calculating lapse rates, while empty diamonds are not used.

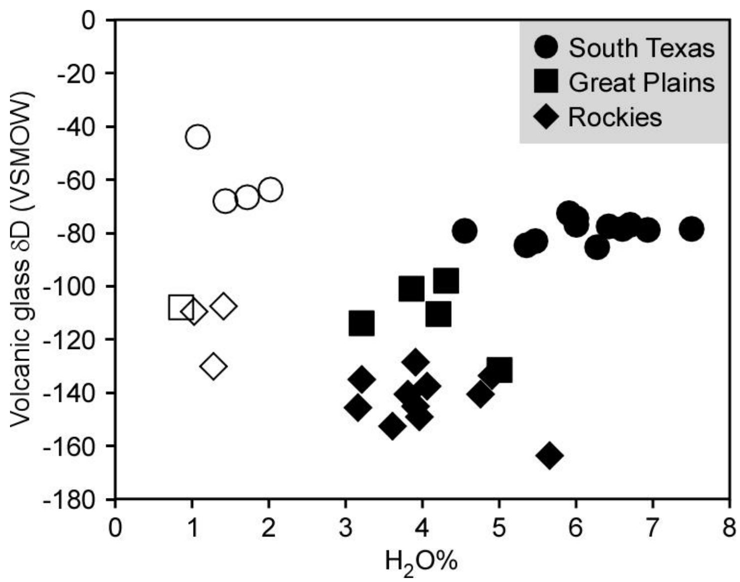

Figure 4-5 δD values of hydrated volcanic glass and their water contents. Volcanic glass that contains less than 2 wt% of water (unfilled symbols), most likely a result incomplete hydration, was not used for paleoelevation reconstruction.

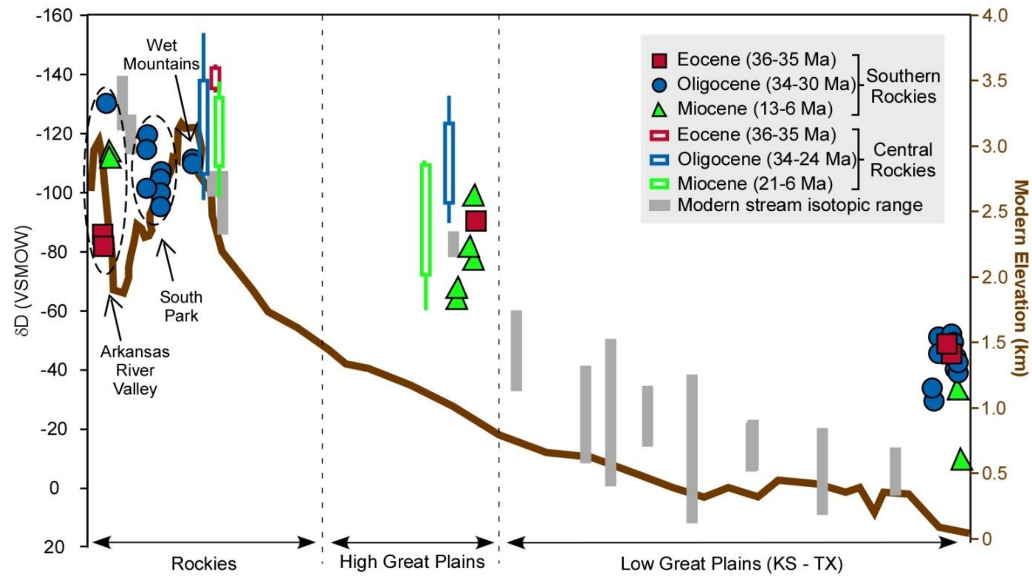

Figure 4-6 Map showing the relationships between the reconstructed surface water δD values and modern river water δD values along the studied transects. Data for the central Rockies and its adjacent Great Plains are compiled from Fan et al. (2014). The ranges within one standard deviation are represented by rectangles, and the maximum and minimum values are represented by bars attached to the rectangles. The scale of x-axis is not proportional to distance.

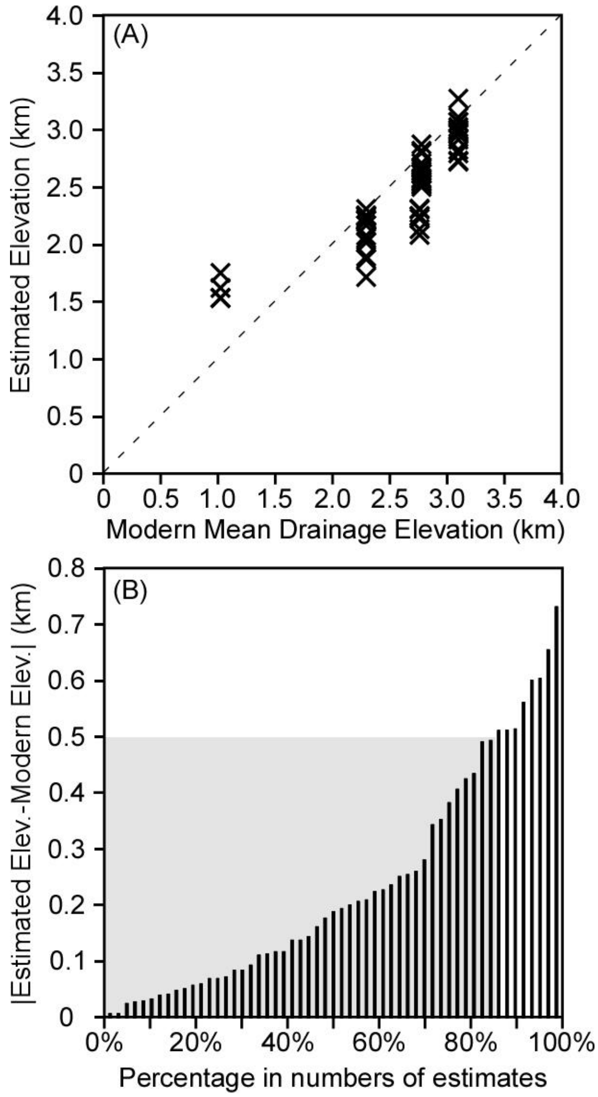

Figure 4-7 Estimated modernmean drainage elevations and the uncertainties. (A) Comparison of the estimated elevations and the true modern elevations. (B) Absolute differences between the estimated and the true modern elevations. The values are plotted in ascending order, and the x-axis represents the percentage of the numbers of estimates. 85% of the estimates are within ±500m uncertainty.

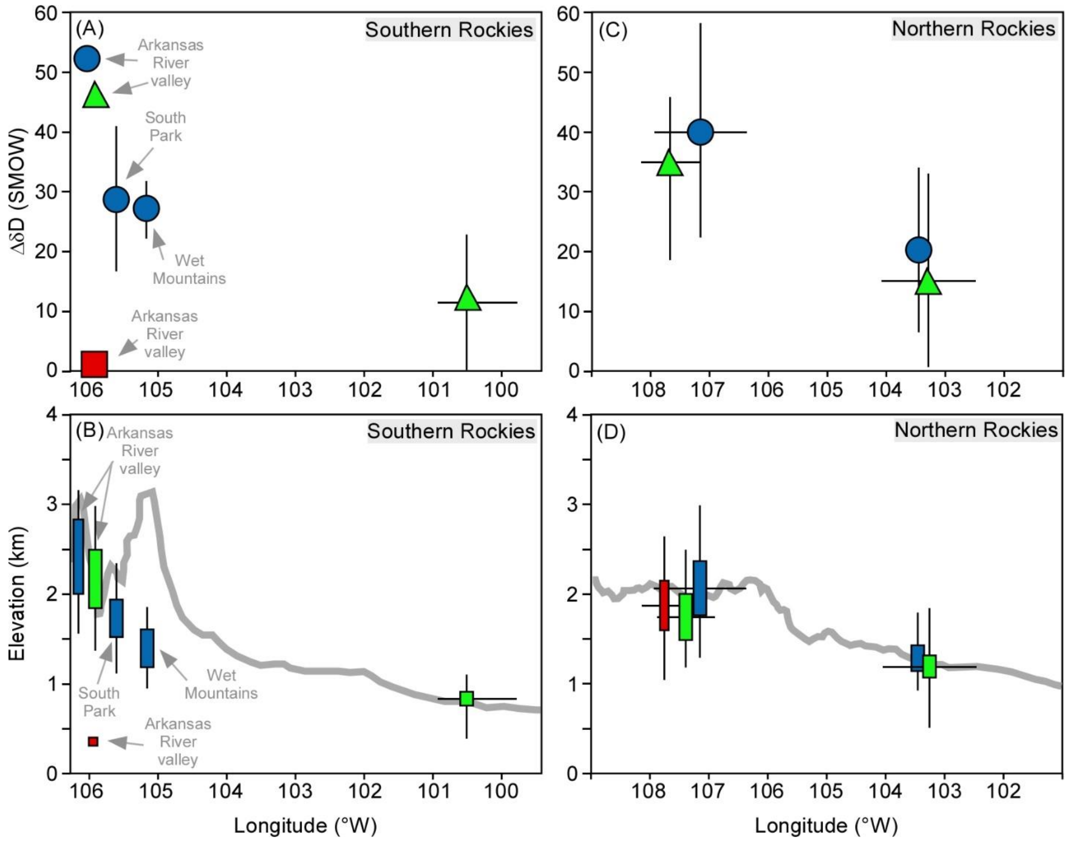

Figure 4-8 Estimates of ΔδD and paleoelevations of the central and southern Rockies and their adjacent Great Plains. ΔδD is the δD difference between the recontruct lowest surface water δD values of the low portion of the Great Plains and and that of the Rockies or the high Great Plains. Estimated ranges of paleoelevation, based on the lapse rates in hot climate (early Eocene) and cold climate (modern), are represented by ractangles. Black bars represent maxium ranges of the values. Red color represents late Eocene samples. Blue color represents Oligocene samples. Green color represents Miocene samples.

Table 4-1 Information of the hydrated volcanic glass samples and calculated water δD values

#	Latitude	Longitude	Elevation	Age (Ma)#	Formation	Lithology	δD glass	H_2O %	δD water*
Late Eocene									
SALIDA-4	38.66994	-106.09844	3010	35.8±0.2 [e2]	Dry Union	sandstone	-108	1.4	-73
SALIDA-6	38.66994	-106.09844	3010	35.8±0.2 [e2]	Dry Union	sandstone	-107	1.0	-73
HPIA3	37.66000	-100.66462	862	35.6-35.4 [c2]		sandstone	-108	0.9	-74
Helms Pit	29.48434	-97.37099	97	35.67±0.05 [d1]	Manning	ash	-82	6.6	-48
Y4	29.45276	-97.33047	77	36-34 [d1]	Manning	ash	-78	6.6	-44
Y1	30.31747	-96.51717	71	36-34 [b1]	Manning	ash	-78	7.5	-44
Oligocene									
GREENHORN1-2 ASH	37.89395	-105.04159	3491	33.5±0.3 [e2]	Devils Hole	sandstone	-140	3.8	-106
GREENHORN4	37.89395	-105.04159	3491	33.5±0.3 [e2]	Devils Hole	sandstone	-130	1.2	-96
SOLIDA 15	38.50828	-106.07244	3010	~33.8 [e2]	Dry Union	sandstone	-164	5.7	-130
WT 14	38.75883	-105.81144	2923	~34.1 [e3]	Balfour	sandstone	-152	3.6	-118
WT 15	38.79397	-105.78683	2923	~34.1 [e3]	Balfour	sandstone	-149	4.0	-115
WT 19	38.79397	-105.78683	2923	~34.1 [e3]	Balfour	sandstone	-135	3.2	-101
WT 20	38.80725	-105.77722	2800	34.1±0.3 [e3]	Balfour	sandstone	-128	3.9	-94
WT 21	38.89517	-105.79364	2800	34.1±0.3 [e3]	Balfour	sandstone	-134	4.9	-100
WT 22	38.89517	-105.79364	2800	34.1±0.3 [e3]	Balfour	sandstone	-138	4.1	-104
WT 23	38.89517	-105.79364	2800	34.1±0.3 [e2]	Balfour	sandstone	-140	4.8	-106
16010901	28.47370	-98.25137	63	~30.4 [a3]	Catahoula	sandstone	-79	4.5	-45
050912 MB2F	28.43154	-98.30160	54	~30.4 [a3]	Catahoula	sandstone	-73	5.9	-39
C150913 MB20	27.90698	-98.57288	217	~30.4 [a3]	Catahoula	sandstone	-67	1.7	-33
A150912 B2	28.58927	-98.21257	61	~30.4 [b1]		ash	-78	6.4	-44
16010904	27.86336	-98.69360	209	~30.4 [a3]	Catahoula	ash	-64	2.0	-30
Conquista	28.87635	-98.10129	138	34.07±0.08 [b1]		ash	-85	5.3	-51
S. Someville L.	30.29126	-96.52406	81	34.10±0.2 [b1]		ash	-85	6.3	-51
Smiley Gonzales	29.19934	-98.10129	162	34.24±0.2 [d1]		ash	-79	6.9	-45
Someville L.S.	30.31793	-96.51695	70	34.5±0.2 [d1]		ash	-83	5.5	-49
Y3	28.43218	-98.30154	51	~32.5 [d3]		ash	-77	6.0	-43
Y5	30.46457	-96.30154	70	30-27 [d3]	Catahoula	ash	-74	6.0	-40

Y6	28.59539	-98.22373	60	~32.7 [d3]		ash	-77	6.7	-43
Miocene									
SOLIDA 12	38.51188	-106.02378	3010	~9.3 [e3]	Dry Union	sandstone	-145	3.9	-111
SOLIDA 14	38.51147	-106.02611	3010	~9.3 [e2]	Dry Union	sandstone	-146	3.2	-112
BC3-350	38.63991	-100.92847	890	8.9±0.5 [f2]	Ogallala	sandstone	-101	3.9	-67
BC8-700	38.63991	-100.92847	890	6.3±0.3 [f2]	Ogallala	sandstone	-114	3.2	-80
CQ1-18	39.84482	-99.75710	706	~11.7 [f3]	Ogallala	sandstone	-110	4.2	-76
CQ1-121	39.84482	-99.75710	706	~11.7 [f2]	Ogallala	sandstone	-132	5.0	-98
DB-2-150	38.64035	-100.91407	877	10.2±0.4 [f2]	Ogallala	sandstone	-98	4.3	-64
160110-04	28.64960	-97.38561	29	14-6 [a3]	Goliad	sandstone	-44	1.1	-10
160111-12	28.29411	-97.96977	45	14-6 [a3]	Goliad	sandstone	-68	1.4	-34

[*]Water δD values are calculated based on the fractionation factor from Friedman et al. (1993).

[#]Code for references: a = (Godfrey et al., 2018); b = (Heintz et al., 2015); c = (Smith et al., 2017); d = (Yancey et al., 2018); e = (Zhu and Fan, 2018); f = (Hallman, 2016). 1 = sanidine $^{40}Ar/^{39}Ar$ dating; 2 = detrital zircon U-Pb dating, maximum depositional age; 3 = stratigraphic correlation.

Chapter 5 Conclusions

This dissertation examines the controlling factors of river water isotope composition in the continental interior of the western USA as well as the uplift history of the southern Rockies. In Chapter 2, I investigated the controlling factors of river water isotope compositions in the central Rockies and the adjacent Great Plains by integrating analyses of spatiotemporal patterns of river water isotope values, back trajectory analysis of precipitation, and statistical analysis of the relationships between river water isotope values and climate and geographic factors. In Chapter 3, I studied detrital zircon U-Pb ages of early Eocene-Miocene sedimentary rocks in south-central Colorado and use their maximum depositional ages and provenance information constrain the landscape and paleodrainage evolution in the southern Rockies. In Chapter 4, I analyzed the spatial patterns and controling factors of modern river water isotope data compiled from a broad region covering near sea-level regions in south Texas, the Great Plains in Oklohoma and Kansas, and the southern Rockies in Colorado. By using reconstructed surface water hydrogne isotope values from those of hydrated volcanic glass and with careful assessment of the large-scale atmospheric circulation pattern and changes in temperature after the Eocene, I reconstructed the late Eocene to the late Miocene paleoelevations of the southern and central Rockies and their adjacent high Great Plains.

In Chapter 2, I found that vapor masses from tropical and high-latitude Pacific, Gulf of Mexico, northern region in the Canadian Rockies and Hudson Bay, and continental recycled moisture all contributed to precipitation in the central Rockies and its adjacent Great Plains, and the Great Plains received more moisture from the Gulf of Mexico than the central Rockies. Therefore, Rayleigh distillation of a single vapor source is not a valid assumption for surface water isotope fractionation in the region. In the Bighorn River drainage, a typical intermontane drainage in the central Rockies, the isotope difference between highland and lowland rivers was small, which was attributed to low $\delta^{18}O$ highland precipitation that governs the isotopic composition of lowland river discharge. In the North Platte River drainage across the central Rockies and Great Plains, river water $\delta^{18}O$ values showed eastward increase east of 105°W, with an average isotope lapse rate of -2.3‰/km. This eastward increase in $\delta^{18}O$ values follows the decreased in elevation and was mainly caused by condensation temperature-induced isotope fractionation in precipitation, and secondarily by more moisture from the Gulf of Mexico on the Great Plains than in the central Rockies and strong evaporation in the headwaters of the North Platte River. The understanding of controlling factors on river water isotope compositions have implications for paleorelief reconstruction. Existence of paleorelief between the Laramide mountain ranges and basin floors can be inferred from the differences of reconstructed river water and basinal precipitation isotope values in the Laramide intermontane basins. By using the modern lapse rate a paleorelief of the central Rockies relative to the Great Plains can be derived for the Oligocene and Neogene.

In Chapter 3, I found the detrital zircons in the Eocene-Miocene strata in the southern Rockies have major populations of 75–11 Ma, 1500–1300 Ma, and 1800–1500 Ma, and minor populations of 1300–950 Ma and 2709–1800 Ma. Maximum depositional ages constrain the absolute ages of the latest Eocene-Oligocene strata because of the presence of abundant air-fall zircons derived from intense synchronous volcanism. The data show that the landscape and paleodrainage pattern in the southern Rockies experienced three distinctive stages including that (1) during the early Eocene, the Wet Mountains was the dominant local topographic feature, and a southward river, likely the paleo-Arkansas River, connected the Wet Mountain Valley with the Huerfano and Raton Basins to the south; (2) during the Eocene-early Oligocene, the Wet Mountain Valley and the Huerfano Basin experienced basin aggradation to form a low-relief surface, and subsequent river erosion on the low-relief surface carved the eastward lower Arkansas River valley; and (3) during the Miocene, the opening of the Rio Grande Rift dissected the low-relief surface and formed the upper Arkansas River valley, and the upper valley was connected with the lower Valley to establish the modern drainage pattern of the Arkansas River in the southern Rockies.

In Chapter 4, I found that the vapors in the southern Rockies and its adjacent Great Plains were from four sources and contienntal recycled moisture contributed a significant amount. The lowest modern river water δD values in the low Great Plains from south Texas to central Kansas had a latitudianl gradient of -3.0 ‰/ degree and the river water δD values in the southern Rockies and its adjacent Great Plains had a lapse rate of -24.9‰/km. Both rates were primarily controled by temperature differences, and secondarily by changing abundance of recycled continental moisture. With careful assessment of the large-scale atmospheric circulation pattern and changes in temperature after the Eocene, I reconstructed the late Eocene to the late Miocene paleoelevations of the southern and central Rockies and their adjacent high Great Plains. The estimates show that the central Rockies established its close-to-modern high elevation by the late Eocene, and its adjacent high Great Plains in western Nebraska was established by the early Oligocene, suggesting that the Neogene epeirogeny had little influence on the topogrpahy of the regions. The estimates also show that the southern Rockies was low during the latest Eocene, and experienced differential uplift during the Oligocene and Neogene. Latest Eocene-early Oligocene magmatism of the San Juan volcanic field has caused surface uplift to the region close to it and its impact on topography dimishes as the study site become furthur away. The Wet Moutnains expereinced major uplift during the Miocene, likely a result of localized uplift associated with the opening of the Rio Grande Rift or difference in lithosphere thickness. The uplift of the high Great Plains adjacent to the central and southern Rockies also show along-strike variation.

Biographical Information

Lu Zhu obtained her Bachelor degree in a joint program from the Missouri University of Science and Technology and the China University of Petroleum (East China) in 2012, and her Master degree in Southern Methodist University in 2014. She then furthered her doctorate education in Earth and Environmental Sciences under the supervision of Dr. Majie Fan at the University of Texas at Arlington. Her research involves field work, laboratory analyses, and data spatial analysis in ArcGIS to unravel tectonic processes, depositional histories, and associated climatic and environmental changes from sedimentary archives. The research tools she uses mainly include stable isotope geochemistry, sedimentology and detrital zircon geochronology.